UNIVERSIDADE DE VIGO

DEPARTAMENTO DE MATEMÁTICA APLICADA II

Modelling, Simulation and Robust Control of Distributed Processes:

Application to Chemical and Biological Systems

Carlos Vilas Fernández

Memoria realizada bajo la dirección de los Investigadores Científicos Dr. D. Antonio Álvarez Alonso y Dr. D. Julio Rodríguez Banga, del Instituto de Investigaciones Marinas de Vigo (CSIC), para optar al grado de Doctor en Matemáticas por la Universidad de Vigo. Marzo de 2008.

Esta memoria fue defendida por D. Carlos Vilas Fernández el día 8 de Mayo de 2008 en la Universidad de Vigo ante el Tribunal compuesto por:

Presidente:

Dr. D. Eduardo Fernández Camacho, Catedrático de Universidad del Departamento de Ingeniería de Sistemas y Automática de la Universidad de Sevilla.

Vocales:

Dr. D. Constantinos Theodoropoulos, *Lecturer* del *Department of Process Integration* de la Universidad de Manchester (Reino Unido).

Dr. D. Fernando Tadeo Rico, Profesor Titular de Universidad del Departamento de Ingeniería de Sistemas y Automática de la Universidad de Valladolid.

Dra. Da. Eva Balsa Canto, Científica Titular del Consejo Superior de Investigaciones Científicas. Instituto de Investigaciones Marinas de Vigo.

Secretario:

Dr. D. Fernando Varas Mérida, Profesor Titular de Universidad del Departamento de Matemática Aplicada II de la Universidad de Vigo.

Calificación: Sobresaliente Cum Laude

Agradecimientos

Me gustaría empezar este apartado agradeciendo a los Doctores y directores de esta tesis Antonio Álvarez Alonso y Julio Rodríguez Banga por brindarme la oportunidad de unirme al grupo de ingeniería de procesos del IIM-CSIC. En especial destaco aquí la gran labor de formación y la confianza depositada en mí por Antonio.

Siguiendo con mi formación me gustaría agradecer a Lino y a Áurea la ayuda prestada con las cuestiones matemáticas más enrevesadas. Sería injusto olvidarme en este apartado del resto de profesores (Durany, Curro, Guillermo,...) del departamento de DMA II de la universidad de Vigo que siempre estuvieron dispuestos a echar un cable.

Por supuesto quiero agradecer la financiación recibida por: los proyectos del ministerio de educación y ciencia del gobierno español PTR1995-0884-OP-02-01 y DPI2004-07444-C04-03; el proyecto de la comunidad europea (BE-FAIR), y las empresas ALIMENTOS AROSA y EMPRESARIOS AGRUPADOS. Dentro de este apartado incluyo también a los otros grupos de investigación con los que colaboramos para llevar a cabo dichos proyectos.

Un alto porcentaje de los resultados de esta tesis fueron desarrollados en estrecha colaboración (que muchas veces se confundía con confrontación) con Míriam. La de cosas que aprendí intentando (y algunas veces consiguiendo) demostrar lo equivocada que estabas. Cuando resultaba ser yo el equivocado, esa noche no dormía bien. Supongo que habremos creado más de un trauma a la gente que no nos conocía y que nos veía trabajar (o pelear) juntos. También recuerdo los primeros tiempos en el grupo en los que empezaba a descubrir Matlab, LaTeX, las ecuaciones en derivadas parciales, el método de diferencias finitas,... gracias Carmen. Y si recuerdo los primeros tiempos, ¿cómo olvidar los últimos? en los que Eva me enseñó a escribir correos electrónicos sin que pareciesen amenazas de muerte; que existen presentaciones de trabajos más allá de las ecuaciones o que una frase en un artículo no tiene que empezar exactamente como la primera vez que se escribió, sino que se puede reescribir toda la frase o incluso todo el párrafo (todo un descubrimiento). También agradezco a Irene su empecinamiento por

querer llevar el coche a todas partes y por estar dispuesta a ayudar aunque estuviese con el agua al cuello, ayuda que también recibí del resto de miembros del grupo: Marcos, Oscar, Luis, María, Jose, Sonia, Dirk, Oliver y Martin.

En mi opinión, todas las tesis que salen del IIM deberían llevar un agradecimiento explícito a Marigel y al resto de miembros de la biblioteca. No creo que pudiésemos hacer mucho sin vosotras. También agradezco los momentos en los que, mucha otra gente del IIM y yo, arreglamos en una comida o en un café todos los problemas que tiene España.

Tradicionalmente éste es el turno para mostrar gratitud a los miembros de la familia. Muchos piensan que no soy una persona tradicional y ahora es el momento de demostrar lo equivocados que están. Agradezco a mis padres la educación que me han dado (si nos olvidamos de la imposición por decreto ley de ir a misa todos los Domingos y fiestas de guardar. Fui un niño temeroso de Dios hasta que me di cuenta de lo bien que se estaba en cama los Domingos lluviosos por la mañana) y por dejarme elegir siempre el camino que deseaba seguir, aunque siempre mostrándome mediante críticas ácidas, que existían otras opciones. También agradezco a mis hermanos que siempre cumplieron cuando se lo pedí.

Por supuesto, no hay tesis que se precie de serlo en la que no se agradezca la influencia de los amigos y yo no voy a ser menos (aunque tampoco más). Muchos emigrasteis (Dani, Jose, Rebeca, Ana, Oso, Inés, Jesús) porque aquí no encontrabais el trabajo adecuado, os fuisteis en busca de un *oráculo* que os guiase y algunos lo encontrasteis en Inglaterra. Otros os quedasteis proporcionándome el entretenimiento necesario en la vida de toda persona (Iñaki, Natalia, Pablo, Iago). Las discusiones entre carnívoros vs. vegetarianos que empezaban con la curiosidad de los primeros acerca de las razones de los segundos y que siempre acababan preguntándonos si comeríamos un extraterrestre o un gorila inteligente, entre muchas otras, fueron el origen de mi eterna devoción por la lógica formal.

También me gustaría agradecer a la gente del Budo Castrelos (tanto a la gente de las nueve y cuarto como a la de las nueve menos cuarto y a la de competición) por dejar que les metiese unos cuantos *mondolio nako chaguis* en momentos de necesidad. Es increíble lo relajante que puede resultar pegar unas cuantas patadas.

Por último me gustaría dedicar un par de líneas a los creadores de software libre y de alternativas a Microsoft. No sé que habría sido de mí sin LaTeX, pero supongo que nada bueno.

Aquello que no nos mata, nos hace más fuertes

Friedrich Wilhelm Nietzsche

Motivación

Las ventajas de disponer de un modelo para la simulación de un determinado proceso son muchas. Entre ellas destacan: poder anticiparse a posibles cambios en las condiciones; ensayar distintos modos de operación o comprobar el efecto de la utilización de equipamiento alternativo. Todo ello de una forma rápida, eficiente y económica.

La mayor parte de los procesos involucrados en campos tan diversos como la biología, la química o la industria alimentaria, entre otros, comparten ciertas características entre las que destacan su carácter distribuido, es decir, los estados asociados a ese proceso evolucionan en el tiempo y están distribuidos en el espacio. Por lo tanto, el modelado y la simulación de los mismos, objetivos de la primera parte de la tesis, llevan asociados por un lado la formulación del sistema en forma de ecuaciones en derivadas parciales (EDP), generalmente no lineales, y por otro lado su resolución. Debido a que en la mayoría de los casos no se conoce la solución analítica de las mismas, generalmente se recurre a las siguientes alternativas:

- Tratar este tipo de sistemas como si fuesen de parámetros concentrados (los estados sólo dependen del tiempo).
- Utilización de métodos numéricos como diferencias finitas (MDF), elementos finitos (MEF) o volúmenes finitos (MVF).

La primera opción sólo es válida cuando la distribución espacial es despreciable frente a la evolución temporal como, por ejemplo, reactores donde mediante agitación se consigue la homogeneización del medio. Sin embargo, en el resto de los casos es necesario recurrir a la segunda alternativa. El mayor inconveniente de ésta es que la solución numérica implica un coste computacional tan grande (especialmente cuando se consideran dominios espaciales 2D o 3D) que resulta poco eficiente, o incluso inservible, para aplicaciones en tiempo real como control u optimización en línea.

En esta tesis se propone, como alternativa a los métodos clásicos, el desarrollo de una sistemática para la proyección de las EDP sobre un subespacio de dimensión reducida. De esta forma la EDP original, se transforma en un conjunto de ecuaciones

diferenciales ordinarias (EDO) conocido como modelo de orden reducido (MOR). Uno de los problemas de los métodos de proyección es tratar con términos no lineales ya que implica llevar a cabo integrales cuya solución analítica se desconoce en muchos casos. Las matrices resultantes del MEF permiten aproximar derivadas e integrales espaciales mediante operaciones algebraicas. En este trabajo se hace uso de dichas matrices para desarrollar una sistemática que permita la obtención de modelos de orden reducido, su resolución de forma eficiente y que sea aplicable tanto a procesos 1D como 2D o 3D con geometrías arbitrariamente complejas.

Por otra parte, en algunos sistemas, el hecho de utilizar un controlador que asegure que el proceso está siendo llevado a cabo en las condiciones adecuadas resulta tan importante como (o incluso más que) disponer de un modelo para la simulación. El diseño de una lógica de control para sistemas reacción-difusión-convección es el principal objetivo de esta tesis.

Los casos estudiados incluyen reactores tubulares y procesos de interés en biología. Dado que en la mayor parte de este tipo de sistemas, tanto los parámetros como los términos no lineales de dichos modelos llevan asociada una cierta incertidumbre, será necesaria la aplicación de técnicas de control robusto capaces de llevar al sistema a una referencia dada a pesar de la presencia de dicha incertidumbre. Para ello se propone la adaptación de la teoría clásica existente de control robusto para sistemas de parámetros concentrados a sistemas distribuidos mediante la utilización de los MOR.

Por último, un problema intrínseco al control de sistemas distribuidos es que, generalmente y debido a restricciones físicas y/o económicas, sólo se dispone de un número finito (normalmente pequeño) de actuadores. Esta cuestión puede provocar que el sistema no sea controlable y, por lo tanto, la referencia deseada no pueda ser alcanzada. Es por ello que también debe prestarse atención a las condiciones (número mínimo de actuadores) que aseguran la controlabilidad del sistema.

Motivation

There is a great amount of advantages in having at our disposal a mathematical model for the simulation of a given process. Among them, the following are highlighted: to enable us to keep abreast of unforeseen changes in the conditions; to explore different ways of operating the plant or to test the effect of using alternative equipment to carry out a given process in a fast, efficient and economical way.

Most of the processes involved in different fields such as biology, chemistry or food industry, among others, share several features such as the distributed nature, i.e., the states associated to those processes evolve in time and are distributed in space. Therefore, the modelling and simulation of them, which are the objectives of the first chapters of the thesis, are associated with, on the one hand the formulation of the system using partial differential equations (PDEs), in general nonlinear, and on the other hand the computation of the solution. Since in most of cases the analytical solution is unknown, the following alternatives are commonly employed:

- To assume that these processes behave like lumped parameter systems (the states are only time dependent).
- To use classical numerical methods like finite differences (FDM), finite elements (FEM) or finite volumes (FVM).

The first option is only valid when the spatial distribution is negligible as compared with the time evolution, for instance in reactors where the homogenisation of the medium is achieved by means of stirring devices. Nevertheless, in the remaining cases it is necessary to use the second alternative. Its main inconvenience is that the numerical solution is computationally involved (especially in 2D or 3D spatial domains) making the approach unsuitable for real time tasks like control or online optimisation.

As an alternative to the classical numerical methods the development of a systematic procedure for the projection of the PDEs onto a low dimensional subspace is proposed in this thesis. In this regard, the original PDE is transformed into a set of ordinary differential equations (ODEs) known as reduced order model (ROM). One

inconvenience of the projection methods is dealing with nonlinear terms since spatial integrals with unknown analytical solutions must be computed. The matrices resulting from the FEM allow us to approximate spatial integrals and derivatives by means of algebraic operations. These matrices are employed in this work in order to develop a systematic procedure, applicable to 1D, 2D or 3D processes with arbitrarily complex geometries, for the construction of ROMs and for the efficient computation of their solution.

On the other hand, in some systems, using a controller ensuring that the process is carried out in adequate conditions, is as important as (or even more than) to have at our disposal a model for simulation. The design of a control logic for reaction-diffusion-convection systems is the main objective of this thesis.

The case studies include tubular reactors and processes of interest in biology. Since the exact values/forms or the parameters and nonlinear terms are unknown in this class of systems, it is necessary to apply robust control techniques able to drive the system to the desired reference despite the presence of uncertainties. To that purpose, the classical theory for the robust control of lumped parameter systems is extended to distributed systems by using the ROMs.

Finally, a problem associated with the control of distributed systems is that, in general and due to physical and/or economical constraints, only a finite (usually low) number of actuators is available. This issue may affect the system controllability and therefore the desired reference may become unreachable. For this reason, special attention must be paid to the conditions (minimum number of actuators) in which the system controllabiltiy is assured.

Objetivos y Estructura de la Tesis

El objetivo principal de este trabajo es el desarrollo de una lógica de control capaz de llevar los estados de un sistema dado a la referencia deseada incluso en presencia de incertidumbre tanto en los parámetros como en la estructura del modelo (*control robusto*). Las siguientes cuestiones, asociadas con el problema de control robusto, se tratan también en esta tesis: la selección del número mínimo de actuadores que aseguran la controlabilidad del sistema; su colocación en el dominio espacial de forma que el esfuerzo de control sea mínimo y el diseño de la lógica de control asociada a los mismos.

Dado que los modelos de orden reducido (MOR) constituyen una pieza fundamental en nuestra propuesta para el control robusto de sistemas distribuidos, la comparación entre las distintas alternativas y el desarrollo de una sistemática eficiente para la obtención de los MOR son objetivos secundarios íntimamente ligados al objetivo principal.

Además, el desarrollo de modelos desde el punto de vista fenomenológico y la resolución de los mismos mediante esquemas numéricos clásicos con los que testar los MOR juegan también un papel fundamental en este trabajo.

Estructura de la Memoria

En el primer capítulo de este trabajo se presenta un enfoque al modelado de sistemas distribuidos distinto, aunque equivalente, al tradicional en ingeniería (basado en balances macroscópicos de materia, energía y cantidad de movimiento). Dicho enfoque hace uso de la primera ley de la termodinámica para llegar a las ecuaciones del modelo. Estas ecuaciones necesitan, sin embargo, ser completadas con las relaciones entre lo que se conoce como fuerzas y los flujos termodinámicos. La segunda ley de la termodinámica nos proporciona el marco en el que encontrar dichas relaciones. La elección del *enfoque termodinámico* frente al tradicional no responde a motivos caprichosos sino que, como se verá a lo largo de esta memoria, dicho enfoque es uno de los pilares sobre los que se asentarán las técnicas de reducción de orden y de control robusto.

El segundo capítulo se centra en los métodos clásicos de resolución de EDP dedicando la mayor parte del mismo al método de elementos finitos ya que será el método clásico empleado en los casos estudiados en esta tesis. Los motivos de elegir el MEF frente a otras posibilidades son, por una parte, su flexibilidad a la hora de tratar problemas con geometrías arbitrariamente complejas y, por otra parte, la utilidad de la estructura resultante de la aplicación del MEF que nos permite aproximar derivadas e integrales espaciales por medio de operaciones algebraicas facilitando la proyección para la obtención de los modelos de orden reducido.

Las distintas técnicas de reducción de orden que se utilizarán para el desarrollo de la lógica de control se describen en el tercer capítulo centrándose especialmente, debido a su eficiencia, en los métodos de descomposición espectral del Laplaciano y de descomposición ortogonal propia. Uno de los principales cuellos de botella de los MOR (la proyección de los términos no lineales) se trata en la tercera sección. Este capítulo concluye con una serie de casos de uso en los que se ilustran los pasos a seguir en cada una de las técnicas de reducción así como sus ventajas e inconvenientes.

En el cuarto capítulo se trata el objetivo principal de esta tesis, el *control robusto*. Para ello se parte de la teoría clásica en sistemas de parámetros concentrados no lineales y se muestra cómo extenderla a sistemas distribuidos mediante los MOR. Además se utilizarán ejemplos sencillos para ilustrar los pasos clave de esta técnica de control. Los detalles a tener en cuenta cuando se afronta el problema de control robusto utilizando un número bajo de actuadores se tratan en la parte final del capítulo.

La segunda parte de esta tesis (capítulos 5 y 6) se dedica a las aplicaciones de las técnicas descritas en los capítulos anteriores. Ya que los reactores tubulares se utilizan ampliamente en la industria y, en general, no son sencillos de controlar, la primera aplicación trata del control robusto de los mismos. Por otra parte, en la segunda aplicación se considera un modelo de interés en biología y en reactores catalíticos conocido como el modelo de FitzHugh-Nagumo.

Finalmente, se presentan de forma resumida las conclusiones de este trabajo desde un punto de vista de crítico y las posibles direcciones que se adoptarán en un futuro próximo y que permitirían fortalecer los puntos débiles del mismo.

Objectives and Thesis Structure

The main objective of this work is the development of a control logic able to drive the states of a given system to the desired reference even in the presence of parametric and/or structural uncertainty (*robust control*). The following issues, associated with the problem of robust control, are considered in this thesis: the selection of the minimum number of actuators that ensures the system controllability; their collocation in the spatial domain and the design of the control logic associated to them.

Since reduced order models (ROMs) play a fundamental role in our approach for the robust control of distributed systems, the comparison among the different alternatives and the development of an efficient systematic procedure for the construction of ROMs are secondary objectives intimately related to the main objective.

Besides, the development of mathematical models from the phenomenological point of view and the computation of their solution by means of classical numerical methods for testing the ROMs also play a key role in this work.

Thesis Structure

In the first chapter of this dissertation an approach for the modelling of distributed systems, which although different is equivalent to the traditional approach employed in engineering (based on mass, energy and momentum macroscopic balances), is presented. This approach makes use of the first law of thermodynamics to derive the model equations. Nevertheless, these equations need to be completed with relationships between the thermodynamic fluxes and forces. The second law of thermodynamics provides us the framework to find such relationships. The reason for choosing the *thermodynamic approach* instead the traditional one is not whimsical but, as it will be shown along the manuscript, such an approach is one of the basis of the order reduction and robust control techniques.

The second chapter is focused on the classical numerical methods for the computation of the solution of PDEs. Most of this chapter is focused on the FEM since it is the classical method employed in the case studies of this thesis. The reasons

for choosing the FEM instead other alternatives are, firstly, its flexibility for dealing with problems with arbitrarily complex geometries and, secondly, the usefulness of the structure resulting from the application of the FEM which allows us to approximate spatial integrals and derivatives by algebraic operations making easier the projection for the derivation of ROMs.

The different order reduction techniques employed for the construction of the control logic are described in the third chapter focusing, due to their efficiency, in the methods of *Proper Orthogonal Decomposition* (POD) and *Laplacian Spectral Decomposition* (LSD). One of the main bottlenecks of ROMs (projection of nonlinear terms) is approached in the third section. This chapter concludes with a number of case studies which illustrate the steps to be followed in each reduction technique showing the main advantages and inconveniences.

The fourth chapter is focused on the main objective of this thesis, the *robust control*. To that purpose, the starting point is the classical theory of robust control for nonlinear lumped parameter systems and it is extended to distributed systems by means of the ROMs. Besides, some simple case studies will be employed so as to illustrate the key steps to be followed in this control technique. The details to take into account when only a low number of actuators are available, are approached in the final part of this chapter.

The second part of this thesis (Chapters 5 and 6) is focused on the applications of the techniques just described in previous chapters. Since tubular reactors are widely employed in the industry and, in general, are challenging examples from the control point of view, the first application is about the robust control of tubular reactors. In the second application a model of interest in biology and catalytic reactors, known as the FitzHugh-Nagumo, is considered.

Finally, the conclusions of this work are briefly discussed from a critical point of view. Furthermore, the possible research directions to be followed in the future to overcome the weak spots of this work will be described.

Notation and General Concepts

Abbreviations

FEM	Finite Element Method
FHN	FitzHugh-Nagumo
LHS	Left Hand Side
LRT	Lyapunov Redesign Technique
LSD	Laplacian Spectral Decomposition
MWR	Method of weighted residuals
ODE	Ordinary Differential Equation
PDE	Partial Differential Equation
POD	Proper Orthogonal Decomposition
RDC	Reaction-Diffusion-Convection
RHS	Right Hand Side
ROM	Reduced Order Model

Typical Symbols

$a(z), b(z)$	Convex functions
$f(z), g(z)$	Nonlinear functions
$\overrightarrow{\mathbf{j}}$	Diffusion flux
J	Thermodynamic fluxes
P	Pressure
$\overrightarrow{\mathbf{q}}$	Heat flux
s	Specific entropy
t	Time
T	Temperature
u	Control input
u_s	Specific internal energy
$\overrightarrow{\mathbf{u}}_i$	Unitary vector on the direction ξ_i
$\overrightarrow{\mathbf{v}}$	Flow velocity
$\overrightarrow{\mathbf{x}}$	Microscopic fluxes through the domain
X	Thermodynamic forces
z	State of a process

Special Characters

A	Intensive variables
$\mathscr{B}$	Boundary of the spatial domain
$\mathscr{B}_e$	Boundary of a finite element spatial domain
$\mathcal{B}$	Lyapunov function
$\mathscr{D}$	Spatial and time domains
$\mathscr{E}$	Set of eigenfunctions
ℓ_0	Invariant set
$\mathscr{L}$	Set of eigenvalues
$\mathscr{M}$	Set of modes
$\mathscr{T}$	Time domain
$\mathscr{V}$	Spatial domain
$\mathscr{V}_e$	Spatial domain of a finite element

Greek symbols

δx	Variation of the quantity x
Γ	Kirchhoff transform
λ	Eigenvalue
μ_i	Chemical potential of the specie i
ϕ	Global basis functions
φ	Local basis functions
ψ	Test functions
ξ	Spatial coordinates

Subindex

a	Finite dimensional set
b	Infinite dimensional set
0	Initial conditions

Superindex

e	Finite element
$*$	Reference

Mathematical operators

$\overrightarrow{\boldsymbol{\nabla}}$	"Nabla" operator. $\overrightarrow{\boldsymbol{\nabla}} = \overrightarrow{\mathbf{u}}_1 \frac{\partial}{\partial \xi_1} + \overrightarrow{\mathbf{u}}_2 \frac{\partial}{\partial \xi_2} + \overrightarrow{\mathbf{u}}_3 \frac{\partial}{\partial \xi_3}$
Δ	Laplacian operator. $\Delta = \nabla^2$
$\langle f, g \rangle_{\mathscr{V}}$	Inner product of two vector functions: $\langle f, g \rangle_{\mathscr{V}} = \int_{\mathscr{V}} f^T g d\boldsymbol{\xi}$
$\|f\|_{\mathscr{V}}$	$\mathcal{L}_2$ norm defined as $\|f\|_{\mathscr{V}} = \langle f, f \rangle_{\mathscr{V}}^{1/2}$
$\frac{D}{Dt}$	Substantial or Lagrangian time derivative. $\frac{D}{Dt} = \frac{\partial}{\partial t} + \overrightarrow{\mathbf{v}} \cdot \overrightarrow{\boldsymbol{\nabla}}$

In general, bold uppercase symbols will represent a matrix while bold lowercase and italic symbols will denote vectors and scalars, respectively.

The different kinds of vectors

In this work the following distinctions will be made regarding vector notation. On the one hand the vectors whose components are referred to the spatial coordinates for instance the Nabla operator ($\overrightarrow{\boldsymbol{\nabla}}$) and, on the other hand the vectors which are composed by different quantities (scalars or vectors), for example a vector collecting the temperature, the concentration and the linear momentum of a given system ($\mathbf{z} = [T, c, \rho\overrightarrow{\mathbf{v}}]^T$)

Vectors and Matrices multiplication

Vectors and matrices can be multiplied in many different ways. In order to distinguish among the different possibilities, the notation followed in (Bird et al., 2002) will be employed in this work. Scalars, vectors and matrices are tensors of zero, one and two, rank respectively. Now, consider that Σ is the summation of the ranks of the elements being multiplied, for instance in the multiplication of a scalar by a vector $\Sigma = 0+1 = 1$ or in the multiplication of a matrix by a vector $\Sigma = 2+1 = 3$, and so on. The different symbols employed in the multiplication will be: None, the cross ($\times$), the single dot ($\cdot$) and the colon (:). The total order of the multiplication is computed as follows:

Operator	Order of the multiplication
None	Σ
$\times$	$\Sigma - 1$
$\cdot$	$\Sigma - 2$
:	$\Sigma - 4$

In this way, for example the order of the multiplication (ab) will be $0+0-0 = 0$ so the result is a scalar, while the order of the multiplication ($\mathbf{a} \cdot \mathbf{B}$) will be $1+2-2 = 1$ so the result is a vector.

The different ways of multiplying vectors and matrices

For the sake of illustration the following vectors and matrices will be considered:

$$\overrightarrow{\mathbf{v}} = [v_{\xi_1}, v_{\xi_2}, v_{\xi_3}] = v_{\xi_1}\overrightarrow{\mathbf{u}}_1 + v_{\xi_2}\overrightarrow{\mathbf{u}}_2 + v_{\xi_3}\overrightarrow{\mathbf{u}}_3; \quad \overrightarrow{\mathbf{w}} = [w_{\xi_1}, w_{\xi_2}, w_{\xi_3}] = w_{\xi_1}\overrightarrow{\mathbf{u}}_1 + w_{\xi_2}\overrightarrow{\mathbf{u}}_2 + w_{\xi_3}\overrightarrow{\mathbf{u}}_3$$

$$\mathbf{P} = \begin{bmatrix} P_{11} & P_{12} & P_{13} \\ P_{21} & P_{22} & P_{23} \\ P_{31} & P_{32} & P_{33} \end{bmatrix}; \qquad \mathbf{Q} = \begin{bmatrix} Q_{11} & Q_{12} & Q_{13} \\ Q_{21} & Q_{22} & Q_{23} \\ Q_{31} & Q_{32} & Q_{33} \end{bmatrix}$$

Furthermore, the *Kronecker delta* (δ_{ij}) and the *Levi-Civita* or *permutation* symbol

(ε_{ijk}) will be employed in some formulas. These parameters are defined by:

$$\begin{cases} \delta_{ij} = 1 & \text{if} \quad i = j \\ \\ \delta_{ij} = 0 & \text{if} \quad i \neq j \end{cases} ; \qquad \begin{cases} \varepsilon_{ijk} = 1 & \text{if} \quad ijk = 123, 231, 312 \\ \\ \varepsilon_{ijk} = -1 & \text{if} \quad ijk = 321, 132, 213 \\ \\ \varepsilon_{ijk} = 0 & \text{otherwise} \end{cases}$$

- Multiplication by a scalar:

  In this case all the elements of the vector or the matrix are multiplied by the scalar

- Vector multiplication:

$$\overrightarrow{\mathbf{v}} \cdot \overrightarrow{\mathbf{w}} = v_{\xi_1} w_{\xi_1} + v_{\xi_2} w_{\xi_2} + v_{\xi_3} w_{\xi_3} = [v_{\xi_1}, v_{\xi_2}, v_{\xi_3}] \begin{bmatrix} w_{\xi_1} \\ w_{\xi_2} \\ v_{\xi_3} \end{bmatrix}$$

  For the sake of simplicity, the scalar product $\overrightarrow{\mathbf{v}} \cdot \overrightarrow{\mathbf{v}}$ will be denoted by v^2 where v is the modulus of $\overrightarrow{\mathbf{v}}$.

$$\overrightarrow{\mathbf{v}} \times \overrightarrow{\mathbf{w}} = \begin{bmatrix} \overrightarrow{\mathbf{u}}_1 & \overrightarrow{\mathbf{u}}_2 & \overrightarrow{\mathbf{u}}_3 \\ v_{\xi_1} & v_{\xi_2} & v_{\xi_3} \\ w_{\xi_1} & w_{\xi_2} & w_{\xi_3} \end{bmatrix}$$

$$\overrightarrow{\mathbf{v}} \overrightarrow{\mathbf{w}} = \begin{bmatrix} v_{\xi_1} w_{\xi_1} & v_{\xi_1} w_{\xi_2} & v_{\xi_1} w_{\xi_3} \\ v_{\xi_2} w_{\xi_1} & v_{\xi_2} w_{\xi_2} & v_{\xi_2} w_{\xi_3} \\ v_{\xi_3} w_{\xi_1} & v_{\xi_3} w_{\xi_2} & v_{\xi_3} w_{\xi_3} \end{bmatrix}$$

- Vector by matrix multiplication:

$$\overrightarrow{\mathbf{v}} \cdot \mathbf{P} = \sum_{k=1}^{3} v_k P_{k1} \overrightarrow{\mathbf{u}}_1 + \sum_{k=1}^{3} v_k P_{k2} \overrightarrow{\mathbf{u}}_2 + \sum_{k=1}^{3} v_k P_{k3} \overrightarrow{\mathbf{u}}_2 = [v_{\xi_1}, v_{\xi_2}, v_{\xi_3}] \begin{bmatrix} P_{11} & P_{12} & P_{13} \\ P_{21} & P_{22} & P_{23} \\ P_{31} & P_{32} & P_{33} \end{bmatrix}$$

$$\mathbf{P} \times \overrightarrow{\mathbf{v}} = \sum_i \sum_l \overrightarrow{\mathbf{u}}_i \overrightarrow{\mathbf{u}}_l \left(\sum_j \sum_k \varepsilon_{jkl} P_{ij} v_k \right)$$

  The case $\overrightarrow{\mathbf{v}}\mathbf{P}$ where the result is third order tensor is not considered in this work.

- Matrix multiplication

$$\mathbf{P} \colon \mathbf{Q} = \sum_i \sum_j P_{ij} Q_{ji}$$

$$\mathbf{P} \cdot \mathbf{Q} = \sum_i \sum_l \overrightarrow{\mathbf{u}}_i \overrightarrow{\mathbf{u}}_l \left(\sum_j P_{ij} Q_{jl} \right)$$

  The cases $\mathbf{P} \times \mathbf{Q}$ and $\mathbf{PQ}$ where the results are third and fourth order tensors are not considered in this work.

In the case of two state vectors $(\mathbf{x}, \mathbf{z})$ the only way of multiplying them considered in this work is the scalar multiplication $\mathbf{x}^T\mathbf{z} = \sum_i x_i z_i$. Likewise, when considered state vectors, $\mathbf{z}^T$ is a row vector while $\mathbf{z}$ is a column vector.

For clarity in the notation, when an operation between vectors whose components are referred to the spatial coordinates $(\overrightarrow{\mathbf{v}})$ and state vectors $(\mathbf{z})$ is carried out, the operation is assumed to apply to all the elements of $\mathbf{z}$, this is:

$$\overrightarrow{\mathbf{v}} \cdot \mathbf{z} = \begin{bmatrix} \overrightarrow{\mathbf{v}} \cdot \mathbf{z}_1 \\ \overrightarrow{\mathbf{v}} \cdot \mathbf{z}_2 \\ \overrightarrow{\mathbf{v}} \cdot \mathbf{z}_2 \end{bmatrix}$$

Integral over a given volume $\mathscr{V}$ will be denoted by:

$$\int_{\mathscr{V}} f d\boldsymbol{\xi} = \int_{\xi_1} \left(\int_{\xi_2} \left[\int_{\xi_3} f d\xi_3 \right] d\xi_2 \right) d\xi_1.$$

Finally, it is assumed that all distributed models considered in this thesis have a unique solution.

Contents

Motivación ix

Motivation xi

Objetivos y Estructura de la Tesis xiii

Objectives and Structure of the Thesis xv

Notation and General Concepts xvii

I Modeling, Simulation and Robust Control of Distributed Process Systems. The Theory 1

1 Modelling of Distributed Processes: A Thermodynamic Approach 3

1.1 Introducción . . . 3

1.2 Introduction . . . 4

1.3 From the First Law to the Model Structure . . . 6

1.4 The Constitutive Equations . . . 9

1.5 Description and Properties of Dissipative Systems . . . 14

2 Simulation of Distributed Processes: The Finite Element Method 23

2.1 Introducción . . . 23

2.2 Introduction . . . 24

2.2.1 The mathematical basis . . . 24

2.3 The Finite Element Method . . . 27

2.3.1 The Basics of the FEM . . . 27

2.3.2 The FEM Matrices: From the Continuous World to its Discrete Version . . . 33

3 Simulation of Distributed Processes: Reduced Order Models 39
3.1 Introducción . . . 39
3.2 Introduction . . . 40
3.2.1 Classification of the Reduced Order Techniques . . . 42
3.3 Nonlinear Terms . . . 43
3.4 The Eigenfunctions Approach . . . 45
3.4.1 The Laplacian Spectral Decomposition Approach . . . 45
3.4.2 The Proper Orthogonal Decomposition . . . 46
3.5 A note on dissipation: The basis of the model reduction . . . 48

4 The Robust Control of Distributed Processes 65
4.1 Introducción . . . 65
4.2 Introduction . . . 68
4.3 The Lyapunov Redesign Technique Revisited . . . 70
4.4 Robust Control in Infinite Dimensional Systems . . . 75
4.5 Control Using a Finite Number of Actuators . . . 81
4.5.1 Robust Control Using a Finite Number of Actuators . . . 84

II Applications: Chemical and Biological Systems 87

5 Application 1: Robust Control of Tubular Reactors 89
5.1 Introducción . . . 89
5.2 Introduction . . . 90
5.3 The Model Equations . . . 91
5.3.1 Dimensional analysis . . . 93
5.3.2 Transformation to Homogeneous Boundary Conditions . . . 95
5.4 The Simulation of Tubular Reactors . . . 96
5.4.1 The Finite Element Method . . . 96
5.4.2 The Laplacian Spectral Decomposition Method . . . 100
5.4.3 The Proper Orthogonal Decomposition Method . . . 102
5.5 The Robust Control of Tubular Reactors . . . 104
5.5.1 Finite Number of Actuators . . . 108

6 Application 2: The Robust Control of the FitzHugh-Nagumo Model 111
6.1 Introducción . . . 111
6.2 Introduction . . . 113
6.3 The model equations . . . 114

6.3.1 The FHN Model as a Representation of a Chemical System . . . 116
6.3.2 The FHN Model as a Representation of a Biological system . . . 118
6.4 Reduced Order Representations . . . 121
6.4.1 ROM in the Chemical Case . . . 121
6.4.2 ROM in the Biological Case . . . 124
6.5 Robust Control . . . 127
6.5.1 Robust Control in the Chemical Case . . . 128
6.5.2 Robust Control in the Biological Case . . . 132

Conclusions **139**

Conclusiones **143**

A Further Notions **147**
A.1 Definitions and Theorems . . . 147
A.2 Alternative development of the state equations . . . 148
A.2.1 Momentum Balance . . . 149
A.2.2 Energy Balance . . . 151
A.2.3 Mass Balance . . . 153
A.3 Initial Value Problem Solvers . . . 154
A.3.1 Explicit Methods . . . 155
A.3.2 Implicit Methods . . . 155
A.4 The Hodgkin-Huxley Model . . . 155

B Proofs of the results **157**
B.1 Proof of Lemma 3.1 . . . 157
B.2 Proof of Lemma 3.2 . . . 158
B.3 Proof of Proposition 3.1 . . . 160
B.4 Proof of Lemma 4.1 . . . 161
B.5 Proof of Proposition 4.1 . . . 162
B.6 Proof of Proposition 4.3 . . . 162
B.7 Proof of Lemma 6.1 . . . 163

References **165**

List of Figures

1.1 Evolution of the distributed temperature. (a) Computed from system (1.37), (b) computed using the Kirchhoff transform -system (1.39)-. . . 18

2.1 From the Fourier series theorem to the family of methods of weighted residuals. 25
2.2 Typical elements considered in the spatial discretization of the FEM. (a) 1D problems, (b) 2D problems. 28
2.3 (a) Solid discretisation. (b) Assembly among the three elements of the spatial domain. The element interior numbers (in red) refer to the local notation while the element exterior numbers (in blue) are related to the global notation. 31
2.4 Typical basis function of the FEM. The white circles represent the element nodes. (a) 1D domains and first order polynomials, (b) 1D domains and second order polynomials, (c) 2D domains with triangular elements and first order polynomials and (d) 2D domains with triangular elements and second order polynomials 34
2.5 1D FEM spatial discretisation using four nodes and linear basis functions. 34
2.6 Graphical interpretation of the relationship between the continuous integral of a function and its discrete counterpart obtained with the $\mathcal{DA}$ FEM matrix. 36
2.7 Evolution and distribution of the temperature in the Fourier problem. The results were obtained (a) analytically and (b) numerically (FEM). 38

3.1 Time evolution of a dissipative system. 44
3.2 Comparison between the eigenfunctions obtained analytically (lines) and numerically (marks). 53
3.3 Evolution of the first six modes, computed with the LSD method, in the Fourier problem. 54

3.4 (a) Numerical solution to the Fourier equation with the LSD with 3 terms. (b) Relative error between the LSD ($p = 3$) and the analytical solution. 55
3.5 (a) Shape of the four more representative PODs basis functions. (b) Energy captured by the PODs 56
3.6 Evolution of the first six modes, computed using the POD method, in the Fourier problem. 57
3.7 (a) Numerical solution to the Fourier equation computed with the POD method ($p = 3$). (b) Relative error between the POD and the analytical solution. 57
3.8 Numerical solution of system (3.24) - (3.26) (a) with $a = c = 0.1$, (b) with $a = c = 2.1$. 59
3.9 The four most representative eigenfunctions on a 1D problem with homogeneous Robin ($\xi = 0$) and Neumann ($\xi = 1$) boundary conditions. 60
3.10 Evolution of the three most representative modes for system (3.24)-(3.25) using the basis of the LSD approach (a) with $a = c = 0.1$, (b) with $a = c = 2.1$. Lines and marks correspond, respectively, with the modes of the FEM and LSD solutions. 61
3.11 Numerical solution of system (3.24) - (3.25) using the LSD approach (a) with $a = c = 0.1$, (b) with $a = c = 2.1$. 61
3.12 Numerical solution of system (3.24) - (3.25) using the POD approach (a) with $a = c = 0.1$, (b) with $a = c = 2.1$. 62
3.13 (a) Evolution of of system (3.24) - (3.25) using the POD approach. (b) Evolution of the three most representative modes obtained from the FEM (continuous lines) and from two different ROMs (marks). 62

4.1 Evolution of a given system with uncertainties under a control law constructed using the LRT. 73
4.2 (a) Evolution of system (4.12) under a proportional control law $u = -Km$. (b) Control effort. 74
4.3 (a) Evolution of system (4.13) under the control law (4.14). (b) Control effort. 75
4.4 Evolution of the field under a control law designed by using different convex functions (a) using function b_1, (b) using function b_2. (c) Control effort for both functions. 80

4.5 (a) Evolution and distribution of z in problem (4.33) with $u = 0$ computed using the FEM. (b) Relative error between the FEM and the ROM. 83
4.6 (a) Field evolution and distribution under the stabilising control law. (b) Control effort. The control enters at $t = 1.5$. 84

5.1 General representation of a tubular reactor with recycle where the reaction $A \rightarrow B$ takes place. 90
5.2 State space representation of the invariant set (ℓ_0) for the System (5.15). The zone where $\ell_0 = 0$ is depicted by the continuous black line (ϖ). . 96
5.3 Solution of system (5.23)-(5.25) without recycle ($r = 0$). (a) For the dimensionless concentration and (b) for the dimensionless temperature. 97
5.4 Solution of system (5.23)-(5.25) with recycle relation $r = 0.5$. (a) For the dimensionless concentration and (b) for the dimensionless temperature. 98
5.5 Representation of the limit cycle reached when $r = 0.5$ in terms of the norm of the states. 98
5.6 Solution of system (5.26)-(5.28) without recycle ($r = 0$). (a) For the dimensionless concentration and (b) for the dimensionless temperature. 99
5.7 Solution of system (5.26)-(5.28) with recycle relation $r = 0.5$. (a) For the dimensionless concentration and (b) for the dimensionless temperature. 100
5.8 First four eigenfunctions and their corresponding eigenvalues computed by solving Eqn (5.29). 100
5.9 Solution of system (5.18)-(5.19) with $r = 0$ using the LSD with 8 eigenfunctions. (a) x_2 field representation, (b) x_2 modes representation. . . 101
5.10 Solution of system (5.18)-(5.19) with $r = 0.5$ using the LSD with 15 eigenfunctions. (a) x_2 field representation, (b) mode representation. . . 102
5.11 (a) Shape of the first three PODs for the fields z_1 (blue lines) and z_2 (red lines). (b) Energy captured by the PODs. 103
5.12 (a) and (c) Evolution and distribution of the fields z_2 with $r = 0$ and z_1 with $r = 0.5$, respectively, computed with the POD technique. (b) and (d) Mode evolution. 104
5.13 Dynamics of the reference trajectory in terms of (a) z_2 and (b) representative modes. 105
5.14 Evolution of the modes corresponding to the sets (a) $(\mathscr{E}_a, \mathscr{L}_a, \mathscr{N}_a)$ and (b) $(\mathscr{E}_b, \mathscr{L}_b, \mathscr{N}_b)$, under the control law. 107
5.15 (a) Evolution of the field z_2 under the control law. (b) control effort. . 107

5.16 Longitudinal section of the tubular reactor showing the optimal position of the zone actuators (pipes). Blank and grey pipes are employed to stabilise the modes belonging to sets $\mathscr{M}_a$ and $\mathscr{M}_b$, respectively. 109

5.17 Evolution of the modes corresponding to the sets (a) $(\mathscr{E}_a, \mathscr{L}_a, \mathscr{N}_a)$ and (b) $(\mathscr{E}_b, \mathscr{L}_b, \mathscr{N}_b)$, under the control law. 109

5.18 (a) Evolution of the field z_2 under the control law using a finite number of actuators. (b) Control effort. 110

6.1 Representation in the phase plane of the nullclines of Eqns (6.1) and (6.2) (a) with three steady states and (b) with one steady state and state trajectory under perturbation. 115

6.2 Evolution and distribution of the field v for the Case 1. The snapshots from (a) to (f) were taken at different (increasing) sampling times. . . . 117

6.3 Evolution and distribution of the field v for the Case 2. The snapshots from (a) to (f) were taken at different (increasing) sampling times. . . . 118

6.4 Snapshots of FHN system corresponding with the travelling plane wave behaviour. 119

6.5 Snapshots of the FHN system corresponding with the spiral behaviour and the irregular forms. 119

6.6 Invariant sets (ℓ_0) for the set of parameters corresponding to (a) Case 1 in the *chemical case*, (b) Case 2 in the *chemical case* and (c) the *biological case*. 121

6.7 (a)-(c) Three eigenfunctions resulted form solving Eqn (6.11). (d)-(f) Absolute error between the eigenfunctions obtained analytically and numerically with the FEM. 122

6.8 Solutions of the FHN model using the LSD technique with (a) 8 eigenfunctions, (b) 15 eigenfunctions and (c) 20 eigenfunctions 123

6.9 First modes of the FHN system (chemical case). Blue lines correspond with the modes obtained using the FEM solution, whereas green dashed lines, red crosses and black dots correspond with ROMs using 8, 15 and 20 eigenfunctions, respectively. 124

6.10 Some PODs for the v-field employed for the construction of the ROM. . 125

6.11 Energy captured by the low dimensional set as a function of the number of PODs chosen. 126

6.12 Evolution of the modes obtained with the finite element scheme (blue lines) and using ROMs capturing the 99.6% (green dashed lines), 99.8% (red crosses) and 99.97% of the energy. (a) First and second modes, (b) third and fourth modes. 127
6.13 v-field snapshots obtained with the ROMs which capture the (a) 99.6%, (b) 99.8% and (c) 99.97% of energy. 127
6.14 Bounds on the nonlinear term $g(v)$. 130
6.15 Evolution of the FHN system exhibiting the "fingerprint" behaviour under the control logic (6.30)-(6.31), (a) before entering the control, (b)-(d) transition period, (e)-(f) after reaching the reference. 130
6.16 Evolution of some modes corresponding to the FHN system. (a) Modes representative of the oscillating front behaviour. The marks represent the reference trajectory. (b) Modes negligible in the oscillating front behaviour. 131
6.17 Evolution of the control effort. (a) In $\mathcal{L}_2$ norm. (b) In three points distributed in the spatial domain. 132
6.18 Bounds on the nonlinear term $g(v)$. 135
6.19 Evolution of some modes under the control law (6.41)-(6.42). (a) Three modes which are representative of the plane wave behavior, (b) three modes negligible in the plane wave behavior. 135
6.20 Snapshots of the FHN system under the control law (6.41)-(6.42). (a) Before entering the control law, (b)-(e) transition period, (f) system under control. 136
6.21 Control effort measured (a) using the norm as defined in Eqn (1.27) and (b) using the value of the control law in three points of the spatial domain. 136
6.22 Mode evolution of the FHN system when applying only control law $\overline{u}_a$. (a) Three modes belonging to the set $\mathbf{m}_{va}$, (b) three modes belonging to the set $\mathbf{m}_{vb}$. 137
6.23 Two snapshots of the activator (v-field) showing the effect of the unstable modes $\mathbf{m}_{vb}$. 137

A.1 Volume element $\delta\xi_1\ \delta\xi_2\ \delta\xi_3$. The arrows indicate the direction in which the component z_{ξ_1} is transported. 149

List of Tables

2.1 Comparison between the real integral and the Simpson's and FEM integrals. 36
2.2 Relationships between the continuous spatial derivatives and integrals and their discrete counterparts using the FEM matrices. 37

3.1 Comparison between the eigenvalues obtained analytically and numerically with the FEM matrices with different levels of discretisation. . . . 54
3.2 Computation time employed in the FEM, LSD and POD techniques. . 58
3.3 Computation required by the FEM, LSD and POD techniques for solving system (3.24) - (3.26) with $a = c = 0.1$ 63
3.4 Computation required by the FEM, LSD and POD techniques for solving system (3.24) - (3.26) with $a = c = 2.1$ 63

6.1 Comparison between the FEM and three ROMs capturing the 99.6%, 99.8% and 99.97% of the energy. 126
6.2 Expressions for the parameters employed in the control law. 130
6.3 Functions and parameters used in the control law. 134

Part I

Modeling, Simulation and Robust Control of Distributed Process Systems. The Theory

Chapter 1

Modelling of Distributed Processes: A Thermodynamic Approach

1.1 Introducción

La representación matemática (modelo) de un fenómeno físico-químico es el primer paso, de importancia fundamental, para su análisis, optimización y control. Existen distintos enfoques para la construcción de un modelo matemático (van den Bosch and van der Klauw, 1994; Ljung, 1999). Por una parte, en el enfoque fenomenológico (caja blanca) los modelos se derivan sobre la base de las leyes físicas obtenidas a partir de los fenómenos de transferencia de materia, energía y cantidad de movimiento (primeros principios). El inconveniente de este método es que requiere un conocimiento completo de los fenómenos físico-químicos involucrados. Por otra parte, en el enfoque experimental (caja negra) las relaciones entre las entradas y las salidas del sistema se establecen mediante fórmulas matemáticas de diferentes grados de complejidad (polinomios, exponenciales, redes neuronales,...). Dichas expresiones se eligen y se ajustan utilizando las medidas de ciertas variables cuando el sistema es sometido a unas perturbaciones específicas. La validez de este método se restringe al rango de condiciones en las que se obtuvieron dichas medidas. La tercera opción (caja gris) resulta de la combinación de los otros dos enfoques. De esta forma, aprovecha las ventajas de ambos métodos minimizando sus inconvenientes.

En este capítulo, el énfasis se pone en el enfoque fenomenológico. En ingeniería, el enfoque clásico para la derivación de modelos de caja blanca se basa en balances los macroscópicos de las cantidades fundamentales (materia, energía y cantidad de

movimiento) (Stephanopoulos, 1984; Bird et al., 2002). En este trabajo se sigue un enfoque distinto aunque equivalente. En este sentido, la primera ley de la termodinámica se utiliza para derivar las ecuaciones matemáticas del modelo (Jou et al., 1993). Sin embargo, dichas ecuaciones tienen que ser completadas con las relaciones entre los flujos de densidad (calor, masa,...) y las fuerzas que impulsan dichos flujos (gradientes de temperatura, masa,...). La segunda ley de la termodinámica nos proporciona el marco para establecer dichas relaciones. La termodinámica no sólo permite derivar la estructura matemática de forma elegante sino que además se puede utilizar como hilo conductor entre las distintas tareas de este trabajo, principalmente la derivación de modelos de orden reducido y de leyes de control robusto.

Como se menciona en Stephanopoulos (1984) el modelado lleva asociado un número de dificultades. La primera se refiere al escaso entendimiento que, en general, se tiene de los fenómenos involucrados en un determinado proceso, por ejemplo las cinéticas de una reacción. El segundo problema radica en determinar de forma precisa los parámetros del modelo. La tercera dificultad es obtener un modelo relativamente sencillo y que a su vez sea preciso. El objetivo de las siguientes secciones es obtener una estructura matemática general para la descripción de los sistemas considerados en este trabajo. Dado que la estructura debe mantenerse lo más general posible, los posible fenómenos involucrados en los procesos no se tratarán en detalle. Por otra parte, la identificación de parámetros para modelos no lineales es por sí sólo un problema bastante complejo fuera de los objetivos de este trabajo. En cualquier caso, se debe señalar que el principal objetivo de esta tesis es diseñar una lógica de control que funcione en presencia de incertidumbre paramétrica y estructural. Por lo tanto los dos primeros inconvenientes del modelado lejos de ser un problema, suponen una motivación para la utilización de controladores robustos. En lo que se refiere a la tercera dificultad se harán ciertas asunciones en la derivación de la estructura matemática para obtener modelos manejables.

1.2 Introduction

The mathematical representation (model) of the physico-chemical phenomena involved in a given process is the first step, of fundamental importance, for its analysis, optimisation and control. There are different approaches to the construction of a mathematical model (van den Bosch and van der Klauw, 1994; Ljung, 1999). On the one hand, in the phenomenological approach (white box) the models are derived on the basis of physical laws obtained from mass, energy and momentum transfer phenomena (first principles). The inconvenience of this method is that it needs a complete knowledge

of the physico-chemical phenomena involved. On the other hand, in the experimental approach (black box), the relationships among system inputs and outputs are stated by means of mathematical formulae of different degrees of complexity (polynomials, exponentials, neural networks,...). Such expressions are chosen and tuned using the measurements of given variables when the system is perturbed in a specific manner. The validity of this method is subject to the range of conditions in which such measurements were obtained. The third option (grey box) results from the combination of the other approaches. In this way, it exploits the advantages of both methods while minimising their inconveniences.

In this chapter emphasis is placed on the grey box approach. In engineering, the classical approach to the derivation of a grey box model is through macroscopic balances of fundamental quantities (mass, energy and momentum) (Stephanopoulos, 1984; Bird et al., 2002) where some expressions, like chemical reactions, are obtained through data fitting. In this work a different, although equivalent, approach is followed. In this regard, the first law of thermodynamics is used to derive the mathematical equations of the model (Jou et al., 1993). Nevertheless, these equations must be completed with the relationships between the density fluxes (heat, mass,...) and thermodynamic forces impulsing such fluxes (gradients of temperature, mass,...). The second law of thermodynamics provide us the framework to establish such relationships. Thermodynamics allows us not only to derive the mathematical structure of a model in an elegant way but it can also be employed as the connecting thread between the different tasks of this work, mainly the derivation of reduced order models and robust control laws.

As pointed out by Stephanopoulos (1984) modelling is associated with a number of difficulties. The first one is the poor understanding of some phenomena involved in a given process, for instance the kinetics of a given reaction. The second problem is to accurately determine the value of the model parameters. The third difficulty is to obtain a sufficiently accurate and tractable model. The objective of the following sections is to obtain a general mathematical structure for describing the systems considered in this work. Since the structure must remain as general as possible in the first section, the involved phenomena will not be dealt with in detail. On the other hand parameter identification for nonlinear models is indeed a quite complex problem which is out of the scope of this work. However, it should be stressed that the main objective of this thesis is to design a control logic which works in the presence of structural and parametric uncertainty. Thus, the first two inconveniences are a motivation to use robust controllers. In order to deal with the third difficulty some assumptions will be made in the derivation of the mathematical structure. This will help us not only with

the size and complexity of the model but with the clarity in its derivation.

This chapter is structured as follows: In the first section the mathematical structure of the model is obtained via the first law of thermodynamics. After this, the second law will be employed to derive the relationships between the density fluxes and the thermodynamic forces. These relationships, together with the boundary conditions, will complete the model. Finally, and using previous concepts, a description (including some useful properties) of the kind of systems considered in this work (*dissipative systems*) is presented. In this context, a new mathematical structure is derived by employing the Kirchhoff transformation so as to deal with non linear diffusive terms. This transformation will be also employed in subsequent chapters to derive reduced order models and to construct a robust control law.

1.3 From the First Law to the Model Structure

Consider a given process $\mathscr{P}$ occurring in a volume element $\mathscr{V} \subset \mathbb{R}^m$ $(m = 1, 2, 3)$ with boundary $\mathscr{B}$ and over the semi-open time interval $\mathscr{T} \subset [0, \infty)$. The first law of thermodynamics states that the energy is neither created nor destroyed, it is only transformed. The energy net flow in a given system must be, then, equal to the energy accumulation in the system, that is:

$$\frac{dE}{dt} = \frac{dQ}{dt} + \frac{dW}{dt}, \tag{1.1}$$

where $E(t) \in \mathcal{H}^1(0, \infty)$ is the total energy, $Q(t) \in \mathcal{H}^1(0, \infty)$ represents the heat exchanged with the surroundings and $W(t) \in \mathcal{H}^1(0, \infty)$ the work applied to the system. E can be split into two contributions: firstly, the internal energy $U(t) \in \mathcal{H}^1(0, \infty)$ and, secondly the kinetic energy $K(t) \in \mathcal{H}^1(0, \infty)$. In terms of the mass density $\rho(\boldsymbol{\xi}, t) \in \mathcal{H}^1(0, \infty; \mathcal{H}^2(\mathscr{V}))$, the specific internal energy $u_s(\boldsymbol{\xi}, t) \in \mathcal{H}^1(0, \infty; \mathcal{H}^2(\mathscr{V}))$ and the fluid velocity $\overrightarrow{\mathbf{v}}(\boldsymbol{\xi}, t) \in \mathcal{H}^1(0, \infty; \mathcal{H}^2(\mathscr{V}))$, U and K are given by:

$$U = \int_{\mathscr{V}} \rho u_s d\boldsymbol{\xi}; \qquad K = \frac{1}{2} \int_{\mathscr{V}} \rho v^2 d\boldsymbol{\xi}, \tag{1.2}$$

with $\boldsymbol{\xi} \in \mathbb{R}^m$ being the spatial coordinates. Applying the Reynolds transport theorem (See the Appendix A.1 for details) to Eqn (1.1) one is led to:

$$\frac{dU}{dt} = \int_{\mathscr{V}} \frac{\partial(\rho u_s)}{\partial t} d\boldsymbol{\xi} + \int_{\mathscr{B}} \rho u_s \overrightarrow{\mathbf{v}} \cdot \overrightarrow{\mathbf{n}} d\boldsymbol{\xi}; \quad \frac{dK}{dt} = \frac{1}{2} \int_{\mathscr{V}} \frac{\partial(\rho v^2)}{\partial t} d\boldsymbol{\xi} + \frac{1}{2} \int_{\mathscr{B}} \rho v^2 \overrightarrow{\mathbf{v}} \cdot \overrightarrow{\mathbf{n}} d\boldsymbol{\xi}, \tag{1.3}$$

where $\overrightarrow{\mathbf{n}} \in \mathbb{R}^m$ is the normal unit vector pointing outwards the boundary $\mathscr{B}$. Q is related to the heat flux $\overrightarrow{\mathbf{q}} \in \mathcal{H}^1(\mathscr{V})$ so that, assuming that the contribution of the

radiation terms can be neglected:

$$\frac{dQ}{dt} = -\int_{\mathscr{B}} \overrightarrow{\mathbf{q}} \cdot \overrightarrow{\mathbf{n}} d\boldsymbol{\xi} = -\int_{\mathscr{V}} \overrightarrow{\boldsymbol{\nabla}} \cdot \overrightarrow{\mathbf{q}} d\boldsymbol{\xi}, \tag{1.4}$$

where use was made of Gauss's theorem (see Appendix A.1). For the sake of clarity neither charged particles nor chemical reactions will be considered in this derivation although they will be included later on. Under these considerations the time derivative of the work applied to the system is given by (Jou et al., 1993):

$$\frac{dW}{dt} = -\int_{\mathscr{B}} (\boldsymbol{\Pi} \cdot \overrightarrow{\mathbf{n}}) \cdot \overrightarrow{\mathbf{v}} d\boldsymbol{\xi} + \int_{\mathscr{V}} \rho \overrightarrow{\mathbf{f}} \cdot \overrightarrow{\mathbf{v}} d\boldsymbol{\xi} = -\int_{\mathscr{V}} \overrightarrow{\boldsymbol{\nabla}} \cdot (\boldsymbol{\Pi} \cdot \overrightarrow{\mathbf{v}}) d\boldsymbol{\xi} + \int_{\mathscr{V}} \rho \overrightarrow{\mathbf{f}} \cdot \overrightarrow{\mathbf{v}} d\boldsymbol{\xi}. \tag{1.5}$$

The terms on the right hand side take into account the contact forces, with $\boldsymbol{\Pi} \in \mathbb{R}^{m \times m}$ being the *stress tensor*, and the body forces $\overrightarrow{\mathbf{f}} \in \mathbb{R}^m$. The stress tensor can be divided into two contributions (Bird et al., 2002), one associated with the thermodynamic pressure P and the other associated with the viscous forces, this is, $\Pi_{ij} = P\delta_{ij} + \tau_{ij}$ where δ_{ij} is the Kronecker delta, P the pressure and τ_{ij} is the viscous stress. $\overrightarrow{\mathbf{f}}$ collects the external forces acting over the system. For instance, if only the gravity is taken into account, then $\overrightarrow{\mathbf{f}} = \overrightarrow{\mathbf{g}}$. When the above expressions are valid for any volume $\mathscr{V}$, the integrands are continuous functions, thus by employing equations (1.3)-(1.5), Eqn (1.1) can be rewritten as follows:

$$\rho \left[\frac{\partial u_s}{\partial t} + \overrightarrow{\mathbf{v}} \cdot \overrightarrow{\boldsymbol{\nabla}} u_s + \overrightarrow{\mathbf{v}} \cdot \left(\frac{\partial \overrightarrow{\mathbf{v}}}{\partial t} + \overrightarrow{\mathbf{v}} \cdot (\overrightarrow{\boldsymbol{\nabla}} \overrightarrow{\mathbf{v}}) \right) \right] + \left(u_s + \frac{1}{2} v^2 \right) \left(\frac{\partial \rho}{\partial t} + \overrightarrow{\mathbf{v}} \cdot \overrightarrow{\boldsymbol{\nabla}} \rho + \rho \overrightarrow{\boldsymbol{\nabla}} \cdot \overrightarrow{\mathbf{v}} \right) =$$

$$-\overrightarrow{\boldsymbol{\nabla}} \cdot \overrightarrow{\mathbf{q}} - \boldsymbol{\Pi}^T : \overrightarrow{\boldsymbol{\nabla}} \overrightarrow{\mathbf{v}} - \overrightarrow{\mathbf{v}} \cdot (\overrightarrow{\boldsymbol{\nabla}} \cdot \boldsymbol{\Pi}) + \rho \overrightarrow{\mathbf{f}} \cdot \overrightarrow{\mathbf{v}}. \tag{1.6}$$

Assuming that all torques are moments of forces, the Cauchy's second law of motion (Truesdell, 1984) asserts that the pressure tensor is symmetric ($\boldsymbol{\Pi} = \boldsymbol{\Pi}^T$). In the remaining of the work, $\boldsymbol{\Pi}$ will be considered symmetric. The last step to obtain the balance equations is to use the Galileo principle. According to it, relation (1.6) must be invariant with respect to the transformation $\overrightarrow{\mathbf{v}} \rightarrow \overrightarrow{\mathbf{v}} + \overrightarrow{\mathbf{v}}_0$, with $\overrightarrow{\mathbf{v}}_0$ being time and spatially independent (Jou et al., 1993). Therefore, by applying such a transformation to (1.6) and subtracting (1.6) from the result, one is led to:

$$\frac{1}{2} v_0^2 \left(\frac{\partial \rho}{\partial t} + \overrightarrow{\mathbf{v}} \cdot \overrightarrow{\boldsymbol{\nabla}} \rho + \rho \overrightarrow{\boldsymbol{\nabla}} \cdot \overrightarrow{\mathbf{v}} \right) + \overrightarrow{\mathbf{v}}_0 \cdot \left[\left(\frac{\partial \rho}{\partial t} + \overrightarrow{\mathbf{v}} \cdot \overrightarrow{\boldsymbol{\nabla}} \rho + \rho \overrightarrow{\boldsymbol{\nabla}} \cdot \overrightarrow{\mathbf{v}} \right) \overrightarrow{\mathbf{v}} + \right.$$

$$\left. \rho \left(\frac{\partial \overrightarrow{\mathbf{v}}}{\partial t} + \overrightarrow{\mathbf{v}} \cdot (\overrightarrow{\boldsymbol{\nabla}} \overrightarrow{\mathbf{v}}) \right) + \overrightarrow{\boldsymbol{\nabla}} \cdot \boldsymbol{\Pi} - \rho \overrightarrow{\mathbf{f}} \right] = 0.$$

Choosing $\overrightarrow{\mathbf{v}}_0 \neq \mathbf{0}$, the following equations must be satisfied:

$$\frac{\partial \rho}{\partial t} = -\overrightarrow{\mathbf{v}} \cdot \overrightarrow{\boldsymbol{\nabla}} \rho - \rho \overrightarrow{\boldsymbol{\nabla}} \cdot \overrightarrow{\mathbf{v}} = -\overrightarrow{\boldsymbol{\nabla}} \cdot (\rho \overrightarrow{\mathbf{v}}), \tag{1.7}$$

$$\rho\frac{\partial\overrightarrow{\mathbf{v}}}{\partial t}=-\rho\overrightarrow{\mathbf{v}}\cdot(\overrightarrow{\boldsymbol{\nabla}}\overrightarrow{\mathbf{v}})-\overrightarrow{\boldsymbol{\nabla}}\cdot\boldsymbol{\Pi}+\rho\overrightarrow{\mathbf{f}}\quad\Longleftrightarrow\quad\frac{\partial\rho\overrightarrow{\mathbf{v}}}{\partial t}=-\overrightarrow{\boldsymbol{\nabla}}\cdot(\boldsymbol{\Pi}+\rho\overrightarrow{\mathbf{v}}\overrightarrow{\mathbf{v}})+\rho\overrightarrow{\mathbf{f}},\tag{1.8}$$

which are, respectively, the balance equations for mass and momentum. Substituting (1.7) and (1.8) into (1.6), the balance equation for energy is obtained:

$$\rho\frac{\partial u_s}{\partial t}=-\rho\overrightarrow{\mathbf{v}}\cdot\overrightarrow{\boldsymbol{\nabla}}u_s-\overrightarrow{\boldsymbol{\nabla}}\cdot\overrightarrow{\mathbf{q}}-\boldsymbol{\Pi}\colon\overrightarrow{\boldsymbol{\nabla}}\overrightarrow{\mathbf{v}}\quad\Longleftrightarrow\quad\frac{\partial\rho u_s}{\partial t}=-\overrightarrow{\boldsymbol{\nabla}}\cdot(\overrightarrow{\mathbf{q}}+\rho u_s\overrightarrow{\mathbf{v}})-\boldsymbol{\Pi}\colon\overrightarrow{\boldsymbol{\nabla}}\overrightarrow{\mathbf{v}}.\tag{1.9}$$

The total energy (kinetic and internal) balance equation is derived by multiplying Eqn (1.8) by $\overrightarrow{\mathbf{v}}$ and adding the result to (1.9).

So far the balance equations for mass, momentum and energy have been derived from the first law of thermodynamics when absence of charged particles, reactions, radiation and intrinsic rotational motions and external force couples are considered. It must be pointed out that when these assumptions do not follow, the same procedure can be applied. In this regard, for example, if one considers a mixture of n components where m chemical reactions take place, the balance equations will share the structure of (1.7), (1.8) and (1.9). Such equations may be found for instance in Truesdell (1984):

$$\frac{\partial\rho_i}{\partial t}=-\overrightarrow{\boldsymbol{\nabla}}\cdot(\rho_i\overrightarrow{\mathbf{v}}_i)+\rho r_i;\quad i=1,...,n\tag{1.10}$$

$$\frac{\partial(\rho_i\overrightarrow{\mathbf{v}}_i)}{\partial t}=-\overrightarrow{\boldsymbol{\nabla}}\cdot(\boldsymbol{\Pi}_i+\rho_i\overrightarrow{\mathbf{v}}_i\overrightarrow{\mathbf{v}}_i)+\rho_i\overrightarrow{\mathbf{f}}_i+\rho\overrightarrow{\mathbf{m}}_i;\quad i=1,...,n\tag{1.11}$$

$$\frac{\partial(\rho_i u_{si})}{\partial t}=-\overrightarrow{\boldsymbol{\nabla}}\cdot(\overrightarrow{\mathbf{q}}_i+\rho_i u_{si}\overrightarrow{\mathbf{v}}_i)-\boldsymbol{\Pi}_i\colon\overrightarrow{\boldsymbol{\nabla}}\overrightarrow{\mathbf{v}}_i+\rho h_i;\quad i=1,...,n\tag{1.12}$$

where r_i, $\overrightarrow{\mathbf{m}}_i$ and h_i are the rates of growth of mass, momentum and energy, respectively. The total density ρ is computed as $\rho=\sum_{i=1}^{n}\rho_i$. Defining the mass fraction c_i, the diffusion velocity $\overrightarrow{\mathbf{w}}_i$ and the diffusion flux $\overrightarrow{\mathbf{j}}_i$ of the i^{th} component as:

$$c_i=\frac{\rho_i}{\rho};\quad\overrightarrow{\mathbf{w}}_i=\overrightarrow{\mathbf{v}}_i-\overrightarrow{\mathbf{v}};\quad\overrightarrow{\mathbf{j}}_i=\rho_i\overrightarrow{\mathbf{w}}_i,$$

Eqn (1.10) may be rewritten as:

$$\frac{\partial(\rho c_i)}{\partial t}=-\overrightarrow{\boldsymbol{\nabla}}\cdot(\overrightarrow{\mathbf{j}}_i+\rho c_i\overrightarrow{\mathbf{v}})+\rho r_i.\tag{1.13}$$

Note that classical approaches to the derivation of the balance equations start with a macroscopic balance of the fundamental quantities (mass, energy, momentum) in a volume element. Finally, this element is reduced to an infinitesimal volume and the desired relations are obtained. In Appendix A.2 the balance equations are obtained as in the classical approach and they are shown to be equivalent to those derived in this section.

On the other hand, other terms can be included into the formulation. For instance, if the system is composed by a mixture of n charged components subject to an electromagnetic field (W_{em}), the expression for the work applied to the system (1.5) should be rewritten so as to include its contribution, which is of the form:

$$\frac{dW_{em}}{dt} = \int_{\mathscr{V}} \sum_{i=1}^{n} \rho_i e_i (\mathbf{E} + \overrightarrow{\mathbf{v}}_i \times \mathbf{B}) \cdot \overrightarrow{\mathbf{v}}_i d\boldsymbol{\xi},$$

where e_i is the electric charge of the i^{th} component, $\mathbf{E}$ corresponds to the electrical field and $\mathbf{B}$ indicates the magnetic induction. A complete derivation of the balance equations including this term can be found in Astarita (1989) or Jou et al. (1993).

1.4 The Constitutive Equations

In order to solve the equations derived in the previous section, an explicit relation between the density fluxes ($\overrightarrow{\mathbf{q}}$, $\overrightarrow{\mathbf{j}}$, ...) and the intensive variables is needed (*constitutive equations*), apart from the boundary conditions, which will be defined in section 1.5. This is the main concern of this section which starts with the second law of thermodynamics. Then, the well-known Gibbs equation will be employed so as to obtain the structure of the entropy production term and to define the variables known as *intensive variables*. With these preliminaries the constitutive equations will be presented and a first order Taylor series approximation will be derived. Finally, the second law will be employed to obtain the constraints on the coefficients of the linear version of the constitutive equation.

The second law states that there exists a state function $S : \mathbb{R}^{ns} \rightarrow \mathbb{R}^{+}$, with ns being the number of states, called *entropy* which is an extensive magnitude and its variation (δS) can be split into two contributions, one corresponding to the internal changes on the system ($\delta_i S$) and the other to the exchanges with the surroundings ($\delta_e S$), so that:

$$\delta S = \delta_i S + \delta_e S; \qquad \text{where} \quad \delta_i S \geq 0. \tag{1.14}$$

Condition $\delta_i S = 0$ holds at equilibrium or when the changes on the system are reversible, otherwise $\delta_i S > 0$. According to relation (1.14), the rate of variation of S is given by:

$$\frac{dS}{dt} = \frac{d_i S}{dt} + \frac{d_e S}{dt}; \qquad \text{where} \quad \frac{d_i S}{dt} \geq 0. \tag{1.15}$$

Similarly to Eqn (1.2), where the internal energy U was expressed in terms of the local specific internal energy u_s, the entropy S can be related to the local specific entropy $s(\boldsymbol{\xi}, t) \in \mathcal{H}^1(0, \infty; \mathcal{H}^2(\mathscr{V}))$. On the other hand, $d_i S/dt$ and $d_e S/dt$ can be expressed

in terms of a local rate production f_s and a local entropy flux $\overrightarrow{\mathbf{j}}_s \in \mathbb{R}^m$, respectively. Thus, by following the methodology of section 1.3 an expression of the form (1.12) or (1.13) can be obtained for s (Jou et al., 1993):

$$\rho\frac{\partial s}{\partial t} = -\rho\overrightarrow{\mathbf{v}}\cdot\overrightarrow{\boldsymbol{\nabla}}s - \overrightarrow{\boldsymbol{\nabla}}\cdot\overrightarrow{\mathbf{j}}_s + f_s, \quad \text{with} \quad f_s \geq 0. \tag{1.16}$$

From Eqn (1.16) one can conclude that the local rate of entropy production, which is never negative independently of the position or the time, is the cause of the irreversibility of a given process: *a given system out of equilibrium will evolve to the equilibrium through irreversible processes producing entropy.* Furthermore, this term will be shown to be a sum of the product of the thermodynamic fluxes J and forces X. In other words, the relationships between fluxes and forces will guide the evolution of the system. The entropy production will be also employed later so as to find out the formal relation between J and X or, to be more specific, to establish the constraints on the coefficients relating the fluxes and the forces.

Classic irreversible thermodynamics is based on the hypothesis of local equilibrium which states that *in a physical system the relations between thermal and mechanical properties, at a given spatial point and time instant, are the same as for the system at equilibrium.* With this in mind, the local specific internal energy u_s and entropy s are homogeneous first-order functions of the extensive variables V, c_i (Callen, 1985). This is $u_s = u_s(s, V, c_1, ..., c_n)$ and $s = s(u_s, V, c_1, ..., c_n)$, with $V = \rho^{-1}$ being the specific volume. In differential form, du is expressed as:

$$du_s = \left(\frac{\partial u_s}{\partial s}\right)_{V,c_i} ds + \left(\frac{\partial u_s}{\partial V}\right)_{u_s,c_i} dV + \sum_{k=1}^{n}\left(\frac{\partial u_s}{\partial c_k}\right)_{s,V,c_i} dc_k; \quad \text{with} \quad k \neq i. \tag{1.17}$$

which is known as the Euler relation. The conventional notation for the above partial derivatives introduces new variables known as *intensive variables*:

$$\left(\frac{\partial u_s}{\partial s}\right)_{V,c_i} = T; \quad \left(\frac{\partial u_s}{\partial V}\right)_{u_s,c_i} = -P; \quad \left(\frac{\partial u_s}{\partial c_k}\right)_{s,V,c_i} = \mu_{si}, \tag{1.18}$$

where T is the temperature, P the pressure and μ_{si} the chemical potential of the i^{th} component[1]. Following the same procedure for the entropy, one is led to:

$$ds = \frac{1}{T}du_s + \frac{P}{T}dV - \sum_{k=1}^{n}\frac{\mu_k}{T}dc_k; \quad \text{with} \quad k \neq i. \tag{1.19}$$

[1]When electric fields or displacements forces are considered, new elements must be included in Eqn (1.17). The form of such equation with the new terms can be seen, for instance, in Demirel (2002). However, for the sake of clarity and since we will not work with this magnitudes, they will be omitted.

Eqn (1.19), known as the Gibbs equation, is the starting point for the derivation of the specific form of the entropy production f_s. Before proceeding with the derivation, a useful version of Eqn (1.7) is expressed in terms of the specific volume V:

$$\rho\frac{\partial V}{\partial t} = -\rho\overrightarrow{\mathbf{v}}\cdot\overrightarrow{\overrightarrow{\boldsymbol{\nabla}}}V + \overrightarrow{\overrightarrow{\boldsymbol{\nabla}}}\cdot\overrightarrow{\mathbf{v}}, \tag{1.20}$$

and the Gibbs equation is formulated in terms of the substantial derivative (Jou et al., 1993):

$$\frac{Ds}{Dt} = \frac{1}{T}\frac{Du_s}{Dt} + \frac{P}{T}\frac{DV}{Dt} - \sum_{k=1}^{n}\frac{\mu_k}{T}\frac{Dc_k}{Dt}; \quad \text{with} \quad k \neq i. \tag{1.21}$$

Multiplying Eqn (1.21) by ρ and using relations (1.9), (1.13) and (1.20), one can get:

$$\rho\frac{Ds}{Dt} = -\frac{1}{T}\left(\overrightarrow{\overrightarrow{\boldsymbol{\nabla}}}\cdot\overrightarrow{\mathbf{q}} - \boldsymbol{\Pi}\colon\overrightarrow{\overrightarrow{\boldsymbol{\nabla}}}\overrightarrow{\mathbf{v}}\right) + \frac{P}{T}\overrightarrow{\overrightarrow{\boldsymbol{\nabla}}}\cdot\overrightarrow{\mathbf{v}} - \sum_{k=1}^{n}\frac{\mu_k}{T}\left(-\overrightarrow{\overrightarrow{\boldsymbol{\nabla}}}\cdot\overrightarrow{\mathbf{j}}_k + r_k\right). \tag{1.22}$$

The reaction terms can be expressed in terms of the stoichiometric coefficients of the component k in the i^{th} reaction (ν_{ki}) and the advancement of the i^{th} reaction ($\dot{\zeta}_i$):

$$r_k = \sum_{i=1}^{m}\nu_{ki}\dot{\zeta}_i; \qquad k = 1, ..., n.$$

If together with r_k, the expression of the affinity of the i^{th} reaction $A_{fi} = -\sum_{k=1}^{n}\nu_{ki}\mu_k$ with $i = 1, ..., m$, is substituted into (1.22) the following relation results:

$$\rho\frac{Ds}{Dt} = -\overrightarrow{\overrightarrow{\boldsymbol{\nabla}}}\cdot\left[\frac{1}{T}\left(\overrightarrow{\mathbf{q}} - \sum_{k=1}^{n}\mu_k\overrightarrow{\mathbf{j}}_k\right)\right] + \overrightarrow{\mathbf{q}}\cdot\overrightarrow{\overrightarrow{\boldsymbol{\nabla}}}\left(\frac{1}{T}\right) - \sum_{k=1}^{n}\overrightarrow{\mathbf{j}}_k\cdot\overrightarrow{\overrightarrow{\boldsymbol{\nabla}}}\left(\frac{\mu_k}{T}\right) -$$

$$\frac{1}{T}\left(\boldsymbol{\Pi} - P\mathbf{I}\right)\colon\overrightarrow{\overrightarrow{\boldsymbol{\nabla}}}\overrightarrow{\mathbf{v}} + \frac{\rho}{T}\sum_{i=1}^{m}A_{fi}\dot{\zeta}_i.$$

Finally, comparing this result with (1.16) the expressions for the entropy flux and production become, respectively:

$$\overrightarrow{\mathbf{j}}_s = \frac{1}{T}\left(\overrightarrow{\mathbf{q}} - \sum_{k=1}^{n}\mu_k\overrightarrow{\mathbf{j}}_k\right),$$

$$f_s = \overrightarrow{\mathbf{q}}\cdot\overrightarrow{\overrightarrow{\boldsymbol{\nabla}}}\left(\frac{1}{T}\right) - \sum_{k=1}^{n}\overrightarrow{\mathbf{j}}_k\cdot\overrightarrow{\overrightarrow{\boldsymbol{\nabla}}}\left(\frac{\mu_k}{T}\right) - \frac{1}{T}\left(\boldsymbol{\Pi} - P\mathbf{I}\right)\colon\overrightarrow{\overrightarrow{\boldsymbol{\nabla}}}\overrightarrow{\mathbf{v}} + \frac{\rho}{T}\sum_{i=1}^{m}A_{fi}\dot{\zeta}_i \geq 0. \tag{1.23}$$

The particular expressions for $\overrightarrow{\mathbf{j}}_s$ and f_s when considering n charged particles and an electromagnetic field $\mathbf{B}$ can be found in Jou et al. (1993). The first and second terms of Eqn (1.23) are the contributions of the energy and mass fluxes to the entropy

production, the third term collects the effects of the mechanical dissipation while the last term refers to the chemical reactions. Note that f_s is, in fact, the sum of products of thermodynamic fluxes J such as $\overrightarrow{\mathbf{q}}$ or $\overrightarrow{\mathbf{j}}_k$ and thermodynamic forces X such as $\overrightarrow{\boldsymbol{\nabla}}(1/T)$ or $\overrightarrow{\boldsymbol{\nabla}}(\mu_k/T)$. Since by the second law one has that $f_s > 0$, the following relation must hold:

$$f_s = \sum_k J_k X_k \geq 0. \tag{1.24}$$

The phenomenological or constitutive equations relate the thermodynamic fluxes with the thermodynamic forces and with the state variables: $J_i = J_i(X_1, X_2, ..., T, p, c_1, ..., c_n)$. In general the constitutive equations are complicated nonlinear functions (Demirel, 2002). A typical procedure to obtain more tractable expressions is to expand J_i in Taylor series around an equilibrium state J_i^{eq}, X_i^{eq}:

$$J_i = J_i^{eq} + \sum_k \left(\frac{\partial J_i}{\partial X_k}\right)_{eq} (X_k - X_k^{eq}) + \frac{1}{2!}\sum_k \sum_j \left(\frac{\partial^2 J_i}{\partial X_k \partial X_j}\right)_{eq} (X_k - X_k^{eq})(X_j - X_j^{eq}) + ...$$

Considering only the first order terms and taking into account that at equilibrium $J_i^{eq} = X_i^{eq} = 0$, the following bilinear expression is obtained:

$$J_i = \sum_k L_{ik} X_k; \qquad \text{with} \quad L_{ik} = \left(\frac{\partial J_i}{\partial X_k}\right)_{eq}. \tag{1.25}$$

The scalars L_{ik} are known as phenomenological coefficients. As pointed out in Jou et al. (1993), statistical mechanics has shown that linear relations of the form (1.25) are valid for a wide class of systems, in particular for those considered in this work.

It must be pointed out that, in isotropic systems and as far as we consider linear relations, some coupling between fluxes and forces are forbidden. To be precise, Hirschfelder et al. (1954) stated that *those terms which correspond to a coupling of tensors whose orders differ by an odd number are forbidden.* This statement is usually referred to as the *Curie symmetry principle* (Prigogine, 1967).

Example 1.1 (The Fourier and Fick laws) *According to (1.25), and taking into account the Curie symmetry principle, the heat and mass fluxes ($\overrightarrow{\mathbf{q}}$, $\overrightarrow{\mathbf{j}}_i$) can be expressed, in an isotropic system, as:*

$$\overrightarrow{\mathbf{q}} = L_{aa} \overrightarrow{\boldsymbol{\nabla}} \left(\frac{1}{T}\right) - \sum_{j=1}^{n} L_{aj} \overrightarrow{\boldsymbol{\nabla}} \left(\frac{\mu_j}{T}\right),$$

$$\overrightarrow{\mathbf{j}}_k = L_{ka} \overrightarrow{\boldsymbol{\nabla}} \left(\frac{1}{T}\right) - \sum_{j=1}^{n} L_{kj} \overrightarrow{\boldsymbol{\nabla}} \left(\frac{\mu_j}{T}\right), \quad k = 1, 2, ..., n.$$

The phenomenological coefficients L_{aa} and L_{kj} are related to the thermal conductivity κ and diffusion D_{kj} coefficients, respectively, by (Jou et al., 1993):

$$L_{aa} = \kappa T^2; \quad D_{kj} = \frac{1}{T}\sum_{i=1}^{n} L_{ki}\left(\frac{\partial \mu_{si}}{\partial c_j}\right)_{T,p,c_{j'}}.$$

The Fourier's law is then obtained by introducing the expression of L_{aa} and neglecting the coupling terms in the heat flux, so one is led to:

$$\overrightarrow{\mathbf{q}} = -\kappa \overrightarrow{\boldsymbol{\nabla}} T.$$

In the same way, the Fick's law is obtained by neglecting the coupling terms, by assuming constant temperature and pressure and introducing the expression of L_{kj} on the mass flux, so that:

$$\overrightarrow{\mathbf{j}}_k = -\sum_{i=1}^{n} D_{ki} \overrightarrow{\boldsymbol{\nabla}} c_i.$$

□

Before concluding this section, some remarks will help completing the description of the system. Introducing the first order approximation of the constitutive equation (1.25) into the general expression for the entropy production (1.24), which is never negative, it follows that:

$$f_s = \sum_{k,j} L_{kj} X_j X_k = [X_1, ..., X_n] \begin{bmatrix} L_{11} & \dots & L_{1n} \\ \vdots & \ddots & \vdots \\ L_{n1} & \dots & L_{nn} \end{bmatrix} \begin{bmatrix} X_1 \\ \vdots \\ X_n \end{bmatrix} \geq 0.$$

According to standard algebraic results the former inequality implies that the coefficient matrix must be semi-positive definite. Thus the phenomenological coefficients must satisfy:

$$L_{kk} \geq 0; \qquad (L_{jk} + L_{kj})^2 \leq 4 L_{kk} L_{jj}.$$

Furthermore, Onsager (1931a,b) proposed other useful relations to be obeyed by the coefficients:

$$L_{kj} = L_{jk}. \tag{1.26}$$

This equation is known as Onsager reciprocal relation and is specially useful in the study of coupling phenomena like the contribution of gradients of mass to the energy density flux (*Dufour effect*) or the relationship between gradients of energy and the mass density flux (*Soret effect*). The Onsager relations have a direct physical interpretation: *if a given thermodynamic force of an irreversible process k affects the irreversible process j then the thermodynamic force of the process j will affect the process k.*

1.5 Description and Properties of Dissipative Systems

As in section 1.3, consider a given process $\mathscr{P}$ occurring in a volume element $\mathscr{V} \subset \mathbb{R}^m$ ($m = 1, 2, 3$) with boundary $\mathscr{B}$ and over the semi-open time interval $\mathscr{T} \subset [0, \infty)$. Functions defined on $\mathscr{V}$ are assumed to be equipped with inner product and $\mathcal{L}_2$ norm of the form:

$$\langle g, h \rangle_{\mathscr{V}} = \int_{\mathscr{V}} g^T h \, d\boldsymbol{\xi}; \qquad \|g\|_{\mathscr{V}} = \langle g, g \rangle_{\mathscr{V}}^{1/2}. \tag{1.27}$$

Let $\mathscr{Z} = \{[z_i]_{i=1}^n\}$ be the set of states and let us collect all the states of the process into the vector function $\mathbf{z} = [z_1, z_2, ..., z_n]^T \in \mathscr{Z}$ known as the field[2]. Equations (1.11)-(1.13) can be rewritten into a more compact form:

$$\frac{\partial \mathbf{z}}{\partial t} + \overrightarrow{\boldsymbol{\nabla}} \cdot \overrightarrow{\mathbf{j}}_f(\mathbf{z}) = \mathbf{f}(\mathbf{z}) + \mathbf{u}(\mathbf{z}), \tag{1.28}$$

where $\mathbf{f}(\mathbf{z}) : \mathscr{Z} \to \mathbb{R}^n$ includes the production terms and the forces that actuate over the system like pressure or viscous forces, $\mathbf{u}(\mathbf{z}) : \mathscr{Z} \to \mathbb{R}^n$ stands for the manipulated variables (control inputs). Typical examples of control inputs include the input/output valve opening to regulate the fluid flow in a given reactor or the actions on the steering wheel, break or accelerator pedal to drive a car. The vector function $\overrightarrow{\mathbf{j}}_f(\mathbf{z}) : \mathscr{Z} \to \mathbb{R}^{n \times m}$ collects the microscopic fluxes through the domain. By comparing (1.28) with (1.12)-(1.13), one can see that $\overrightarrow{\mathbf{j}}_f(\mathbf{z})$ is composed by convective and diffusive parts:

$$\overrightarrow{\mathbf{j}}_f(\mathbf{z}) = \overrightarrow{\mathbf{v}}\mathbf{z} - \mathbf{L}(\mathbf{A})\overrightarrow{\mathbf{x}}(\mathbf{A}). \tag{1.29}$$

$\mathbf{L}(\mathbf{A}) \in \mathbb{R}^{n \times n}$ is the positive definite matrix of phenomenological coefficients and $\overrightarrow{\mathbf{x}}(\mathbf{A})$ collects the thermodynamic forces impulsing the different fluxes. The set of the intensive parameters $\mathbf{A} = [A_1, ..., A_n]^T \in \mathbb{R}^n$ will be denoted by $\mathscr{A}$. As shown in the previous section, both $\mathbf{L}(\mathbf{A})$ and $\overrightarrow{\mathbf{x}}(\mathbf{A})$ are functions of the intensive parameters. In fact, the forces are in general gradients of the intensive variables ($\overrightarrow{\mathbf{x}}(\mathbf{A}) = \overrightarrow{\boldsymbol{\nabla}}\mathbf{A}$). Furthermore a relationship between the extensive $\mathbf{z}$ and the intensive $\mathbf{A}$ parameters was obtained by means of the entropy function -see Eqn (1.18)-. In this section, the concept of intensive parameters will be employed in a broader sense than in the previous section. In this way, use is made of a general convex[3] function $a(\mathbf{z}) : \mathscr{Z} \to \mathbb{R}$ to establish the

[2]For the sake of clarity in the notation, all the components of $\mathbf{z}$ are considered as scalars. Note that this implies that the components of $\overrightarrow{\mathbf{j}}_f(\mathbf{z})$ and $\mathbf{u}(\mathbf{z})$ are vectors and scalars respectively. However, the same arguments apply when a component of $\mathbf{z}$ is a vector (for instance the momentum).

[3]The convention employed in this work for the definition of *convex* is: A given function is convex if its tangents remain below the function.

connections between $\mathbf{z}$ and $\mathbf{A}$. The set of intensive variables is defined, now, as the derivative of $a(\mathbf{z})$ with respect to the field:

$$\mathbf{A} = \frac{\partial a(\mathbf{z})}{\partial \mathbf{z}}.$$

Note that when this function equals the negative of the entropy (i.e., $a(\mathbf{z}) = -s(\mathbf{z})$) the intensive variables are the ones included in the Gibbs equation (1.19), so that:

$$\mathbf{A} = \left[-\frac{1}{T}, -\frac{P}{T}, \frac{\mu_1}{T}, ..., \frac{\mu_n}{T}\right]^T.$$

For the sake of clarity, from now on, the arguments of the functions that were already defined will be omitted. Alternatively to the "thermodynamic" selection of the convex function, other criteria of interest in control, might be employed like, for instance, the use of a quadratic function $a = \mathbf{z}^T\mathbf{z}$. In this sense, for convenience, a new convex function $b(\mathbf{z}, \mathbf{z}^*) : \mathscr{Z} \times \mathscr{Z} \to \mathbb{R}^+ \cup \{0\}$ will be constructed as the difference between the original function a and its supporting hyperplane (*tangent*) at a given reference state ($\mathbf{z}^*$):

$$b = a - [a^* + \mathbf{m}^T(\mathbf{z} - \mathbf{z}^*)]; \qquad \text{where} \quad \mathbf{m}^T = \left(\frac{\partial a}{\partial \mathbf{z}}\right)_{\mathbf{z}=\mathbf{z}^*} = (\mathbf{A}^*)^T. \tag{1.30}$$

In the words of Alonso and Ydstie (2001) this term *is related to the minimum amount of work needed to perform a certain task using fixed resources and Carnot engines* and is referred to as the *available storage*. This function will also play a central role in the derivation of reduced order models (Chapter 3) and in the construction of a robust nonlinear control law (Chapter 4). It must be pointed out that, as shown in Alonso and Ydstie (2001), the available storage is bounded by the field so that:

$$0 \leq q_0\|\mathbf{z} - \mathbf{z}^*\|^2 \leq b \leq q_1\|\mathbf{z} - \mathbf{z}^*\|^2, \qquad \text{with} \quad \|\mathbf{z} - \mathbf{z}^*\|^2 = (\mathbf{z} - \mathbf{z}^*)^T(\mathbf{z} - \mathbf{z}^*), \tag{1.31}$$

and where $q_0, q_1 > 0$. Since function b is strictly convex, the map $\mathscr{Z} \longleftrightarrow \mathscr{A}$ is one to one and onto. The same holds for deviations from arbitrary references $\mathbf{z}^*$, $\mathbf{A}^*$, since by the Taylor's theorem for vectorial fields -see Appendix A.1- one has that:

$$\mathbf{A} - \mathbf{A}^* = \mathbf{Q}(\mathbf{z} - \mathbf{z}^*), \tag{1.32}$$

with

$$\mathbf{Q} = \int_0^1 \mathbf{M}(\mathbf{z}^* + \varepsilon(\mathbf{z} - \mathbf{z}^*))d\varepsilon; \quad M_{ij} = \frac{\partial^2 b}{\partial z_i \partial z_j},$$

Matrices $\mathbf{Q}$ and $\mathbf{M}$ are positive definite since b is convex (Alonso and Ydstie, 2001).

At this point, a new mathematical representation will be introduced to deal with the nonlinearity of the phenomenological coefficients in reaction-diffusion-convection (RDC) systems. Depending on the nonlinearity of these terms, classical numerical methods may be computationally expensive or even may fail. Phase change processes, among others, are typical examples where this issue is relevant. The Kirchhoff transform (Saro et al., 1995) allows us to reformulate the problem in such a way that the field-dependent diffusivity is removed from the equations. This methodology was successfully applied in different fields such as freezing/thawing of foods with arbitrary 3D geometries (Scheerlinck et al., 2001), melting processes or thermal processes induced by laser irradiation (Conde et al., 2005), among others. The advantages of using this transformation are not only numerical but theoretical as well since the structure of the problem reformulated in this way allows us to extract interesting properties of this kind of systems for control and stability analysis purposes (Alonso et al., 2004a). In the new mathematical representation, the field dependent diffusion matrix $\mathbf{L}$ is substituted in Eqn (1.28) by the corresponding Kirchhoff transformation:

$$\mathbf{\Gamma} = \int_{\mathbf{A}^0}^{\mathbf{A}} \mathbf{L}(\mathbf{A}) d\mathbf{A}, \tag{1.33}$$

with $\mathbf{A}^0$ being a given reference state. The set of Kirchhoff transforms $\{[\Gamma_i]\}_{i=1}^n$ will be denoted by $\mathscr{G}$. Eqn (1.33) is introduced into System (1.28) after the substitution of relation (1.29) so as to obtain:

$$\frac{\partial \mathbf{z}}{\partial t} + \vec{\boldsymbol{\nabla}} \cdot (\vec{\mathbf{v}} \mathbf{z}) = \Delta \mathbf{\Gamma} + \mathbf{f}(\mathbf{z}) + \mathbf{u}. \tag{1.34}$$

The integral (1.33) has an unique solution provided that it is path independent. This is the case when the differential

$$d\Gamma_i = \sum_{j=1}^{ns} L_{ij}(\mathbf{A}) dA_j = \sum_{j=1}^{ns} \frac{\partial \Gamma_{ij}}{\partial A_j} dA_j, \quad \forall i, j = 1, ..., ns, \tag{1.35}$$

is exact.

Definition 1.1 (Exact differential) *The differential (1.35) is exact whenever the following relations hold among functions $\{L_{ij}\}_{i,j=1}^{ns}$ (Smith et al., 1996):*

$$\left(\frac{\partial L_{im}}{\partial A_n} \right)_{A^{[n]}} = \left(\frac{\partial L_{in}}{\partial A_m} \right)_{A^{[m]}}; \quad \forall i, m, n = 1, ..., ns; \quad m \neq n, \tag{1.36}$$

where the notation $A^{[k]}$ is employed to represent the set $\{A_p\}_{p=1}^{ns} \setminus A_k$.

Example 1.2 (Exact and Inexact differentials) *Consider a vectorial field of the form* $\overrightarrow{\mathbf{v}} = [3\xi_2, 4\xi_3, -6\xi_1]$. *Consider also the spatial coordinates in differential form* $d\overrightarrow{\boldsymbol{\xi}} = [d\xi_1, d\xi_2, d\xi_3]^T$. *According to Definition 1.1 the differential* $df = \overrightarrow{\mathbf{v}} \cdot d\overrightarrow{\boldsymbol{\xi}}$ *is inexact since:*

$$3 = \frac{\partial v_1}{\partial \xi_2} \neq \frac{\partial v_2}{\partial \xi_1} = 0; \qquad 0 = \frac{\partial v_1}{\partial \xi_3} \neq \frac{\partial v_3}{\partial \xi_1} = -6; \qquad 4 = \frac{\partial v_2}{\partial \xi_3} \neq \frac{\partial v_3}{\partial \xi_2} = 0.$$

In order to illustrate the implications of this, consider the curve $\mathscr{C} = \{(\xi_1, \xi_2, \xi_3) \,/\, \xi_1^2 + \xi_2^2 = 9;\ \xi_3 = 0\}$. *Using polar coordinates, curve* $\mathscr{C}$ *can be expressed as:*

$$\begin{cases} \xi_1 = 3\cos(\theta) \\ \xi_2 = 3\sin(\theta) \\ \xi_3 = 0 \end{cases}, \quad \theta \in [0, 2\pi].$$

With the new coordinates $\overrightarrow{\mathbf{v}} = [9\sin\theta, 0, -18\cos(\theta)]$ *and* $d\overrightarrow{\boldsymbol{\xi}} = [-3\sin\theta, 3\cos\theta, 0]$ *so that:*

$$\int_{\mathscr{C}} df = \int_0^{2\pi} -27\sin^2(\theta) d\theta = -27\pi.$$

Note that this integral is clearly path dependent since $\int_{\mathscr{C}} df \neq 0$ *with* $\mathscr{C}$ *being a closed curve*[4]. *Consider now the vectorial field* $\overrightarrow{\mathbf{v}} = [2\xi_1\xi_2^3, 3\xi_1^2\xi_2^2, 0]$. *In this case:*

$$6\xi_1\xi_2^2 = \frac{\partial v_1}{\partial \xi_2} = \frac{\partial v_2}{\partial \xi_1} = 6\xi_1\xi_2^2; \qquad 0 = \frac{\partial v_1}{\partial \xi_3} = \frac{\partial v_3}{\partial \xi_1} = 0; \qquad 0 = \frac{\partial v_2}{\partial \xi_3} = \frac{\partial v_3}{\partial \xi_2} = 0,$$

so the differential $df = \overrightarrow{\mathbf{v}} \cdot d\overrightarrow{\boldsymbol{\xi}}$ *is exact. Note that now the integral over the closed curve* $\mathscr{C}$ *is:*

$$\int_{\mathscr{C}} df = \int_0^{2\pi} -3\sin^4(\theta)\cos(\theta) + 729\sin^2(\theta)\cos^3(\theta) d\theta = 0.$$

□

It should be remarked that, since $\mathbf{L}$ is positive definite and assuming that the differential is exact, the map $\mathscr{G} \longleftrightarrow \mathscr{A}$ is one to one and onto. In the remaining of this work the systems considered will be restricted to those obeying condition (1.36), as it is characteristic of many isothermal and non-isothermal distributed reaction systems.

Example 1.3 (Kirchhoff) *This example is a modified version of the case study described in Antoniades and Christofides (2000). The system consists of a RD process where the zeroth order, exothermic reaction* $A \rightarrow B$ *takes place. The spatial domain*

[4]If a differential df is path independent then $\int_a^b df = F(b) - F(a)$, so that if $a = b$ the integral is zero.

is defined as $\mathscr{V} = \{\xi \,/\, 0 < \xi < \pi\}$ *with boundary* $\mathscr{B} = \{0, \pi\}$. *For this example, the temperature distribution satisfies:*

$$\frac{\partial T}{\partial t} = \vec{\boldsymbol{\nabla}} \cdot \left[\kappa \vec{\boldsymbol{\nabla}} T\right] + f(T); \quad f(T) = \beta_T \left[\exp\left(-\frac{\gamma}{1+T}\right) - \exp\left(-\gamma\right)\right] + \beta_H (u - T), \tag{1.37}$$

where $\kappa = 1 - \alpha T$ *represents the field dependent diffusion coefficient.* γ *is the activation energy, and* β_T, β_H *denote the dimensionless heat of reaction and heat transfer coefficient, respectively. Finally,* u *is the control input. System description is completed with boundary and initial conditions of the form:*

$$T|_{\mathscr{B}} = 0; \quad T(\xi, 0) = T_0 = 0.4 \sin(2\xi). \tag{1.38}$$

The values of the parameters and initial conditions are: $\alpha = 0.05, \beta_T = 2, \beta_H = 50, \gamma = 4, u = 0$. *As shown in section 1.4, by neglecting the coupling terms, the phenomenological coefficient in the heat equation becomes* $L = \kappa T^2$. *Thus, the corresponding Kirchhoff transform (1.33) applied to this system results into:*

$$\Gamma = \int_{T^0=0}^{T} \kappa T^2 d\left(-\frac{1}{T}\right) = \int_{T^0=0}^{T} (1 - \alpha T) dT = T - \frac{\alpha}{2} T^2.$$

Using the Kirchhoff transform, Eqn (1.37) can be rewritten as:

$$\frac{\partial T}{\partial t} = \Delta \Gamma + f(T). \tag{1.39}$$

Equations (1.37) and (1.39) have been numerically solved using the finite element method (see Chapter 2) and the results have been plotted in Figures 1.1(a) and (b), respectively. The pictures show that both representations are equivalent. □

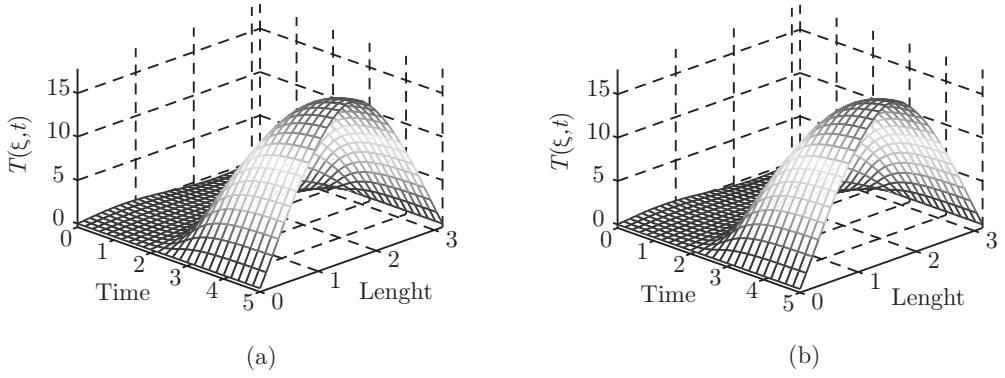

Figure 1.1: Evolution of the distributed temperature. (a) Computed from system (1.37), (b) computed using the Kirchhoff transform -system (1.39)-.

Let us now continue with the description and properties of dissipative systems. For convenience, the following reference is defined:

$$\frac{\partial \mathbf{z}^*}{\partial t} + \overrightarrow{\boldsymbol{\nabla}} \cdot (\overrightarrow{\mathbf{v}} \mathbf{z}^*) = \Delta \boldsymbol{\Gamma}^* + \mathbf{f}^*(\mathbf{z}^*) + \mathbf{u}^*; \quad \boldsymbol{\Gamma}^* = \int_{\mathbf{A}^0}^{\mathbf{A}^*} \mathbf{L}(\mathbf{A}) d\mathbf{A}.$$

System (1.34) in deviation form with respect to this reference can be rewritten as:

$$\frac{\partial \overline{\mathbf{z}}}{\partial t} + \overrightarrow{\boldsymbol{\nabla}} \cdot (\overrightarrow{\mathbf{v}} \overline{\mathbf{z}}) = \Delta \overline{\boldsymbol{\Gamma}} + \overline{\mathbf{f}}(\mathbf{z}, \mathbf{z}^*) + \overline{\mathbf{u}}. \tag{1.40}$$

where the bar indicates that the term is expressed in deviation form. The production terms $\overline{\mathbf{f}}$ in Eqn (1.40) are assumed to be Lipschitz continuous. As in Alonso et al. (2004a), this is formally expressed in terms of $\overline{\mathbf{A}}$ through the following condition:

Condition 1.1 *There exists a positive constant μ and a reference $\mathbf{z}^*$ such that*

$$[\mathbf{A} - \mathbf{A}^*]^T [\mathbf{f} - \mathbf{f}^*] + \ell_\mu(\mathbf{z}; \mathbf{z}^*) = \mu [\mathbf{A} - \mathbf{A}^*]^T [\mathbf{A} - \mathbf{A}^*], \tag{1.41}$$

with $\ell_\mu(\mathbf{z}; \mathbf{z}^*) > 0$ for every $\mathbf{z} \neq \mathbf{z}^*$, $\ell_\mu(\mathbf{z}^*; \mathbf{z}^*) = 0$.

This condition allows us to establish connections with the states operating both near and far from the equilibrium (Alonso et al., 2004a). It is also employed to define what is understood in this work as *dissipative systems*.

Definition 1.2 (Dissipative system) *Consider a given convex function $b(\mathbf{z}, \mathbf{z}^*)$. System (1.28) is said to be* dissipative *with respect to the function $b(\mathbf{z}, \mathbf{z}^*)$ if for $\mu = 0$ in Condition (1.1), $\ell_0(\mathbf{z}; \mathbf{z}^*) \geq 0$ for $\mathbf{z}$ such that $\|\mathbf{z} - \mathbf{z}^*\| \geq \varrho$ for some positive ϱ. Furthermore if $\ell_0(\mathbf{z}; \mathbf{z}^*) > 0$ for every $\mathbf{z} \neq \mathbf{z}^*$ and $\ell_0(\mathbf{z}^*; \mathbf{z}^*) = 0$ the system is* purely dissipative.

The description of the system is completed with appropriate boundary conditions. To that purpose, in this work, the methodology employed in Astarita (1989) and Alonso et al. (2000) will be also used and the boundary will be split into three disjoint sets $\mathscr{B} = \mathscr{B}_d \cup \mathscr{B}_0 \cup \mathscr{B}_c$. Second order boundary conditions are defined on $\mathscr{B}_d$:

$$\left[\mathbf{L}(\mathbf{A}) \frac{d\overline{\mathbf{A}}}{d\mathbf{n}}\right]_{\mathscr{B}_d} = -\mathbf{H}\overline{\mathbf{A}}, \tag{1.42}$$

where $\mathbf{H}$ is a positive definite matrix whose elements are the transfer coefficients. The second set ($\mathscr{B}_0$) corresponds with that part associated with zero flux boundary conditions:

$$\left[\mathbf{L}(\mathbf{A}) \frac{d\overline{\mathbf{A}}}{d\mathbf{n}}\right]_{\mathscr{B}_0} = 0. \tag{1.43}$$

$\mathscr{B}_c$ refers to the part of the boundary through which material flows with velocity $\overrightarrow{\mathbf{v}}$. This boundary is divided into two disjoint sets $\mathscr{B}_c^+$ and $\mathscr{B}_c^-$ satisfying:

$$\overrightarrow{\mathbf{v}} \cdot \overrightarrow{\mathbf{n}}(\mathscr{B}_c^+) \geq 0; \qquad \overrightarrow{\mathbf{v}} \cdot \overrightarrow{\mathbf{n}}(\mathscr{B}_c^-) \leq 0,$$

these conditions characterise the regions of the boundary where the material leaves and enters, respectively. Choosing the reference as the value of the field in $\mathscr{B}_c^-$, boundary conditions on this region become:

$$\overline{\mathbf{z}}(\mathscr{B}_c^-) = 0. \tag{1.44}$$

Finally, in order to illustrate the definition of dissipative systems and to motivate Condition 1.1 the following example, taken from Gorban et al. (2000), will be employed.

Example 1.4 *Let us consider an isolated and well-mixed (homogeneous) material system where n chemical species (involving p types of atoms) participate on a network of r reactions of the form:*

$$\alpha_{1j}\mathcal{C}_1 + \alpha_{2j}\mathcal{C}_2 + ... + \alpha_{nj}\mathcal{C}_n \rightleftharpoons \beta_{1j}\mathcal{C}_1 + \beta_{2j}\mathcal{C}_2 + ... + \beta_{nj}\mathcal{C}_n, \quad j = 1, ..., r.$$

$\mathcal{C}_i$ represents the i^{th} chemical specie and α_{ij} and β_{ij} are its corresponding stoichiometric coefficients for the j-reaction. Since the system is assumed to be isolated and well mixed, the time evolution of the concentrations for the n species can be described by a set of ordinary differential equations of the form:

$$\frac{d\mathbf{c}}{dt} = \sum_{j=1}^{r} \nu_j \dot{\zeta}_j, \tag{1.45}$$

where ν_j are stoichiometric vectors having as elements $\nu_{ij} = \beta_{ij} - \alpha_{ij}$: The vector $\mathbf{c}$ represents chemical species concentrations and $\dot{\zeta}_j$ are the net reaction rates, which are assumed to obey the mass action law*:*

$$\dot{\zeta}_j = k_j^+ \prod_{i=1}^{n} c_i^{\alpha_{ij}} - k_j^- \prod_{i=1}^{n} c_i^{\beta_{ij}}, \tag{1.46}$$

with k_j^+ and k_j^- being positive kinetic parameters for the direct and inverse j-reaction rates, respectively. The phase space for this system is the space of positive concentrations constrained by the set of atomic conservation laws. Next it is shown that the system we just described is in fact purely dissipative (see Definition 1.2) with respect to a constant reference $\mathbf{c}^*$, defined as

$$\dot{\zeta}_j^* = 0; \quad j = 1, ...r. \tag{1.47}$$

To that purpose, let us consider the convex function:

$$a(\mathbf{c}) = \sum_{i=1}^{n} c_i \left(ln\left(c_i\right) - 1 \right). \tag{1.48}$$

As discussed by Gorban et al. (2000), this function is closely related to the free energy for systems at constant temperature and volume. The dual $\mathbf{A}$ *to the field* $\mathbf{c}$ *is obtained by computing the directional derivative of* $a(\mathbf{c})$*, being its elements* $A_i = ln(c_i)$ *for* $i = 1, ..., n$*. Function* $b(\mathbf{c}; \mathbf{c}^*)$ *-see Eqn (1.30)- in this example is now constructed as the difference between* $a(\mathbf{c})$ *and its supporting hyperplane at* $\mathbf{c}^*$ *so that*

$$b = a - a^* - \mathbf{A}^{*T}(\mathbf{c} - \mathbf{c}^*). \tag{1.49}$$

Substituting (1.48) and the expression for A into (1.49), and rearranging terms, one is led to

$$b(\mathbf{c}; \mathbf{c}^*) = \sum_{i=1}^{n} c_i \left[\ln\left(\frac{c_i}{c_i^*}\right) - 1 \right] + \sum_{i=1}^{n} c_i^*. \tag{1.50}$$

It is an easy matter to check that $b(\mathbf{c}, \mathbf{c}^*)$ *is, in fact, positive for* $\mathbf{c} \neq \mathbf{c}^*$ *and* $b(\mathbf{c}^*, \mathbf{c}^*) = 0$*. Taking the time derivative of b along (1.45) and using (1.41) with* $\mu = 0$ *one has that:*

$$\frac{db}{dt} = (\mathbf{A} - \mathbf{A}^*)^T(\mathbf{f} - \mathbf{f}^*) = -\ell_0(\mathbf{c}, \mathbf{c}^*), \qquad \mathbf{f} = \sum_{j=1}^{r} \nu_j \dot{\zeta}_j,$$

$$\ell_0(\mathbf{c}, \mathbf{c}^*) = -(\mathbf{A} - \mathbf{A}^*)^T \sum_{j=1}^{r} \nu_j (\dot{\zeta}_j - \dot{\zeta}_j^*). \tag{1.51}$$

Note that $\ell_0(\mathbf{c}^*, \mathbf{c}^*) = 0$ *so, in order to check whether this system is purely dissipative (Definition 1.2) one must show that* $\ell_0(\mathbf{c}, \mathbf{c}^*) > 0$ *for any* $\mathbf{c} \neq \mathbf{c}^*$*. To that purpose, the following auxiliary variables will be defined:*

$$x_j = \prod_{i=1}^{n} c_i^{\alpha_{ij}}; \quad y_j = \prod_{i=1}^{n} c_i^{\beta_{ij}}; \quad z_j = \varphi_j x_j; \quad \lambda_j = \frac{y_j}{z_j}, \tag{1.52}$$

for $j = 1, ...r$*, and* $\varphi_j = k_j^+ / k_j^-$*. Using (1.52), Eqn (1.51) can be rewritten as*

$$\ell_0(\mathbf{c}; \mathbf{c}^*) = \sum_{j=1}^{r} k_j^- (\overline{\mathbf{A}}^T \nu_j)(y_j - \varphi_j x_j) = \sum_{j=1}^{r} k_j^- \ln\left(\frac{y_j}{z_j}\right)(y_j - z_j) =$$

$$\sum_{j=1}^{r} k_j^- z_j (\lambda_j - 1)\ln(\lambda_j) = \sum_{j=1}^{r} k_j^- z_j g(\lambda_j),$$

with $g(\lambda_j) = (\lambda_j - 1)\ln(\lambda_j)$*. Since the phase space for the system is that of positive concentrations and* $g(\lambda_j)$ *is positive definite for every* $\lambda_j \neq 1$*, then it follows that*

$\ell_0(\mathbf{c};\mathbf{c}^*) > 0$ except at $\lambda_j = 1$ for all j. Recovering the original variables, $\lambda_j = 1$ implies that for all j:

$$k_j^+ \prod_{i=1}^{n} c_i^{\alpha_{ij}} = k_j^- \prod_{i=1}^{n} c_i^{\beta_{ij}},$$

which coincides with the reference (1.47).

□

Chapter 2

Simulation of Distributed Processes: The Finite Element Method

2.1 Introducción

En el capítulo anterior se ha derivado la estructura matemática de los modelos empleados para describir los sistemas reacción-difusión-convección (RDC). Como resultado se ha obtenido un sistema de ecuaciones en derivadas parciales (EDP). Uno de los inconvenientes de este tipo de sistemas es que, con la excepción de unos pocos casos sencillos, no existen métodos analíticos para encontrar la solución de las ecuaciones involucradas. Los métodos numéricos se presentan, pues, como una alternativa para solventar dicho inconveniente. Estos métodos se basan en técnicas de discretización que nos permiten aproximar el conjunto infinito de números que representa un función continua mediante un conjunto finito de parámetros.

El primer objetivo de este capítulo es proporcionar las herramientas matemáticas que se emplean en la mayoría de los métodos numéricos para resolver EDPs y, en base a esto, resumir brevemente las técnicas empleadas más comúnmente. Entre las distintas alternativas, aquellas basadas en el método de Galerkin serán descritas más en detalle y algunas serán utilizadas en este trabajo. En particular se elegirán: el método de elementos finitos (MEF) debido a su flexibilidad y los modelos de orden reducido (descritos en el Capítulo 3) en base a su eficiencia. El segundo objetivo de este capítulo es describir el MEF prestando especial atención a la estructura de las

matrices resultantes de la aplicación de esta técnica. Estas matrices nos permitirán aproximar derivadas e integrales espaciales mediante ecuaciones algebraicas, siendo una pieza fundamental en la derivación de los modelos de orden reducido.

2.2 Introduction

In the previous chapter, the mathematical structure of the models employed for describing reaction-diffusion-convection (RDC) systems was derived. As a result, a system of partial differential equations (PDEs) was obtained. One of the inconveniences of this kind of systems is that, with the exception of a few simple cases, there are no analytical methods for finding the solution of the involved equations. Numerical methods have emerged as the alternative to avoid this problem. These methods are based on discretisation techniques which allow us to approximate the infinite set of numbers that represent a continuous function by means of a finite set of parameters.

The first objective of this chapter is to provide the mathematical tools, which are used for most of numerical methods, for solving PDEs and, on this basis, to give a brief outline of the most commonly employed techniques. Among the different alternatives, some based on the Garlerkin scheme will be described and used in this work. In particular, the finite element method (FEM) will be chosen on the basis of its flexibility and reduced order models (described in Chapter 3) since they are the most efficient. The second objective of this chapter is to describe the FEM, paying special attention to the particular structure of the matrices resulting from the application of this technique. These matrices will allow us to approximate spatial integrals and derivatives by using algebraic equations and, due to this property, they will play a key role in the derivation of reduced order models.

2.2.1 The mathematical basis

As said above, before proceeding with the description of the numerical methods, the basic mathematical concepts employed by them will be presented. The PDEs derived in Chapter 1 have the following general structure -see Eqn (1.28)-:

$$da\frac{\partial z}{\partial t} + \overrightarrow{\boldsymbol{\nabla}}\cdot(\overrightarrow{\mathbf{v}}z) = \overrightarrow{\boldsymbol{\nabla}}\cdot\left(\kappa(z)\overrightarrow{\boldsymbol{\nabla}}z\right) + f(z), \tag{2.1}$$

defined on the domain $\mathscr{D} = \mathscr{V} \times \mathscr{B} \times \mathscr{T}$ where $\mathscr{V} \subset \mathbb{R}^m$ $(m = 1, 2, 3)$ is the spatial domain with boundary $\mathscr{B}$ and $\mathscr{T}$ is the semi-open time interval $[0, \infty)$. For the sake of clarity and without loss of generality, $z(\boldsymbol{\xi}, t) \in \mathcal{H}^1(0, \infty; \mathcal{H}^2(\mathscr{V}))$ is considered in this Chapter as a scalar field. It is worth mentioning that the same results apply to vector

fields. da is a scalar parameter while $\kappa(z) : \mathscr{Z} \rightarrow \mathbb{R}^+$ and $f(z) : \mathscr{Z} \rightarrow \mathbb{R}$ are functions (possibly nonlinear) of the field. The boundary conditions are of the form:

$$\overrightarrow{\mathbf{n}} \cdot \kappa \overrightarrow{\boldsymbol{\nabla}} z + qz = g, \qquad \text{in } \mathscr{B}. \tag{2.2}$$

Dirichlet boundary conditions (BC), also known as essential BC, are not included in this formulation since they can be approximated using Neumann (or natural) BC (2.2) by selecting a large transfer coefficient q and $g = qz^*$ where z^* is the value of z on the boundary. The reason for employing this approximation is that Neumann BC can be included into the FEM formulation in a natural way. This point will be illustrated in Section 2.3.

The *Fourier series theorem* (Reddy, 1998) plays a central role in the numerical techniques for solving PDEs (see Figure 2.1). For this reason a version of this theorem,

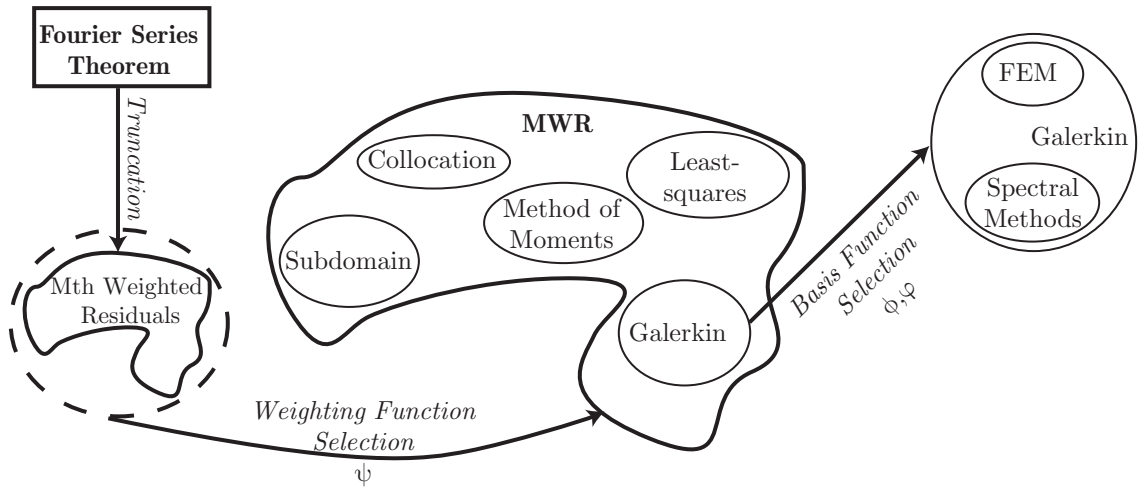

Figure 2.1: From the Fourier series theorem to the family of methods of weighted residuals.

suitable for the computations, will be first discussed. Essentially, the Fourier series theorem establishes that: given an orthonormal basis set on a Hilbert space $\mathcal{L}_2$ (i.e., a maximal orthonormal set $\Phi = \{\varphi_i(\boldsymbol{\xi})\}_{i=1}^{\infty}$, with $\varphi_i : \mathbb{R}^m \rightarrow \mathbb{R}$)[1] any function $g(\cdot, t) \in \mathcal{L}_2(\mathscr{V})$ can be expanded in convergent series of the form:

$$g(\boldsymbol{\xi}, t) = \sum_{i=1}^{\infty} \langle \varphi_i(\boldsymbol{\xi}), g(\boldsymbol{\xi}, t) \rangle_{\mathscr{V}} \varphi_i(\boldsymbol{\xi}) = \sum_{i=1}^{\infty} r_i(t) \varphi_i(\boldsymbol{\xi}). \tag{2.3}$$

[1] Although here the notation φ is employed in a general sense, in further sections and chapters φ and ϕ will be employed to represent, respectively, local and global basis functions. It must be pointed out that some of the approaches based on the MWR relax the requirement of orthogonality of the basis functions. Furthermore, functions φ may depend on both time and spatial coordinates. However, for the sake of convenience, in this work they are considered to be only functions depending on the spatial coordinates.

Most of the numerical methods employed for solving PDE systems belong to the family of *methods of weighted residuals* (MWR) in which, the solution of the PDE (2.1) is approximated by truncating the series (2.3) as follows:

$$z(\boldsymbol{\xi},t) \approx \tilde{z}(\boldsymbol{\xi},t) = \sum_{i=1}^{N} Z_i(t)\varphi_i(\boldsymbol{\xi}). \tag{2.4}$$

The substitution of approximation (2.4) into Eqn (2.1) results into the following residual:

$$da\frac{\partial \tilde{z}}{\partial t} + \overrightarrow{\boldsymbol{\nabla}}\cdot(\overrightarrow{\boldsymbol{\nu}}\tilde{z}) - \overrightarrow{\boldsymbol{\nabla}}\cdot\left(\kappa(\tilde{z})\overrightarrow{\boldsymbol{\nabla}}\tilde{z}\right) - f(\tilde{z}) = R.$$

The best approximation will be that minimising R and it is found by searching the set of time dependent functions $\mathfrak{Z} = \{Z_i(t)\}_{i=1}^{N}$ which provides:

$$\int_{\mathscr{V}} R(\boldsymbol{\xi},t)d\boldsymbol{\xi} = 0. \tag{2.5}$$

In order to compute the N elements of $\mathfrak{Z}$, N equations are required. To that purpose, Eqn (2.5) is multiplied by N weighting functions $\psi(\boldsymbol{\xi}) : \mathbb{R}^m \rightarrow \mathbb{R}$ resulting into the following system of ODEs:

$$\int_{\mathscr{V}} R(\boldsymbol{\xi},t)\psi_i(\boldsymbol{\xi})d\boldsymbol{\xi} = 0; \quad i = 1,...,N. \tag{2.6}$$

This system can be numerically solved by using any of the initial value problems (IVP) solvers described in Appendix A.3. Depending on the selection of the weighting functions different methods arise (see Figure 2.1). Among them, the most commonly employed are briefly described below.

The **Collocation** method is the simplest scheme of the MWR. The weighting functions are chosen as the Dirac delta $\psi_i = \delta(\boldsymbol{\xi} - \boldsymbol{\xi}_i)$ (Lapidus and Pinder, 1999). The location of the collocation points ($\boldsymbol{\xi}_i$) will determine the accuracy of the method. There exist techniques such as the *orthogonal collocation* (Constantinides and Mostoufi, 1999) which select the adequate locations of these points. The *finite difference method* can be included into these schemes. In the **Subdomain** method the spatial domain is divided into N sub-regions. The weighting functions ψ_i with $i = 1,...,N$ are selected to be 1 on a sub-region $\mathscr{V}_i$ and 0 on the rest of the domain $\mathscr{V}\backslash\mathscr{V}_i$. In this family of techniques, probably the best known is the *finite volume method* (Fletcher, 1984). The weighting functions in the **Least-squares** method are chosen as the derivatives of the residual with respect the time dependent functions $\psi_i = \frac{\partial R}{\partial Z_i}$. For dynamic problems Eqn (2.4) has to be modified to include time dependent trial functions so the coefficients Z_i are constant. When the weighting functions take the form $\psi_i(\boldsymbol{\xi}) = \xi_i$

the technique is known as **method of moments** which is very effective when dealing with boundary-layer problems (Fletcher, 1984). Finally, in the **Galerkin** scheme, the weighting functions ψ_i coincide with the basis functions φ_i which form a complete set for the N dimensional subspace where the approximated solution is found. Due to this property, the larger the number N, the better the approximation, so that in the limit when $N \to \infty$ it follows that $z = \tilde{z}$. The basis functions in this method can be locally (φ) or globally (ϕ) defined. Among the Galerkin schemes with locally defined functions probably the most employed due to its flexibility is the *finite element method* (FEM). This feature, the flexibility when solving problems with irregular spatial domains or with non homogeneous boundary conditions, is one of the reasons why the FEM is the classical method chosen in this work. This technique is described more in detail in the following section. When the basis functions are globally defined these schemes are also known as *spectral methods* and will be described in Chapter 3.

2.3 The Finite Element Method

This section is not intended to provide a complete description of the FEM but only to present the basics, including the derivation of the FEM matrices which will allow us to approximate spatial integrals and derivatives by algebraic operations. Such matrices will be employed along this work. Detailed analysis of the FEM, including error analysis, can be found elsewhere in the literature, see for instance (Reddy, 1993; Akin, 2005; Zienkiewicz et al., 2005).

2.3.1 The Basics of the FEM

The finite element formulation of a PDE problem is obtained through a number of steps. Namely the following: the discretisation of the spatial domain which allows us to represent complex spatial domains; the derivation of the weak form which as will become clear later on this Chapter coincides with the structure of Eqn (2.6); the approximation of the solution on an element of the grid which allows us to systematise the FEM and the extension to the whole spatial domain by ensuring continuity of the solution and, finally the selection of the basis functions. These steps are briefly described below.

1. **Discretisation of the Spatial Domain**

As said above, this technique employs local basis functions, thus the spatial domain must be divided into a number of finite discrete elements (*finite element mesh*) so as to define such basis. In this chapter, the number of discretisation points of the

FEM is denoted by N. In 1D problems the elements are segments (see Figure 2.2 (a)) while in 2D or 3D problems the range of possibilities for choosing the form of the elements increase. These possibilities include: triangular (see Figure 2.2 (b)), rectangular, tetrahedral or rectangular prism elements among others. As shown in

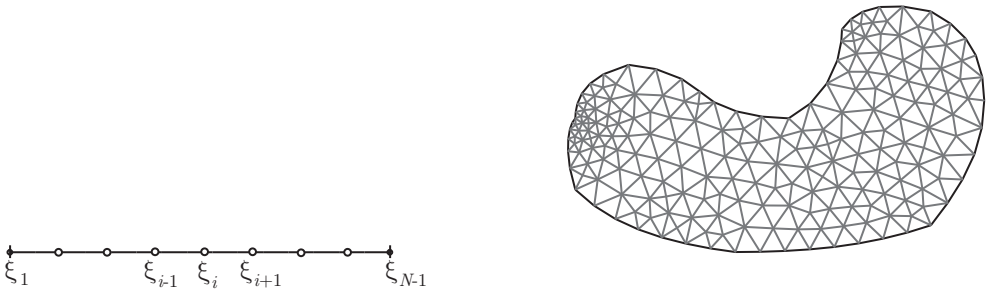

(a) (b)

Figure 2.2: Typical elements considered in the spatial discretization of the FEM. (a) 1D problems, (b) 2D problems.

Figure 2.2 (b), the elements allow us to represent complex spatial geometries as well (Reddy, 1993). The basis functions of the Galerkin method (see section 2.2) for the FEM correspond to polynomials constructed by means of interpolation points known as *nodes*. These nodes, represented by circles in Figure 2.2 (a), are usually located at the vertices of the mesh elements but depending on the degree of the polynomials more nodes may be required. These extra nodes can be located in the boundary or inside the element. The accuracy of the method will depend on the number of elements considered as well as on the geometry, on the degree of the polynomials and on the complexity of the problem.

2. **Derivation of the Variational or Weak Form**

The reader should note that solution of Eqn (2.1) requires that the field z, and the basis functions φ of the Galerkin approximation, must belong to the Sobolev space $\mathcal{H}^2(\mathscr{V})$. Such condition can be relaxed to $\mathcal{H}^1(\mathscr{V})$ by using a new formulation known as the *weak form*. If the solution of the weak form belongs to $\mathcal{H}^2(\mathscr{V})$ then it coincides with the solution of problem (2.1). Another advantage of the weak form is that it contains the natural boundary conditions of the problem. This new mathematical representation is derived by multiplying Eqn (2.1) by an arbitrary test function ψ and integrating the result over the spatial domain, so that:

$$\int_{\mathscr{V}} da\psi \frac{\partial z}{\partial t} d\boldsymbol{\xi} + \int_{\mathscr{V}} \psi \overrightarrow{\boldsymbol{\nabla}} \cdot (\overrightarrow{\boldsymbol{\nabla}} z)\, d\boldsymbol{\xi} = \int_{\mathscr{V}} \psi \overrightarrow{\boldsymbol{\nabla}} \cdot \left(\kappa \overrightarrow{\boldsymbol{\nabla}} z\right) d\boldsymbol{\xi} + \int_{\mathscr{V}} \psi f d\boldsymbol{\xi}. \tag{2.7}$$

Note that this coincides with the procedure followed in the family of MWR -see section 2.2.1-. Since the FEM is based on the Galerkin approach, the test functions ψ will coincide with the basis functions φ of the field approximation. The issues related to the basis and test functions will be discussed in the third and fifth steps. By means of the Green's first identity -see Appendix A.1-, the first term of the RHS of Eqn (2.7) can be expressed as:

$$\int_{\mathscr{V}} \psi \overrightarrow{\boldsymbol{\nabla}} \cdot \left(\kappa \overrightarrow{\boldsymbol{\nabla}} z \right) d\boldsymbol{\xi} = \int_{\mathscr{B}} \psi \overrightarrow{\mathbf{n}} \cdot \kappa \overrightarrow{\boldsymbol{\nabla}} z d\boldsymbol{\xi} - \int_{\mathscr{V}} \overrightarrow{\boldsymbol{\nabla}} \psi \cdot \left(\kappa \overrightarrow{\boldsymbol{\nabla}} z \right) d\boldsymbol{\xi},$$

and substituting this expression into Eqn (2.7), results

$$\int_{\mathscr{V}} da \psi \frac{\partial z}{\partial t} d\boldsymbol{\xi} + \int_{\mathscr{V}} \psi \overrightarrow{\boldsymbol{\nabla}} \cdot \left(\overrightarrow{\mathbf{v}} z \right) d\boldsymbol{\xi} + \int_{\mathscr{V}} \overrightarrow{\boldsymbol{\nabla}} \psi \cdot \left(\kappa \overrightarrow{\boldsymbol{\nabla}} z \right) d\boldsymbol{\xi} = \int_{\mathscr{B}} \psi \overrightarrow{\mathbf{n}} \cdot \kappa \overrightarrow{\boldsymbol{\nabla}} z d\boldsymbol{\xi} + \int_{\mathscr{V}} \psi f d\boldsymbol{\xi},$$

which introducing the boundary conditions (2.2) now reads:

$$\int_{\mathscr{V}} da \psi \frac{\partial z}{\partial t} d\boldsymbol{\xi} + \int_{\mathscr{V}} \psi \overrightarrow{\boldsymbol{\nabla}} \cdot \left(\overrightarrow{\mathbf{v}} z \right) d\boldsymbol{\xi} + \int_{\mathscr{V}} \overrightarrow{\boldsymbol{\nabla}} \psi \cdot \left(\kappa \overrightarrow{\boldsymbol{\nabla}} z \right) d\boldsymbol{\xi} + \int_{\mathscr{B}} \psi q z d\boldsymbol{\xi} = \int_{\mathscr{B}} \psi g d\boldsymbol{\xi} + \int_{\mathscr{V}} \psi f d\boldsymbol{\xi}, \quad (2.8)$$

Note that the second spatial derivatives have vanished from the formulation.

3. **Element-wise approximation of the solution**

When dealing with the derivation of a systematic procedure for the FEM, it may be more convenient to consider the weak form over an arbitrary finite element $\mathscr{V}_e$ instead of over the whole domain $\mathscr{V}$. In such a case, the weak form can be expressed as:

$$\int_{\mathscr{V}_e} \psi^e da \frac{\partial z^e}{\partial t} d\boldsymbol{\xi} + \int_{\mathscr{V}_e} \psi^e \overrightarrow{\boldsymbol{\nabla}} \cdot \left(\overrightarrow{\mathbf{v}} z^e \right) d\boldsymbol{\xi} + \int_{\mathscr{V}_e} \overrightarrow{\boldsymbol{\nabla}} \psi^e \cdot \left(\kappa \overrightarrow{\boldsymbol{\nabla}} z^e \right) d\boldsymbol{\xi} + \int_{\mathscr{B}_e} \psi^e q z^e d\boldsymbol{\xi} =$$

$$\int_{\mathscr{B}_e} \psi^e g^e d\boldsymbol{\xi} + \int_{\mathscr{V}_e} \psi^e f^e d\boldsymbol{\xi}, \quad (2.9)$$

where ψ^e is the test function in the element $\mathscr{V}_e$ and the solution z^e is approximated over each element, so that:

$$z^e \approx \tilde{z}^e = \sum_{i=1}^{n} Z_i^e \varphi_i^e, \quad (2.10)$$

with Z_i^e being the values of the solution at the nodes of the element $\mathscr{V}_e$. φ_i^e corresponds to the basis functions over the same element and n is the number of nodes of $\mathscr{V}_e$.

Substituting expression (2.10) into (2.9) and choosing the test functions ψ so as to coincide with the basis functions φ^e, the following set of n equations is obtained:

$$\int_{\mathscr{V}_e} \varphi_k^e da \frac{\partial \sum_{i=1}^{n} Z_i^e \varphi_i^e}{\partial t} d\boldsymbol{\xi} + \int_{\mathscr{V}_e} \varphi_k^e \overrightarrow{\boldsymbol{\nabla}} \cdot \left(\overrightarrow{\mathbf{v}} \sum_{i=1}^{n} Z_i^e \varphi_i^e \right) d\boldsymbol{\xi} + \int_{\mathscr{V}_e} \overrightarrow{\boldsymbol{\nabla}} \varphi_k^e \cdot \left(\kappa \overrightarrow{\boldsymbol{\nabla}} \sum_{i=1}^{n} Z_i^e \varphi_i^e \right) d\boldsymbol{\xi} +$$

$$\int_{\mathscr{B}_e} \varphi_k^e q \sum_{i=1}^{n} Z_i^e \varphi_i^e d\boldsymbol{\xi} = \int_{\mathscr{B}_e} \varphi_k^e g^e d\boldsymbol{\xi} + \int_{\mathscr{V}_e} \varphi_k^e f^e d\boldsymbol{\xi}; \quad k = 1, 2, ..., n,$$

or in a more compact form:

$$\sum_{i=1}^{n} da\mathcal{DA}_{ki}^e \frac{\partial Z_i^e}{\partial t} + \sum_{i=1}^{n} \left(\mathcal{BE}_{ki}^e + \kappa \mathcal{C}_{ki}^e + q\mathcal{Q}_{ki}^e\right) Z_i^e = \mathcal{G}_k^e + \mathcal{F}_k^e; \quad k = 1, 2, ..., n, \tag{2.11}$$

where the matrices in the former expression are:

$$\mathcal{DA}_{ki}^e = \int_{\mathscr{V}_e} \varphi_k^e \varphi_i^e d\boldsymbol{\xi}; \quad \mathcal{BE}_{ki}^e = \int_{\mathscr{V}_e} \varphi_k^e \overrightarrow{\boldsymbol{\nabla}} \cdot \left(\overrightarrow{\mathbf{v}} \varphi_i^e\right) d\boldsymbol{\xi}; \quad \mathcal{C}_{ki}^e = \int_{\mathscr{V}_e} \overrightarrow{\boldsymbol{\nabla}} \varphi_k^e \cdot \overrightarrow{\boldsymbol{\nabla}} \varphi_i^e d\boldsymbol{\xi};$$

$$\mathcal{Q}_{ki}^e = \int_{\mathscr{B}_e} \varphi_k^e \varphi_i^e d\boldsymbol{\xi}; \quad \mathcal{G}_k^e = \int_{\mathscr{B}_e} \varphi_k^e g^e d\boldsymbol{\xi}; \quad \mathcal{F}_k^e = \int_{\mathscr{V}_e} \varphi_k^e f^e d\boldsymbol{\xi}; \qquad k = 1, ..., n. \tag{2.12}$$

4. **Extension to the whole domain**

The formulation presented in the previous point was derived for an arbitrary isolated element of the mesh. In order to obtain the desired solution of Eqn (2.1), this formulation must be extended to the whole domain. To that purpose, all the isolated elements must be first ordered and then assembled. The first part consists of assigning a number $(e^1, e^2, ..., e^p)$ to each element and to each node. Although the numbers can be arbitrarily assigned to each element, an appropriate order may help to improve the efficiency of the algorithms when solving the final ODE system.

Finally, in order to assemble the elements, one should realise that the value of the field in the shared nodes must be the same (continuity of the solution). This will become clear in the following example where a simple case is chosen so as to illustrate all these steps of the FEM.

Example 2.1 (A stationary reaction-diffusion system) *Consider a given isolated homogeneous solid where a reaction takes place. On the steady state, the distribution of the temperature z is described by:*

$$\kappa \Delta z + f = 0, \tag{2.13}$$

$$\overrightarrow{\mathbf{n}} \cdot \overrightarrow{\boldsymbol{\nabla}} z = 0, \tag{2.14}$$

where $\kappa = 1$ is a constant conduction coefficient and f corresponds with the reaction term. Note that Eqns (2.13) and (2.14) are particular cases of Eqns (2.1) and (2.2) with $da = q = g = 0$, $\overrightarrow{\mathbf{v}} = \mathbf{0}$.

For the sake of illustration, the solid will be split only into three finite elements (Figure 2.3 (a)). Note also that this discretisation scheme results into six global nodes. This implies that the solution is expanded into a Fourier series of the form (2.4) with

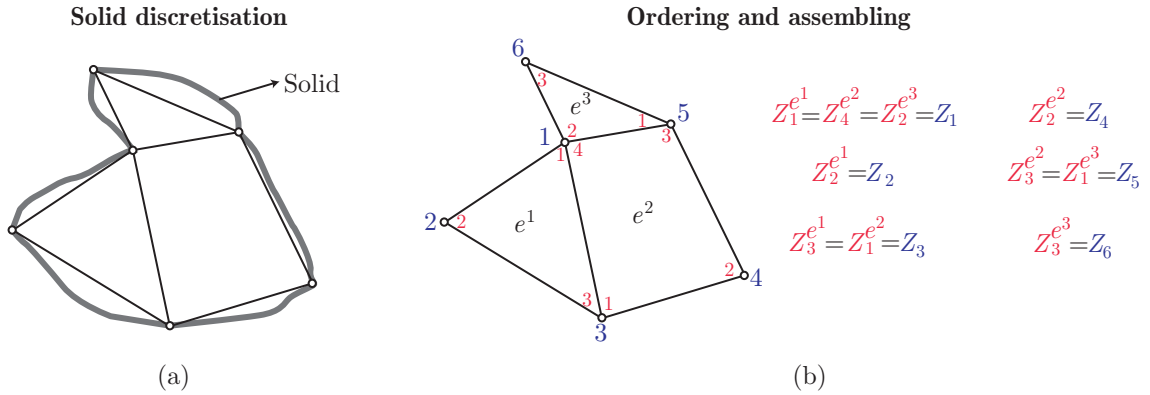

(a) (b)

Figure 2.3: (a) Solid discretisation. (b) Assembly among the three elements of the spatial domain. The element interior numbers (in red) refer to the local notation while the element exterior numbers (in blue) are related to the global notation.

$N = 6$. *Therefore, six coefficients* Z_i *must be computed and six equations are required. In the remaining of this example, we will search for a matrix* $\mathcal{C} \in \mathbb{R}^{6\times 6}$ *and a vector* $\mathcal{F} \in \mathbb{R}^6$ *so that the solution* $\mathcal{Z}$ *can be expressed as* $\mathcal{Z} = \mathcal{C}^{-1}\mathcal{F}$.

After the discretisation, the first step to obtain the FEM solution is the derivation of the weak form, which for the case considered in this example and after substituting the test functions, reads as follows in the element-wise form:

$$\int_{\mathscr{V}_e} \overrightarrow{\boldsymbol{\nabla}}\varphi_k^e \cdot \left(\overrightarrow{\boldsymbol{\nabla}} \sum_{i=1}^{n} Z_i^e \varphi_i^e \right) d\boldsymbol{\xi} = \int_{\mathscr{V}_e} \varphi_k^e f^e d\boldsymbol{\xi}; \qquad k = 1, ..., n$$

Note that, in this expression, use was made of the approximation (2.10). It is also worth mentioning that, in this case, since different kind of elements were considered (see Figure 2.3) the number of nodes n *of each element will differ. Using the matrices defined in relations (2.12) the former expression can be rewritten as:*

$$\sum_{i=1}^{n} \mathcal{C}_{ki}^{e^j} Z_i^{e^j} = \mathcal{F}_k^{e^j}; \qquad k = 1, ..., n; \qquad j = 1, ..., n_e. \tag{2.15}$$

where n_e *is the number of elements. The last step is the element assembly. To that purpose, note that the first global node coincides with the first local node of the element* e^1*, with the fourth local node of the element* e^2 *and with the second local node of the element* e^3 *(see Figure 2.3 (b)). Let us now concentrate on Eqn (2.15) and on the first* $(k = 1)$ *node of the element* e^1*. In this particular case, Eqn (2.15) reads:*

$$\mathcal{C}_{11}^{e^1} Z_1^{e^1} + \mathcal{C}_{12}^{e^1} Z_2^{e^1} + \mathcal{C}_{13}^{e^1} Z_3^{e^1} = \mathcal{F}_1^{e^1}. \tag{2.16}$$

Similarly, when considering the fourth ($k = 4$) local node of the element e^2 and the second ($k = 2$) local node of the element e^3, Eqn (2.15) leads to the following set of algebraic equations:

$$\mathcal{C}_{41}^{e^2} Z_1^{e^2} + \mathcal{C}_{42}^{e^2} Z_2^{e^2} + \mathcal{C}_{43}^{e^2} Z_3^{e^2} + \mathcal{C}_{44}^{e^2} Z_4^{e^2} = \mathcal{F}_4^{e^2}, \tag{2.17}$$

$$\mathcal{C}_{21}^{e^3} Z_1^{e^3} + \mathcal{C}_{22}^{e^3} Z_2^{e^3} + \mathcal{C}_{23}^{e^3} Z_3^{e^3} = \mathcal{F}_2^{e^3}. \tag{2.18}$$

Furthermore, in order to ensure continuity of the solution one has that $Z_1^{e^1} = Z_4^{e^2} = Z_2^{e^3} = Z_1$ (see Figure 2.3 (b)). Likewise, $Z_2^{e^1} = Z_2$, $Z_3^{e^1} = Z_1^{e^3} = Z_3$, $Z_2^{e^2} = Z_4$, $Z_3^{e^2} = Z_1^{e^3} = Z_5$ and $Z_3^{e^3} = Z_6$, thus Eqns (2.16), (2.17) and (2.18) can be rewritten as follows:

$$\mathcal{C}_{11}^{e^1} Z_1 + \mathcal{C}_{12}^{e^1} Z_2 + \mathcal{C}_{13}^{e^1} Z_3 = \mathcal{F}_1^{e^1}. \tag{2.19}$$

$$\mathcal{C}_{41}^{e^2} Z_3 + \mathcal{C}_{42}^{e^2} Z_4 + \mathcal{C}_{43}^{e^2} Z_5 + \mathcal{C}_{44}^{e^2} Z_1 = \mathcal{F}_4^{e^2}, \tag{2.20}$$

$$\mathcal{C}_{21}^{e^3} Z_5 + \mathcal{C}_{22}^{e^3} Z_1 + \mathcal{C}_{23}^{e^3} Z_6 = \mathcal{F}_2^{e^3}. \tag{2.21}$$

Adding Eqns (2.19)-(2.21) one has that:

$$\left(\mathcal{C}_{11}^{e^1} + \mathcal{C}_{44}^{e^2} + \mathcal{C}_{22}^{e^3}\right) Z_1 + \mathcal{C}_{12}^{e^1} Z_2 + \left(\mathcal{C}_{13}^{e^1} + \mathcal{C}_{41}^{e^2}\right) Z_3 + \mathcal{C}_{42}^{e^2} Z_4 + \left(\mathcal{C}_{43}^{e^2} + \mathcal{C}_{21}^{e^3}\right) Z_5 + \mathcal{C}_{23}^{e^3} Z_6 =$$

$$\mathcal{F}_1^{e^1} + \mathcal{F}_4^{e^2} + \mathcal{F}_2^{e^3}, \tag{2.22}$$

which is one of the six equations required to obtain the solution. The second equation is obtained through the second global node. Note that this node coincides only with the second local node of element e^1. In this case Eqn (2.15) leads to the following equations:

$$\mathcal{C}_{21}^{e^1} Z_1^{e^1} + \mathcal{C}_{22}^{e^1} Z_2^{e^1} + \mathcal{C}_{23}^{e^1} Z_3^{e^1} = \mathcal{F}_2^{e^1} \quad \Longleftrightarrow \quad \mathcal{C}_{21}^{e^1} Z_1 + \mathcal{C}_{22}^{e^1} Z_2 + \mathcal{C}_{23}^{e^1} Z_3 = \mathcal{F}_2^{e^1}, \tag{2.23}$$

where use was made of the local and global node notation. The third global node is shared by the third node of the element e^1 and by the first node of the element e^2. Making again use of Eqn (2.15) and taking into account the continuity of the solution, one has:

$$\left(\mathcal{C}_{31}^{e^1} + \mathcal{C}_{14}^{e^2}\right) Z_1 + \mathcal{C}_{32}^{e^1} Z_2 + \left(\mathcal{C}_{33}^{e^1} + \mathcal{C}_{11}^{e^2}\right) Z_3 + \mathcal{C}_{12}^{e^2} Z_4 + \mathcal{C}_{13}^{e^2} Z_5 = \mathcal{F}_3^{e^1} + \mathcal{F}_1^{e^2}. \tag{2.24}$$

So far, three global nodes were employed to obtain three equations. The remaining equations are derived by applying the same procedure to the rest of global nodes. The final result is:

$$\mathcal{C}_{24}^{e^2} Z_1 + \mathcal{C}_{21}^{e^2} Z_3 + \mathcal{C}_{22}^{e^2} Z_4 + \mathcal{C}_{23}^{e^2} Z_5 = \mathcal{F}_2^{e^2}, \tag{2.25}$$

$$\left(\mathcal{C}_{34}^{e^2} + \mathcal{C}_{12}^{e^3}\right) Z_1 + \mathcal{C}_{31}^{e^2} Z_3 + \mathcal{C}_{32}^{e^2} Z_4 + \left(\mathcal{C}_{33}^{e^2} + \mathcal{C}_{11}^{e^3}\right) Z_5 + \mathcal{C}_{13}^{e^3} Z_6 = \mathcal{F}_3^{e^2} + \mathcal{F}_1^{e^3}, \tag{2.26}$$

$$\mathcal{C}_{32}^{e^3} Z_1 + \mathcal{C}_{31}^{e^3} Z_5 + \mathcal{C}_{33}^{e^3} Z_6 = \mathcal{F}_3^{e^3}. \tag{2.27}$$

Eqns (2.22), (2.23) and (2.24)-(2.27) form a system of six equations with six unknown quantities which can be solved. Note also that this system can be rewritten into a more compact form: $\mathcal{C}\mathcal{Z} = \mathcal{F}$*, where matrix* $\mathcal{C}$ *and vectors* $\mathcal{Z}$ *and* $\mathcal{F}$ *correspond with:*

$$\mathcal{C} = \begin{bmatrix} \mathcal{C}_{11}^{e^1} + \mathcal{C}_{44}^{e^2} + \mathcal{C}_{22}^{e^3} & \mathcal{C}_{12}^{e^1} & \mathcal{C}_{13}^{e^1} + \mathcal{C}_{41}^{e^2} & \mathcal{C}_{42}^{e^2} & \mathcal{C}_{43}^{e^2} + \mathcal{C}_{21}^{e^3} & \mathcal{C}_{23}^{e^3} \\ \mathcal{C}_{21}^{e^1} & \mathcal{C}_{22}^{e^1} & \mathcal{C}_{23}^{e^1} & 0 & 0 & 0 \\ \mathcal{C}_{31}^{e^1} + \mathcal{C}_{14}^{e^2} & \mathcal{C}_{32}^{e^1} & \mathcal{C}_{33}^{e^1} + \mathcal{C}_{11}^{e^2} & \mathcal{C}_{12}^{e^2} & \mathcal{C}_{13}^{e^2} & 0 \\ \mathcal{C}_{24}^{e^2} & 0 & \mathcal{C}_{21}^{e^2} & \mathcal{C}_{22}^{e^2} & \mathcal{C}_{23}^{e^2} & 0 \\ \mathcal{C}_{34}^{e^2} + \mathcal{C}_{12}^{e^3} & 0 & \mathcal{C}_{31}^{e^2} & \mathcal{C}_{32}^{e^2} & \mathcal{C}_{33}^{e^2} + \mathcal{C}_{11}^{e^3} & \mathcal{C}_{13}^{e^3} \\ \mathcal{C}_{32}^{e^3} & 0 & 0 & 0 & \mathcal{C}_{31}^{e^3} & \mathcal{C}_{33}^{e^3} \end{bmatrix}; \quad \mathcal{Z} = \begin{bmatrix} Z_1 \\ Z_2 \\ Z_3 \\ Z_4 \\ Z_5 \\ Z_6 \end{bmatrix};$$

$$\mathcal{F} = \left[\begin{array}{cccccc} \mathcal{F}_1^{e^1} + \mathcal{F}_4^{e^2} + \mathcal{F}_2^{e^3}, & \mathcal{F}_2^{e^1}, & \mathcal{F}_3^{e^1} + \mathcal{F}_1^{e^2}, & \mathcal{F}_2^{e^2}, & \mathcal{F}_3^{e^2} + \mathcal{F}_1^{e^3}, & \mathcal{F}_1^{e^3} \end{array} \right]^T.$$

It should be remarked from the definition of the FEM matrices -see relations (2.12)- it follows that $\mathcal{C}_{ij}^{e^k} = \mathcal{C}_{ji}^{e^k}$ *and thus matrix* $\mathcal{C}$ *is symmetric.*

□

In this example a simple stationary case was presented. When other terms, like convection or accumulation, are taken into account, the same procedure can be applied to obtain:

$$da\mathcal{D}\mathcal{A}\frac{d\mathcal{Z}}{dt} + (\kappa\mathcal{C} + \mathcal{B}\mathcal{E} + q\mathcal{Q})\,\mathcal{Z} = \mathcal{F} + \mathcal{G}, \tag{2.28}$$

where the matrices $\mathcal{D}\mathcal{A}$ and $\mathcal{Q}$ are also symmetric.

5. **Selection of the basis functions**

In the FEM, the basis functions φ_i are selected to be algebraic polynomials as shown in Figure 2.4. The degree of the polynomial is a key factor in the quality of the approximation. In general the higher the order of the polynomial the better the approximation but it will also produce a larger number of equations. For practical reasons, the value of φ is the unity on one node of an element $\mathscr{V}_e$ and zero on the remaining (Figure 2.4):

$$\varphi_j^e(\boldsymbol{\xi}_i^e) = \begin{cases} 1 & \text{if} \quad i = j \\ \\ 0 & \text{if} \quad i \neq j \end{cases}$$

Finally, it should be remarked that since the FEM is based on the Galerkin technique, the test functions ψ will coincide with the basis functions φ.

2.3.2 The FEM Matrices: From the Continuous World to its Discrete Version

An interesting and useful property of the matrices resulting from the FEM is that *they can be employed to approximate spatial integrals and derivatives by means of algebraic*

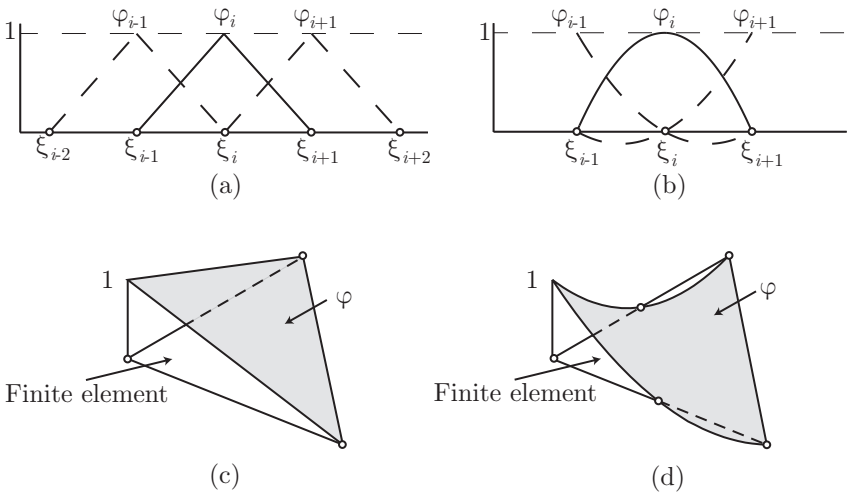

Figure 2.4: Typical basis function of the FEM. The white circles represent the element nodes. (a) 1D domains and first order polynomials, (b) 1D domains and second order polynomials, (c) 2D domains with triangular elements and first order polynomials and (d) 2D domains with triangular elements and second order polynomials

operations. In this section the relationships between the continuous operators and their discrete counterparts are established. For illustrative purposes, a detailed derivation of the connections between the $\mathcal{DA}$ FEM matrix and the spatial integral will be presented in the 1D case. Since the derivation of the other relationships can be obtained following the same procedure, it will not be included in this work. For more details one can consult García et al. (2007).

Consider a 1D spatial domain $\mathscr{V} \subset \mathbb{R}$ with boundary $\mathscr{B}$. Let us divide $\mathscr{V}$ into three finite elements (i.e. four nodes) as depicted in Figure 2.5. Numbers and symbols in

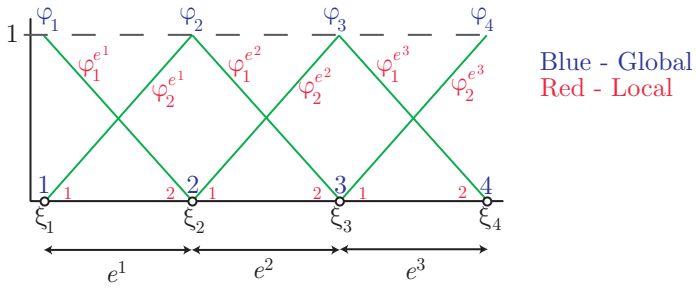

Figure 2.5: 1D FEM spatial discretisation using four nodes and linear basis functions.

red are related with local node/element notation while the blue ones refer to the global node/element notation. The linear basis functions of the FEM are also represented in

this figure (green lines). For this particular case, the $\mathcal{DA}$ matrix takes the form (see Example 2.1 for details on the derivation of the FEM matrices):

$$\mathcal{DA} = \begin{bmatrix} \mathcal{DA}_{11}^{e^1} & \mathcal{DA}_{12}^{e^1} & 0 & 0 \\ \mathcal{DA}_{21}^{e^1} & \mathcal{DA}_{22}^{e^1} + \mathcal{DA}_{11}^{e^2} & \mathcal{DA}_{12}^{e^2} & 0 \\ 0 & \mathcal{DA}_{21}^{e^2} & \mathcal{DA}_{22}^{e^2} + \mathcal{DA}_{11}^{e^3} & \mathcal{DA}_{12}^{e^3} \\ 0 & 0 & \mathcal{DA}_{21}^{e^3} & \mathcal{DA}_{22}^{e^3} \end{bmatrix}.$$

Now consider two given functions $f(\xi), g(\xi) \in \mathcal{L}_2(\mathscr{V})$ with $g(\xi) = 1$, $\forall \xi \in \mathscr{V} \cup \mathscr{B}$. Denoting by f_i, g_i the value of f and g at the global node i, the discrete counterparts of f and g are, respectively $\mathcal{F} = [f_1, f_2, f_3, f_4]^T$ and $\mathcal{G} = [g_1, g_2, g_3, g_4]^T = [1, 1, 1, 1]^T$. Using the $\mathcal{DA}$ matrix, one has that:

$$\mathcal{G}^T\mathcal{DAF} = \mathcal{F}^T\mathcal{DAG} = \left(\mathcal{DA}_{11}^{e^1} + \mathcal{DA}_{21}^{e^1}\right) f_1 + \left(\mathcal{DA}_{12}^{e^1} + \mathcal{DA}_{22}^{e^1} + \mathcal{DA}_{11}^{e^2} + \mathcal{DA}_{21}^{e^2}\right) f_2 +$$

$$\left(\mathcal{DA}_{12}^{e^2} + \mathcal{DA}_{22}^{e^2} + \mathcal{DA}_{11}^{e^3} + \mathcal{DA}_{21}^{e^3}\right) f_3 + \left(\mathcal{DA}_{12}^{e^3} + \mathcal{DA}_{22}^{e^3}\right) f_4.$$

Taking into account that the specific form of the *element-wise* $\mathcal{DA}$ matrix is

$$\mathcal{DA}_{ij}^{e^k} = \mathcal{DA}_{ji}^{e^k} = \int_{\xi_k}^{\xi_{k+1}} \varphi_i^{e^k} \varphi_j^{e^k} \, d\xi; \quad k = 1, 2, 3; \quad i, j = 1, 2,$$

the previous expression can be rewritten, using the global node/element notation, as

$$\mathcal{G}^T\mathcal{DAF} = \int_{\xi_1}^{\xi_2} (\varphi_1 + \varphi_2)(\varphi_1 f_1 + \varphi_2 f_2)\, d\xi + \int_{\xi_2}^{\xi_3} (\varphi_2 + \varphi_3)(\varphi_2 f_2 + \varphi_3 f_3)\, d\xi +$$

$$\int_{\xi_3}^{\xi_4} (\varphi_3 + \varphi_4)(\varphi_3 f_3 + \varphi_4 f_4)\, d\xi.$$

By construction (see Figure 2.5) one has that, $\varphi_1(\xi) + \varphi_2(\xi) = 1$, $\forall \xi \in [\xi_1, \xi_2]$. Similarly, $\varphi_2(\xi) + \varphi_3(\xi) = 1$, $\forall \xi \in [\xi_2, \xi_3]$ and $\varphi_3(\xi) + \varphi_4(\xi) = 1$, $\forall \xi \in [\xi_3, \xi_4]$. Then, the previous expression can be rewritten as:

$$\mathcal{G}^T\mathcal{DAF} = \int_{\xi_1}^{\xi_2} (\varphi_1 f_1 + \varphi_2 f_2)\, d\xi + \int_{\xi_2}^{\xi_3} (\varphi_2 f_2 + \varphi_3 f_3)\, d\xi + \int_{\xi_3}^{\xi_4} (\varphi_3 f_3 + \varphi_4 f_4)\, d\xi \approx \int_{\xi_1}^{\xi_4} f\, d\xi. \tag{2.29}$$

The graphical interpretation of this approximation is presented in Figure 2.6. Function f (black line) is approximated by a piecewise linear function (blue lines). Note that the expression for the piecewise linear function in each interval coincides with the expression for each integral in the relation (2.29). Larger discretisations will produce better approximations between the nonlinear and the piecewise linear functions thus

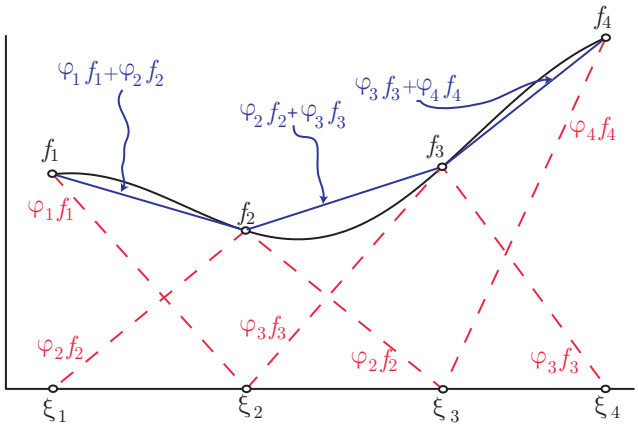

Figure 2.6: Graphical interpretation of the relationship between the continuous integral of a function and its discrete counterpart obtained with the $\mathcal{DA}$ FEM matrix.

leading to better computations of the integral. If an arbitrary nonlinear function g is chosen instead of $g = 1$ then $\mathcal{G}^T\mathcal{DAF} = \int_{\xi_1}^{\xi_4} g f d\xi$.

In Table 2.1 the results of integrating two given functions (1D and 2D) with the FEM matrices are compared with the analytical and the Simpson's rule results. The FEM is able to approximate fairly accurately the analytical solution. It should be stressed that the computations in the case of the FEM are straightforward (they only consist of matrix multiplications). In the case of the 1D function, 31 points were employed in both the FEM and the Simpson's cases while in the 2D function the number of nodes was 216 for the FEM and 221 for the Simpson method.

Function	**Real Integral**	**Simpson**	**FEM**
$f(\xi) = \xi^3 + \xi^2 - \exp(\xi/10);\ \xi = [1, 3]$	26.2198	26.2198	26.2198
$f(\xi_1, \xi_2) = \xi_1\xi_2 + \xi_1^2/\xi_2 - \exp(\xi_2/10);$ $(\xi_1, \xi_2) = [2, 4] \times [1, 2]$	19.6141	19.6141	19.6279

Table 2.1: Comparison between the real integral and the Simpson's and FEM integrals.

The other relationships between continuous and discrete operators can be obtained in a similar way and they are summarised in Table 2.2 for homogeneous boundary conditions. The subindex i in the second and fourth rows of the table is employed to indicate the direction of the derivative. For instance, the derivation with respect to ξ_1 corresponds with $i = 1$. In this case the velocity for constructing the $\mathcal{BE}$ matrix -see relations (2.12)- must be chosen as $\vec{\mathbf{v}} = [1, 0, 0]$. Finally, the approximations to

	Continuous	**Discrete**
1	$\int_{\mathscr{V}} g(\boldsymbol{\xi}) f(\boldsymbol{\xi}) d\boldsymbol{\xi}$	$\mathcal{G}^T \mathcal{D}\mathcal{A}\mathcal{F}$
2	$\int_{\mathscr{V}} g(\boldsymbol{\xi}) \frac{\partial f(\boldsymbol{\xi})}{\partial \xi_i} \, \mathrm{d}\boldsymbol{\xi}$	$\mathcal{G}^T \mathcal{B}\mathcal{E}_i \mathcal{F}$
3	$\int_{\mathscr{V}} g(\boldsymbol{\xi}) \Delta f(\boldsymbol{\xi}) \, \mathrm{d}\boldsymbol{\xi}$	$-\mathcal{G}^T \left(\mathcal{C} + \mathcal{Q}\right) \mathcal{F}$
4	$\frac{\partial}{\partial \xi_i}$	$\mathcal{D}\mathcal{A}^{-1}\mathcal{B}\mathcal{E}_i$
5	$\Delta = \frac{\partial^2}{\partial \xi_1^2} + \frac{\partial^2}{\partial \xi_2^2} + \frac{\partial^2}{\partial \xi_3^2}$	$-\mathcal{D}\mathcal{A}^{-1}\left(\mathcal{C} + \mathcal{Q}\right)$

Table 2.2: Relationships between the continuous spatial derivatives and integrals and their discrete counterparts using the FEM matrices.

the first and second spatial derivatives (4^{th} and 5^{th} rows in the table) were obtained from their integral counterparts (2^{nd} and 3^{rd} rows in the table). In this way, note that integral $\int_{\mathscr{V}} g \frac{\partial f}{\partial \xi_i} d\boldsymbol{\xi}$ can be approximated by using both the $\mathcal{B}\mathcal{E}$ or the $\mathcal{D}\mathcal{A}$ matrices as:

$$\int_{\mathscr{V}} g \frac{\partial f}{\partial \xi_i} d\boldsymbol{\xi} = \mathcal{G}^T \mathcal{B}\mathcal{E}_i \mathcal{F} \quad \text{or} \quad \int_{\mathscr{V}} g \frac{\partial f}{\partial \xi_i} d\boldsymbol{\xi} = \mathcal{G}^T \mathcal{D}\mathcal{A}\, \mathcal{S}_i \mathcal{F},$$

where $\mathcal{S}_i$ represents the discrete version of the first spatial derivative in the ξ_i direction. This relation holds for all g, f, thus $\mathcal{B}\mathcal{E}_i = \mathcal{D}\mathcal{A}\mathcal{S}_i$ or, equivalently, $\mathcal{S}_i = \mathcal{D}\mathcal{A}^{-1}\mathcal{B}\mathcal{E}_i$.

Example 2.2 (Application to the Fourier Equation) *Consider the Fourier equation in a 1D spatial domain $\mathscr{V} = [0, 1]$:*

$$\frac{\partial z(\xi, t)}{\partial t} = \kappa \Delta z(\xi, t), \tag{2.30}$$

with $\kappa = 0.1$ and boundary and initial conditions of the form:

$$\overrightarrow{\mathbf{n}} \cdot \overrightarrow{\boldsymbol{\nabla}} z(0, t) = \overrightarrow{\mathbf{n}} \cdot \overrightarrow{\boldsymbol{\nabla}} z(1, t) = 0, \quad z(\xi, 0) = z_0 = 5 \left(\frac{\xi^2}{2} - \frac{\xi^4}{4} \right) + 1.$$

The analytical solution of this problem is (Polyanin, 2002):

$$z(\xi, t) = \int_0^1 z_0(x) \left[1 + 2 \sum_{n=1}^{\infty} \cos\left(n\pi\xi\right) \cos\left(n\pi x\right) \exp\left(-\kappa n^2 \pi^2 t\right) \right] dx.$$

After the spatial discretisation, the formulation of the variational form and the basis function selection, the FEM matrices can be obtained as indicated previously. Since no convection term ($\overrightarrow{\mathbf{v}} = \mathbf{0}$) or nonlinear functions ($f = 0$) are included into the problem

formulation and the boundary conditions are homogeneous ($q = g = 0$) the FEM matrices $\mathcal{Q}, \mathcal{BE}, \mathcal{G}, \mathcal{F}$ are null, thus the discrete FEM counterpart of (2.30) becomes:

$$\mathcal{DA}\frac{d\mathcal{Z}}{dt} = -\kappa\mathcal{CZ}, \quad or \quad \frac{d\mathcal{Z}}{dt} = -\kappa\mathcal{DA}^{-1}\mathcal{CZ},$$

where $\mathcal{Z} = [Z_1, Z_2, ..., Z_N]^T$ is the discrete version of the temperature field. The solution of this system of ODEs can be obtained by using any of the numerical methods mentioned in Appendix A.3. As mentioned above, the accuracy of the FEM depends on the number of discretisation points N employed. In this regard when using $N = 31$ and performing the simulation till the steady state ($t = 4$), the maximum relative and absolute errors between the analytical and numerical results are:

$$\epsilon_{rel} = \left|\max\left(\frac{z_{ana} - z_{num}}{z_{ana}}\right)\right| 100 = 0.0145\%;\ \epsilon_{abs} = |\max(z_{ana} - z_{num})| = 2.2 \times 10^{-4}.$$

When the steady state is reached, the maximum relative error reduces to $\epsilon_{rel} = 2.7 \times 10^{-3}\%$. Using a finer mesh ($N = 61$) the maximum relative and absolute errors are:

$$\epsilon_{rel} = \left|\max\left(\frac{z_{ana} - z_{num}}{z_{ana}}\right)\right| 100 = 3.6{\times}10^{-3}\%;\ \epsilon_{abs} = |\max(z_{ana} - z_{num})| = 5.5{\times}10^{-5}.$$

When $N \to \infty$ the error goes to zero but the computational cost to solve the ODE system increases. It should be stressed that when using $N = 31$ the differences between the analytical and the FEM results appear, in the worst case, in the fourth decimal number so the FEM with $N = 31$ is considered accurate.

A graphical comparison between the analytical and the numerical solution with $N = 31$ is presented in Figure (2.7). As shown in the Figure, the differences are negligible.

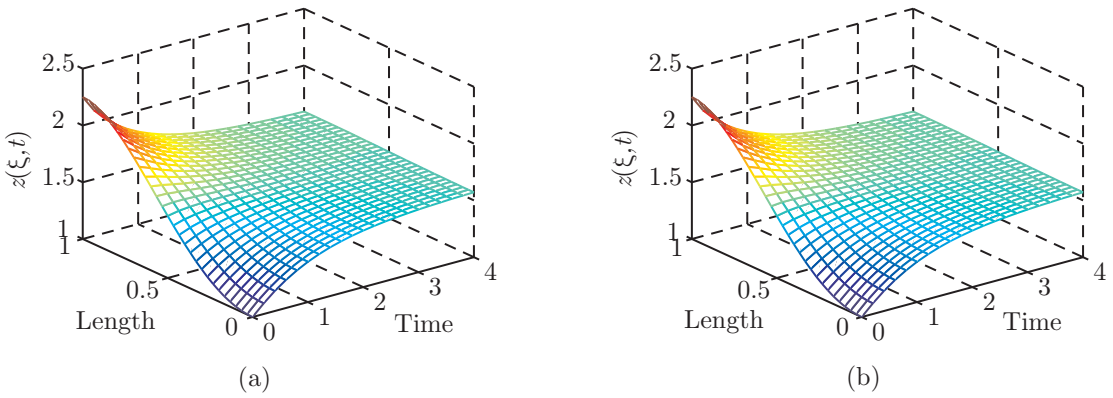

Figure 2.7: Evolution and distribution of the temperature in the Fourier problem. The results were obtained (a) analytically and (b) numerically (FEM).

Chapter 3

Simulation of Distributed Processes: Reduced Order Models

3.1 Introducción

La aplicación de los métodos numéricos clásicos, como diferencias finitas o elementos finitos, descrito en el capítulo anterior, para calcular la solución de ecuaciones en derivadas parciales (EDP) normalmente lleva asociado la resolución de un número elevado de ecuaciones diferenciales ordinarias. Este punto es especialmente crítico cuando se consideran dominios espaciales 2D o 3D, donde el número de ecuaciones necesarias para obtener un resultado satisfactorio se puede incrementar a decenas o centenas de miles. Por lo tanto, estos enfoques se vuelven prohibitivos para aplicaciones como optimización o control en tiempo real ya que el tiempo necesario para resolver estas ecuaciones puede superar la escala de tiempos en la que ocurren las dinámicas relevantes del proceso real. Hay una clara necesidad, pues, de alternativas con un coste computacional menor al de los métodos clásicos. Estas alternativas se conocen como *modelos de orden reducido* (MOR) o *métodos espectrales* (Fletcher, 1984) y se basan en obviar las dinámicas que ocurren a escalas de tiempo mucho más rápidas que las relevantes. De alguna forma esto está relacionado con la idea de compresión empleada hoy en día para almacenar imágenes o música (jpg, mp3) donde las características no relevantes (información que no puede captar el ojo o el oído) se eliminan.

Se ha dedicado una gran cantidad de esfuerzo al desarrollo de técnicas para la reducción de modelos lineales. Entre éstas se encuentra por ejemplo: *Balance and Truncate* (Tombs and Postlethwaite, 1987; Varga, 1991) o la *Aproximación de Hankel*

(Lemouel et al., 1994; Sasane, 2002). En cualquier caso, las técnicas de reducción de sistemas lineales no se considerarán en este trabajo ya que la mayoría de las aplicaciones en sistemas químicos y biológicos son no lineales. Además, las técnicas no lineales se pueden aplicar a sistemas lineales.

Los esquemas para la obtención de MOR en sistemas distribuidos no lineales emplean el método de Galerkin (ver Capítulo 2) con funciones base globales en lugar de locales. Estas bases forman un conjunto completo ortogonal que puede ser normalizado. Otras técnicas íntimamente relacionadas con el método de Garlerkin emplean funciones base globales, por ejemplo los métodos *tau* o *pseudo espectral*. En el método tau las funciones base no tienen que cumplir las condiciones frontera pero en general requiere resolver un número grande de ecuaciones. En el método pseudo espectral el dominio espacial se divide en un número de puntos (puntos de colocación) y la solución en cada punto se aproxima mediante series de Fourier. Este método depende de la colocación de los puntos y puede producir que altas frecuencias de la solución aparezcan como frecuencias bajas. Para una descripción detallada de ambos métodos ver, por ejemplo, Gottlieb and Orszag (1977); Fletcher (1984). Las técnicas de reducción de orden se han aplicado en una amplia gama de sistemas en las últimas seis décadas. Algunos ejemplos incluyen modelado atmosférico (Silberman, 1954; Lorenz, 1960), simulación de turbulencias (Orszag and Kruskal, 1968; Berkooz et al., 1993), reactores químicos (Antoniades and Christofides, 2000; Alonso et al., 2004b) o el tratamiento térmico de comida enlatada (Balsa-Canto et al., 2002b) entre otros. Las ventajas de los MOR no se limitan a la simulación sino que además se han empleado para tratar de forma eficiente problemas en control (Shvartsman and Kevrekidis, 1998; Christofides, 2001), estimación de parámetros (Park et al., 1998) o reconstrucción de estados (Alonso et al., 2000; García et al., 2007) entre otros. Las cuestiones relacionadas con la utilización de los MOR para el control de sistemas distribuidos se discutirán en el Capítulo 4.

El objetivo de este capítulo es presentar las técnicas de reducción de orden más comúnmente empleadas y describir en detalles las más eficientes: la *descomposición espectral del Laplaciano* y *la descomposición ortogonal propia*.

3.2 Introduction

The application of the classical numerical methods, such as finite differences or the FEM, described in the previous chapter, for computing the solution of PDEs usually results into a large number of ordinary differential equations to be solved. This is particularly critical when considering 2D or 3D spatial domains, where the number of

equations necessary to obtain a satisfactory result may increase to tens or hundreds of thousands. Therefore, these approaches become unsuitable for tasks to be performed in real time like control or optimisation. This is because the time needed to solve such number of equations is, in many cases, much larger than the time scale in which the relevant dynamics of the real process occur. Thus, there is a need for alternatives computationally cheaper than the classical numerical methods. These alternatives are known as *reduced order models* (ROMs) or *spectral methods* (Fletcher, 1984). The main idea behind the alternatives to classical numerical methods is to neglect the dynamics that occur at time scales much faster than the relevant ones. This can be somehow quite close to the idea of data compression employed nowadays to store images or music (jpg,mp3) where non relevant features (information that cannot be captured by the eye or the ear) are neglected.

Many efforts have been spent in the development of techniques for the reduction of linear models. Amongst them one can find the *Balance and Truncate* (Tombs and Postlethwaite, 1987; Varga, 1991) or the *Hankel approximation* (Lemouel et al., 1994; Sasane, 2002). However, the reduction of linear models will not be considered in this work since most of applications in chemical and biological systems are nonlinear. Furthermore the reduction techniques for nonlinear systems can be also applied to linear problems.

The schemes to obtain ROMs of nonlinear distributed process systems employ the Galerkin method (see Chapter 2) with global functions instead of the local functions employed by the FEM. Such basis functions must satisfy the boundary conditions individually, and form a complete orthogonal set which can be normalised so as to obtain

$$\langle \phi_i, \phi_j \rangle_{\mathscr{V}} = \begin{cases} 1 & \text{if} \quad i = j \\ \\ 0 & \text{if} \quad i \neq j \end{cases} . \tag{3.1}$$

It should be pointed out that other techniques, closely related to the Galerkin spectral method, like the *tau* or the *pseudo spectral* methods also employ global basis functions. In the *tau* method, the basis functions are not required to satisfy the BC. The inconvenience is that, in general, this technique requires to solve a larger number of ODE. In the *pseudo spectral* method the spatial domain is divided into a number of points known as *collocation points*. The solution in each point is approximated by a series of the form of (2.4) where only the values of the basis functions at the collocation points are considered. This method depends strongly on these points and may produce *aliasing*. That is, high frequencies of the solution on the discrete grid appear as low frequencies. A detailed description of both methods can be found in

Gottlieb and Orszag (1977); Fletcher (1984). The reduction order methods have been applied to the simulation of a wide range of systems during the last six decades. Some examples include atmospheric modelling (Silberman, 1954; Lorenz, 1960), turbulence simulation (Orszag and Kruskal, 1968; Berkooz et al., 1993), chemical reactors (Antoniades and Christofides, 2000; Alonso et al., 2004b) or thermal treatment of canned food (Balsa-Canto et al., 2002b) among others. The advantages of using ROMs are not only limited to simulation but their features allow us to efficiently handle problems in control (Shvartsman and Kevrekidis, 1998; Christofides, 2001), parameter estimation (Park et al., 1998) or state reconstruction (Alonso et al., 2000; García et al., 2007) among others, in distributed process systems. The issues related to the use of ROMs for the control of DPS will be further discussed in Chapter 4.

3.2.1 Classification of the Reduced Order Techniques

As it was said above, the ROMs discussed in this work are particular cases of the Galerkin method where the basis functions are globally defined. Depending on the selection of the basis set, a wide family of different approaches arise. This selection will determine the accuracy of the technique, thus in order to choose the appropriate alternatives, the main weaknesses and strengths of the more commonly basis employed are briefly discussed next:

- **Polynomials**. Typically, Legendre and Chebyshev polynomials. These techniques are the most robust in the sense that they can be applied to a wider range of applications like, for instance, problems with non-periodic boundary conditions. Nevertheless, Legendre polynomials present convergence problems when internal discontinuities occur. The main inconvenience of the Chebyshev polynomials is that their efficiency is lower than in other approaches since they are not strictly orthogonal and produce off-diagonal contributions to the mass matrix in the projection.

- **Fourier series**. The convergence rate of the approximation using these basis is greater than that of Chebyshev polynomials with periodic boundary conditions (Fletcher, 1984). However, the application of general Fourier series to problems with non periodic BC will produce a constant overshoot in the neighbourhood of one boundary (Gottlieb and Orszag, 1977).

- **Eigenfunctions**. This approach presents two main inconveniences. Firstly, the analytical computation of eigenfunctions is limited to simple geometries and spa-

tial operators and, secondly, the range of application is limited to some types (typically homogeneous) of boundary conditions (Fletcher, 1984). However, these basis produce higher convergence rates than the others presented before thus resulting into a lower number of equations.

It should be remarked that most of systems considered in this work present homogeneous boundary conditions. Furthermore, as it will be shown later, a system with non homogeneous BC can be converted into an equivalent one with homogeneous BC by means of state transformations. On the other hand, a new systematic alternative for the numerical computation of eigenfunctions will be proposed in this work. This alternative, based on the FEM, will allow us to apply the eigenfunctions approach to complex spatial domains. Since the main inconveniences of the eigenfunctions technique can be circumvented and it is the most efficient in the sense of number of equations, this approach is considered as the best option for obtaining reduced order models.

This chapter is structured as follows: First, issues related to the projection of the nonlinear terms will be discussed. In this regard, a new systematic approach based on the FEM is proposed as an alternative to the existing techniques. After this, the eigenfunctions approach is described more in detail in Section 3.4. Then, in Section 3.5, some concepts presented in Chapter 1 and related to thermodynamics are employed to show that constructing a finite dimensional approximation in dissipative systems is always possible under certain conditions. Finally, the eigenfunctions method will be applied to a number of case studies and the results will be compared with the analytical and/or the FEM solutions.

3.3 Nonlinear Terms

As it will be shown in Section 3.5, in dissipative systems *the states evolve to a low dimensional subspace (hyperplane) and remain in it in the future* (Balsa-Canto, 2001; Christofides, 2001; Alonso et al., 2004b). This property is schematically depicted in Figure 3.1. ROMs are then projections of the original PDE system into a low dimensional subspace. The main difficulty of projection methods lies in the projection of the nonlinear terms. In this way, consider a nonlinear function $f(\boldsymbol{\xi}, t) : \mathbb{R}^m \times \mathscr{T} \rightarrow \mathbb{R}$, with $m = 1, 2, 3$ and $\mathscr{T}$ being the semiopen time interval $[0, \infty)$, expanded in a truncated Fourier series, so that:

$$f(\boldsymbol{\xi}, t) \approx \sum_{i=1}^{p} \sigma_i(t)\phi_i(\boldsymbol{\xi}).$$

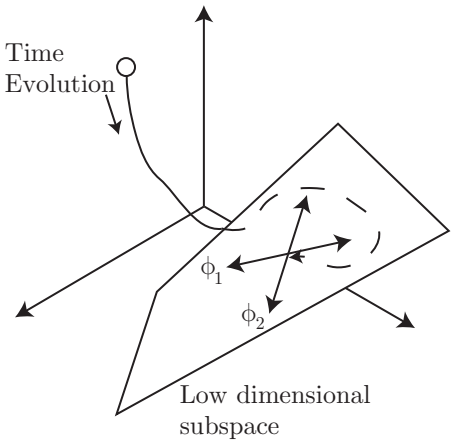

Figure 3.1: Time evolution of a dissipative system.

In order to compute the p coefficients $\sigma_i(t)$, the following p integrals must be solved:

$$\sigma_i(t) = \int_{\mathscr{V}} f(\boldsymbol{\xi}, t)\phi_i(\boldsymbol{\xi})d\boldsymbol{\xi}; \qquad i = 1, ..., p.$$

A first option to evaluate the integral could be to employ a quadrature formula like the Simpson's rule, but this is computationally expensive so the main advantage of ROMs is lost. The fast Fourier transform (Cooley and Tukey, 1965; Brigham, 1974) is a more efficient alternative that can be employed when Fourier series are considered as basis functions. Orszag (1980) stated that similar fast transforms are possible for other orthogonal basis. Although this approach reduces the number of equations as compared with quadrature techniques it still remains into a large number of equations, especially in 2D or 3D. Form another perspective, Rico-Martínez et al. (1995) employed neural networks to deal with the nonlinear terms. The problem of this approach is that training a neural network is a hard task. Balsa-Canto et al. (2002a, 2004) proposed a field transformation leading to a system of PDEs in which the nonlinear terms are polynomials whose integration is straightforward. The number of PDEs increase with this transformation but the integrals can be evaluated analytically. However, this approach is problem-dependent and different transformations must be defined for each nonlinear term. In this work an alternative based on the FEM is proposed. It consists on using the $\mathcal{DA}$ matrix of the FEM, as described in Section 2.3.2 (see Table 2.2), to compute the integrals. This alternative does not require to increase the number of equations, the computational cost to evaluate the integrals is very low and, since the $\mathcal{DA}$ matrix only depends on the spatial domain and the number of discretisation points, the approach can be employed for any nonlinear term. This allows us to systematise the procedure for a given spatial domain. The computation of the p coefficients $\sigma_i(t)$

is as follows:

$$\boldsymbol{\sigma} = \mathcal{F}^T \mathcal{D} \mathcal{A} \boldsymbol{\Phi}; \quad \text{with} \quad \mathbf{c} = [c_1, ..., c_p]^T; \quad \boldsymbol{\Phi} = [\boldsymbol{\phi}_1, ..., \boldsymbol{\phi}_p],$$

where $\mathcal{F}$ and $\boldsymbol{\phi}_i$ are, respectively, the discrete versions of the nonlinear function $f(\boldsymbol{\xi}, t)$ and the eigenfunctions $\phi_i(\boldsymbol{\xi})$.

3.4 The Eigenfunctions Approach

In the eigenfunctions approach, the basis functions are selected as the solution of an eigenvalue problem of the form:

$$\phi_i(\boldsymbol{\xi}) = \lambda_i \int_{\mathcal{V}} \mathcal{K}(\boldsymbol{\xi}, \boldsymbol{\xi}') \phi_i(\boldsymbol{\xi}') d\boldsymbol{\xi}' \tag{3.2}$$

The eigenvalues λ_i may be arranged so that $|\lambda_i| \leq |\lambda_j|$ for $i < j$ (Courant and Hilbert, 1989). Furthermore, it can be shown that $\lambda_p \to \infty$ as $p \to \infty$ (Smoller, 1994; Reddy, 1998). Depending on the nature of the kernel, two different approaches, which will be described in the following sections, arise: the *Laplacian Spectral Decomposition* (LSD) and the *Proper Orthogonal Decomposition* (POD). For convenience, in the POD method, a new parameter defined as $\mu_i = 1/\lambda_i$ will be employed.

3.4.1 The Laplacian Spectral Decomposition Approach

By selecting the kernel as the Green's function associated with the Laplacian operator, solving the integral equation (3.2) is equivalent to finding the solution to the differential equation (Courant and Hilbert, 1989):

$$\Delta \phi_i(\boldsymbol{\xi}) = -\lambda_i \phi_i(\boldsymbol{\xi}), \tag{3.3}$$

with appropriate boundary conditions. This a classical possibility of functional analysis. For more details see, for instance, Rudin (1973); Curtain and Pritchard (1977); Brezis (1984); Eidelman et al. (2004). Some authors have also considered the selection of the kernel as the Green's function associated with the whole spatial operator (Laplacian and gradient). The integral equation leads in this case to the differential equation:

$$\left(\Delta - \overrightarrow{\boldsymbol{\nabla}} \cdot \overrightarrow{\mathbf{v}}\right) \phi_i(\boldsymbol{\xi}) = -\lambda_i \phi_i(\boldsymbol{\xi}).$$

The inconvenience is that now, the kernel is non-symmetric so theorems on symmetric kernels such as the *expansion theorem* are not applicable. Furthermore, other properties of symmetric kernels like the eigenvalues are real numbers do not hold in the case of

non symmetric kernels. In this work the eigenvalue problem will only consider the Laplacian operator.

Finally, the FEM matrices can be also employed to approximate the PDE (3.3) by a discrete eigenvalue problem:

$$\mathcal{D}\mathcal{A}^{-1}\left(\mathcal{C}+\mathcal{Q}\right)\boldsymbol{\phi}_i = -\lambda_i \boldsymbol{\phi}_i.$$

In this case, the BC are required to be homogeneous. Fortunately, when dealing with systems with non homogeneous BC some transformations can be defined to obtain equivalent systems with homogeneous boundary conditions (Vilas et al., 2007).

3.4.2 The Proper Orthogonal Decomposition

This method, first proposed by Sirovich (1987), arose in the context of turbulence simulation. Since that paper, this technique has been employed in many different fields like chemical reactors (Alonso et al., 2004b), reconstruction of pictures (Everson and Sirovich, 1995), fluid dynamics (Berkooz et al., 1993; Holmes et al., 1996) or thermal treatment of canned food (Balsa-Canto et al., 2002b), among others.

In this case, the kernel $\mathcal{K}(\boldsymbol{\xi}, \boldsymbol{\xi}')$ corresponds to a two point correlation kernel of the form (Alonso et al., 2004c):

$$\mathcal{K}(\boldsymbol{\xi}, \boldsymbol{\xi}') = \lim_{T\to\infty} \frac{1}{T}\int_0^T z(\boldsymbol{\xi}, t) z(\boldsymbol{\xi}', t) dt, \tag{3.4}$$

where T stands for a given time horizon and the snapshots $z(\boldsymbol{\xi}, t)$ can be obtained either from numerical simulation or from experiments. In the remaining of the work, the term POD will be employed to denote the eigenfunctions obtained with this technique in order to differentiate them from the basis functions obtained with the LSD. It is important to point out that the set of PODs forms a complete orthonormal basis set on a Hilbert space. Since the kernel $\mathcal{K}$ is real symmetric, its eigenvalues are real numbers (Courant and Hilbert, 1989).

Constructing a POD basis from a discrete set of data

So far the POD methodology was presented in its variational (infinite dimensional) form. However, in practice, only a finite discrete set of measurements is available which calls for a discrete counterpart of Eqn (3.2). In what follows a description of the discrete formulation, which although equivalent is more convenient for practical purposes, will be provided.

Let $\mathcal{Z}_i \in \mathbb{R}^N$ be the vector of values of the field $z(\boldsymbol{\xi}, t_i) \in \mathcal{H}^1(0, \infty; \mathcal{H}^2(\mathscr{V}))$ at a finite number N of spatial points and at a given time t_i (snapshot). The problem is stated as follows: *Given a set of snapshots* $\mathfrak{Z} = \{\mathcal{Z}_i\}_{i=1}^k$, *find a basis* $\boldsymbol{\Phi} = [\Phi_1, \Phi_2, ..., \Phi_p]$ *which maximises the projection over the original set* $\mathfrak{Z}$. Note also that in infinite dimensions, the problem is formally stated as (Holmes et al., 1997):

$$\max_{\Phi} \mathcal{J} = \max_{\Phi} \left(\frac{1}{k} \sum_{i=1}^{k} \langle \Phi, z_i \rangle_{\mathscr{V}}^2 \right) - \boldsymbol{\mu} \left(\langle \Phi, \Phi \rangle_{\mathscr{V}} - 1 \right),$$

where k represents a sufficiently large number of snapshots representative of the system and its dynamic behaviour. The solution of this optimisation problem, in its discrete version, leads to the associated eigenvalue problem (3.2) where now the kernel is:

$$\mathcal{K} = \frac{1}{k} \sum_{i=1}^{k} \mathcal{Z}_i \mathcal{Z}_i^T. \tag{3.5}$$

Note that the *Proper Orthogonal Decomposition* (POD) method provides a set of empirical basis functions which are optimal with respect to other possible expansions. This set is optimal in the sense that for a given number of basis functions, it captures most of the relevant dynamic behaviour of the original distributed system in the range of initial conditions, parameters, inputs, and/or perturbations of the experimental data (Balsa-Canto et al., 2004).

It must be pointed out that for large values of N, solving Eqn (3.2) can be computationally involved. In order to avoid this problem and save computation time, a useful alternative, proposed by Sirovich (1987) and known as the *method of snapshots* or *strobes*, is briefly discussed. In this method, each eigenfunction is expressed in terms of the original data as:

$$\boldsymbol{\phi}_j = \sum_{i=1}^{k} w_i^j \mathcal{Z}_i, \tag{3.6}$$

where w_i^j are the weights to be computed. To this purpose, a new matrix is defined as:

$$\mathcal{M}_{ij} = \frac{1}{k} \langle \mathcal{Z}_i, \mathcal{Z}_j \rangle_{\mathscr{V}}. \tag{3.7}$$

Introducing Eqns (3.5) and (3.6) in the eigenvalue problem (3.2), results into:

$$\mathcal{M}\mathcal{W}_j = \mu_j \mathcal{W}_j, \tag{3.8}$$

where the eigenvectors $\mathcal{W}_j$ have as elements the weights in equation (3.6) so that $\mathcal{W}_j = [w_1^j, w_2^j, ..., w_k^j]^T$.

The FEM matrices can also help in the computation of the PODs since Eqn (3.2) can be approximated as:

$$\mu_i \boldsymbol{\phi}_i = \mathcal{K}\mathcal{D}\mathcal{A}\boldsymbol{\phi}_i, \qquad \text{or} \qquad \boldsymbol{\phi}_i = \lambda_i \mathcal{K}\mathcal{D}\mathcal{A}\boldsymbol{\phi}_i,$$

with $\mathcal{K}$ constructed as in Eqn (3.5). Finally it should be stressed that the eigenvalues λ_i, or to be precise their inverses μ_i, can be employed as an *a priori* measurement of the accuracy of the approximation. In this sense, the total energy captured by the full set of PODs is computed through the eigenvalues as $E = \sum_{i=1}^{N} \mu_i$. Thus the percentage of energy captured by a given number p of PODs is:

$$E(\%) = \frac{\sum_{i=1}^{p} \mu_i}{\sum_{i=1}^{N} \mu_i} 100. \tag{3.9}$$

The more the energy captured, the better the quality of the approximation.

3.5 A note on dissipation: The basis of the model reduction

Let $\mathscr{E} = \{\phi_i(\boldsymbol{\xi})\}_{i=1}^{\infty}$ and $\mathscr{L} = \{\lambda_i\}_{i=1}^{\infty}$ be, respectively, the complete sets of eigenfunctions and their associated eigenvalues satisfying (3.3). Consider the subsets of natural numbers $\mathcal{N}_a$ and $\mathcal{N}_b$ where $\mathcal{N}_a$ is a finite subset of arbitrary numbers and $\mathcal{N}_b = \mathbb{N} \setminus \mathcal{N}_a$ corresponds with its complement. These sub-sets will allow us to split the eigenset $(\mathscr{E}, \mathscr{L}, \mathbb{N})$ into two disjoint sets: $(\mathscr{E}_a, \mathscr{L}_a, \mathcal{N}_a)$ and $(\mathscr{E}_b, \mathscr{L}_b, \mathcal{N}_b)$ with $\mathscr{E}_a = \{\phi_i\}_{i\in\mathcal{N}_a}$, $\mathscr{L}_a = \{\lambda_i\}_{i\in\mathcal{N}_a}$ and $\mathscr{E}_b$ and $\mathscr{L}_b$ their corresponding complements. Using these subsets, all the terms of Eqn (1.40) can be split as:

$$\overline{\mathbf{z}} = \overline{\mathbf{z}}_a + \overline{\mathbf{z}}_b = \sum_{i\in\mathcal{N}_a} \mathbf{m}_i(t)\phi_i(\boldsymbol{\xi}) + \sum_{i\in\mathcal{N}_b} \mathbf{m}_i(t)\phi_i(\boldsymbol{\xi}), \tag{3.10}$$

$$\overline{\mathbf{A}} = \overline{\mathbf{A}}_a + \overline{\mathbf{A}}_b = \sum_{i\in\mathcal{N}_a} \boldsymbol{\alpha}_i(t)\phi_i(\boldsymbol{\xi}) + \sum_{i\in\mathcal{N}_b} \boldsymbol{\alpha}_i(t)\phi_i(\boldsymbol{\xi}), \tag{3.11}$$

$$\overrightarrow{\boldsymbol{\nabla}} \cdot (\overrightarrow{\mathbf{v}}\overline{\mathbf{z}}) = \overrightarrow{\boldsymbol{\nabla}} \cdot (\overrightarrow{\mathbf{v}}\overline{\mathbf{z}}_a) + \overrightarrow{\boldsymbol{\nabla}} \cdot (\overrightarrow{\mathbf{v}}\overline{\mathbf{z}}_b) = \sum_{i\in\mathcal{N}_a} \boldsymbol{\tau}_i(t)\phi_i(\boldsymbol{\xi}) + \sum_{i\in\mathcal{N}_b} \boldsymbol{\tau}_i(t)\phi_i(\boldsymbol{\xi}), \tag{3.12}$$

$$\overline{\mathbf{f}} = \overline{\mathbf{f}}_a + \overline{\mathbf{f}}_b = \sum_{i\in\mathcal{N}_a} \boldsymbol{\sigma}_i(t)\phi_i(\boldsymbol{\xi}) + \sum_{i\in\mathcal{N}_b} \boldsymbol{\sigma}_i(t)\phi_i(\boldsymbol{\xi}), \tag{3.13}$$

$$\overline{\boldsymbol{\Gamma}} = \overline{\boldsymbol{\Gamma}}_a + \overline{\boldsymbol{\Gamma}}_b = \sum_{i\in\mathcal{N}_a} \boldsymbol{\gamma}_i(t)\phi_i(\boldsymbol{\xi}) + \sum_{i\in\mathcal{N}_b} \boldsymbol{\gamma}_i(t)\phi_i(\boldsymbol{\xi}), \tag{3.14}$$

$$\overline{\mathbf{u}} = \overline{\mathbf{u}}_a + \overline{\mathbf{u}}_b = \sum_{i\in\mathcal{N}_a} \boldsymbol{\pi}_i(t)\phi_i(\boldsymbol{\xi}) + \sum_{i\in\mathcal{N}_b} \boldsymbol{\pi}_i(t)\phi_i(\boldsymbol{\xi}). \tag{3.15}$$

Consider that any of the functions $\overline{\mathbf{z}}, \overline{\mathbf{A}}, \overline{\mathbf{f}}, \overline{\mathbf{\Gamma}}, \overline{\mathbf{u}} \in \mathbb{R}^n$ are denoted using the symbol $\overline{\mathbf{x}}$, thus $\overline{\mathbf{x}} = [\overline{x}_1, \overline{x}_2, ..., \overline{x}_n]^T$. Likewise, using $\mathbf{q}_i$ to represent the time dependent functions $\mathbf{m}_i, \boldsymbol{\alpha}_i, \boldsymbol{\sigma}_i, \boldsymbol{\gamma}_i, \boldsymbol{\pi}_i \in \mathbb{R}^n$ one has that $\mathbf{q}_i = [q_i^1, q_i^2, ..., q_i^n]^T$ where indices $1, 2, 3, ..., n$ indicate that the function is associated with the fields $\overline{z}_1, \overline{z}_2, ..., \overline{z}_n$, respectively.

In what follows, the concept of *passivity* will be employed to show that the field $\overline{\mathbf{z}}$ and the term $\overrightarrow{\boldsymbol{\nabla}}\overline{\mathbf{z}}$ are square integrable (i.e., their $\mathcal{L}_2$ norms -as defined in Eqn (1.27)- are bounded). In consequence, they belong to the Hilbert space $\mathcal{L}_2$ and they can be expanded in infinite convergent series. Then the relationships between $\overline{\mathbf{z}}$ and the other terms of the left hand side of Eqns (3.13)-(3.14) will be employed to show that the expansion is also possible for these terms.

Definition 3.1 (Passive systems) *Let us denote the set of the states of the system* $\mathbf{z}$ *by* $\mathscr{Z}$*. A system is said to be* passive *if there exists a function* $\mathcal{B}(\mathbf{z}) : \mathscr{Z} \to \mathbb{R}^+ \cup \{0\}$ *bounded from below so that*

$$\mathcal{B}(\mathbf{z}(t+T)) - \mathcal{B}(\mathbf{z}(t)) \leq \int_t^{t+T} \langle y, \mathfrak{u} \rangle_{\mathscr{Y}} ds, \quad \forall t, T > 0, \tag{3.16}$$

with $\mathfrak{u}$ *and* y *being the input and the output of the system, respectively.*

Boundedness of the field $\overline{\mathbf{z}}$

Consider a system of the form (1.40) to be dissipative according to Definition 1.2 and let split the state space into two disjoint sets, Ω and Ω' where:

- Ω is the region where $\ell_0 \leq 0$.
- Ω' is the complement of Ω, i.e., the set where $\ell_0 > 0$.

With this separation, the discussion on the boundedness of $\overline{\mathbf{z}}$ is divided into two parts. First, in the region Ω by Definition 1.2, the norm of the field is bounded by the parameter ϱ. The boundedness of $\overline{\mathbf{z}}$ on the second part (region Ω') is more complicated to prove. To that purpose, consider the function $a(\mathbf{z})$ of Section 1.3 and let us define a new convex function $b(\mathbf{z}, \mathbf{z}^*) : \mathscr{Z} \times \mathscr{Z} \to \mathbb{R}^+ \cup \{0\}$ as in Eqn (1.30).

Lemma 3.1 *Under Condition 1.1, system (1.40) is passive with respect to an output* $y = \overline{\mathbf{A}}$ *and an input* $\mathfrak{u} = \overline{\mathbf{u}} + \mu y$*. In particular, for the region* Ω' *and* $\mu = 0$*, one has that:*

$$\mathcal{B}(\overline{\mathbf{z}}(T)) \leq \mathcal{B}(\overline{\mathbf{z}}(0)) + \int_0^T \langle \overline{\mathbf{A}}, \overline{\mathbf{u}} \rangle_{\mathscr{Y}} dt. \tag{3.17}$$

where $\mathcal{B}(\overline{\mathbf{z}}(t))$ *denote the spatial integral of* $b(\overline{\mathbf{z}}, \overline{\mathbf{z}}^*)$.

For the sake of clarity, the proof of this lemma is included in Appendix B.1. Lemma 3.1 implies that function $\mathcal{B}(\overline{\mathbf{z}}(T))$ is bounded for all $T > 0$, provided that the controls are bounded so that $\int_0^T \langle \overline{\mathbf{A}}, \overline{\mathbf{u}} \rangle_{\mathscr{V}} dt < \infty$. On the other hand, as it was demonstrated in Alonso and Ydstie (2001), function $b(\mathbf{z}; \mathbf{z}^*)$ is bounded by the field as indicated in expression (1.31) which is rewritten here for the sake of clarity:

$$q_0 \|\mathbf{z} - \mathbf{z}^*\|^2 \leq b(\mathbf{z}; \mathbf{z}^*) \leq q_1 \|\mathbf{z} - \mathbf{z}^*\|^2, \qquad \text{with} \quad \|\mathbf{z} - \mathbf{z}^*\|^2 = (\mathbf{z} - \mathbf{z}^*)^T (\mathbf{z} - \mathbf{z}^*),$$

and where q_0 and q_1 are strictly positive constants. Integrating this inequality over the spatial domain, the following bound in the $\mathcal{L}_2$ norm is obtained: $\|\overline{\mathbf{z}}\|^2_{\mathscr{V}} \leq \mathcal{B}/q_0 < \infty$. Thus, $\overline{\mathbf{z}}$ can be expanded as an infinite convergent series.

Boundedness of the convective term

As shown in Appendix B.1 the derivatives of $\mathcal{B}$ along the trajectories (1.40) satisfy:

$$\dot{\mathcal{B}} = \langle \overline{\mathbf{A}}, \Delta \overline{\Gamma} \rangle_{\mathscr{V}} - \langle \overline{\mathbf{A}}, \overrightarrow{\boldsymbol{\nabla}} \cdot (\overline{\mathbf{v}} \overline{\mathbf{z}}) \rangle_{\mathscr{V}} - L_\mu + \langle y, \mathfrak{p} \rangle_{\mathscr{V}}.$$

Since, as shown in Appendix (B.1), the convective term in the previous equation is non positive, one is led to:

$$\dot{\mathcal{B}} \leq -\langle \overrightarrow{\boldsymbol{\nabla}} \overline{\mathbf{A}}, \mathbf{L}(\mathbf{A}) \overrightarrow{\boldsymbol{\nabla}} \overline{\mathbf{A}} \rangle_{\mathscr{V}} - L_\mu + \langle y, \mathfrak{u} \rangle_{\mathscr{V}} \Rightarrow$$

$$\mathcal{B}(\mathbf{z}(T)) - \mathcal{B}(\mathbf{z}(0)) \leq -\int_0^T \langle \overrightarrow{\boldsymbol{\nabla}} \overline{\mathbf{A}}, \mathbf{L}(\mathbf{A}) \overrightarrow{\boldsymbol{\nabla}} \overline{\mathbf{A}} \rangle_{\mathscr{V}} dt + \int_0^T (-L_\mu + \langle y, \mathfrak{u} \rangle_{\mathscr{V}}) dt. \tag{3.18}$$

$\mathbf{L}(\mathbf{A})$ is positive definite and therefore there exists a constant $\delta_1 > 0$ such that $\delta_1 \|\overrightarrow{\boldsymbol{\nabla}} \overline{\mathbf{A}}\|^2_{\mathscr{V}} \leq \langle \overrightarrow{\boldsymbol{\nabla}} \overline{\mathbf{A}}, \mathbf{L}(\mathbf{A}) \overrightarrow{\boldsymbol{\nabla}} \overline{\mathbf{A}} \rangle_{\mathscr{V}}$. With this inequality Eqn (3.18) can be rewritten as:

$$\delta_1 \|\overrightarrow{\boldsymbol{\nabla}} \overline{\mathbf{A}}\|^2_{\mathscr{V}} \leq \mathcal{B}(\mathbf{z}(0)) - \mathcal{B}(\mathbf{z}(T)) + \int_0^T (-L_\mu + \langle y, \mathfrak{u} \rangle_{\mathscr{V}}) ds.$$

Since the RHS is bounded for $\mu = 0$ (see Appendix B.1) it follows that $\|\overrightarrow{\boldsymbol{\nabla}} \overline{\mathbf{A}}\|^2_{\mathscr{V}} < \infty$ and $\overrightarrow{\boldsymbol{\nabla}} \cdot (\overline{\mathbf{v}} \overline{\mathbf{z}}) < \infty$.

Boundedness of the nonlinear terms $\overline{\mathbf{f}}$

As stated in Condition 1.1, the production terms $\overline{\mathbf{f}}$ are Lipschitz so they are bounded by the field and thus they belong to $\mathcal{L}_2$.

Boundedness of the Kirchhoff term

The systems considered in this work will satisfy a relation of the type:

$$\langle\overline{\mathbf{\Gamma}},\overline{\mathbf{\Gamma}}\rangle_{\mathscr{V}} = \|\overline{\mathbf{\Gamma}}\|^2_{\mathscr{V}} \leq k_1^2\|\overline{\mathbf{A}}\|^2_{\mathscr{V}},$$

where k_1 is a given positive parameter. In this way, function $\overline{\mathbf{\Gamma}}$ can also be expanded in infinite series of the form (3.14).

Boundedness of the control terms

This restriction was already imposed to show that the field was bounded. The control inputs considered are then restricted to those bounded in the $\mathcal{L}_2$ norm ($\|\overline{\mathbf{u}}\|^2_{\mathscr{V}} < \infty$).

Note that the restrictions just described are satisfied by most of chemical reactions, fluid dynamics or biological distributed systems. Now the following lemma useful in further computations is introduced.

Lemma 3.2 *Projections of the different terms of Eqn (1.40) over the subfield $\overline{\mathbf{A}}_b$ satisfy the following relations:*

1. $\langle\overline{\mathbf{A}}_b, \frac{\partial\overline{\mathbf{z}}}{\partial t}\rangle_{\mathscr{V}} = \boldsymbol{\alpha}_b^T\frac{d\mathbf{m}_b}{dt}$.
2. $\langle\overline{\mathbf{A}}_b, \Delta\overline{\Gamma}\rangle_{\mathscr{V}} \leq -\zeta\lambda_\ell\boldsymbol{\alpha}_b^T\boldsymbol{\alpha}_b$.
3. $-\langle\overline{\mathbf{A}}_b, \overrightarrow{\boldsymbol{\nabla}}\cdot(\overrightarrow{\mathbf{v}}\overline{\mathbf{z}})\rangle_{\mathscr{V}} \leq 0$.
4. $\langle\overline{\mathbf{A}}_b, \overline{\mathbf{f}}\rangle_{\mathscr{V}} \leq \mu\boldsymbol{\alpha}_b^T\boldsymbol{\alpha}_b$.

where the vectors $\boldsymbol{\alpha}_b$ and $\mathbf{m}_b$ are of the form: $\boldsymbol{\alpha}_b = [\boldsymbol{\alpha}_b^1, \boldsymbol{\alpha}_b^2, ..., \boldsymbol{\alpha}_b^n]^T$ and $\mathbf{m}_b = [\mathbf{m}_b^1, \mathbf{m}_b^2, ..., \mathbf{m}_b^n]^T$. The elements inside the former vectors correspond with $\boldsymbol{\alpha}_b^i = [\alpha^i_{\mathcal{N}_b(1)}, \alpha^i_{\mathcal{N}_b(2)}, ...]^T$ and $\mathbf{m}_b^i = [m^i_{\mathcal{N}_b(1)}, m^i_{\mathcal{N}_b(2)}, ...]^T$. The parameters on the RHS of the previous relations are: $\lambda_\ell = \min_{\mathscr{L}_b}(\lambda(\Delta))$, $\zeta = \min_{\overline{\mathbf{A}}}\inf_i[\lambda_i(\mathbf{L})]$.

The proof of this lemma is included in Appendix B.2. On the other hand, the following Proposition establishes the conditions for constructing low dimensional approximations of dissipative systems. This is, the proposition states that dissipative systems evolve towards finite dimensional hyperplanes and remain in them in the future.

Proposition 3.1 *Consider a particular subset $(\mathscr{E}_a, \mathscr{L}_a, \mathcal{N}_a)$ as that containing the p smallest eigenvalues and their associated eigenfunctions. Then, if p is large enough, the subfield $\overline{\mathbf{z}}_b$ associated with the subset $(\mathscr{E}_b, \mathscr{L}_b, \mathcal{N}_b)$ is exponentially stable. In addition, the larger the value of p, the faster the exponential decaying of the dynamic modes of the stable subsystem.*

The proof of this proposition, which uses the relations of Lemma 3.2, can be found in Appendix B.3. As a consequence of the fast decaying of the modes belonging to the set $(\mathscr{E}_b, \mathscr{L}_b, \mathcal{N}_b)$, the series expansion (3.10) can be truncated to obtain an approximated solution of the form:

$$\overline{\mathbf{z}}(\xi,t) \approx \widetilde{\mathbf{z}}(\xi,t) = \sum_{i\in\mathcal{N}_a} \mathbf{m}_i(t)\phi_i(\xi), \tag{3.19}$$

which constitutes the basis for the reduced order model (ROM) development (Shvartsman and Kevrekidis, 1998; Alonso et al., 2004b). Usually the number of modes necessary to obtain a good approximation is much lower than the number of equations required in classical methods such as *finite elements* or *finite differences*. This property will be employed to derive the control laws in subsequent chapters.

The ROM is obtained following the steps of other MWR. This is by projecting PDE (1.40) over the eigenfunctions belonging to the set $\mathscr{E}_a$ so that:

$$\langle \Phi_a, \frac{\partial \overline{\mathbf{z}}}{\partial t}\rangle_{\mathscr{V}} + \langle \Phi_a, \overrightarrow{\overline{\boldsymbol{\nabla}}} \cdot (\overrightarrow{\overline{\mathbf{v}}}\overline{\mathbf{z}})\rangle_{\mathscr{V}} = \langle \Phi_a, \Delta\overline{\boldsymbol{\Gamma}}\rangle_{\mathscr{V}} + \langle \Phi_a, \overline{\mathbf{f}}\rangle_{\mathscr{V}} + \langle \Phi_a, \overline{\mathbf{u}}\rangle_{\mathscr{V}}, \tag{3.20}$$

with $\Phi_a = [\phi_{\mathcal{N}_a(1)}, ..., \phi_{\mathcal{N}_a(p)}]$. Applying expressions (3.10)-(3.15) to Eqn (3.20), one has that:

$$\langle \Phi_a, \sum_{i\in\mathcal{N}_a} \phi_i \frac{d\mathbf{m}_i}{dt} + \sum_{i\in\mathcal{N}_b} \phi_i \frac{d\mathbf{m}_i}{dt}\rangle_{\mathscr{V}} + \langle \Phi_a, \sum_{i\in\mathcal{N}_a} \phi_i \boldsymbol{\tau}_i + \sum_{i\in\mathcal{N}_b} \phi_i \boldsymbol{\tau}_i\rangle_{\mathscr{V}} =$$

$$-\langle \Phi_a, \sum_{i\in\mathcal{N}_a} \phi_i\lambda_i\boldsymbol{\gamma}_i + \sum_{i\in\mathcal{N}_b} \phi_i\lambda_i\boldsymbol{\gamma}_i\rangle_{\mathscr{V}} + \langle \Phi_a, \sum_{i\in\mathcal{N}_a} \phi_i\boldsymbol{\sigma}_i + \sum_{i\in\mathcal{N}_b} \phi_i\boldsymbol{\sigma}_i\rangle_{\mathscr{V}} + \langle \Phi_a, \sum_{i\in\mathcal{N}_a} \phi_i\boldsymbol{\pi}_i + \sum_{i\in\mathcal{N}_b} \phi_i\boldsymbol{\pi}_i\rangle_{\mathscr{V}}.$$

Finally, and since the eigenfunctions are orthonormal, the previous expression becomes:

$$\frac{d\mathbf{m}_a}{dt} = -\Lambda_a\boldsymbol{\gamma}_a - \boldsymbol{\tau}_a + \boldsymbol{\sigma}_a + \boldsymbol{\pi}_a,$$

where Λ_a is a diagonal matrix containing the eigenvalues of the set $\mathscr{L}_a$ and $\boldsymbol{\gamma}_a$, $\boldsymbol{\tau}_a$, $\boldsymbol{\sigma}_a$ and $\boldsymbol{\pi}_a$ are the time dependent vector functions employed in Eqns (3.10)-(3.15).

The global spatial dependent functions in Eqn (3.19) were obtained by solving the eigenvalue problem (3.3). It must be pointed out that alternative functions such as the PODs could be employed in the approximation.

In order to illustrate and to compare the reduced order techniques two simple examples will be employed. The first one is the well-known Fourier problem with homogeneous BC. The second consists on a 1D reaction-diffusion equation.

Example 3.1 (The Fourier Problem) *Consider the Fourier equation in the 1D spatial domain $\mathscr{V} = [0,1]$:*

$$\frac{\partial z}{\partial t} = \kappa\Delta z, \tag{3.21}$$

with $\kappa = 0.1$ *and initial and homogeneous boundary conditions of the form:*

$$z(\xi,0) = 5\left(\frac{\xi^2}{2} - \frac{\xi^4}{4}\right) + 1; \quad \vec{\mathbf{n}}\cdot\vec{\boldsymbol{\nabla}} z(0,t) = \vec{\mathbf{n}}\cdot\vec{\boldsymbol{\nabla}} z(1,t) = 0.$$

Note that this example coincides with Eqn (2.30) and has been solved both analytically and numerically by using the FEM matrices in Section 2.3.2.

Solution with the LSD approach

The basis functions are obtained by solving Eqn (3.3). It should be remarked that in this particular case they can be obtained either analytically

$$\phi_i(\xi) = \begin{cases} \cos\left((i-1)\pi\xi\right) & \textit{for} \quad i = 1 \\ -1^{i-1}\sqrt{2}\cos\left((i-1)\pi\xi\right) & \textit{for} \quad i = 2,3,4,... \end{cases} ; \quad \lambda_i = (i-1)^2\pi^2,$$

or by using the FEM matrices (see Table 2.2) so that:

$$\Delta\phi_i = -\lambda_i\phi_i \Longleftrightarrow \mathcal{D}\mathcal{A}^{-1}\mathcal{C}\boldsymbol{\phi}_i = -\lambda_i\boldsymbol{\phi}_i. \tag{3.22}$$

In Figure 3.2 the first four basis functions obtained analytically (lines) and numerically (marks) with the FEM matrices and 31 discretisation points are plotted. In addition, in

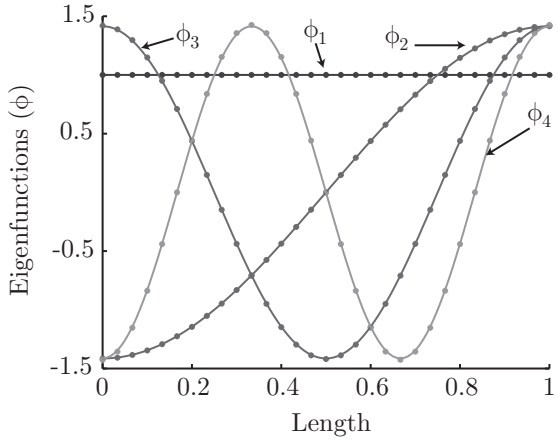

Figure 3.2: Comparison between the eigenfunctions obtained analytically (lines) and numerically (marks).

Table 3.1 the first four eigenvalues obtained analytically and numerically with different levels of discretisation are shown. The Figure and the Table show good agreement between the numerical and the analytical results. The quality of the approximation increases with the number of discretisation points.

	Analytical	**Numerical**		
N. Discret. points	–	61	31	16
λ_1	0	$\sim 10^{-12}$	$\sim 10^{-12}$	$\sim 10^{-12}$
λ_2	9.8696	9.8718	9.8786	9.9057
λ_3	39.4784	39.5145	39.6229	40.0589
λ_4	88.8264	89.0092	89.5593	91.7855

Table 3.1: Comparison between the eigenvalues obtained analytically and numerically with the FEM matrices with different levels of discretisation.

Now, the solution $z(\xi,t)$ is approximated by a series of the form (3.19), thus Eqn (3.21) reads:

$$\sum_{i=1}^{p} \phi_i \frac{dm_i}{dt} = \kappa \sum_{i=1}^{p} m_i \Delta\phi_i.$$

In order to obtain a system of ODEs representing the time evolution of the modes m_i, this equation is multiplied by each eigenfunction and the result is integrated over the spatial domain (MWR) to obtain:

$$\frac{dm_i}{dt} = \kappa \sum_{i=1}^{p} m_i \int_{\mathscr{V}} \phi_i^T \Delta\phi_i d\xi = -\kappa m_i \lambda_i \qquad with \;\; i = 1, 2, .., p.$$

The time evolution of the first six modes ($p = 6$) is represented in Figure 3.3. The

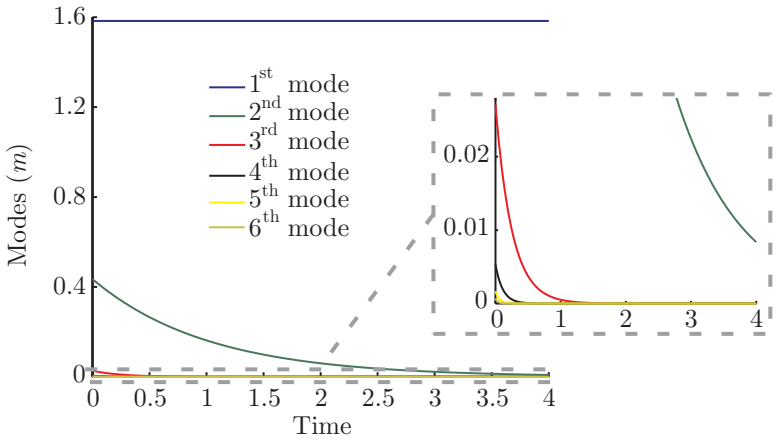

Figure 3.3: Evolution of the first six modes, computed with the LSD method, in the Fourier problem.

picture shows that the first three modes are much more important than the remaining so using $p = 3$ should be enough to accurately represent the solution $z(\xi,t)$. Note also, in the augmented image, that the contribution of the third mode can be neglected beyond

$t = 1$. *If the simulation is performed to* $t = 10$ *one could see that even the second mode can be also neglected after* $t = 8$.

So far the eigenfunctions and the weighting parameters (modes) of approximation (3.19) were obtained so the solution $z(\xi, t)$ *can be now recovered. Figure 3.4 (a) shows the evolution and distribution of* $z(\xi, t)$ *obtained by means of the LSD method with* $p = 3$ *modes. This solution is close to the analytical one (see Section 2.3.2). In fact*

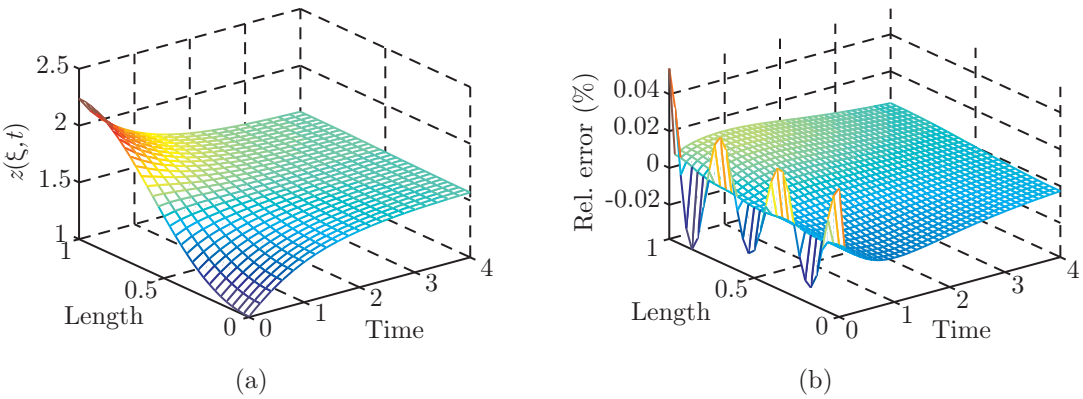

Figure 3.4: (a) Numerical solution to the Fourier equation with the LSD with 3 terms. (b) Relative error between the LSD ($p = 3$) and the analytical solution.

the relative error between the analytical result and the LSD is never larger than 0.054%[1] *(Figure 3.4 (b)) being the absolute error lower than* 1.2×10^{-3} *and both absolute and relative errors decrease very fast with time. Most of the contribution to the error at the first times is due to the fourth mode which was neglected. Note that this mode is very small as compared with the firsts three, but it is enough to alter the fourth decimal number of the solution. It should be highlighted that when this mode vanishes at* $t > 0.3$ *(Figure 3.3), the error in the LSD, approaches to the error in the FEM.*

Solution with the POD approach

As pointed out before, the first step to obtain the PODs basis is the construction of a representative set of data. In this example such set will be obtained from the FEM simulation of system (3.21). To that purpose the time domain $t = [0, 4]$ *is divided into three parts. This separation is based on the dynamic behaviour of the system:*

- *First interval* $t = [0, 0.5]$. *In this part, the changes in the dynamic behaviour are more appreciable so the time interval* (δt) *between two consecutive measurements should be lower than in the rest of the time domain. In this case* $\delta t = 0.02$.

[1]Note that this implies that the differences between the analytical and the LSD solutions appear in the third decimal number.

- *Second interval* $t = (0.5, 2]$. *The dynamics approximates to the steady state so the measurement interval may be larger than in the previous case* $\delta t = 0.1$.

- *Third interval* $t = (2, 4]$. *This part corresponds with the evolution of the system close to the steady state. A couple of measurements here are enough* ($\delta t = 0.5$).

The PODs basis are now computed by following the methodology described in Section 3.4.2. Figure 3.5 (a) shows the shape of the four more representative PODs while the energy captured (see Eqn 3.9) when employing different numbers of PODs is depicted in Figure 3.5 (b). As shown in the Figure, three PODs are able to capture more than

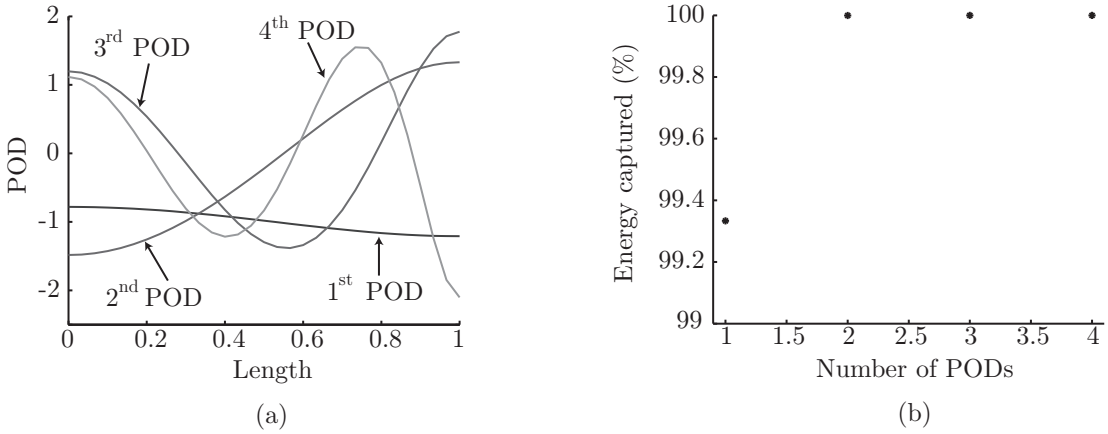

Figure 3.5: (a) Shape of the four more representative PODs basis functions. (b) Energy captured by the PODs

the 99.99% *of the energy. Note that, as in the case of the LSD functions, the number of spatial oscillations in the PODs decreases when the POD becomes more representative (i.e. more energy is captured). In general, the number of spatial oscillations can be employed to determine their contribution to the behaviour in a qualitative manner. Projecting Eqn (3.21) over the p more representative PODs results:*

$$\frac{d\mathbf{m}}{dt} = \kappa \mathcal{A}\mathbf{m} \tag{3.23}$$

where $\mathbf{m} = [m_1, ..., m_p]^T$ *and* $\mathcal{A}$ *is the projection of the Laplacian of the PODs over the PODs, that is:*

$$\mathcal{A} = \int_{\mathscr{V}} \Phi^T \Delta \Phi d\xi \approxeq -\mathbf{\Phi}^T \mathcal{C} \mathbf{\Phi},$$

where $\Phi = [\phi_1(\xi), ..., \phi_p(\xi)]$ *and* $\mathbf{\Phi} = [\boldsymbol{\phi}_1, ..., \boldsymbol{\phi}_p]$ *with* $\boldsymbol{\phi}_i$ *being the discrete counterpart of the PODs. The time evolution of the firsts six modes* ($p = 6$) *is represented in Figure 3.6. The plot shows that, as in the LSD case, the firsts three modes are much*

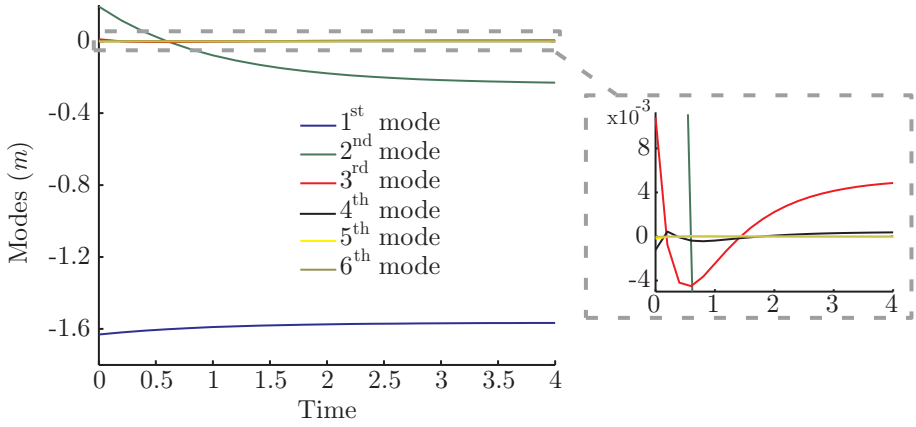

Figure 3.6: Evolution of the first six modes, computed using the POD method, in the Fourier problem.

more important than the remaining, thus using $p = 3$ should be enough to accurately represent the solution $z(\xi, t)$. In this case, the contribution of the fourth mode is less important than in the LSD at the beginning ($t < 0.3$).

Since both the PODs and the modes were computed, the solution $z(\xi, t)$ - see Figure 3.7 (a)- can be recovered by using Eqn (3.19). In this case the relative error between

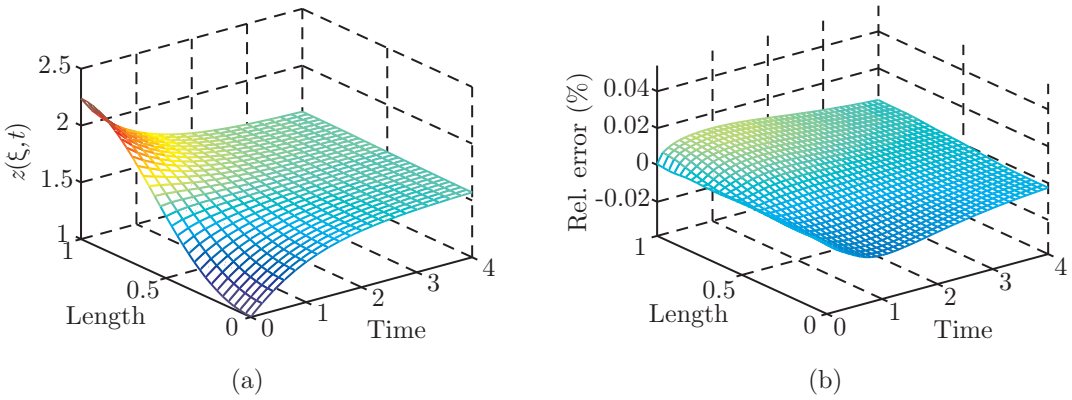

Figure 3.7: (a) Numerical solution to the Fourier equation computed with the POD method ($p = 3$). (b) Relative error between the POD and the analytical solution.

the ROM and the analytical solution (Figure 3.7 (b)) is never larger than 0.0147%. *This result is better than the LSD at the first times of the simulation and is quite near to the FEM error. This is in agreement with the mode evolution (Figure 3.6). The contribution of the fourth mode to the solution is much lower than in the LSD case. This is particularly true at the beginning ($t < 0.3$). In fact, in the POD, the relative magnitude between the first and the fourth modes is around 1500 while in the LSD case*

this relation reduces to 500. In general, using the same number of elements the POD method will result into a better approximation than the LSD.

Comparison between the FEM, LSD and POD methods

Table 3.2 shows the computational time required to solve problem (3.21) with the FEM, LSD and POD methods. In all cases, the simulation runs from $t = 0$ to $t = 4$ with a

Method	FEM		LSD		POD	
N. Eqns	31		3		3	
IVP	BDF	Adams	BDF	Adams	BDF	Adams
CPU Time (s)	4.34	0.60	0.31	0.15	0.31	0.15

Table 3.2: Computation time employed in the FEM, LSD and POD techniques.

time interval $\delta t = 0.005$. As illustrated in the Table, the ROMs are able to reduce in one order of magnitude the computational time required by the FEM.

□

In order to show the importance of an adequate selection of the set of data for computing the PODs, a system with different behaviours will be considered next.

Example 3.2 (1D Reaction-Diffusion System) *In this example, known as the* brusselator*, a system in which a number of reversible reactions take place is considered. There are six species (A, B, C, D, Z_1, Z_2) and four reactions of the form (Nicolis and Nicolis, 1999):*

$$A \rightleftarrows Z_1; \qquad Z_1 \rightleftarrows C; \qquad B + Z_1 \rightleftarrows D + Z_2; \qquad 2Z_1 + Z_2 \rightleftarrows 3Z_1.$$

Assuming that the concentrations of species A, B, C and D can be maintained at a constant value, the following model equations are obtained:

$$\frac{\partial z_1}{\partial t} = \kappa \Delta z_1 + f(z_1, z_2); \quad f(z_1, z_2) = a + c - (b+2)z_1 + dz_2 + z_1^2 z_2 - z_1^3 \tag{3.24}$$

$$\frac{\partial z_2}{\partial t} = \kappa \Delta z_2 + g(z_1, z_2); \quad g(z_1, z_2) = bz_1 - dz_2 - z_1^2 z_2 + z_1^3 \tag{3.25}$$

where a, b, c, d, z_1 and z_2 represent the concentrations of the species A, B, C, D, Z_1 and Z_2 respectively and κ is the diffusion coefficient. Boundary and initial conditions are of the form:

$$\vec{\mathbf{n}} \cdot \kappa \vec{\boldsymbol{\nabla}} z_i(0,t) = -z_i(0,t); \qquad \vec{\mathbf{n}} \cdot \vec{\boldsymbol{\nabla}} z_i(L,t) = 0; \quad z_i(\xi, 0) = z_{i0}; \quad i = 1, 2. \tag{3.26}$$

Solution with the FEM approach

Depending on the value of the parameters, this system can exhibit different dynamical behaviours (steady states, limit cycles,...). In order to illustrate this point, the FEM matrices are employed to solve system (3.24) - (3.26), so that we obtain:

$$\frac{d\mathcal{Z}_1}{dt} = -\mathcal{D}\mathcal{A}^{-1}(\kappa\mathcal{C} + \mathcal{Q})\mathcal{Z}_1 + \mathcal{F} \tag{3.27}$$

$$\frac{d\mathcal{Z}_2}{dt} = -\mathcal{D}\mathcal{A}^{-1}(\kappa\mathcal{C} + \mathcal{Q})\mathcal{Z}_2 + \mathcal{G} \tag{3.28}$$

where $\mathcal{Z}_1$, $\mathcal{Z}_2$, $\mathcal{F}$ and $\mathcal{G}$ are the FEM discrete versions of the states z_1, z_2 and nonlinear functions $f(z_1, z_2)$ and $g(z_1, z_2)$, respectively. Consider now that the parameters a and b can be modified and the remaining have the following values: $L = 1$, $\kappa = 0.1$, $d = 0.5$ and $b = 16$. Figure 3.8 (a) shows the evolution of $\mathcal{Z}_1$ with $a = c = 0.1$ and initial conditions $z_{10} = z_{20} = 0.05(\xi^2/2 - \xi^4/4)$. As one can see in the Figure, a stable steady

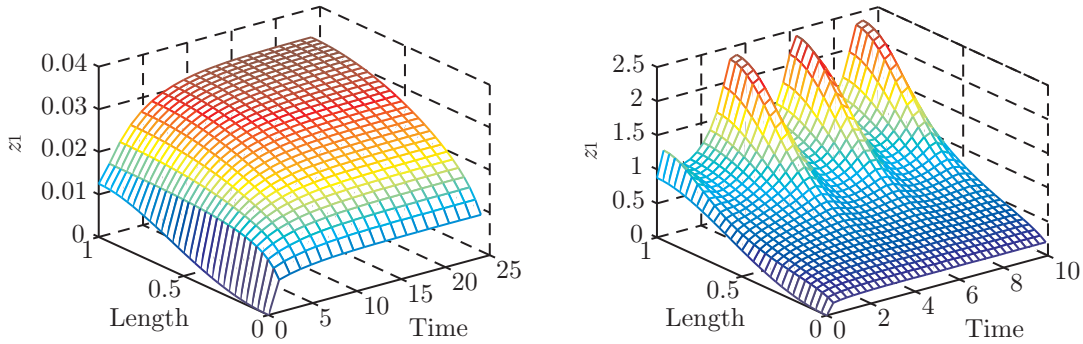

Figure 3.8: Numerical solution of system (3.24) - (3.26) (a) with $a = c = 0.1$, (b) with $a = c = 2.1$.

state is reached after a transition period. On the other hand, choosing $a = c = 2.1$ and initial conditions $z_{10} = 3.5(\xi^2/2 - \xi^4/4)$ and $z_{20} = 50(\xi^2/2 - \xi^4/4)$ the system evolves in the form of a limit cycle as shown in Figure 3.8 (b).

Solution with the LSD approach

The first step is to obtain the basis functions resulting from the eigenvalue problem (3.3). As indicated before, this step can be carried out in a straightforward manner by using the FEM matrices, so that:

$$\mathcal{D}\mathcal{A}^{-1}(\kappa\mathcal{C} + \mathcal{Q})\boldsymbol{\phi}_i = -\lambda_i\boldsymbol{\phi}_i.$$

In this case, since Robin boundary conditions are considered in the first point ($\xi = 0$), the FEM matrix $\mathcal{Q}$ must be included into the problem. The four more representative eigenfunctions with their corresponding eigenvalues are plotted in Figure 3.9.

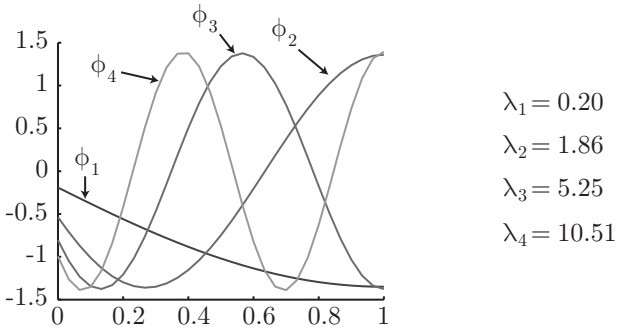

Figure 3.9: The four most representative eigenfunctions on a 1D problem with homogeneous Robin ($\xi = 0$) and Neumann ($\xi = 1$) boundary conditions.

The same procedure applied in the former example is employed here. Projecting Eqns (3.27) - (3.28) over the p most representative eigenfunctions one is led to:

$$\frac{d\mathbf{m}_{z_1}}{dt} = -\Lambda \mathbf{m}_{z_1} + \int_{\mathscr{V}} \Phi^T f d\xi,$$

$$\frac{d\mathbf{m}_{z_2}}{dt} = -\Lambda \mathbf{m}_{z_2} + \int_{\mathscr{V}} \Phi^T g d\xi,$$

where $\mathbf{m}_{z_i}$ is a vector containing the p most representative modes of the field z_i, Λ is a diagonal matrix with the eigenvalues as elements and $\Phi = [\phi_1, \phi_2, ..., \phi_p]$. The integrals in the previous equations are computed using the $\mathcal{DA}$ FEM matrix so that $\int_{\mathscr{V}} \Phi^T h d\xi \approx \mathbf{\Phi}^T \mathcal{DAH}$ where h can be either f or g, and $\mathbf{\Phi}$ and $\mathcal{H}$ are the discrete versions of Φ and h. Initial conditions for this system are computed as:

$$\mathbf{m}_{z_1}(0) = \mathbf{\Phi}^T \mathcal{DAZ}_{10}; \qquad \mathbf{m}_{z_2}(0) = \mathbf{\Phi}^T \mathcal{DAZ}_{20}.$$

The evolution of the three most representative modes for the steady state behaviour and limit cycle is shown in Figures 3.10 (a) and (b), respectively. These figures were obtained using seven eigenfunctions ($p = 7$). Continuous lines represent the modes obtained with the FEM scheme while marks corresponds with the LSD computation. As one can see, both representations coincide. This is also verified when recovering the fields from the modes and the PODs ($\mathcal{Z}_i = \mathbf{\Phi}\mathbf{m}_{z_i}$) as shown in Figures 3.11 (a) ($a = c = 0.1$) and 3.11 (b) ($a = c = 2.1$).

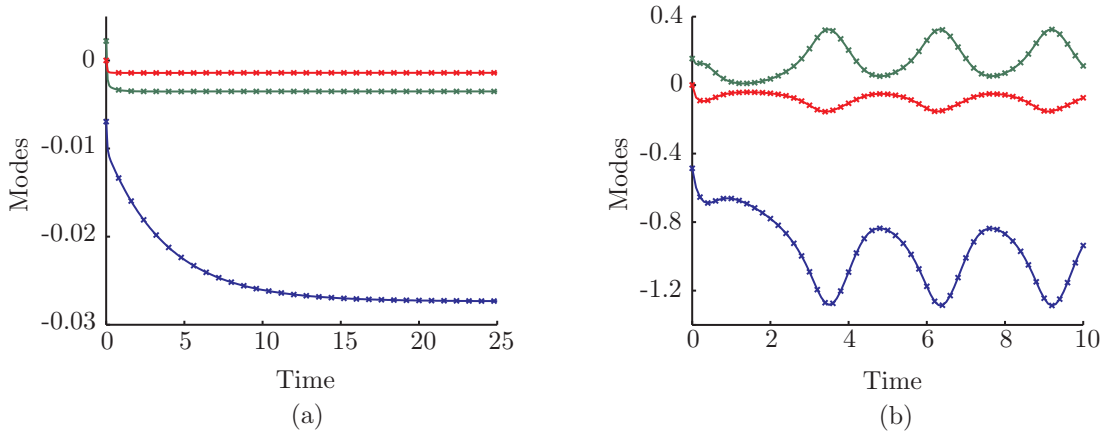

Figure 3.10: Evolution of the three most representative modes for system (3.24)-(3.25) using the basis of the LSD approach (a) with $a = c = 0.1$, (b) with $a = c = 2.1$. Lines and marks correspond, respectively, with the modes of the FEM and LSD solutions.

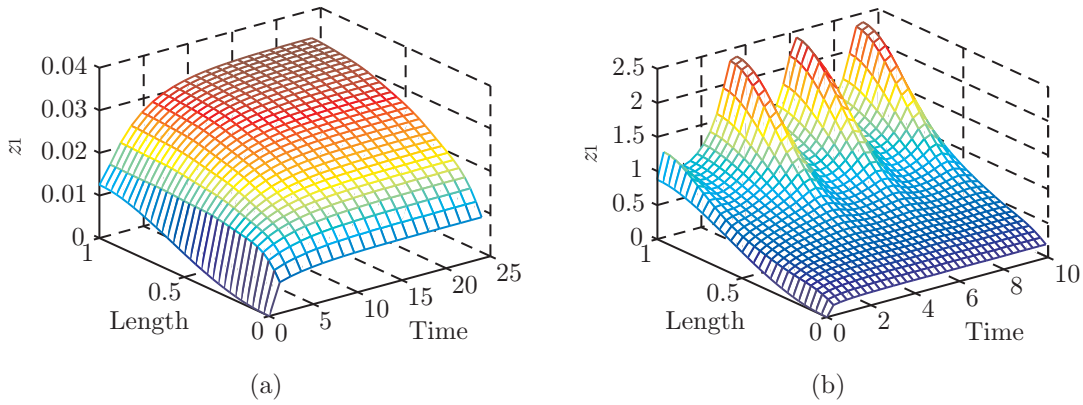

Figure 3.11: Numerical solution of system (3.24) - (3.25) using the LSD approach (a) with $a = c = 0.1$, (b) with $a = c = 2.1$.

Solution with the POD approach

In order to show that the selection of the data set is a key step in the POD approach, in this example, the snapshots will be taken only from the simulation of the first behaviour ($a = c = 0.1$) and close to the steady state. Once the data set is constructed, the PODs can be obtained following the procedure described in Section 3.4.2. Now, projecting Eqns (3.24) - (3.26) over the PODs one is led to:

$$\frac{d\mathbf{m}_{z_1}}{dt} = -\mathcal{A}_{z_1}\mathbf{m}_{z_1} + \int_{\mathscr{V}} \Phi_{z_1}^T f d\xi; \qquad \frac{d\mathbf{m}_{z_2}}{dt} = -\mathcal{A}_{z_2}\mathbf{m}_{z_2} + \int_{\mathscr{V}} \Phi_{z_2}^T g d\xi,$$

where $\mathcal{A}_{z_i}$ results from the projection of the Laplacian over the PODs, this is $\mathcal{A}_{z_i} = \kappa \int_{\mathscr{V}} \Phi_{z_1} \Delta \Phi_{z_1} d\xi$ and the integrals are computed as in the previous example. The initial

conditions are computed as:

$$\mathbf{m}_{z_1}(0) = \mathbf{\Phi}_{z_1}^T \mathcal{DAZ}_1(0); \qquad \mathbf{m}_{z_2}(0) = \mathbf{\Phi}_{z_2}^T \mathcal{DAZ}_2(0).$$

In this case using 4 PODs is enough to describe the steady state behaviour ($a = c = 0.1$) as shown in Figure 3.12 (a). However, the limit cycle cannot be reproduced neither

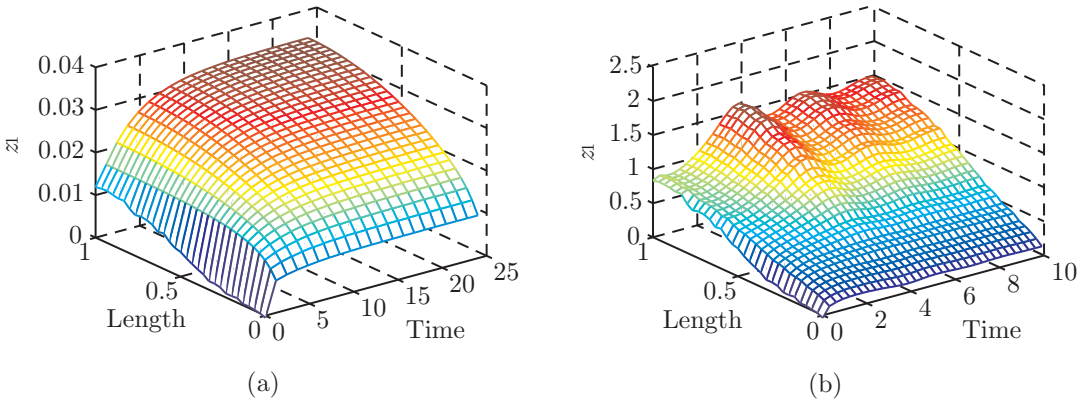

Figure 3.12: Numerical solution of system (3.24) - (3.25) using the POD approach (a) with $a = c = 0.1$, (b) with $a = c = 2.1$.

using 7 PODs (Figure 3.12 (b)) nor using the complete set (Figure 3.13 (a)), thus illustrating that the selection of the data set for the construction of the PODs is a determining factor in the derivation of the ROM. The FEM and the POD approaches

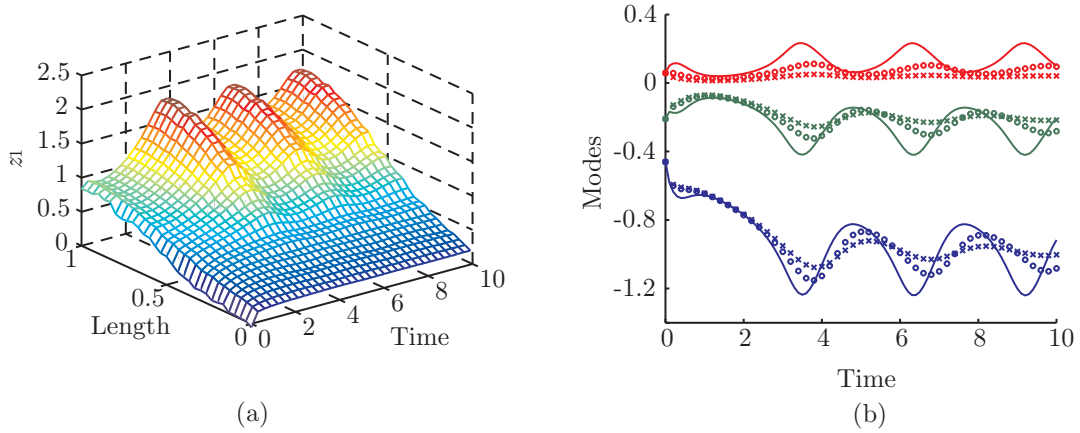

Figure 3.13: (a) Evolution of of system (3.24) - (3.25) using the POD approach. (b) Evolution of the three most representative modes obtained from the FEM (continuous lines) and from two different ROMs (marks).

are also compared in terms of the modes. In Figure 3.13 (b) continuous lines represent

the modes obtained with the FEM while marks are related to the POD. Although using the complete set (circles) improves the results of the ROM with seven PODs (crosses), none of them are adequate to represent the limit cycle.

Comparison between the FEM, LSD and POD methods

The computational effort required for solving problem (3.24) - (3.26) with the FEM, LSD and POD methods is represented in Table 3.3 for the steady state solution and Table 3.4 for the limit cycle behaviour. The simulation when $a = c = 0.1$ *runs from* $t = 0$ *to* $t = 25$ *with a time interval* $\delta t = 0.02$*. On the other hand, when* $a = c = 2.1$ *the final time is* $t = 10$*. As shown in the Tables, the computational time can be reduced in one order of magnitude when using ROMs.*

Method	FEM		LSD		POD	
N. Eqns	31×2		7×2		4×2	
IVP Solver	BDF	Adams	BDF	Adams	BDF	Adams
CPU Time (s)	22.8	12.1	3.8	0.6	2.9	3.6

Table 3.3: Computation required by the FEM, LSD and POD techniques for solving system (3.24) - (3.26) with $a = c = 0.1$.

Method	FEM		LSD		POD	
N. Eqns	31×2		7×2		7×2	
IVP Solver	BDF	Adams	BDF	Adams	BDF	Adams
CPU Time (s)	18.8	5.3	3.1	0.5	2.6	2.3

Table 3.4: Computation required by the FEM, LSD and POD techniques for solving system (3.24) - (3.26) with $a = c = 2.1$.

□

In general, when the differences in terms of number of equations between the LSD and the POD are not significant, it may result more convenient to use the LSD since it can be employed in a wider range of conditions.

Chapter 4

The Robust Control of Distributed Processes

4.1 Introducción

El primer paso para controlar un sistema es disponer de una representación del mismo. Las capacidades predictivas del modelo determinarán en parte la calidad del control. Debido a fuentes de error como incertidumbre en los parámetros, simplificaciones del modelo o perturbaciones no medidas, en el mundo real los modelos son sólo aproximaciones de los sistemas de forma que la misma entrada puede producir distintas salidas en el modelo y en la planta real. El *control robusto* es la parte de la teoría de control que trata con la incertidumbre en los modelos. Por otra parte, los sistemas considerados en este trabajo, tienen una naturaleza no lineal. Los primeros intentos para tratar el control de procesos con comportamiento no lineal fueron mediante aproximaciones del modelo utilizando una versión lineal sobre la que se pudiese aplicar los controladores convencionales PID. Sin embargo, este enfoque sólo es efectivo con términos no lineales muy suaves y cuando se trabaja cerca del estado estacionario nominal. En el resto de los casos, el ajuste de los controladores PID tiene que ser muy conservativo llevando a la degradación de la realización del control (Seborg and Henson, 1997). La técnicas de control no lineal no sólo mejoran las lineales y nos permite analizar términos no lineales abruptos sino que además nos permite tratar con la incertidumbre de los modelos e incluso pueden resultar en un diseño más simple que la versión lineal (Slotine and Li, 1991). El objetivo de este capítulo es diseñar una lógica de control capaz de conducir los estados de un sistema no lineal distribuido a la referencia deseada incluso

en presencia de fuentes de error. En los siguientes párrafos los enfoques clásicos al control robusto no lineal se describen brevemente. Dicha descripción no pretende ser exhaustiva sino sólo proporcionar las nociones básicas, incluyendo algunas referencias representativas, para que el lector interesado pueda profundizar en la materia.

Una de las técnicas de control no lineal más extendidas es la *linealización por estados retroalimentados* (Slotine and Li, 1991; Khalil, 1996) que hace uso de transformaciones algebraicas para obtener un sistema en lazo cerrado lineal. Al contrario que en el enfoque clásico, este método es exacto. Los principales inconvenientes son: el problema de seguir una trayectoria de referencia puede llevar a transformaciones muy complejas y, la incertidumbre del modelo afecta al rendimiento del control. En lo que respecta a las técnicas robustas, probablemente una de las más empleadas para tratar con perturbaciones no medidas es el *control por modelo interno* (Garcia and Morari, 1982; Morari and Zafiriou, 1989). Las perturbaciones no medidas, utilizadas como señales de retroalimentación, se estiman utilizando las salidas del modelo y de la planta. Además el modelo se separa en dos partes: una invertible y otra que contiene los aspectos no invertibles. El controlador se construye en base a la parte invertible. Se puede extender a sistemas no lineales pero está restringido a procesos estables en lazo abierto (Henson and Seborg, 1997).

Prosigamos la discusión con las técnicas clásicas para el control robusto no lineal. En los enfoques de *Backstepping* y *Forwarding* (Sepulchre et al., 1997) se utilizan unas transformaciones en los estados para obtener un sistema con conexiones en cascada que es estable en el origen. Esto se aprovecha para diseñar el controlador. La incertidumbre se trata incluyendo términos en las transformaciones que la dominan. Las transformaciones de estado también juegan un papel importante en el *control por modos deslizantes* (Slotine and Li, 1991; Åström and Wittenmark, 1995). En este caso el objetivo es sustituir un problema de orden n por otro equivalente de orden 1. Se puede mostrar que una regularización perfecta pueder ser alcanzada incluso en presencia de incertidumbre pero la trayectoria de referencia debe ser suave para no excitar las dinámicas no modeladas asociadas con frecuencias altas (Slotine and Li, 1991). En el *control adaptativo* (Slotine and Li, 1991; Khalil, 1996) la robustez se afronta permitiendo que los parámetros del controlador sean variables. Dichos parámetros se ajustan en línea mediante un algoritmo alimentado con medidas de los estados de salida de la planta. Otra técnica que ha recibido gran atención en los últimos años es el *control predictivo basado en modelos* (MPC) (Allgöwer and Zheng, 1997; Camacho and Bordons, 1999). La idea básica es utilizar un modelo para predecir el comportamiento de la planta, en combinación con una técnica de optimización para definir una secuencia

de control que minimiza una cierta función objetivo. El primer paso de la secuencia de control se aplica a la planta y, en el siguiente intervalo se vuelve a repetir el procedimiento utilizando las nuevas medidas de los estados de la planta. Esto nos permite tener en cuenta la incertidumbre en el modelo. El problema es que esta técnica requiere un gran esfuerzo computacional que puede ser innecesario. El *método directo de Lyapunov* (Slotine and Li, 1991) y la *técnica de rediseño de Lyapunov* (LRT) (Corless, 1993; Khalil, 1996) son enfoques muy extendidos para el análisis y para el diseño de control cuando se trabaja en sistemas distribuidos. Si la energía total del sistema se disipa continuamente, el sistema debe evolucionar a un estado de equilibrio (Ydstie and Alonso, 1997; Alonso and Ydstie, 2001). Esto permite el estudio de la estabilidad del sistema utilizando una función escalar (*función de Lyapunov*). Otras alternativas especialmente útiles cuando se trabaja con procesos complejos o con modelos poco precisos son: el *control borroso* (White and Sofge, 1992), *control por métodos de aprendizaje* (Syafiie et al., 2007) o el *control mediante redes neuronales* (Norgaard et al., 2000).

Las técnicas mencionadas hasta el momento se han creado en el contexto de sistemas de parámetros concentrados. Muchas de ellas se han adaptado a sistemas distribuidos como es el caso de MPC, backstepping (Bošković et al., 2003) o el método directo de Lyapunov (Christofides, 2001). En los últimos años se ha dedicado un esfuerzo importante al diseño de políticas de control para sistemas distribuidos. Los enfoques estándar se basan en la discretización espacial del conjunto original de EDP para obtener un conjunto de ecuaciones diferenciales ordinarias. Esto permite emplear los métodos clásicos para sistemas de dimensión finita (Dochain et al., 1992; Gundepudi and Friedly, 1998). Sin embargo, la controlabilidad y observabilidad depende del número de puntos de discretización y de su localización. Además, en procesos donde la distribución es fuerte puede afectar a la calidad del control (Christofides, 2001). Por otra parte, resolver el conjunto de ecuaciones resultante puede ser muy costoso lo que hace que este enfoque sea poco apropiado para tareas en tiempo real. Debido a estas desventajas han surgido nuevos métodos basados en técnicas de descomposición espectral que tienen en cuenta la naturaleza distribuida de estos sistemas. Para diseñar el controlador en este enfoque se aprovecha la estructura del operador espacial y se usa el método de Galerkin para aproximar el sistema mediante un conjunto de ecuaciones diferenciales ordinarias de dimensión baja (Shvartsman and Kevrekidis, 1998). Christofides y colaboradores -ver, por ejemplo Christofides and Daoutidis (1996); Shi et al. (2006)- han empleado esta técnica en combinación con el método directo de Lyapunov para obtener controladores estabilizantes y la han aplicado a sistemas químicos como reactores tubulares, entre otros. Esta metodología ha sido ampliamente usada por otros autores en el contexto

de control de reactores químicos -ver (Hoo and Zheng, 2001; Alonso et al., 2004b) y referencias- o sistemas biológicos (Vilas et al., 2006).

4.2 Introduction

The first step to control a system is to have available a representation of this system (model). The predictive capabilities of the model will influence the control quality. Due to error sources like parameter uncertainty, model simplifications or unmeasured disturbances, in the real world, models are only approximations of systems so the same input will produce different outputs in the system and in the model. The *robust control* is the part of the control theory which deals with model uncertainty. On the other hand, the systems considered in this work, have a nonlinear nature. The first attempts to deal with the control of processes exhibiting nonlinear behaviour were by approximating the original model by a linear counterpart and using conventional PID controllers. Nevertheless, this approach is only effective with mild nonlinearities or when working close to the nominal steady state. In other cases, the tuning of the PID controllers must be very conservative which may result into the degradation of the control system performance (Seborg and Henson, 1997). Nonlinear control techniques not only improves the linear control methods and allows the analysis of hard nonlinearities but it also allows us to deal with model uncertainties and even the controller design may result simpler than in its linear counterpart (Slotine and Li, 1991). The aim of this chapter is to design a control logic able to drive the states of a nonlinear distributed system to the desired reference despite the error sources. In the following paragraphs the classical approaches to nonlinear robust control will be briefly described. Such description is not intended to be exhaustive but just to provide an outline including some representative references so the interested reader can go deeper into the subject.

A widely extended nonlinear control technique is the *Feedback Linearisation* (Slotine and Li, 1991; Khalil, 1996) which makes use of algebraic transformations to obtain a closed loop linear system in which the conventional control techniques can be applied. It should be stressed that, contrary to the classical approach, the feedback linearisation is exact. The main inconveniences of this technique are two: firstly, the tracking control problem may lead to complex transformations and secondly, model uncertainty may affect the control performance. Regarding robust techniques, probably one of the most employed to deal with unmeasured disturbances in linear systems is the *Internal Model Control* (Garcia and Morari, 1982; Morari and Zafiriou, 1989). The unmeasured disturbances, used as feedback signals, are estimated by means of the model and plant

outputs (Ogunnaike and Ray, 1994). Besides, the process model is separated into two parts: one invertible and the other containing the noninvertible aspects. The controller is based on the invertible part. It can be extended to nonlinear systems but it is restricted to open-loop stable processes (Henson and Seborg, 1997).

Let us now proceed with the classical nonlinear robust control techniques. In the *Backstepping* and *Forwarding* approaches (Sepulchre et al., 1997) state transformations are used to obtain a system with cascade connections which is stable at the origin with input zero. This fact is employed in the controller design. Model uncertainties in these techniques are approached by including, in the transformations, some terms constructed to dominate such uncertainties. State transformations are also a key concept in *Sliding Mode Control* (Slotine and Li, 1991; Åström and Wittenmark, 1995). In this case the objective of the transformations is to replace a n^{th} order problem into a 1^{st} order equivalent one which is easier to control. It can be shown that perfect performance can be achieved in the presence of model uncertainty although the desired reference trajectory must be smooth in order not to excite unmodelled dynamics usually associated with high frequencies (Slotine and Li, 1991). In *Adaptive Control* (Slotine and Li, 1991; Khalil, 1996) the robustness is approached by allowing variable controller parameters which are tuned online by means of an algorithm fed with output state plant measurements. Other techniques which have received a great amount of attention during recent years is the *Model Predictive Control* (MPC) (Allgöwer and Zheng, 1997; Camacho and Bordons, 1999). The basic idea is to use a model to predict the process behaviour in combination with an optimization technique to define a control sequence minimizing a certain objective function. The first step of the control sequence is applied and in the following interval the procedure is repeated using the new plant outputs which allows us to take into account the uncertainties. However, this technique requires a large amount of computation which may be unnecessary. The *Lyapunov's Direct Method* (Slotine and Li, 1991) and the *Lyapunov's Redesign Technique* (Corless, 1993; Khalil, 1996) are very extended for analysis and control design when working on distributed systems. If the total energy of a system is continuously dissipated, the system must evolve to an equilibrium point (Ydstie and Alonso, 1997; Alonso and Ydstie, 2001). This allows us to study the stability of the system by using a single scalar function (*Lyapunov function*). Other alternatives especially useful when working with very complex processes or with inaccurate mathematical models include the *Fuzzy Control* (White and Sofge, 1992), *Learning Methods* (Syafiie et al., 2007) or *Neural Networks* (Norgaard et al., 2000).

The techniques just mentioned have arisen in the context of lumped parameter

systems. Many of them have been adapted to distributed process systems as it is the case of MPC, backstepping (Bošković et al., 2003) or Lyapunov's direct method (Christofides, 2001). Over recent years, a considerable research effort concentrated on the design of control policies for distributed process systems (Christofides, 2001). Standard approaches to the control of this kind of systems are based on the spatial discretisation of the original set of partial differential equations (PDEs) to obtain a set of ordinary differential equations (ODEs). This allows us to employ standard finite-dimensional methods just described above to construct the controller (Dochain et al., 1992; Gundepudi and Friedly, 1998). However, there exist several disadvantages in this approach. For instance, the controllability and observability properties would depend on the number of discretisation points as well as its location. Moreover, in processes where the distribution is strong, these approaches may lead to a poor control quality (Christofides, 2001). In addition, the resulting set of ODEs is computationally involved due to its high dimensionality which could make the approach unsuitable for real time applications. Due to these disadvantages, new methods based on spectral decomposition techniques, which take into account the spatially distributed nature of these systems, have emerged. This approach takes advantage of the spatial differential operator structure and uses the Galerkin method so as to approximate the system by a low-dimensional set of ODEs to design the controller (Shvartsman and Kevrekidis, 1998). Christofides and coworkers -see, for example (Christofides and Daoutidis, 1996; Shi et al., 2006)- employed this approach in combination with the Lyapunov's direct method to derive stabilising controllers and applied it to chemical systems such as tubular reactors or particulate processes, among others. This methodology has been widely employed by many authors in the context of control of chemical reactors -see (Hoo and Zheng, 2001; Alonso et al., 2004b) and references therein- or biological systems (Vilas et al., 2006).

This chapter is structured as follows: In the first section and for the sake of completeness, the classical approach to the robust control of finite dimensional systems as developed in Khalil (1996) is presented. Then, in Section 4.4 it is extended to DPS by means of the ROMs described in Chapter 3. Finally, Section 4.5 deals with the problem of controlling DPS when only a finite number of actuators are available.

4.3 The Lyapunov Redesign Technique Revisited

The objective of this section is to briefly present one of the main tools employed in this work for the robust control of distributed systems. This tool is known as the *Lyapunov*

redesign technique (LRT) (Khalil, 1996) and deals with the issue of controlling finite dimensional systems in the presence of uncertainties.

Let us denote by $\mathscr{T}$ the semiopen time interval $[0, \infty)$ and by $\mathscr{M} \subset \mathbb{R}^n$ the set of states of a given system. Consider that such system is described by the following set of ODEs:

$$\frac{d\mathbf{m}}{dt} = \mathbf{h}(\mathbf{m}, t) + \mathbf{H}(\mathbf{m}, t)\left[\mathbf{u} + \boldsymbol{\delta}(\mathbf{m}, t, \mathbf{u})\right], \tag{4.1}$$

where $\mathbf{m} \in \mathscr{M}$ is the state vector, $\mathbf{h} : \mathscr{M} \times \mathscr{T} \to \mathbb{R}^n$ and $\mathbf{H} : \mathscr{M} \times \mathscr{T} \to \mathbb{R}^n \times \mathbb{R}^q$, with q being the number of inputs, are known functions locally Lipschitz in $\mathbf{m}$ and piecewise continuous in time, $\mathbf{u} \in \mathbb{R}^q$ corresponds with the control inputs. Finally, the model uncertainties (error sources) are collected in $\boldsymbol{\delta} : \mathscr{M} \times \mathscr{T} \times \mathbb{R}^p \to \mathbb{R}^q$. The control law is now split into two parts $\mathbf{u} = \mathbf{u}_{\mathbf{h},\mathbf{H}} + \mathbf{u}_{\boldsymbol{\delta}}$ where $\mathbf{u}_{\mathbf{h},\mathbf{H}}$ will be employed to stabilise the nominal system:

$$\frac{d\mathbf{m}}{dt} = \mathbf{h} + \mathbf{H}\mathbf{u}_{\mathbf{h},\mathbf{H}},$$

and $\mathbf{u}_{\boldsymbol{\delta}}$ will be constructed to compensate the uncertain terms. To be precise, the LRT is only concerned with the design of $\mathbf{u}_{\boldsymbol{\delta}}$ for finite dimensional systems. To that purpose, the perturbation $\boldsymbol{\delta}$ must enter the state equation at the point where the control enters (*matching condition*). Systems not satisfying this conditions are considered in Corless (1993). The perturbation is also required to be bounded by a known function. This is formally stated in the following assumption.

Assumption 4.1 *The uncertain term $\boldsymbol{\delta}$ is bounded as:*

$$\|\boldsymbol{\delta}(\mathbf{m}, t, \mathbf{u})\|_2 \leq \eta(\mathbf{m}, t) + k\|\mathbf{u}_{\boldsymbol{\delta}}\|_2, \qquad \textit{with} \;\; 0 \leq k < 1 \tag{4.2}$$

where $\eta : \mathscr{M} \times \mathscr{T} \to \mathbb{R}^+ \cup \{0\}$ is a known continuous function.

The construction of $\mathbf{u}_{\boldsymbol{\delta}}$ begins with the definition of a Lyapunov function $\mathcal{B}(\mathbf{m}) : \mathscr{M} \to \mathbb{R}^+ \cup \{0\}$ so that:

$$q_1(\|\mathbf{m}\|_2) \leq \mathcal{B}(\mathbf{m}) \leq q_2(\|\mathbf{m}\|_2), \tag{4.3}$$

$$\frac{\partial \mathcal{B}(\mathbf{m})}{\partial t} + \mathbf{A}\left[\mathbf{h} + \mathbf{H}\mathbf{u}_{\mathbf{h},\mathbf{H}}\right] \leq -q_3(\|\mathbf{m}\|_2), \qquad \text{with} \;\; \mathbf{A} = \frac{\partial \mathcal{B}(\mathbf{m})}{\partial \mathbf{m}}, \tag{4.4}$$

where $q_i(\cdot)$ with $i = 1, 2, 3$ are class $\mathcal{K}$ functions. The definition of class $\mathcal{K}$ and $\mathcal{KL}$ functions, employed later on this section, is included in Appendix A. For convenience, the arguments of some functions will be omitted in the remaining of this section. The derivative of $\mathcal{B}$ along the trajectories (4.1) can be bounded as follows:

$$\dot{\mathcal{B}} = \frac{\partial \mathcal{B}}{\partial t} + \mathbf{A}\left(\mathbf{h} + \mathbf{H}\mathbf{u}_{\mathbf{h},\mathbf{H}}\right) + \mathbf{A}\mathbf{H}\left(\mathbf{u}_{\boldsymbol{\delta}} + \boldsymbol{\delta}\right) \leq -q_3 + \mathbf{A}\mathbf{H}(\mathbf{u}_{\boldsymbol{\delta}} + \boldsymbol{\delta}),$$

which by using $\omega^T = \mathbf{AH}$, can be rewritten as:

$$\dot{\mathcal{B}} \leq -q_3 + \omega^T \boldsymbol{\delta} + \omega^T \mathbf{u}_{\boldsymbol{\delta}}. \tag{4.5}$$

Taking into account the bound on $\boldsymbol{\delta}$ - see relation (4.2)- and using the Cauchy-Schwarz inequality, a more convenient form of Eqn (4.5) is obtained:

$$\dot{\mathcal{B}} \leq -q_3 + \|\omega\|_2 \left(\eta + k\|\mathbf{u}_{\boldsymbol{\delta}}\|_2\right) + \omega^T \mathbf{u}_{\boldsymbol{\delta}}. \tag{4.6}$$

Now, consider a control law of the form:

$$\mathbf{u}_{\boldsymbol{\delta}} = \begin{cases} -\frac{\eta}{1-k}\frac{\omega}{\|\omega\|_2}, & \text{if} \quad \eta\|\omega\|_2 \geq \theta \\ \\ -\frac{\eta^2}{1-k}\frac{\omega}{\theta}, & \text{if} \quad \eta\|\omega\|_2 < \theta \end{cases}, \tag{4.7}$$

where θ is a tuning parameter chosen by the user and the second condition (that where $\eta\|\omega\|_2 < \theta$) was chosen so as to avoid the discontinuity at the origin ($\|\omega\|_2 = 0$). By substituting the control law (4.7) on inequality (4.6) two cases arise:

- If $\eta\|\omega\|_2 \geq \theta$ then

$$\dot{\mathcal{B}} \leq -q_3 + \eta\|\omega\|_2 + \frac{k\eta}{1-k}\|\omega\|_2 - \frac{\eta}{1-k}\frac{1}{\|\omega\|_2}\omega^T\omega \leq -q_3. \tag{4.8}$$

- If $\eta\|\omega\|_2 < \theta$ then

$$\dot{\mathcal{B}} \leq -q_3 + \eta\|\omega\|_2 + \frac{k\eta^2}{(1-k)\theta}\|\omega\|_2^2 - \frac{\eta^2}{(1-k)\theta}\omega^T\omega = -q_3 + \eta\|\omega\|_2 - \frac{\eta^2}{\theta}\|\omega\|_2^2.$$

  Function $\Psi = \eta\|\omega\|_2 - \frac{\eta^2}{\theta}\|\omega\|_2^2$ attains its maximum value ($\Psi_{\max} = \theta/4$) at $\eta\|\omega\|_2 = \theta/2$. Therefore we have:

$$\dot{\mathcal{B}} \leq -q_3 + \Psi_{\max} = -q_3 + \frac{\theta}{4}. \tag{4.9}$$

Note that inequality (4.9) is also satisfied in the case $\eta\|\omega\|_2 \geq \theta$. Since q_3 is a class $\mathcal{K}$ the derivative of the Lyapunov function $\dot{\mathcal{B}}$ is negative outside a given ball. As shown in (Khalil, 1996) the following relation holds independently of the value of $\eta\|\omega\|_2 \geq \theta$:

$$\dot{\mathcal{B}} \leq -\frac{q_3(\|\mathbf{m}\|_2)}{2}, \qquad \forall\, \mu(\theta) \leq \|\mathbf{m}\|_2 < r,$$

where $\theta < 2q_3(q_2^{-1}(q_1(r)))$ and $\mu(\theta) = q_3^{-1}(\theta/2) < q_2^{-1}(q_1(r))$. Thus $\dot{\mathcal{B}}$ is negative outside the ball of radius $\mu(\theta)$. Under these conditions, for initial vectors satisfying $\|\mathbf{m}(t_0)\|_2 \leq q_2^{-1}(q_1(r))$, there exists a finite time t_1 such that the solution of the closed

loop system (4.1), with $\mathbf{u_{h,H}}$ stabilising the nominal system and $\mathbf{u_\delta}$ of the form (4.7), satisfies:

$$\|\mathbf{m}\|_2 \leq \beta(\|\mathbf{m}(t_0)\|_2, t - t_0), \quad \forall t_0 \leq t < t_1, \tag{4.10}$$

$$\|\mathbf{m}\|_2 \leq g(\theta) = q_1^{-1}(q_2(q_3^{-1}(\theta/2))), \quad \forall t \geq t_1, \tag{4.11}$$

where $\beta(\cdot,\cdot)$ is a class $\mathcal{KL}$ function. Since $g(\cdot)$ is a class $\mathcal{K}$ function, the lower the value of θ, the lower the value of g. If all the assumptions hold globally and $q_1(\cdot)$ belongs to class $\mathcal{K}_\infty$ then (4.10) and (4.11) hold for any initial state $\mathbf{m}(t_0)$ (Khalil, 1996). Finally, if $q_i(r) = u_i r^c$ with $i = 1, 2, 3$ and $u_i, c > 0$ it follows that $\beta(r, s) = ur\exp(-\gamma s)$, with $u, \gamma > 0$. In other words, the convergence of the vector state to the reference between t_0 and t_1 is exponential and beyond t_1 the vector state is bounded by g (*ultimately bounded*). The effect of the control law (4.7) on system (4.1) is sketched in Figure 4.1. When the control law enters in action at t_0, it drives the state exponentially fast to

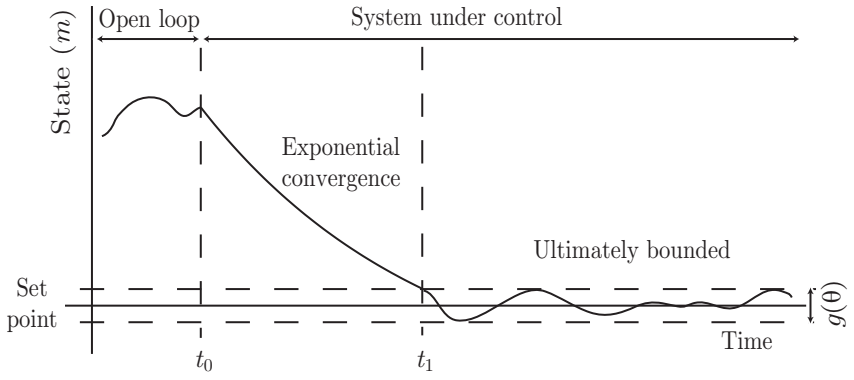

Figure 4.1: Evolution of a given system with uncertainties under a control law constructed using the LRT.

a region close to the reference. Once the state reaches this region (t_1), it will remain there in the future. Note that, since uncertainties are considered, the convergence to the set point cannot be ensured but only to a region around it. This region can be arbitrarily reduced by an appropriate selection of the control parameters. It should be highlighted that considering too conservative bounds on the uncertain terms may lead to sharp control actions producing chattering.

The procedure for deriving a robust control law and the behaviour of a given system under such control is illustrated in the following simple example.

Example 4.1 (One state case) *Consider the following nominal system:*

$$\frac{dm}{dt} = -\kappa m + m - m^3 + u, \tag{4.12}$$

with $\kappa = 0.85$. *It is clear that using a control law* $u = -Km$ *with* $K > (1 - \kappa) = 0.15$, *the nominal system is stabilised. The blue line in Figure 4.2 (a) represents the evolution of the system with* $K = 0.3$. *Now, let us consider a perturbation of the form*

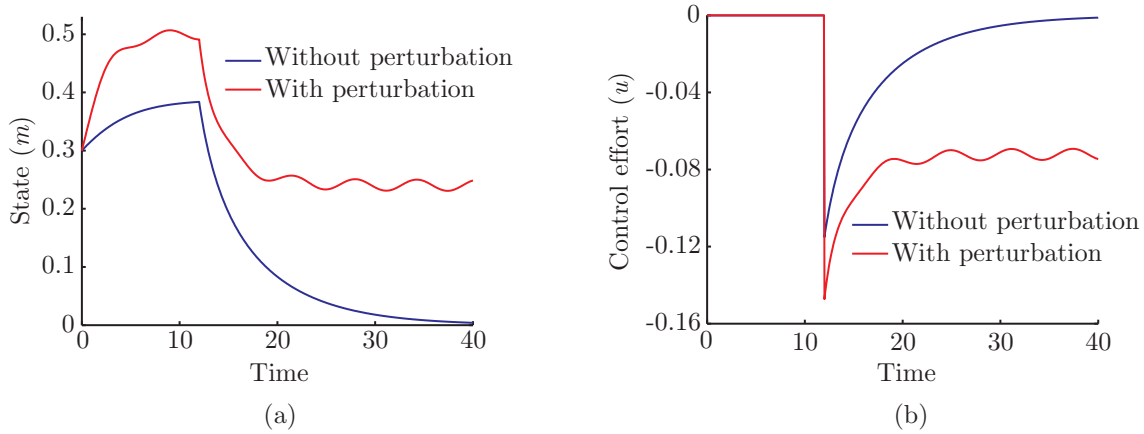

Figure 4.2: (a) Evolution of system (4.12) under a proportional control law $u = -Km$. (b) Control effort.

$\delta = 0.05 + 0.01 \sin(t)$. *System (4.12) is rewritten as follows:*

$$\frac{dm}{dt} = -\kappa m + m - m^3 + 0.05 + 0.01 \sin(t) + u. \tag{4.13}$$

Note that this system match into Eqn (4.1) with $h = -\kappa m + m - m^3$, $H = 1$. *The control law* $u = -Km$ *now fails to stabilise this system, as shown in Figure 4.2 (red line). In order to derive a control law able to deal with the uncertainty, consider the Lyapunov function* $\mathcal{B} = m^2/2$. *In this case the dual of the field coincides with the field, i.e.* $A = m$, *and since* $H = 1$ *then* $\omega = m$. *The exact value of the perturbation is assumed to be unknown. The only information on* δ *is a bound of the form* $\delta < \eta = 0.062$. *In this case, control law (4.7) reads with* $k = 0$*:*

$$u_\delta = \begin{cases} -\eta \frac{m}{\|m\|_2}, & \text{if} \quad \eta \|m\|_2 \geq \theta \\ -\eta^2 \frac{m}{\theta}, & \text{if} \quad \eta \|m\|_2 < \theta \end{cases}. \tag{4.14}$$

The results of applying this control to system (4.13) with $\theta = 5 \times 10^{-3}$ *(green line),* $\theta = 1 \times 10^{-3}$ *(blue line) and* $\theta = 1 \times 10^{-4}$ *(red line) are shown in Figure 4.3. As it can be seen in the figure, the lower the value of* θ *the closer the state to 0 and also the larger the control effort.*

□

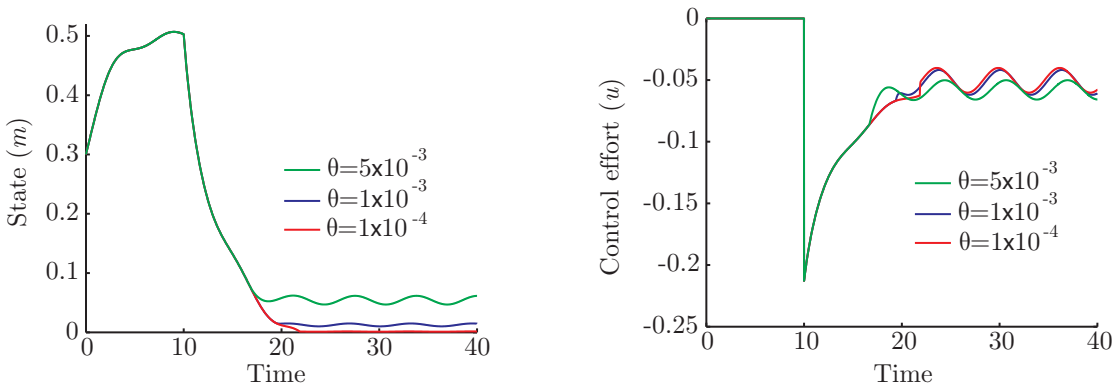

Figure 4.3: (a) Evolution of system (4.13) under the control law (4.14). (b) Control effort.

4.4 Robust Control in Infinite Dimensional Systems

The main idea behind the approach proposed in this work to the robust control of infinite dimensional systems is to combine the ROMs derived in Section 3.2 with the classical theory on robust control just presented in section 4.3. As shown in Section 3.2, PDEs can be approximated with arbitrary accuracy by finite dimensional approximations (ROMs) in which it is possible to apply the LRT. Consider the general equation for RDC systems (see Eqn 1.34 in Chapter 1):

$$\frac{\partial \mathbf{z}}{\partial t} = \Delta\boldsymbol{\Gamma} - \overrightarrow{\boldsymbol{\nabla}} \cdot (\overrightarrow{\mathbf{v}}\mathbf{z}) + \mathbf{f}(\mathbf{z}) + \mathbf{u}, \quad \boldsymbol{\Gamma} = \int_{\mathbf{A}^0}^{\mathbf{A}} \mathbf{L}(\mathbf{A}) d\mathbf{A}.$$

and the reference trajectory:

$$\frac{\partial \mathbf{z}^*}{\partial t} = \Delta\boldsymbol{\Gamma}^* - \overrightarrow{\boldsymbol{\nabla}} \cdot (\overrightarrow{\mathbf{v}}\mathbf{z}^*) + \mathbf{f}^* + \mathbf{u}^*, \quad \boldsymbol{\Gamma}^* = \int_{\mathbf{A}^0}^{\mathbf{A}^*} \mathbf{L}^*(\mathbf{A}) d\mathbf{A}.$$

Note that, contrary to the reference chosen in Chapter 1, this can be a dynamic reference and the term $\mathbf{L}^*(\mathbf{A})$ can be different from $\mathbf{L}(\mathbf{A})$. The system in deviation form can be rewritten as:

$$\frac{\partial \overline{\mathbf{z}}}{\partial t} = \Delta\boldsymbol{\Gamma} - \Delta\boldsymbol{\Gamma}^* - \overrightarrow{\boldsymbol{\nabla}} \cdot (\overrightarrow{\mathbf{v}}\overline{\mathbf{z}}) + \overline{\mathbf{f}} + \overline{\mathbf{u}}. \tag{4.15}$$

For convenience let us now operate the term $\boldsymbol{\Gamma} - \boldsymbol{\Gamma}^*$:

$$\boldsymbol{\Gamma} - \boldsymbol{\Gamma}^* = \int_{\mathbf{A}^0}^{\mathbf{A}} \mathbf{L}(\mathbf{A}) d\mathbf{A} - \int_{\mathbf{A}^0}^{\mathbf{A}^*} \mathbf{L}^*(\mathbf{A}) d\mathbf{A} = \int_{\mathbf{A}^0}^{\mathbf{A}} \mathbf{L}(\mathbf{A}) d\mathbf{A} - \int_{\mathbf{A}^0}^{\mathbf{A}^*} \mathbf{L}^*(\mathbf{A}) d\mathbf{A} +$$

$$\int_{\mathbf{A}^0}^{\mathbf{A}^*} \mathbf{L}(\mathbf{A}) d\mathbf{A} - \int_{\mathbf{A}^0}^{\mathbf{A}^*} \mathbf{L}(\mathbf{A}) d\mathbf{A} = \int_{\mathbf{A}^*}^{\mathbf{A}} \mathbf{L}(\mathbf{A}) d\mathbf{A} - \int_{\mathbf{A}^0}^{\mathbf{A}^*} \chi(\mathbf{A}) d\mathbf{A} = \overline{\boldsymbol{\Gamma}} - \boldsymbol{\Gamma}_d$$

where $\chi(\mathbf{A}) = \mathbf{L}^*(\mathbf{A}) - \mathbf{L}(\mathbf{A})$. Substituting this expression into equation (4.15), one is led to:

$$\frac{\partial \overline{\mathbf{z}}}{\partial t} = \Delta\overline{\mathbf{\Gamma}} - \Delta\mathbf{\Gamma}_d - \overrightarrow{\mathbf{\nabla}} \cdot (\overrightarrow{\mathbf{v}}\overline{\mathbf{z}}) + \overline{\mathbf{f}} + \overline{\mathbf{u}}. \tag{4.16}$$

On the other hand, defining the subsets $(\mathscr{E}_a, \mathscr{L}_a, \mathcal{N}_a)$ and $(\mathscr{E}_b, \mathscr{L}_b, \mathcal{N}_b)$ as in section 3.5 and making use of previous results, discussed in Chapter 3, the set of modes for the reference trajectory $\mathscr{M}^* = \{\mathbf{m}_i^*\}_{i\in\mathbb{N}}$ can be separated into two disjoint sets: $\mathscr{M}_a^*$ and $\mathscr{M}_b^*$. The set $\mathscr{M}_b^* = \{\mathbf{m}_i^*\}_{i\in\mathcal{N}_b}$ is composed of the exponentially stable modes which will be referred to as *non representative modes*. $\mathscr{M}_a^* = \{\mathbf{m}_i^*\}_{i\in\mathcal{N}_a}$ collects the remaining modes which will be referred to as *representative modes*. Note that the number of elements in $\mathscr{M}_a^*$ is finite. The same separation procedure is applied to the modes of the system to be controlled $\mathscr{M} = \{\mathbf{m}_i\}_{i\in\mathbb{N}}$. The control law is then designed so as to achieve two different objectives: on the one hand the stabilisation of those modes belonging $\mathscr{M}_b$ and on the other hand, to force the remaining (those belonging to $\mathscr{M}_a$) to follow the reference trajectory given by the modes of $\mathscr{M}_a^*$.

Projection of Eqn (4.16) over each eigenfunction of the set $\mathscr{E} = \{\phi_i(\boldsymbol{\xi})\}_{i=1}^{\infty}$ leads to:

$$\langle\phi_i, \frac{\partial \overline{\mathbf{z}}}{\partial t}\rangle_{\mathscr{V}} = \frac{d\overline{m}_i}{dt} = \langle\phi_i, \Delta\overline{\mathbf{\Gamma}}\rangle_{\mathscr{V}} - \langle\phi_i, \Delta\mathbf{\Gamma}_d\rangle_{\mathscr{V}} - \langle\phi_i, \overrightarrow{\mathbf{\nabla}} \cdot (\overrightarrow{\mathbf{v}}\overline{\mathbf{z}})\rangle_{\mathscr{V}} +$$

$$\langle\phi_i, \overline{\mathbf{f}}\rangle_{\mathscr{V}} + \langle\phi_i, \overline{\mathbf{u}}\rangle_{\mathscr{V}}, \quad i = 1, ..., \infty. \tag{4.17}$$

The former relation represents an infinite number of equations which, by using the sets $\mathcal{N}_a$ and $\mathcal{N}_b$, can be grouped into two vector equations so that:

$$\frac{d\overline{\mathbf{m}}_a}{dt} = \langle\Phi_a, \Delta\overline{\mathbf{\Gamma}}\rangle_{\mathscr{V}} - \langle\Phi_a, \Delta\mathbf{\Gamma}_d\rangle_{\mathscr{V}} - \langle\Phi_a, \overrightarrow{\mathbf{\nabla}} \cdot (\overrightarrow{\mathbf{v}}\overline{\mathbf{z}})\rangle_{\mathscr{V}} + \langle\Phi_a, \overline{\mathbf{f}}\rangle_{\mathscr{V}} + \langle\Phi_a, \overline{\mathbf{u}}\rangle_{\mathscr{V}}, \tag{4.18}$$

$$\frac{d\overline{\mathbf{m}}_b}{dt} = \langle\Phi_b, \Delta\overline{\mathbf{\Gamma}}\rangle_{\mathscr{V}} - \langle\Phi_b, \Delta\mathbf{\Gamma}_d\rangle_{\mathscr{V}} - \langle\Phi_b, \overrightarrow{\mathbf{\nabla}} \cdot (\overrightarrow{\mathbf{v}}\overline{\mathbf{z}})\rangle_{\mathscr{V}} + \langle\Phi_b, \overline{\mathbf{f}}\rangle_{\mathscr{V}} + \langle\Phi_b, \overline{\mathbf{u}}\rangle_{\mathscr{V}},$$

where $\Phi_a = [\phi_{\mathcal{N}_a(1)}, ..., \phi_{\mathcal{N}_a(n)}]$ and $\Phi_b = [\phi_{\mathcal{N}_b(1)}, \phi_{\mathcal{N}_b(2)}, ...]$. Note that the set $\mathcal{N}_b$ was chosen in order for the modes $\mathbf{m}_b^*$ to be exponentially stable. This implies that $\mathbf{m}_b^*$ (and thus $\Delta\mathbf{\Gamma}_b^*$) can be neglected and the previous expression can be rewritten as:

$$\frac{d\overline{\mathbf{m}}_b}{dt} = \langle\Phi_b, \Delta\mathbf{\Gamma}\rangle_{\mathscr{V}} - \langle\Phi_b, \overrightarrow{\mathbf{\nabla}} \cdot (\overrightarrow{\mathbf{v}}\overline{\mathbf{z}})\rangle_{\mathscr{V}} + \langle\Phi_b, \overline{\mathbf{f}}\rangle_{\mathscr{V}} + \langle\Phi_b, \overline{\mathbf{u}}\rangle_{\mathscr{V}}. \tag{4.19}$$

It should be remarked that stabilising the modes in deviation form $\overline{\mathbf{m}}_a$ and $\overline{\mathbf{m}}_b$ is equivalent to force $\mathbf{m}_a \to \mathbf{m}_a^*$ and $\mathbf{m}_b \to \mathbf{m}_b^* = 0$ (and thus $\mathbf{z} \to \mathbf{z}^*$), since $\overline{\mathbf{m}}_a = \mathbf{m}_a - \mathbf{m}_a^*$ and $\overline{\mathbf{m}}_b = \mathbf{m}_b - \mathbf{m}_b^*$. The control law will be then split into two contributions: $\overline{\mathbf{u}}_a$ and $\overline{\mathbf{u}}_b$ responsible for stabilising $\overline{\mathbf{m}}_a$ and $\overline{\mathbf{m}}_b$, respectively.

Let us continue with the design of $\overline{\mathbf{u}}_a$. The same procedure can be applied to $\mathbf{m}_b$ so as to obtain an expression for $\overline{\mathbf{u}}_b$. Multiplying Eqn (4.18) by the time dependent functions $\boldsymbol{\alpha}_a^T$ in Eqn (3.11), we obtain:

$$\boldsymbol{\alpha}_a^T \frac{d\overline{\mathbf{m}}_a}{dt} = \langle \overline{\mathbf{A}}_a, \Delta\overline{\boldsymbol{\Gamma}} \rangle_{\mathscr{V}} - \langle \overline{\mathbf{A}}_a, \Delta\boldsymbol{\Gamma}_d \rangle_{\mathscr{V}} - \langle \overline{\mathbf{A}}_a, \overrightarrow{\boldsymbol{\nabla}} \cdot (\overrightarrow{\mathbf{v}}\overline{\mathbf{z}}) \rangle_{\mathscr{V}} + \langle \overline{\mathbf{A}}_a, \overline{\mathbf{f}} \rangle_{\mathscr{V}} + \langle \overline{\mathbf{A}}_a, \overline{\mathbf{u}_a} \rangle_{\mathscr{V}}. \quad (4.20)$$

Now the following lemma useful in further computations is introduced.

Lemma 4.1 *Projections of the different terms of Eqn (1.40) over the subfield* $\overline{\mathbf{A}}_a$ *satisfy the following relations:*

1. $\langle \overline{\mathbf{A}}_a, \Delta\overline{\boldsymbol{\Gamma}} \rangle_{\mathscr{V}} \leq -\zeta\lambda_m \boldsymbol{\alpha}_a^T \boldsymbol{\alpha}_a.$
2. $-\langle \overline{\mathbf{A}}_a, \Delta\boldsymbol{\Gamma}_d \rangle_{\mathscr{V}} \leq \lambda_q \|\gamma_{da}\|_2 \|\overline{\mathbf{A}}_a\|_{\mathscr{V}}.$
3. $-\langle \overline{\mathbf{A}}_a, \overrightarrow{\boldsymbol{\nabla}} \cdot (\overrightarrow{\mathbf{v}}\overline{\mathbf{z}}) \rangle_{\mathscr{V}} \leq 0.$
4. $\langle \overline{\mathbf{A}}_a, \overline{\mathbf{f}} \rangle_{\mathscr{V}} \leq \zeta_a \|\overline{\mathbf{A}}_a\|_{\mathscr{V}}.$

where $\boldsymbol{\alpha}_a \in \mathbb{R}^p$*, with* p *being the number of elements in the set* $\mathscr{E}_a$*. The vector* $\boldsymbol{\alpha}_a$ *is of the form:* $\boldsymbol{\alpha}_a = [\boldsymbol{\alpha}_a^1, \boldsymbol{\alpha}_a^2, ..., \boldsymbol{\alpha}_a^n]^T$ *and the elements inside this vector correspond with* $\boldsymbol{\alpha}_a^i = [\alpha^i_{\mathcal{N}_a(1)}, \alpha^i_{\mathcal{N}_a(2)}, ..., \alpha^i_{\mathcal{N}_a(p)}]^T$*. The parameters on the RHS of the previous relations are:* $\zeta = \min_{\overline{\mathbf{A}}} \inf_i[\lambda_i(\mathbf{L})]$*,* $\lambda_m = \min_{\mathscr{L}_a}(\lambda(\Delta))$*,* $\lambda_q = \max_{\mathscr{L}_a}(\lambda(\Delta))$*, and* $\zeta_a \geq \|\overline{\mathbf{f}}_a\|_{\mathscr{V}}$*.*

The proof of this lemma is included in Appendix B.4. Substituting expressions of Lemma 4.1 into equation (4.20), the following inequality is obtained:

$$\boldsymbol{\alpha}_a^T \frac{d\overline{\mathbf{m}}_a}{dt} \leq -\zeta\lambda_m \boldsymbol{\alpha}_a^T \boldsymbol{\alpha}_a + \lambda_q \|\gamma_{da}\|_2 \|\overline{\mathbf{A}}_a\|_{\mathscr{V}} + \zeta_a \|\overline{\mathbf{A}}_a\|_{\mathscr{V}} + \langle \overline{\mathbf{A}}_a, \overline{\mathbf{u}}_a \rangle_{\mathscr{V}}. \quad (4.21)$$

A new convex function $b_a(\overline{\mathbf{z}}_a)$ can be defined as in Eqn (1.30) for the field $\overline{\mathbf{z}}_a$ so that $b_a = \frac{1}{2}\overline{\mathbf{z}}_a^T \overline{\mathbf{z}}_a$. The time derivative of b_a reads:

$$\dot{b}_a = \frac{\partial b_a}{\partial \overline{\mathbf{z}}_a} \frac{\partial \overline{\mathbf{z}}_a}{\partial t} = \overline{\mathbf{A}}_a^T \frac{\partial \overline{\mathbf{z}}_a}{\partial t} \Rightarrow \dot{\mathcal{B}}_a = \int_{\mathscr{V}} \dot{b}_a d\xi = \boldsymbol{\alpha}_a^T \frac{d\overline{\mathbf{m}}_a}{dt}.$$

In addition, $\overline{\mathbf{A}}_a$ relates to $\overline{\mathbf{z}}_a$ through an expression of the form (1.32) so that

$$\boldsymbol{\alpha}_a^T \boldsymbol{\alpha}_a = \langle \overline{\mathbf{A}}_a, \overline{\mathbf{A}}_a \rangle_{\mathscr{V}} = \langle Q_a \overline{\mathbf{z}}_a, Q_a \overline{\mathbf{z}}_a \rangle_{\mathscr{V}} \geq \delta_{0a}^2 \mathbf{m}_a^T \mathbf{m}_a \geq \frac{\delta_{0a}^2}{q_{1a}} \mathcal{B}_a, \quad (4.22)$$

where δ_{0a} is the minimum eigenvalue of Q_a. Using these relations, inequality (4.21) can be rewritten as:

$$\dot{\mathcal{B}}_a \leq -\zeta\lambda_m \frac{\delta_{0a}^2}{q_{1a}} \mathcal{B}_a + \lambda_q \|\gamma_{da}\|_2 \|\overline{\mathbf{A}}_a\|_{\mathscr{V}} + \zeta_a \|\overline{\mathbf{A}}_a\|_{\mathscr{V}} + \langle \overline{\mathbf{A}}_a, \overline{\mathbf{u}}_a \rangle_{\mathscr{V}}. \quad (4.23)$$

The exact forms of the nonlinear terms and the diffusive parameters are assumed to be unknown although a given bound should be available. In this regard, one can define

a known function η_a such that $\eta_a > \lambda_q \|\gamma_{da}\|_2 + \zeta_a$. Using this bound, relation (4.23) reads:

$$\dot{\mathcal{B}}_a \leq -\zeta \lambda_m \frac{\delta_0^2}{q_1} \mathcal{B}_a + \eta_a \|\overline{\mathbf{A}}_a\|_{\mathscr{V}} + \langle \overline{\mathbf{A}}_a, \overline{\mathbf{u}}_a \rangle_{\mathscr{V}}. \tag{4.24}$$

The last step consists of selecting a control law in order to cancel the uncertain term of Eqn (4.24). The following proposition suggests a possible controller capable of attaining this objective.

Proposition 4.1 *A control law of the form*

$$\overline{\mathbf{u}}_a = \begin{cases} -\eta_a \frac{\overline{\mathbf{A}}_a}{\|\overline{\mathbf{A}}_a\|_{\mathscr{V}}} & \text{if} \quad \eta_a \|\overline{\mathbf{A}}_a\|_{\mathscr{V}} \geq \theta_a \\ \\ -\eta_a^2 \frac{\overline{\mathbf{A}}_a}{\theta_a} & \text{if} \quad \eta_a \|\overline{\mathbf{A}}_a\|_{\mathscr{V}} < \theta_a \end{cases}, \tag{4.25}$$

will make the field $\overline{\mathbf{z}}_a$ to be ultimately bounded.

The proof of this Proposition can be found in Appendix B.5. As mentioned above, the same procedure can be applied to obtain an expression of the form of (4.23) using a Lyapunov function $\mathcal{B}_b$ defined as in Eqn (1.30) for the field $\overline{\mathbf{z}}_b$:

$$\dot{\mathcal{B}}_b \leq -\zeta \lambda_\ell \frac{\delta_{0b}^2}{q_{1b}} \mathcal{B}_b + \zeta_b \|\overline{\mathbf{A}}_b\|_{\mathscr{V}} + \langle \overline{\mathbf{A}}_b, \overline{\mathbf{u}}_b \rangle_{\mathscr{V}}, \tag{4.26}$$

where $\zeta_b > \|\overline{\mathbf{f}}_b\|_{\mathscr{V}}$.

Proposition 4.2 *Consider a given known function η_b of the form $\eta_b \geq \zeta_b$. A control law of the form:*

$$\overline{\mathbf{u}}_b = \begin{cases} -\eta_b \frac{\overline{\mathbf{A}}_b}{\|\overline{\mathbf{A}}_b\|_{\mathscr{V}}} & \text{if} \quad \eta_b \|\overline{\mathbf{A}}_b\|_{\mathscr{V}} \geq \theta_b \\ \\ -\eta_b^2 \frac{\overline{\mathbf{A}}_b}{\theta_b} & \text{if} \quad \eta_b \|\overline{\mathbf{A}}_b\|_{\mathscr{V}} < \theta_b \end{cases}, \tag{4.27}$$

will make the field $\overline{\mathbf{z}}_b$ to be ultimately bounded.

The same line of arguments employed in the proof of Proposition 4.1 can be applied in a straightforward manner to show that the control law (4.27) stabilises the set $\mathscr{M}_b$. The proof of Proposition 4.1 also shows that the price to pay for robustness is that asymptotic convergence cannot be ensured but only convergence to a region around the reference. It must be pointed out that this region can be arbitrarily reduced by decreasing the control parameters θ_a and θ_b but at the cost of larger control efforts.

Although any convex positive definite function b could be employed, it may be worth searching for a given b capturing the nonlinearity of the process, especially when considering bounds on the controls. This point is illustrated through the following example.

Example 4.2 (Selection of the Lyapunov function) *The system considered here is that described in Example 1.3 of Section 1.5. In this process, the heat produced by the reaction is removed from the system through a cooling jacket. The interaction between the diffusion, the reaction heat and the cooling medium can produce runaway phenomena. The objective is to construct a control law able to stabilise the system. For convenience, let us rewrite the model equations:*

$$\frac{\partial T}{\partial t} = \Delta\Gamma + f + \beta_H u; \quad f = \beta_T \left[\exp\left(-\frac{\gamma}{1+T} \right) - \exp\left(-\gamma\right) \right] - \beta_H T, \tag{4.28}$$

with boundary and initial conditions of the form:

$$T|_{\mathscr{B}} = 0; \quad T(\xi, 0) = T_0 = 0.4 \sin\left(2\xi\right). \tag{4.29}$$

The controller is now designed as follows: first, let us choose a convex function b and compute its time derivative along the trajectories (4.28) so that:

$$\dot{b} = \overline{A}^T \frac{\partial T}{\partial t} = \overline{A}^T \Delta\Gamma + \overline{A}^T f + \beta_H \overline{A}^T u,$$

where $\overline{A}^T = \frac{\partial b}{\partial T}$. Integrating over the spatial domain and denoting $\mathcal{B} = \int_{\mathscr{V}} b d\xi$ results:

$$\dot{\mathcal{B}} = \langle \overline{A}, \Delta\Gamma \rangle_{\mathscr{V}} + \langle \overline{A}, f \rangle_{\mathscr{V}} + \beta_H \langle \overline{A}, u \rangle_{\mathscr{V}}. \tag{4.30}$$

As shown in Section 3.5, the first term of the RHS is non positive. Since the nonlinear term is Lipschitz, Eqn (4.30) can be rewritten as follows:

$$\dot{\mathcal{B}} \leq \mu \langle \overline{A}, \overline{A} \rangle_{\mathscr{V}} - L_\mu + \beta_H \langle \overline{A}, u \rangle_{\mathscr{V}} \leq \mu \langle \overline{A}, \overline{A} \rangle_{\mathscr{V}} + \beta_H \langle \overline{A}, u \rangle_{\mathscr{V}},$$

where use was made of Condition 1.1 which states that there exists a $\mu > 0$ so that $L_\mu > 0$. Now let us choose a control law of the form $u = -\frac{\omega}{\beta_H} \overline{A}$ with $\omega > \mu$. Using expressions (1.32) and (1.31) one has that $\dot{\mathcal{B}} \leq r\mathcal{B}$ where $r = \frac{\delta_0^2}{q_1}(\mu - \omega) < 0$. Finally, by means of the Gronwall-Bellman lemma (Khalil, 1996) one is led to:

$$\mathcal{B} \leq \mathcal{B}(0) \exp(rt),$$

which implies that the field T evolves exponentially to zero.

The dual $\overline{A}$ of the field T is closely connected with the convex function b so the control effort will strongly depend on the selection of such a function. In order to illustrate this point, two possibilities have been considered:

$$b_1 = \frac{1}{2} T^2,$$

$$b_2 = \frac{1}{2}T^2 - 1 - \sigma T + \exp(\sigma T),$$

where σ is a positive design parameter. b_2 has been selected so as to take into account the structure of the nonlinear term as proposed in Alonso et al. (2002). The intensive counterparts of the field for b_1 and b_2 are:

$$\overline{A}_1 = T,$$

$$\overline{A}_2 = T + \sigma[-1 + \exp(\sigma T)].$$

Using Eqn (1.41) one can check that for $\mu_1 > 4.155$ and $\mu_2 > 0.99$ with $\sigma = 1.26$, ℓ_μ is positive for all T. The gains ω in the control law are chosen accordingly.

Figures 4.4(a) and 4.4(b) show the evolution of the field under the control $u_i = -\frac{\omega_i}{\beta_H}\overline{A}_i$ with $i = 1$ and $i = 2$, respectively. The effort of both control laws is represented in Figure 4.4(c). As shown in the Figure, using function b_2 (red line) results into smoother control actions as compared with b_1 (blue line).

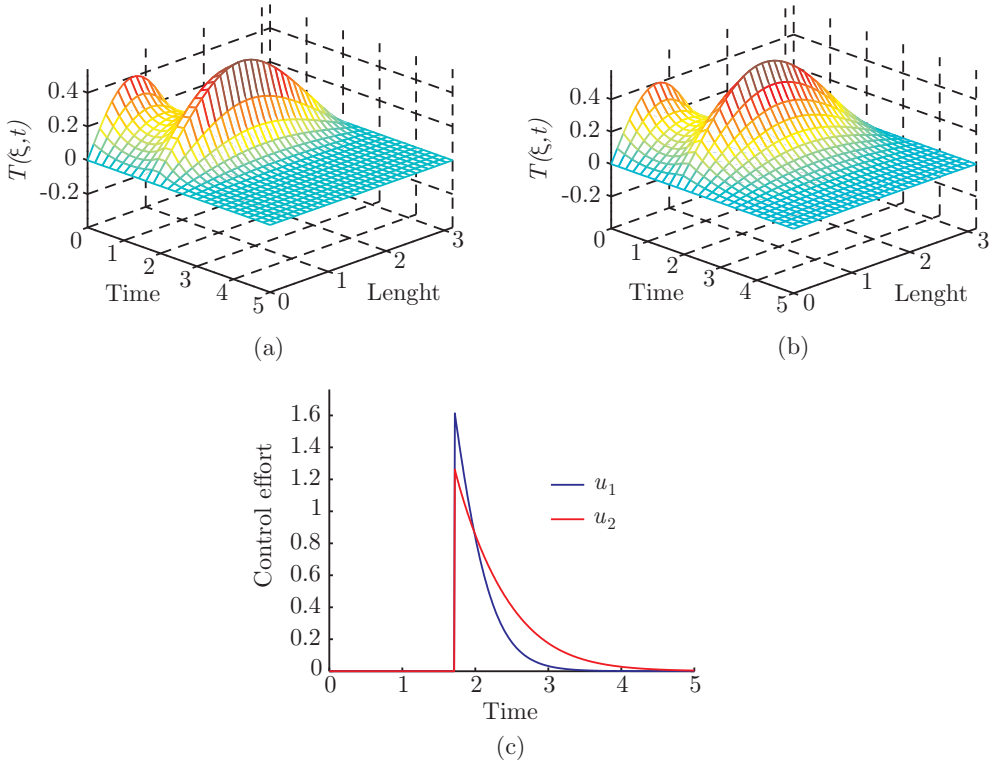

Figure 4.4: Evolution of the field under a control law designed by using different convex functions (a) using function b_1, (b) using function b_2. (c) Control effort for both functions.

4.5 Control Using a Finite Number of Actuators

So far, a control law able to drive a given dissipative system to either steady or dynamic reference trajectories was derived. However, it should be stressed that this control law is distributed throughout the spatial domain which calls for an infinite number of actuators. In practice, only a finite (and usually low) number of actuators is available. Here, this issue is approached using some concepts presented in previous sections. For the sake of clarity, the section will start with the problem of stabilising a system perfectly described by the model when all the terms of the model are known. After this, model uncertainty will be included in the problem and a robust control law will be constructed.

Consider a given dissipative system in deviation form with respect to a stationary reference trajectory $\mathbf{z}^*$ -see Section 1.5-:

$$\frac{\partial \overline{\mathbf{z}}}{\partial t} + \overrightarrow{\overline{\boldsymbol{\nabla}}} \cdot (\overrightarrow{\overline{\boldsymbol{\nu}}} \overline{\mathbf{z}}) = \Delta \overline{\boldsymbol{\Gamma}} + \overline{\mathbf{f}}(\mathbf{z}, \mathbf{z}^*) + \overline{\mathbf{u}}_m,$$

where $\overline{\mathbf{u}}_m$ is the control applied at a number m of intervals. The actuator is usually denoted by the couple (Ω, g) where Ω is the geometric support of the actuator, that is the region of the spatial domain where the actuator is located, and g the spatial distribution of the action on the support Ω (Zerrik et al., 2001). Although many authors have considered point-wise instead of zone actuators, in this work, for practical reasons only zone actuators will be employed[1]. Nevertheless it should be remarked that the same procedure applies to point-wise actuators.

As shown in Chapter 3, the solution $\overline{\mathbf{z}}$ can be approximated by a finite series of the form (3.19). Substituting this approximation on the previous equation and projecting the result over the finite dimensional set of eigenfunctions $\mathscr{E}_a = \{\phi_i\}_{i \in \mathcal{N}_a}$, an expression of the form of (4.20) is obtained:

$$\boldsymbol{\alpha}_a^T \frac{d\overline{\mathbf{m}}_a}{dt} = \langle \overline{\mathbf{A}}_a, \Delta \overline{\boldsymbol{\Gamma}} \rangle_{\mathscr{V}} - \langle \overline{\mathbf{A}}_a, \overrightarrow{\overline{\boldsymbol{\nabla}}} \cdot (\overrightarrow{\overline{\boldsymbol{\nu}}} \overline{\mathbf{z}}) \rangle_{\mathscr{V}} + \langle \overline{\mathbf{A}}_a, \overline{\mathbf{f}} \rangle_{\mathscr{V}} + \langle \overline{\mathbf{A}}_a, \overline{\mathbf{u}}_{am} \rangle_{\mathscr{V}}.$$

Using the convex function $\mathcal{B}_a$ as in the previous section and assuming that the nonlinear term is Lipschitz (see Condition 1.1), one has that:

$$\dot{\mathcal{B}}_a \leq -\zeta \lambda_m \|\overline{\mathbf{A}}_a\|_{\mathscr{V}}^2 + \mu_a \|\overline{\mathbf{A}}_a\|_{\mathscr{V}}^2 + \langle \overline{\mathbf{A}}_a, \overline{\mathbf{u}}_{am} \rangle_{\mathscr{V}}.$$

or, in terms of the modes $\boldsymbol{\alpha}_a(t)$:

$$\dot{\mathcal{B}}_a \leq -\zeta \lambda_m \boldsymbol{\alpha}_a^T \boldsymbol{\alpha}_a + \mu_a \boldsymbol{\alpha}_a^T \boldsymbol{\alpha}_a + \langle \overline{\mathbf{A}}_a, \overline{\mathbf{u}}_{am} \rangle_{\mathscr{V}}. \tag{4.31}$$

[1] In RDC systems, most of the controllers actuate over a region and not over a single point.

The number of elements in the set $\mathscr{E}_a = \{\phi_i\}_{i\in\mathcal{N}_a}$ was chosen so that the modes belonging to the set $\mathscr{M}_b$ remain stable. Therefore, a control law stabilising $\overline{\mathbf{z}}_a$ will stabilise the original system as well. Consider a matrix $\mathscr{G}$ whose elements are of the form[2]: $\mathscr{G}_{ij} = \langle \phi_j, g_i \rangle_{\mathscr{V}}$. As pointed out in Alonso et al. (2004b) and demonstrated in Zerrik et al. (2001) if the number of actuators is greater than or equal to the number of elements of $\mathcal{N}_a$, this is $m \geq n$ and $rank(\mathscr{G}) = m$, then the system is controllable. Let us now make use of the Heaviside function H to define g. In this way, the control law can be expressed as:

$$\overline{\mathbf{u}}_{am}(\xi,t) = \sum_{k=1}^{m} \left[H(\xi-\xi_k) - H(\xi-(\xi_k+d))\right] \mathfrak{u}_{ak}(\xi,t),$$

where $\mathfrak{u}_{ak}(\xi,t)$ is the control applied in each interval $\mathscr{V}_k = [\xi_k, \xi_k + d]$. For clarity in the notation, let us define the function $\mathcal{H}_k$ as: $\mathcal{H}_k = H(\xi-\xi_k) - H(\xi-(\xi_k+d))$. Consider that $\mathfrak{u}_{ak}(\xi,t) = -\omega\overline{\mathbf{A}}_a$, with ω being a scalar parameter, then:

$$\langle \overline{\mathbf{A}}_a, \overline{\mathbf{u}}_{am} \rangle_{\mathscr{V}} = -\omega \langle \overline{\mathbf{A}}_a, \sum_{k=1}^{m} \mathcal{H}_k \overline{\mathbf{A}}_a \rangle_{\mathscr{V}}.$$

Taking into account that $\overline{\mathbf{A}}_a$ can be expressed in terms of the modes $\boldsymbol{\alpha}_a(t)$ and the eigenfunctions $\phi_a(\boldsymbol{\xi})$ as: $\overline{\mathbf{A}}_a = \sum_{i\in\mathcal{N}_a} \boldsymbol{\alpha}_i(t)\phi_i(\boldsymbol{\xi})$, one is led to:

$$\langle \overline{\mathbf{A}}_a, \overline{\mathbf{u}}_{am} \rangle_{\mathscr{V}} = -\omega \langle \sum_{i\in\mathcal{N}_a} \boldsymbol{\alpha}_i\phi_i, \sum_{k=1}^{m} \mathcal{H}_k \sum_{i\in\mathcal{N}_a} \boldsymbol{\alpha}_i\phi_i \rangle_{\mathscr{V}} = -\omega \langle \sum_{k=1}^{m} \mathcal{H}_k \sum_{i\in\mathcal{N}_a} \boldsymbol{\alpha}_i\phi_i, \sum_{k=1}^{m} \mathcal{H}_k \sum_{i\in\mathcal{N}_a} \boldsymbol{\alpha}_i\phi_i \rangle_{\mathscr{V}}.$$

Since the elements of the set $\boldsymbol{\alpha}_a$ are independent of the spatial coordinates, the previous expression can be rewritten as:

$$\langle \overline{\mathbf{A}}_a, \overline{\mathbf{u}}_{am} \rangle_{\mathscr{V}} = -\omega \boldsymbol{\alpha}_a^T \mathbf{P} \boldsymbol{\alpha}_a,$$

where $\mathbf{P}$ is a matrix with elements:

$$\mathbf{P}_{ij} = \sum_{k=1}^{m} \int_{\mathscr{V}} \mathcal{H}_k \phi_i(\xi)\phi_j(\xi) d\xi = \sum_{k=1}^{m} \int_{\mathscr{V}_k} \phi_i(\xi)\phi_j(\xi) d\xi.$$

Choosing the parameter $\underline{\lambda}$ as the minimum eigenvalue of $\mathbf{P}$, inequality (4.31) becomes:

$$\dot{\mathcal{B}}_a \leq \left(-\zeta\lambda_m + \mu_a - \omega\underline{\lambda}\right) \boldsymbol{\alpha}_a^T \boldsymbol{\alpha}_a.$$

Selecting the control gain ω as:

$$\omega > \frac{(\mu_a - \zeta\lambda_m)}{\underline{\lambda}}, \tag{4.32}$$

[2]In the case of point-wise actuators the elements of the matrix would have the form $\mathscr{G}_{ij} = \phi_j(b_i)$ where b_i with $i = 1, .., m$ are the locations of the actuators.

and taking into account that $\mathcal{B}_a$ is related to $\boldsymbol{\alpha}_a$ through $q_{1a}, \delta_{0a} > 0$ -see Eqn (4.22)-, we obtain that $\dot{\mathcal{B}}_a \leq -r\mathcal{B}_a$, where $r = (\zeta\lambda_m - \mu_a + \omega\underline{\lambda})\,\delta_{0a}^2 q_{1a}^{-1} > 0$. Making use of the Gronwall-Bellman lemma (Khalil, 1996), one can show that $\mathcal{B}_a$ and thus $\overline{z}_a$ vanish as $t \to \infty$. It should be remarked that the best distribution of the actuators (that producing the lowest control effort) is that which maximises $\underline{\lambda}$.

Example 4.3 (A simple reaction-diffusion case) *Consider a system obeying the following PDE:*

$$\frac{\partial z}{\partial t} = \kappa\Delta z + z - 0.2z^3 + u, \tag{4.33}$$

with boundary and initial conditions of the form:

$$\overrightarrow{\mathbf{n}} \cdot \overrightarrow{\boldsymbol{\nabla}} z(\xi, t)|_{\mathscr{B}} = 0; \quad z(\xi, 0) = 5\left(\frac{\xi^2}{2} - \frac{\xi^4}{4}\right) + 1,$$

where z is the variable to be stabilised, $\kappa = 0.1$ is a diffusion coefficient and u stands for the control term.

Consider now a reduced order model for system (4.33) constructed with the LSD technique (see Section 3.4). Choosing the first four modes as the representative ones (i.e., $\mathcal{N}_a = [1, 2, 3, 4]$) the maximum relative error between the FEM and the ROM is $\varepsilon_{max} = 0.21\%$ and decreases very quickly with the time as shown in Figure 4.5 (b).

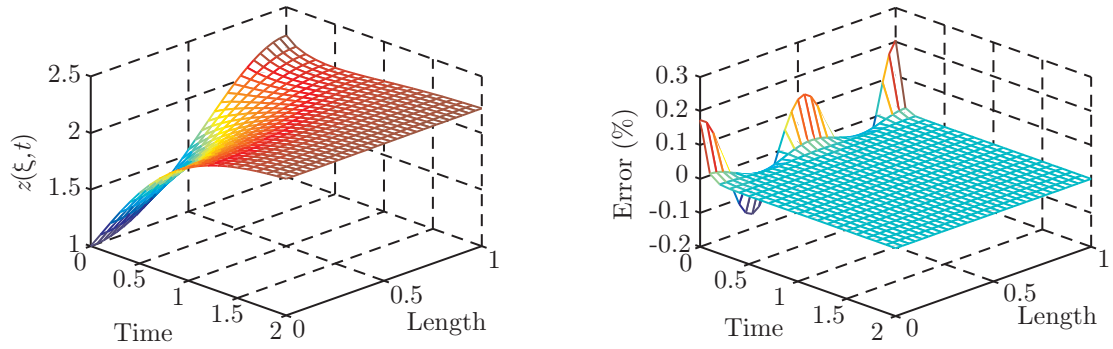

Figure 4.5: (a) Evolution and distribution of z in problem (4.33) with $u = 0$ computed using the FEM. (b) Relative error between the FEM and the ROM.

A control law which stabilises the first four modes will also stabilise the field. According to Zerrik et al. (2001) at least four actuators are necessary. The length of the zone of each actuator will be chosen so as to coincide with the length of a finite element, this is $d = L/30 = 1/30$. The number of possibilities for locating the actuators is about 3×10^4. Among these, the following maximises the minimum eigenvalue of $\mathbf{P}$ $(\underline{\lambda})$:

$$\Omega_1 = [0.0667, 0.1]; \quad \Omega_2 = [0.3333, 0.3667]; \quad \Omega_3 = [0.6, 0.63337]; \quad \Omega_4 = [0.8667, 0.9].$$

This notation indicates that the first actuator occupies the part of the domain defined by Ω_1, the second actuator is located on the spatial interval defined by Ω_2 and so on. Using these locations, we obtain $\underline{\lambda} = 0.125$. In this case, the Lipschitz condition holds for any parameter $\mu > 1$, and in particular it holds for $\mu = 1.5$. Finally, with these boundary conditions the minimum eigenvalue of the problem: $\Delta\phi_i = -\lambda_i\phi_i$, is $\lambda_m = 0$ and therefore the control gain takes the form $\omega > \mu/\underline{\lambda}$ - see Eqn (4.32)-. Consider now a control law of the form $\overline{\mathbf{u}}_{am}(\xi, t) = \sum_{k=1}^{m} \mathcal{H}_k \mathfrak{u}_k(\xi, t)$ with:

$$\mathfrak{u}_{ak} = -\omega \overline{\mathbf{A}}_a; \qquad \omega > \frac{\mu}{\underline{\lambda}} = \frac{1.5}{0.125}.$$

As shown in Figure 4.6 when this control is switched on ($t > 1.5$), system (4.33) is stabilised. □

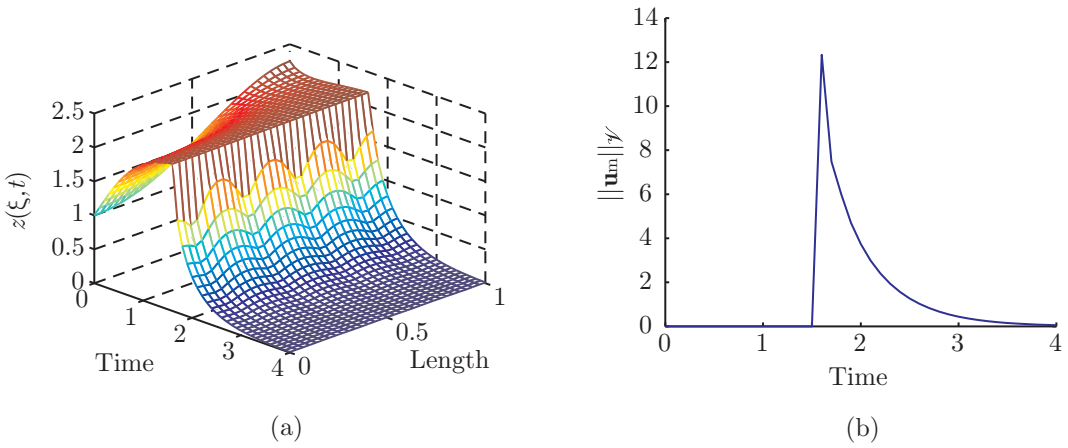

Figure 4.6: (a) Field evolution and distribution under the stabilising control law. (b) Control effort. The control enters at $t = 1.5$.

4.5.1 Robust Control Using a Finite Number of Actuators

In this section, model uncertainty is introduced into the problem of control of dissipative systems using a finite number of actuators. The basic idea is to combine the results of Section 4.4 with the main concepts presented in the first part of Section 4.5.

Consider a given RDC system where the diffusive parameters and the nonlinear terms are unknown. Consider also a reference trajectory $\mathbf{z}^*$ to be followed by the states $\mathbf{z}$ of the RDC system as in Section 4.4. Following the same procedure of Section 4.4, the state evolution can be expressed in terms of the modes - see expressions (4.18) and (4.19)-. These equations are rewritten here for the sake of clarity:

$$\frac{d\overline{\mathbf{m}}_a}{dt} = \langle \Phi_a, \Delta\overline{\mathbf{\Gamma}} \rangle_{\mathcal{Y}} - \langle \Phi_a, \Delta\mathbf{\Gamma}_d \rangle_{\mathcal{Y}} - \langle \Phi_a, \overrightarrow{\mathbf{\nabla}} \cdot (\overrightarrow{\mathbf{v}}\overline{\mathbf{z}}) \rangle_{\mathcal{Y}} + \langle \Phi_a, \overline{\mathbf{f}} \rangle_{\mathcal{Y}} + \langle \Phi_a, \overline{\mathbf{u}}_{am} \rangle_{\mathcal{Y}},$$

$$\frac{d\overline{\mathbf{m}}_b}{dt} = \langle \Phi_b, \Delta\mathbf{\Gamma}\rangle_{\mathscr{V}} - \langle \Phi_b, \overrightarrow{\overline{\mathbf{\nabla}}} \cdot (\overrightarrow{\overline{\mathbf{v}}}\overline{\mathbf{z}})\rangle_{\mathscr{V}} + \langle \Phi_b, \overline{\mathbf{f}}\rangle_{\mathscr{V}} + \langle \Phi_b, \overline{\mathbf{u}}_{bm}\rangle_{\mathscr{V}}.$$

The difference with respect to Section 4.4 is that now the control is applied at a finite number m of zones. The objective is to stabilise $\overline{\mathbf{m}}_a$ and $\overline{\mathbf{m}}_b$ through the control laws $\overline{\mathbf{u}}_{am}$ and $\overline{\mathbf{u}}_{bm}$, respectively. Using the relations of Lemmas 3.2 and 4.1, the Lipschitz condition 1.1 , the convex functions $b_a = 1/2\overline{\mathbf{z}}_a^T\overline{\mathbf{z}}_a$ and $b_b = 1/2\overline{\mathbf{z}}_b^T\overline{\mathbf{z}}_b$ and their integral counterparts $\mathcal{B}_a$ and $\mathcal{B}_b$, one has that:

$$\dot{\mathcal{B}}_a \leq -\zeta\lambda_m \boldsymbol{\alpha}_a^T\boldsymbol{\alpha}_a + \lambda_q\|\gamma_{da}\|_2\|\boldsymbol{\alpha}_a\|_2 + \zeta_a\|\boldsymbol{\alpha}_a\|_2 + \langle \overline{\mathbf{A}}_a, \overline{\mathbf{u}}_{am}\rangle_{\mathscr{V}}, \tag{4.34}$$

$$\dot{\mathcal{B}}_b \leq -\zeta\lambda_\ell \boldsymbol{\alpha}_b^T\boldsymbol{\alpha}_b + \zeta_b\|\boldsymbol{\alpha}_b\|_2 + \langle \overline{\mathbf{A}}_b, \overline{\mathbf{u}}_{bm}\rangle_{\mathscr{V}}. \tag{4.35}$$

$\overline{\mathbf{u}}_{am}$ and $\overline{\mathbf{u}}_{bm}$ must be constructed to drive, respectively, $\mathcal{B}_a$ and $\mathcal{B}_a$ to zero. Employing concepts of the first part of Section 4.5, $\overline{\mathbf{u}}_{am}$ and $\overline{\mathbf{u}}_{bm}$ are written, using the Heaviside function, as:

$$\overline{\mathbf{u}}_{am}(\xi,t) = \sum_{k=1}^{m} \mathcal{H}_k \mathfrak{u}_{ak}(\xi,t); \qquad \overline{\mathbf{u}}_{bm}(\xi,t) = \sum_{k=1}^{m} \mathcal{H}_k \mathfrak{u}_{bk}(\xi,t).$$

Proposition 4.3 *Consider that two given functions η_a and η_b bounding the uncertain parameters and nonlinear terms of the form: $\eta_a > \underline{\lambda}^{-1}(\lambda_q\|\gamma_{da}\|_2 + \zeta_a)$ and $\eta_b > \underline{\lambda}^{-1}(\zeta_b)$ are known. The control laws $\overline{\mathbf{u}}_{am}$ and $\overline{\mathbf{u}}_{bm}$ with $\mathfrak{u}_{ak}$ and $\mathfrak{u}_{bk}$ constructed as:*

$$\mathfrak{u}_{ak}(\xi,t) = \begin{cases} -\eta_a \frac{\overline{\mathbf{A}}_a}{\|\overline{\mathbf{A}}_a\|_{\mathscr{V}}} & \text{if} \quad \eta_a\|\overline{\mathbf{A}}_a\|_{\mathscr{V}} \geq \theta_a \\ \\ -\eta_a^2 \frac{\overline{\mathbf{A}}_a}{\theta_a} & \text{if} \quad \eta_a\|\overline{\mathbf{A}}_a\|_{\mathscr{V}} < \theta_a \end{cases}, \tag{4.36}$$

$$\mathfrak{u}_{bk}(\xi,t) = \begin{cases} -\eta_b \frac{\overline{\mathbf{A}}_b}{\|\overline{\mathbf{A}}_b\|_{\mathscr{V}}} & \text{if} \quad \eta_b\|\overline{\mathbf{A}}_b\|_{\mathscr{V}} \geq \theta_b \\ \\ -\eta_b^2 \frac{\overline{\mathbf{A}}_b}{\theta_b} & \text{if} \quad \eta_b\|\overline{\mathbf{A}}_b\|_{\mathscr{V}} < \theta_b \end{cases}, \tag{4.37}$$

will stabilise system (4.34)-(4.35) and thus will drive the field $\mathbf{z}$ to the reference $\mathbf{z}^*$.

The proof of this proposition for the control law $\overline{\mathbf{u}}_{am}$ can be found in Appendix B.6. The same procedure can be applied to obtain the proof for the control law $\overline{\mathbf{u}}_{bm}$.

Part II

Applications: Chemical and Biological Systems

Chapter 5

Application 1: Robust Control of Tubular Reactors

5.1 Introducción

Los reactores tubulares se emplean ampliamente en la industria química debido a sus múltiples ventajas entre las que se encuentran: presentan una elevada conversión volumétrica; el calor transferido mediante un medio de enfriamiento/calentamiento se puede optimizar incrementando el número de tubos y disminuyendo su área de contacto; o que pueden trabajar de forma continua durante largos periodos de tiempo. Entre sus principales desventajas cabe mencionar: que son difíciles de controlar y que cuando se llevan a cabo reacciones exotérmicas se pueden producir puntos calientes (Fogler, 1992). Esto hace que los reactores tubulares sean buenos candidatos para testar la teoría de control presentada en el capítulo anterior.

La representación esquemática de un reactor tubular típico se puede ver en la Figura 5.1. La alimentación fresca de reactivo entra por la izquierda con una concentración C_{Af}[1]. El componente A fluye a lo largo del reactor produciendo el compuesto deseado (B en la figura) que junto con la parte de A que no reaccionó sale por el extremo derecho. Cuando la reacción es exotérmica, el calor liberado incrementa la temperatura lo que puede producir daños en el reactor o incluso su explosión (Silebi and Schiesser, 1992). La temperatura del sistema se controla mediante un medio de calentamiento/enfriamiento (T_c en la Figura) que consiste en un número de tubos alrededor del reactor. Dentro de los tubos pasa un fluido cuya temperatura se puede manipu-

[1]Por conveniencia sólo se considerará un reactivo A

lar. El modelado, simulación y control son puntos clave cuando se trabaja con este tipo de reactores. Finalmente y para aumentar la eficiencia del reactor, la corriente de salida se introduce en un separador y el componente A se recicla y se mezcla con la alimentación fresca. El objetivo de este capítulo es probar las leyes de control y las técnicas de reducción de orden, propuestas en capítulos anteriores, en un caso de interés industrial.

5.2 Introduction

Tubular reactors are widely employed in the chemical industry due to their advantages among which the most important are listed next: they present a high volumetric conversion; the heat transfer with the heating/cooling media can be optimised by increasing the number of pipes and decreasing their contact area; or they are able to work continuously for long time periods. However, its main disadvantages are that they are difficult to control and when the reaction is exothermic hot spots can occur (Fogler, 1992) thus making tubular reactors good candidates to test the control theory presented in the previous chapter. A schematic representation of a typical tubular reactor is presented in Figure 5.1. The fresh feed of reactant enters the left end with concentra-

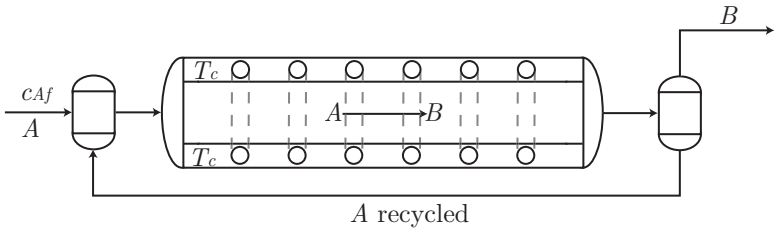

Figure 5.1: General representation of a tubular reactor with recycle where the reaction $A \rightarrow B$ takes place.

tion C_{Af}[2]. The component A flows through the vessel reacting to produce the desired compound (B in the Figure) which together with the part of A which did not react flow out the right end. When the reaction is exothermic the heat released increases the temperature, which may produce damages or even explosion (Silebi and Schiesser, 1992). The temperature of the system is controlled through a heating/cooling media (T_c in the Figure) which consists of a number of pipes around the reactor. A fluid with a manipulable temperature flows inside the pipes. The modelling, simulation and control are critical issues when working with this kind of reactors. Finally, and in order to

[2]For the sake of simplicity only one reactant, referred to as A, will be considered

increase the reactor efficiency, the outlet stream is introduced into a separator and the component A is recycled and mixed with the fresh feed. The objective of this chapter is to test the control and order reduction techniques, presented in previous chapters, on a case study of industrial interest.

The chapter is structured as follows: In Section 5.3 the models equations are derived from the theory presented in Chapter 1 and a dimensionless analysis will be performed to reduce the number of parameters. After this, the mathematical equations will be solved through the FEM technique and the behaviour of the system will be discussed. Besides, reduced order models will be shown to be a useful alternative to the FEM scheme. Finally in Section 5.5, the robust control technique derived in Chapter 4 will be applied to this system.

5.3 The Model Equations

The model equations employed to describe the behaviour of tubular reactors are the 3D version of those derived in Chapter 1 -see Eqns (1.11)-(1.13)-. However, for the sake of clarity, a number of assumptions will be made to simplify the model. For instance, usually in industrial reactors the radius is much lower than the length what allows us to neglect the dynamics and distribution in the radial direction, thus the system can be described by a 1D model. For a detailed discussion of models for tubular reactors see for instance Levenspiel (1962); Aris (1973); Fogler (1992). In general the following assumptions can be considered in ideal reactors.

Assumption 5.1 *The system is perfectly mixed in the radial direction.*

Assumption 5.2 *All the molecules stay the same time in the reactor.*

Assumption 5.3 *There is no void volume and turbulence is not considered.*

Assumption 5.4 *The axial velocity is constant and homogeneous.*

In a 3D model we have to specify the conditions at the boundary related with the radial direction. In the 1D version, these are included as transfer terms. Under these assumptions, the model equations, describing mass and energy balances, are of the form (Fogler, 1992; Levenspiel, 2004):

$$\frac{\partial(\rho c_A)}{\partial t} + \overrightarrow{\mathbf{v}} \cdot \overrightarrow{\boldsymbol{\nabla}}(\rho c_A) = -\overrightarrow{\boldsymbol{\nabla}} \cdot \overrightarrow{\mathbf{j}} + \rho r_A, \tag{5.1}$$

$$\frac{\partial(\rho u_s)}{\partial t} + \overrightarrow{\mathbf{v}} \cdot \overrightarrow{\boldsymbol{\nabla}}(\rho u_s) = -\overrightarrow{\boldsymbol{\nabla}} \cdot \overrightarrow{\mathbf{q}} + \rho h, \tag{5.2}$$

where c_A is the concentration of the component A, ρ indicates the density, v stands for the axial velocity, $\overrightarrow{\mathbf{j}}$ and $\overrightarrow{\mathbf{q}}$ are, respectively, the mass and heat fluxes in the axial direction, u_s represents the specific internal energy and r_A and h are the rates of growth of mass and energy, respectively. In general, when the fluids are liquids, the density can be considered constant and homogeneous. In addition, the contributions of the coupling terms to the mass and energy fluxes can be neglected so that Fick's and Fourier's laws hold. Thus, the mass balance referred to the component A can be rewritten as follows:

$$\frac{\partial c_A}{\partial t} + \overrightarrow{\mathbf{v}} \cdot \overrightarrow{\boldsymbol{\nabla}} c_A = \overrightarrow{\boldsymbol{\nabla}} \cdot \left(D_A \overrightarrow{\boldsymbol{\nabla}} c_A \right) + f_1(c_A, T), \tag{5.3}$$

where D_A is the diffusion coefficient and f_1 coincides with the reaction rate at which A is consumed (r_A).

On the other hand, the internal energy can be expressed as a function of a variable that turns out to be much easier to be measured, *the temperature*. In this regard for processes at constant volume, one has that:

$$du_s = \left(\frac{\partial u_s}{\partial T} \right)_V dT = c_V dT,$$

where V is the volume and c_V the specific heat at constant volume. In the case of liquids $c_V \approx c_p$. Introducing this expression into Eqn (1.12) the following PDE results:

$$\rho c_p \frac{\partial T}{\partial t} + \rho c_p \overrightarrow{\mathbf{v}} \cdot \overrightarrow{\boldsymbol{\nabla}} T = \overrightarrow{\boldsymbol{\nabla}} \cdot \left(\kappa \overrightarrow{\boldsymbol{\nabla}} T \right) + f_2(c_A, T) + Q_{tr}, \tag{5.4}$$

where the rate of energy growth, h in Eqn (5.2), is expressed as the contribution of two terms: the heat generated by the reaction (f_2) and the rate of heat exchanged between the cooling/heating device and the reactor (Q_{tr}). The expression for this last term is $Q_{tr} = h_U A_w (T_c - T)$ with h_U being the overall heat transfer coefficient, A_w is the contact area between the cooling device and the reactor and T_c represents the temperature of the cooling device.

In order to complete the description of the system, the boundary conditions must be specified. In this regard, the following assumptions will help us to simplify the derivation of such conditions:

Assumption 5.5 *There is no reaction taking place in the recycling stream.*

Assumption 5.6 *The residence time in the reactor is much longer than the delay in the recycling stream, thus the mixture with the fresh feed can be considered instantaneous.*

Under these assumptions, boundary conditions take the form:

$$\left[\overrightarrow{\mathbf{n}}\cdot\left(D_A\overrightarrow{\boldsymbol{\nabla}}c_A\right) = -v\left(c_A-(1-r)c_{Af}-rc_A(L,t)\right)\right]_{\xi=0}; \qquad \left[\overrightarrow{\mathbf{n}}\cdot\overrightarrow{\boldsymbol{\nabla}}c_A = 0\right]_{\xi=L}, \quad (5.5)$$

$$\left[\overrightarrow{\mathbf{n}}\cdot\left(\kappa\overrightarrow{\boldsymbol{\nabla}}T\right) = -\rho c_p v\left(T-(1-r)T_f-rT(L,t)\right)\right]_{\xi=0}; \qquad \left[\overrightarrow{\mathbf{n}}\cdot\overrightarrow{\boldsymbol{\nabla}}T = 0\right]_{\xi=L}, \quad (5.6)$$

where r is the recycle relation, c_{Af} and T_f correspond with the concentration and temperature of the fresh feed, respectively, and L is the reactor length.

5.3.1 Dimensional analysis

The dimensional analysis is a technique employed to make the analysis of given physical systems easier and to check the correctness of an equation which has been derived after some algebraic manipulations. It allow us to reduce the original set of dimensional parameters by employing a lower set of dimensionless parameters. For a detailed discussion about the dimensional analysis see, for instance, Aris (1999). One way of defining the dimensionless variables and parameters is to choose the characteristic length L and the fluid velocity v, so that:

$$\xi^* = \frac{\xi}{L}; \qquad t^* = \frac{tv}{L}, \quad (5.7)$$

are the dimensionless versions of the spatial and time coordinates. Using these transformations, the time and spatial operators take the form:

$$\frac{\partial}{\partial t} = \frac{v}{L}\frac{\partial}{\partial t^*}; \qquad \nabla = \frac{1}{L}\nabla^*; \qquad \Delta = \frac{1}{L^2}\Delta^*.$$

State and control dimensionless variables can also be obtained by defining the following transformations:

$$z_1 = \frac{c_A - c_A^{ref}}{c_A^{ref}}; \qquad z_2 = \frac{T - T^{ref}}{T^{ref}}; \qquad u = \frac{T_c - T^{ref}}{T^{ref}}, \quad (5.8)$$

where c_A^{ref} and T^{ref} are given references that, for simplicity when dealing with the boundary conditions, will be chosen as the concentration and the temperature of the fresh feed (c_{Af}, T_f), respectively. In order to simulate the behaviour of the reactor, expressions for the nonlinear terms are required. In this chapter, and for illustration purposes, a first order reaction term will be considered although other kinetic rates can be considered as well. Therefore, terms $f_1(c_A, T)$ and $f_2(c_A, T)$ in Eqns (5.3) and (5.4) are given by:

$$f_1(c_A,T) = -k\exp\left(\frac{-E_a}{RT}\right)c_A; \qquad f_2(c_A,T) = -\Delta Hk\exp\left(\frac{-E_a}{RT}\right)c_A, \quad (5.9)$$

where k is the pre-exponential factor, E_a denotes the activation energy, R represents the universal constant of gases and ΔH is the heat of reaction. A new set of dimensionless parameters can be defined from k, E_a, R and ΔH as follows:

$$\gamma = \frac{E_a}{RT_f}; \qquad B_{c_A} = \frac{kL\exp(-\gamma)}{v}; \qquad B_T = \frac{-\Delta H c_{Af}}{\rho c_p T_f}. \tag{5.10}$$

It is an easy task to show that, using (5.7)-(5.10) and assuming that the thermal conductivity κ and the mass diffusivity D_A are constant, Eqns (5.3) - (5.6) can be rewritten as:

$$\frac{\partial z_1}{\partial t^*} + \nabla^* z_1 = \frac{1}{Pe_{z_1}}\Delta^* z_1 - B_{c_A} f^*(z_1, z_2), \tag{5.11}$$

$$\frac{\partial z_2}{\partial t^*} + \nabla^* z_2 = \frac{1}{Pe_{z_2}}\Delta^* z_2 + B_T B_{c_A} f^*(z_1, z_2) + \beta_T (u - z_2), \tag{5.12}$$

$$[\nabla^* z_1 = Pe_{z_1}(z_1 - r z_1(1, t^*))]_{\xi=0}; \quad [\nabla^* z_1 = 0]_{\xi=1}, \tag{5.13}$$

$$[\nabla^* z_2 = Pe_{z_2}(z_2 - r z_2(1, t^*))]_{\xi=0}; \quad [\nabla^* z_2 = 0]_{\xi=1}, \tag{5.14}$$

where

$$Pe_{z_1} = \frac{Lv}{D_A}; \quad Pe_{z_2} = \frac{Lv\rho c_p}{\kappa}; \quad \beta_T = \frac{h_U A_w L}{\rho c_p v}; \quad f^*(z_1, z_2) = \exp\left(\frac{\gamma z_2}{z_2 + 1}\right)(1 + z_1).$$

For the sake of clarity and with some abuse of notation, dimensionless variables t^*, ξ^*, nonlinear function f^* and spatial operators ∇^* and Δ^* will be denoted by t, ξ, f, ∇ and Δ, respectively, in the remaining of this chapter.

Finally, collecting the state variables z_1 and z_2 into the vector state $\mathbf{z} = [z_1, z_2]^T$, equations (5.11)-(5.14) can be rewritten in a more compact form as:

$$\frac{\partial \mathbf{z}(\xi, t)}{\partial t} + \nabla \mathbf{z}(\xi, t) = D\Delta \mathbf{z}(\xi, t) + \Sigma(\mathbf{z}) + \mathbf{u}(\xi, t), \tag{5.15}$$

$$[\nabla \mathbf{z} = Pe_{\mathbf{z}}(r\mathbf{z}(1, t) - \mathbf{z}(t, 0))]_{\xi=0}; \qquad [\nabla \mathbf{z} = \mathbf{0}]_{\xi=1}, \tag{5.16}$$

where the diffusion and Peclet matrices, nonlinear terms and control inputs are of the form:

$$D = \begin{bmatrix} \frac{1}{Pe_{z_1}} & 0 \\ 0 & \frac{1}{Pe_{z_2}} \end{bmatrix}; \quad Pe_{\mathbf{z}} = \begin{bmatrix} Pe_{z_1} & 0 \\ 0 & Pe_{z_2} \end{bmatrix};$$

$$\Sigma(\mathbf{z}) = \begin{bmatrix} -B_{c_A} f(z_1, z_2) \\ \\ B_T B_{c_A} f(z_1, z_2) - \beta_T z_2 \end{bmatrix}; \quad \mathbf{u} = \begin{bmatrix} 0 \\ \\ \beta_T u \end{bmatrix}.$$

5.3.2 Transformation to Homogeneous Boundary Conditions

As mentioned in Section 3.4, in order to apply the LSD method, homogeneous boundary conditions are required. In this section, use is made of the state transformation proposed in Balsa-Canto et al. (2004) to obtain a mathematical model equivalent to system (5.15)-(5.16) with homogeneous boundary conditions.

Consider the following state transformation:

$$\mathbf{x} = \mathbf{z} - \boldsymbol{\chi}(\xi)\boldsymbol{\pi}(t), \tag{5.17}$$

with

$$\mathbf{x} = \begin{bmatrix} x_1(\xi,t) \\ x_2(\xi,t) \end{bmatrix}; \quad \boldsymbol{\chi}(\xi) = \begin{bmatrix} \chi_1(\xi) & 0 \\ 0 & \chi_2(\xi) \end{bmatrix}; \quad \boldsymbol{\pi}(\xi) = \begin{bmatrix} \pi_1(t) \\ \pi_2(t) \end{bmatrix}.$$

Introducing (5.17) into Eqns (5.15)-(5.16) and selecting the functions $\boldsymbol{\chi}(\xi)$ and $\boldsymbol{\pi}(t)$ so that:

$$\boldsymbol{\pi}(t) = \mathbf{z}(1,t); \qquad \chi_1(\xi) = \chi_2(\xi) = r; \quad \forall t, \xi,$$

the behaviour of the reactor can be described by the following PDE system:

$$\frac{d\mathbf{x}}{dt} = D\Delta\mathbf{x} - \nabla\mathbf{x} + \Sigma(\mathbf{x}) - r\frac{d\mathbf{z}(1,t)}{dt} + \mathbf{u}, \tag{5.18}$$

$$[\nabla\mathbf{x} = -Pe_{\mathbf{z}}\mathbf{x}]_{\xi=0}\,; \qquad [\nabla\mathbf{x} = 0]_{\xi=1}\,, \tag{5.19}$$

where the nonlinear term is of the form:

$$\Sigma(\mathbf{x}) = \begin{bmatrix} -B_{c_A}(1 + x_1 + rz_1(1,t)) \exp\left(\frac{\gamma(x_2+rz_2(1,t))}{1+x_2+rz_2(1,t)}\right) \\ \\ B_T B_{c_A}(1 + x_1 + rz_1(1,t)) \exp\left(\frac{\gamma(x_2+rz_2(1,t))}{1+x_2+rz_2(1,t)}\right) - \beta_T(x_2 + rz_2(1,t)) \end{bmatrix}.$$

Note that an expression for the term $\frac{d\mathbf{z}(1,t)}{dt}$ is required to solve the system. This expression is obtained through the Dirac delta $\delta(\xi-\xi')$ with $\xi' = 1$. When $\delta(\xi-\xi')$ acts over transformation (5.17) and Eqn (5.18) and after spatial integration, the following expressions are obtained:

$$\mathbf{x}(1,t) = \mathbf{z}(1,t) - r\mathbf{z}(1,t) \Rightarrow \frac{d\mathbf{x}(1,t)}{dt} = (1-r)\frac{d\mathbf{z}(1,t)}{dt}, \tag{5.20}$$

$$\frac{d\mathbf{x}(1,t)}{dt} = D\Delta\mathbf{x}(1,t) - \nabla\mathbf{x}(1,t) + \Sigma(\mathbf{x})^L - r\frac{d\mathbf{z}(1,t)}{dt} + \mathbf{u}^L,$$

where $\Sigma(\mathbf{x})^L$ and $\mathbf{u}^L$ represent the values of functions $\Sigma(\mathbf{x})$ and $\mathbf{u}$, respectively, in $\xi = 1$. Finally, the combination of the previous equation with expression (5.20) results into:

$$\frac{d\mathbf{z}(1,t)}{dt} = D\Delta\mathbf{x}(1,t) - \nabla\mathbf{x}(1,t) + \Sigma(\mathbf{x})^L + \mathbf{u}^L. \tag{5.21}$$

5.4 The Simulation of Tubular Reactors

In order to illustrate the different aspects of the theory presented in previous chapters on tubular reactors, let us consider a reactor described by Eqns (5.15)-(5.16) with the following set of parameters (Antoniades and Christofides, 2001):

$$Pe_{z_1} = Pe_{z_2} = 7; \quad B_{c_A} = 0.1; \quad \gamma = 10; \quad B_T = 2.5; \quad \beta_T = 2.$$

Initial conditions are chosen of the form:

$$z_1(\xi, 0) = z_2(\xi, 0) = 0. \tag{5.22}$$

Before proceeding with the simulation of the reactor, let us show that according to Definition 1.2 this system is dissipative with respect to $b = \frac{1}{2}(c_A^2 + T^2)$. To illustrate this point the invariant set $\ell_0 = -\mathbf{A}^T\Sigma(\mathbf{z})$ -see Eqn (1.41) in Condition 1.1- where $\mathbf{A}^T = \partial b/\partial \mathbf{z}$, is represented in Figure 5.2. The continuous black line (ϖ) corresponds with the region where $\ell_0 = 0$, while the area denoted by Ω depicts the zone where $\ell_0 < 0$. The unreachable region ($c_A > c_{Af}$) is represented by a gray rectangle. The picture

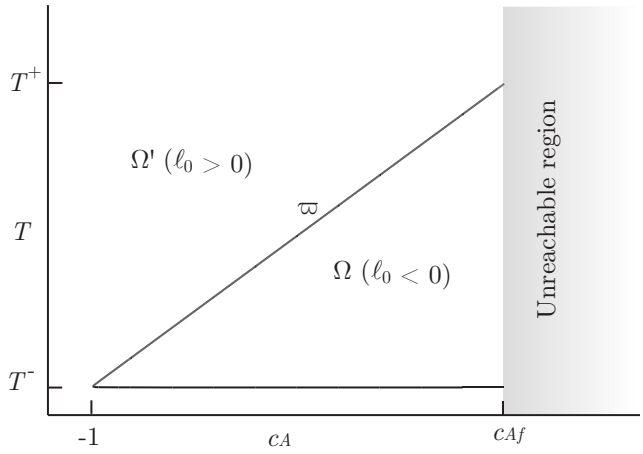

Figure 5.2: State space representation of the invariant set (ℓ_0) for the System (5.15). The zone where $\ell_0 = 0$ is depicted by the continuous black line (ϖ).

shows that, for a given feed concentration c_{Af}, there exists an upper temperature (T^+) so that, outside the bounded region $\mathcal{D} = \Omega \cup \varpi$, ℓ_0 is positive.

5.4.1 The Finite Element Method

The steps described in Section 2.3 are applied in this example so as to obtain and use the FEM matrices. The flexibility of the FEM allows us to employ it for both homogeneous and inhomogeneous boundary conditions.

Inhomogeneous boundary conditions

In this case, the system is described by Eqns (5.15)-(5.16). After the discretisation of the spatial domain into N nodes and the selection of the basis functions φ (in this example first order polynomials) the FEM matrices can be obtained as described in section 2.3. Using these matrices, the original infinite dimensional system can be approximated by a finite number of ODEs of the form:

$$\frac{d\mathcal{Z}_1}{dt} = -\mathcal{D}\mathcal{A}^{-1}\left(\frac{1}{Pe_{z_1}}\mathcal{C} + \mathcal{B}\mathcal{E} + \mathcal{Q}\right)\mathcal{Z}_1 - B_{c_A}\mathcal{F}(\mathcal{Z}_1, \mathcal{Z}_2) + \mathcal{D}\mathcal{A}^{-1}\mathcal{G}_1, \tag{5.23}$$

$$\frac{d\mathcal{Z}_2}{dt} = -\mathcal{D}\mathcal{A}^{-1}\left(\frac{1}{Pe_{z_2}}\mathcal{C} + \mathcal{B}\mathcal{E} + \mathcal{Q}\right)\mathcal{Z}_2 + B_T B_{c_A}\mathcal{F}(\mathcal{Z}_1, \mathcal{Z}_2) + \beta_T(\mathcal{U} - \mathcal{Z}_2) + \mathcal{D}\mathcal{A}^{-1}\mathcal{G}_2, \tag{5.24}$$

where $\mathcal{Z}_1, \mathcal{Z}_2, \mathcal{F}$ and $\mathcal{U}$ are, respectively, the FEM discrete counterparts of the fields z_1 and z_2, nonlinear function f and control term u. Likewise, initial conditions (5.22) become:

$$\mathcal{Z}_1(0) = \mathcal{Z}_2(0) = \mathbf{0}. \tag{5.25}$$

The dynamic evolution of this system is highly conditioned by the value of the recycle relation. In order to illustrate this point, system (5.23)-(5.25) has been numerically solved using different recycle relations. The results for $r = 0$ are represented in Figure 5.3. Note that in this case a steady state is reached after $t = 2$. On the contrary, when

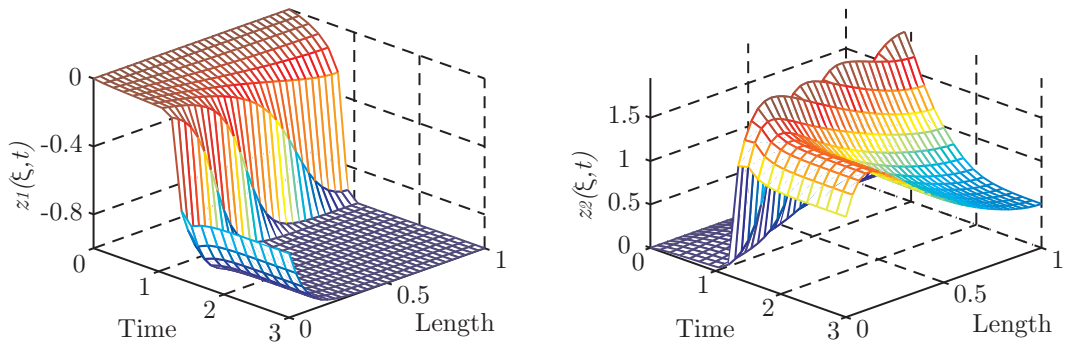

(a) (b)

Figure 5.3: Solution of system (5.23)-(5.25) without recycle ($r = 0$). (a) For the dimensionless concentration and (b) for the dimensionless temperature.

the recycle relation is $r = 0.5$ an oscillatory behaviour is produced in the evolution of the system (see Figure 5.4). Such oscillatory behaviour corresponds to a limit cycle as shown in Figure 5.5 where the $\mathcal{L}_2$ norms of fields z_1 and z_2 are plotted.

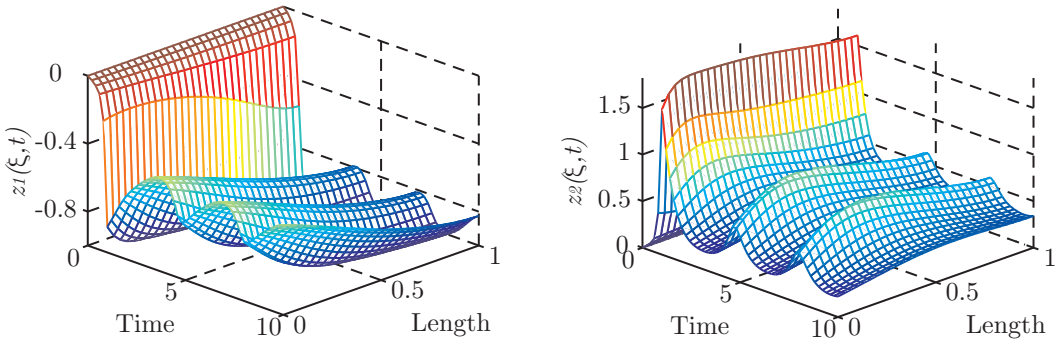

Figure 5.4: Solution of system (5.23)-(5.25) with recycle relation $r = 0.5$. (a) For the dimensionless concentration and (b) for the dimensionless temperature.

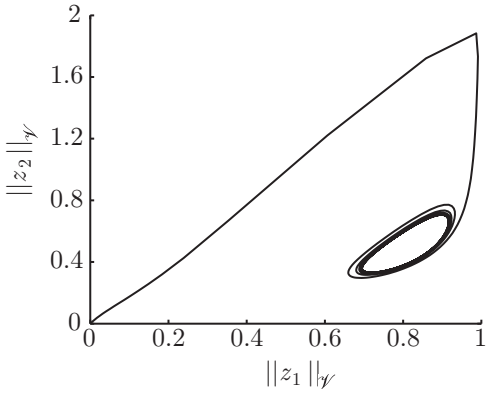

Figure 5.5: Representation of the limit cycle reached when $r = 0.5$ in terms of the norm of the states.

It should be stressed that this simulation was carried out using a discretisation scheme of 31 nodes ($N = 31$). No further improvements in the solution were achieved for larger number of nodes.

Homogeneous boundary conditions

In this case, the system is described by Eqns (5.18)-(5.19). As in the previous case, the FEM matrices are employed to approximate the infinite dimensional system by a finite number of ODEs of the form:

$$\frac{d\mathcal{X}_1}{dt} = -\mathcal{D}\mathcal{A}^{-1}\left(\frac{1}{Pe_{z_1}}\mathcal{C} + \mathcal{B}\mathcal{E} + \mathcal{Q}\right)\mathcal{X}_1 - B_{c_A}\mathcal{F}(\mathcal{X}_1, \mathcal{X}_2) - r\frac{d\mathcal{Z}_1(1,t)}{dt}, \tag{5.26}$$

$$\frac{d\mathcal{X}_2}{dt} = -\mathcal{D}\mathcal{A}^{-1}\left(\frac{1}{Pe_{z_2}}\mathcal{C} + \mathcal{B}\mathcal{E} + \mathcal{Q}\right)\mathcal{X}_2 + B_T B_{c_A}\mathcal{F}(\mathcal{X}_1, \mathcal{X}_2) + \beta_T(\mathcal{U} - \mathcal{X}_2) - r\frac{d\mathcal{Z}_2(1,t)}{dt}, \tag{5.27}$$

where $\mathcal{X}_1, \mathcal{X}_2$ and $\mathcal{F}$ are, respectively, the FEM discrete counterparts of the fields x_1 and x_2 and nonlinear function $f(\mathbf{x})$. The time derivative of each vector $\mathcal{Z}_i$ with $i = 1, 2$ - see Eqn (5.21)- is computed using the FEM matrices by the following relation:

$$\frac{d\mathcal{Z}_i}{dt} = -\mathcal{D}\mathcal{A}^{-1}\left(\frac{1}{Pe_{z_1}}\mathcal{C}(i_L,:) + \mathcal{B}\mathcal{E}(i_L,:) + \mathcal{Q}(i_L,:)\right)\mathcal{X}_i + \Sigma_i^L + \mathcal{U}^L$$

where the notation $(i_L, :)$ in the FEM matrices indicates the row corresponding to the point $\xi = L = 1$ and the superindex L refers to the value of the function at the point $\xi = L = 1$. According to transformation (5.17), the initial conditions are in this case:

$$\mathcal{X}_1(0) = \mathcal{X}_2(0) = \mathbf{0}. \tag{5.28}$$

Obviously, since this system of equations is just an alternative representation of the reactor dynamics, their solutions will be also highly conditioned by the value of the recycle relation. Once again, the system has been numerically solved using different recycle relations. Figure 5.6 shows the results obtained when $r = 0$. Note that accord-

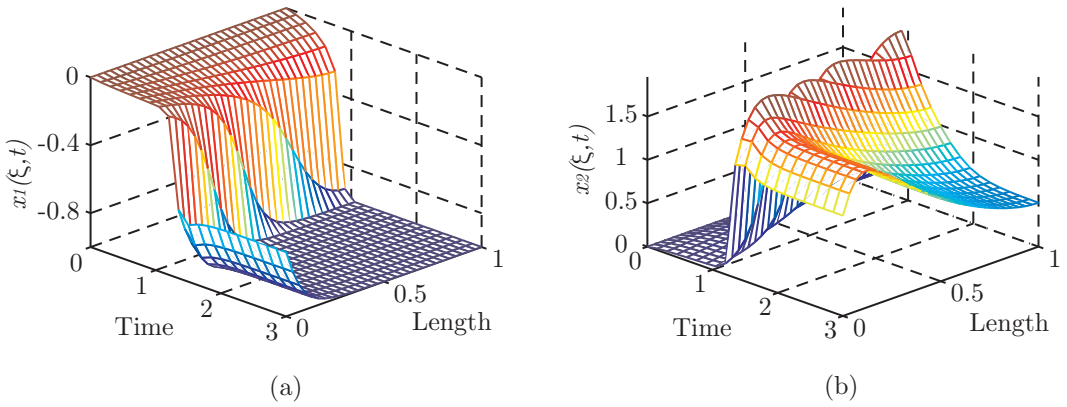

Figure 5.6: Solution of system (5.26)-(5.28) without recycle ($r = 0$). (a) For the dimensionless concentration and (b) for the dimensionless temperature.

ing to transformation (5.17) if $r = 0$ then $\mathbf{z}$ should coincide with $\mathbf{x}$. This fact becomes clear when comparing Figures 5.3 and 5.6. On the contrary, when the recycle relation is $r = 0.5$, although a limit cycle is also obtained (see Figure 5.7) the value of $\mathbf{z}$ differs from $\overrightarrow{\mathbf{x}}$.

It should be remarked that negligible differences (below 1×10^{-4}) between the original field $\mathbf{z}$ and the field computed using the transformation $\mathbf{x}$ arise, mainly because of time discretisation errors.

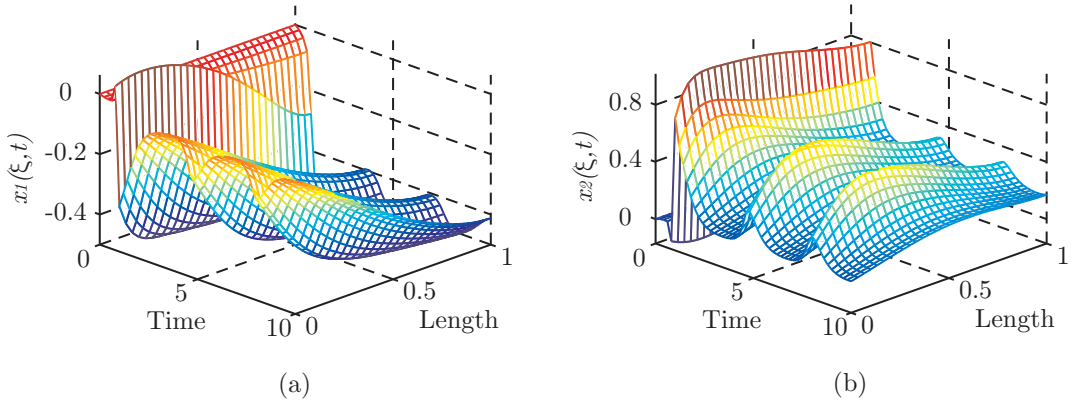

Figure 5.7: Solution of system (5.26)-(5.28) with recycle relation $r = 0.5$. (a) For the dimensionless concentration and (b) for the dimensionless temperature.

5.4.2 The Laplacian Spectral Decomposition Method

Since the LSD method fails when inhomogeneous boundary conditions are taken into account, this technique will be applied to the transformed system (5.18)-(5.19). The first step is to obtain the eigenfunctions by solving the eigenvalue equation $\Delta\phi_i = -\lambda_i\phi_i$ with appropriate boundary conditions. Using the FEM matrices the following discrete counterpart of the problem is obtained:

$$\mathcal{D}\mathcal{A}^{-1}\left(\frac{1}{Pe_z}\mathcal{C} + \mathcal{Q}\right)\boldsymbol{\phi}_i = -\lambda_i\boldsymbol{\phi}_i. \tag{5.29}$$

The first four eigenfunctions with the corresponding eigenvalues are plotted in Figure 5.8. As expected, the frequency of the spatial oscillations for the eigenfunction ϕ_i is

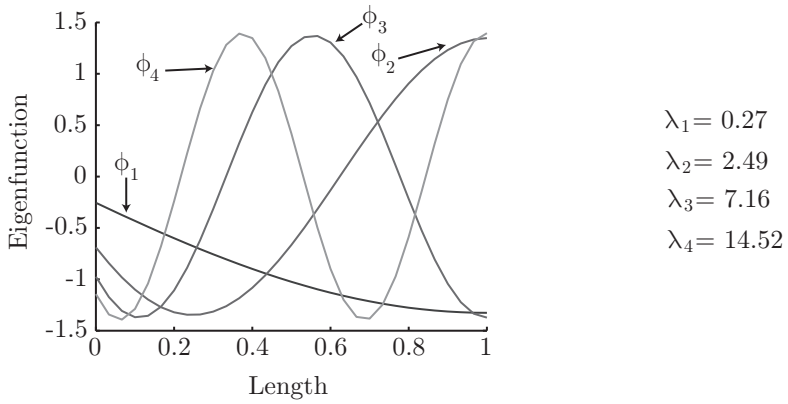

Figure 5.8: First four eigenfunctions and their corresponding eigenvalues computed by solving Eqn (5.29).

higher than that corresponding with the eigenfunction ϕ_j whenever $i > j$. Projection

of system (5.18) over the eigenfunctions leads to the following set of ODEs:

$$\frac{d\mathbf{m}_{x_1}}{dt} = \mathcal{A}\mathbf{m}_{x_1} - B_{c_A}\mathscr{F} - r\mathbf{\Phi}^T\mathcal{D}\mathcal{A}\frac{d\mathcal{Z}_1(1,t)}{dt},$$

$$\frac{d\mathbf{m}_{x_2}}{dt} = \mathcal{A}\mathbf{m}_{x_2} + B_T B_{c_A}\mathscr{F} + \beta_T(\mathscr{U} - \mathbf{m}_{x_2}) - r\mathbf{\Phi}^T\mathcal{D}\mathcal{A}\frac{d\mathcal{Z}_2(1,t)}{dt},$$

where:

$$\mathcal{A} = -\mathbf{\Phi}^T\left(\frac{1}{Pe_{z_1}}\mathcal{C} + \mathcal{B}\mathcal{E} + \mathcal{Q}\right)\mathbf{\Phi}; \quad \mathscr{F} = \mathbf{\Phi}^T\mathcal{D}\mathcal{A}F(\mathcal{X}_1, \mathcal{X}_2); \quad \mathscr{U} = \mathbf{\Phi}^T\mathcal{D}\mathcal{A}\mathcal{U}.$$

First let us start by showing the results for $r = 0$. In this case, the first 8 eigenfunctions are enough to obtain a maximum relative error between the FEM and the LSD results lower than the 1%. As shown in Figure 5.9 the LSD is able to reproduce the tubular reactor behaviour. From another perspective (a comparison in terms of

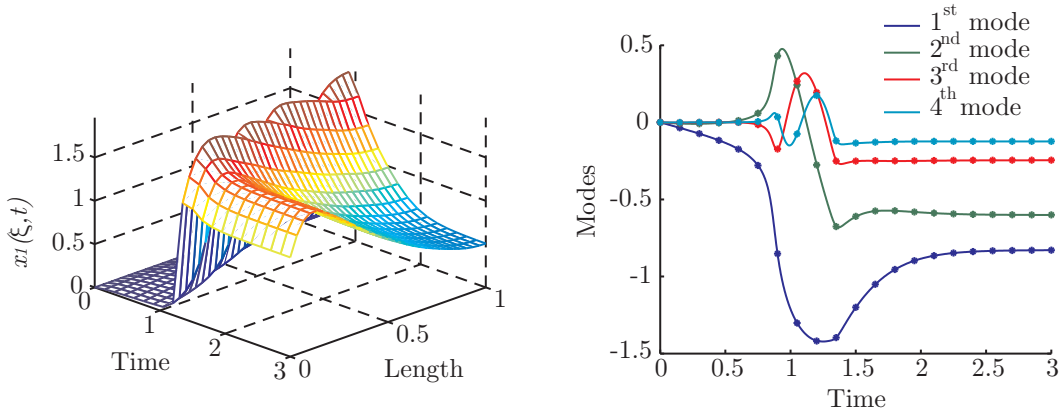

Figure 5.9: Solution of system (5.18)-(5.19) with $r = 0$ using the LSD with 8 eigenfunctions. (a) x_2 field representation, (b) x_2 modes representation.

the modes), Figure 5.9 (b) shows that the solution obtained with the FEM (continuous lines), coincides with the solution obtained with the LSD (marks). Note that the number of equations in the LSD is almost four times lower than in the FEM.

When the recycle relation is set to $r = 0.5$ the LSD does not work as accurately as for the same number of eigenfunctions when $r = 0$ thus leading to relative errors between the LSD and the FEM greater than the 50% when using 8 eigenfunctions. This number must be then increased. Using 15 eigenfunctions the maximum relative error is reduced to the 5% and, as shown in Figure 5.10 (a), the tubular reactor behaviour can be reproduced. However slight differences between the FEM and the LSD solutions still remain (see Figure 5.10 (b)) even with such number of eigenfunctions.

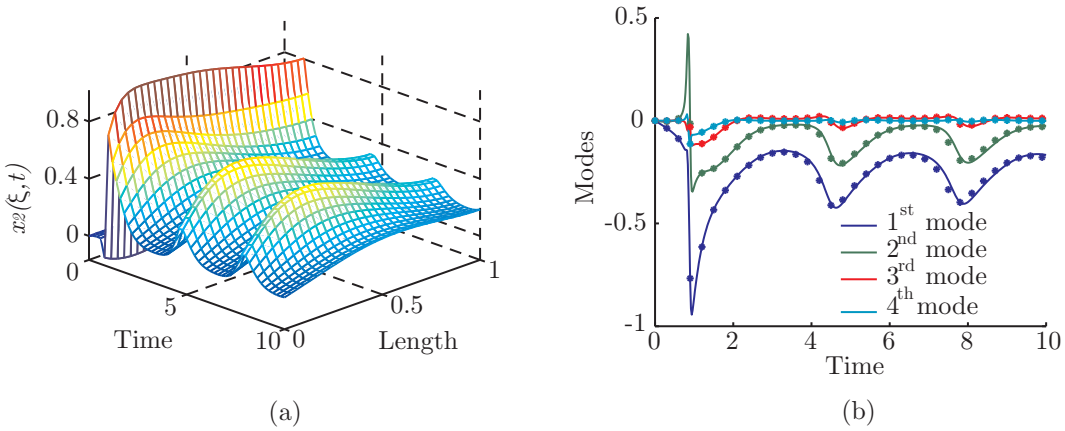

Figure 5.10: Solution of system (5.18)-(5.19) with $r = 0.5$ using the LSD with 15 eigenfunctions. (a) x_2 field representation, (b) mode representation.

5.4.3 The Proper Orthogonal Decomposition Method

The first step in the construction of the basis set is to obtain a set of snapshots representative of the behaviour of the system (5.15)-(5.16). In this case, the objective is to derive a ROM capable of reproducing the original system for both $r = 0$ and $r = 0.5$. It should be also able to represent transition periods as well as steady states attained and limit cycles. The snapshots are obtained from direct numerical simulation using initial conditions $z_1(\xi, 0) = z_2(\xi, 0) = 0$. When $r = 0$, the data were taken using a time interval of $\delta t = 0.03$. After the steady state is reached at $t \approx 2.7$ only four snapshots were selected. When the recycle relation is set to $r = 0.5$, the time interval between to consecutive measurements is reduced to $\delta t = 0.01$ in order to accurately capture the limit cycle. The last snapshot was taken at $t = 8$, which is enough to capture the information of one cycle.

Once the snapshots are obtained, the PODs can be computed using any of the methods described in Section 3.4.2. In this case, since the number of snapshots is much larger than the number of nodes N, the *direct method* is more convenient (see Section 3.4.2). Using the FEM matrices, this is equivalent to solving:

$$\boldsymbol{\phi}_i^{z_j} = \lambda_i \mathcal{K}_{z_j} \mathcal{D}\mathcal{A} \boldsymbol{\phi}_i^{z_j}; \qquad \mathcal{K}_{z_j} = \frac{1}{\ell} \sum_{k=1}^{\ell} \mathcal{Z}_j(t_k) \mathcal{Z}_j^T(t_k); \qquad j = 1, 2; \quad i = 1, ..., N,$$

Figure 5.11(a) shows the shape of the first three PODs for the fields z_1 (blue lines) and z_2 (red lines). Note that the higher the number of the POD, the larger the frequency of the spatial oscillations. The energy captured by the first nine PODs is depicted in Figure 5.11(b). As shown in the figures, using 8 and 9 PODs for the fields $z1$ and z_2,

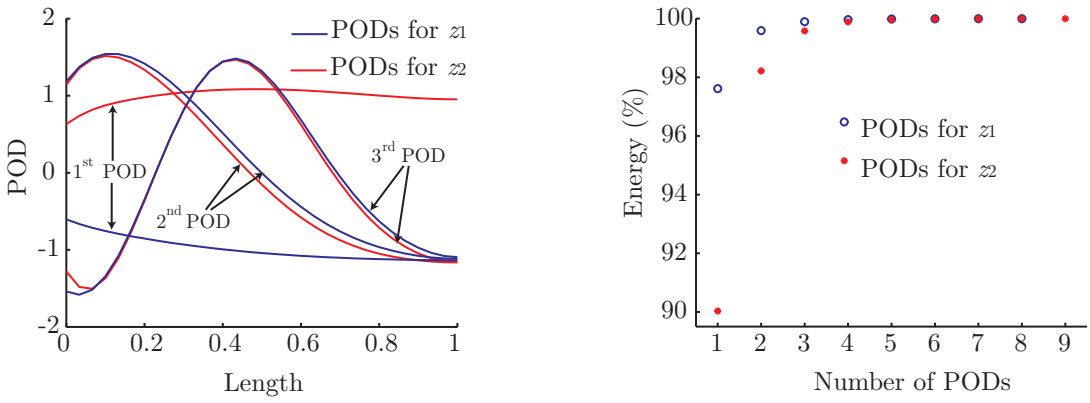

Figure 5.11: (a) Shape of the first three PODs for the fields z_1 (blue lines) and z_2 (red lines). (b) Energy captured by the PODs.

respectively, is enough to capture the 99.999% of the energy.

As described in Section 5.4.1, Eqns (5.15)-(5.16) can be numerically approximated by a set of ODEs using the FEM matrices -see Eqns (5.23)-(5.24)-. The projection of these equations into the PODs leads to the following ODE set:

$$\frac{d\mathbf{m}_{z_1}}{dt} = \mathcal{A}_{\mathbf{m}_{z1}}\mathbf{m}_{z_1} - B_{c_A}\mathscr{F}_{z_1} + \mathscr{G}_{z_1},$$

$$\frac{d\mathbf{m}_{z_2}}{dt} = \mathcal{A}_{\mathbf{m}_{z2}}\mathbf{m}_{z_2} + B_T B_{c_A}\mathscr{F}_{z_2} + \beta_T(\mathscr{U} - \mathbf{m}_{z_2}) + \mathscr{G}_{z_2}.$$

Collecting the representative PODs ($\boldsymbol{\phi}_i^{z_j}$, with $j = 1, 2$) into the matrix $\boldsymbol{\Phi}^{z_j}$, the different terms of the previous relations can be expressed as:

$$\mathcal{A}_{\mathbf{m}_{zj}} = -(\boldsymbol{\Phi}^{z_j})^T \left(1/Pe_{z_j}\mathcal{C} + \mathcal{Q} + \mathcal{B}\mathcal{E}\right)\boldsymbol{\Phi}^{z_j}; \quad \mathscr{F}_{z_j} = (\boldsymbol{\Phi}^{z_j})^T\mathcal{D}\mathcal{A}\mathcal{F};$$

$$\mathscr{G}_{z_j} = (\boldsymbol{\Phi}^{z_j})^T\mathcal{G}_j; \quad \mathscr{U} = (\boldsymbol{\Phi}^{z_2})^T\mathcal{D}\mathcal{A}\mathbf{U}.$$

The FEM matrices can be also employed to compute the initial conditions, so that:

$$\mathbf{m}_{z_j}(0) = (\boldsymbol{\Phi}^{z_j})^T\mathcal{D}\mathcal{A}\mathcal{Z}_j(0); \qquad j = 1, 2.$$

Once these equations are solved, the field is recovered by applying $\mathcal{Z}_j = \boldsymbol{\Phi}^{z_j}\mathbf{m}_{z_j}$. For $r = 0$, the field z_2 computed using the POD technique capturing the 99.999% of the energy is plotted in Figure 5.12 (a), for $r = 0.5$ the field z_1 is represented in Figure 5.12 (c). The relative error between the FEM and the POD solution remains below the 0.5% with the exception of a few points, in the case of $r = 0$, coinciding with the sharp regions of the transient period. In these points the relative error increases to 5%.

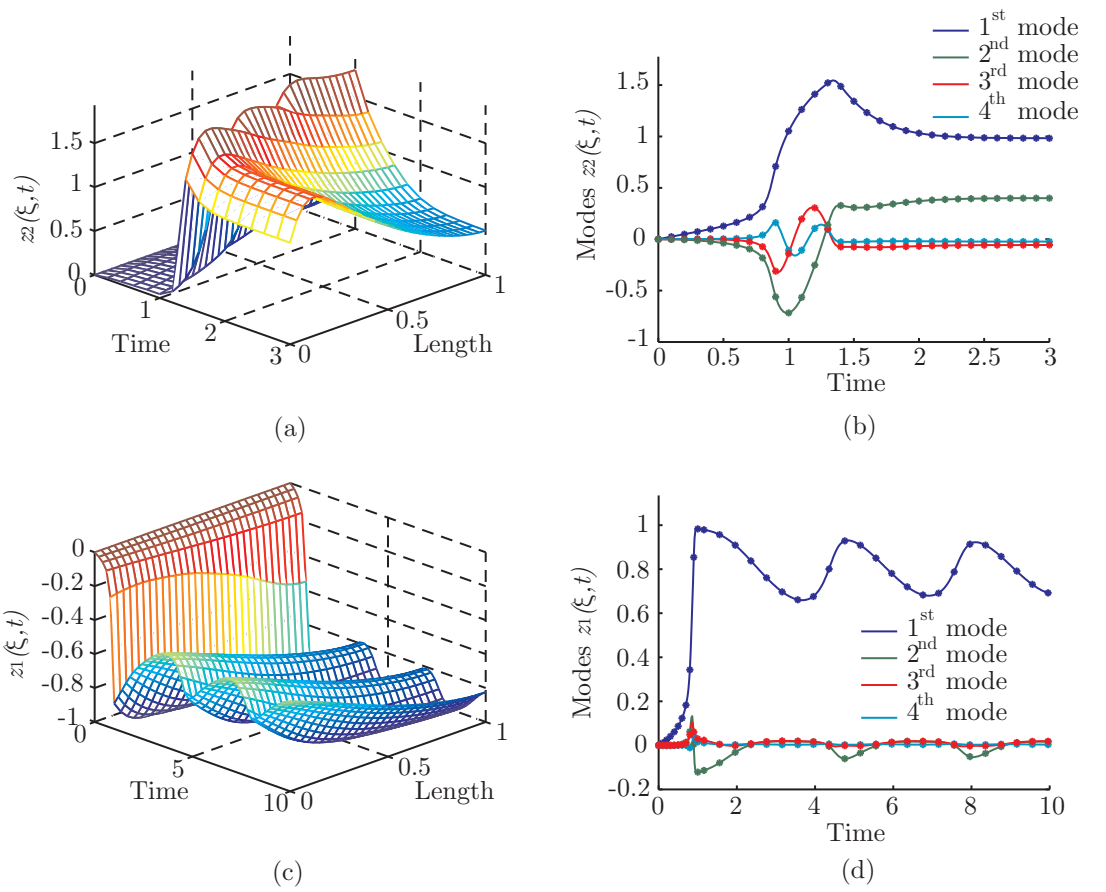

Figure 5.12: (a) and (c) Evolution and distribution of the fields z_2 with $r = 0$ and z_1 with $r = 0.5$, respectively, computed with the POD technique. (b) and (d) Mode evolution.

The main reason for this is that, in the case of $r = 0.5$, a better set of snapshots were considered for the computation of the PODs. From the point of view of mode evolution (Figures 5.12 (b) and (d)), the POD technique (marks) also shows good agreement with the FEM results (continuous lines).

5.5 The Robust Control of Tubular Reactors

In this section, the theory presented in Chapter 4 is applied to the tubular reactor with recycle just described in previous sections. As shown before, the dynamics of this class of reactors is highly conditioned by the recycle relation. In this sense, when $r = 0$ a steady state is reached while with $r = 0.5$ the evolution is in form of a limit cycle. The objective is to design a control law able to force the reactor to follow the limit cycle (reference trajectory) even when the recycle relation is $r = 0$. The control

variable corresponds with the temperature of the heating/cooling media u. Finally, It is assumed that the nonlinear reaction term f is unknown thus calling for robust controllers.

As mentioned in Chapter 4, ROMs are a key aspect of the approach to the robust control of RDC systems developed in this work. The POD technique was shown to be more appropriate in this case study since it results into a set of ODEs much lower than the LSD method. It should be remarked that the ROM is not required to describe the complete dynamic behaviour of the system but only that representative of the reference trajectory (limit cycle). For this reason, in this section new POD basis will be obtained only from the limit cycle data[3] with $u = 0$. In this case, using four PODs for both z_1 and z_2 are enough to capture the 99.9999% of the energy while the relative errors between the FEM and the ROM solution remain below the 0.3%.

The evolution of the system to control and the reference is given by Eqns (5.15)-(5.16) with $r = 0$ and $r = 0.5$, respectively. The dynamics of the reference trajectory are plotted in Figure 5.13. The representation on the left (Figure 5.13 (a)) shows the evolution and distribution of the field z_2 while the evolution of the representative modes is depicted in Figure 5.13 (b).

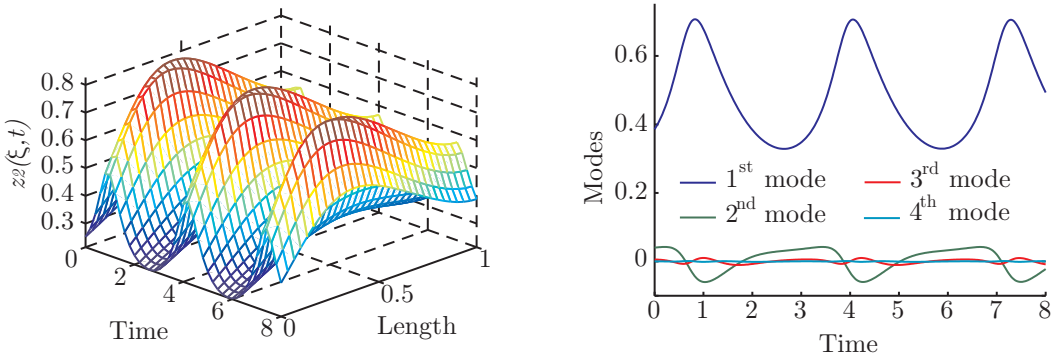

Figure 5.13: Dynamics of the reference trajectory in terms of (a) z_2 and (b) representative modes.

The system in deviation form with respect to the reference is described by the following set of PDEs:

$$\frac{\partial \overline{\mathbf{z}}}{\partial t} + \nabla \overline{\mathbf{z}} = D\Delta \overline{\mathbf{z}} + \overline{\Sigma} + \overline{\mathbf{u}}, \tag{5.30}$$

$$[\nabla \overline{\mathbf{z}} = Pe_{\mathbf{z}}\,(r\overline{\mathbf{z}}(1,t) - \overline{\mathbf{z}}(t,0))]_{\xi=0}\,; \qquad [\nabla \overline{\mathbf{z}} = \mathbf{0}]_{\xi=1}\,. \tag{5.31}$$

[3]The PODs of the previous section were obtained from data corresponding to limit cycle ($r = 0.5$), steady state ($r = 0$) and transient dynamics.

Construction of the control law proceeds as follows: First, choose the sets $(\mathscr{E}_a, \mathscr{L}_a, \mathcal{N}_a)$ and $(\mathscr{E}_b, \mathscr{L}_b, \mathcal{N}_b)$ with $\mathcal{N}_a = 1, 2, 3, 4$ and $\mathcal{N}_b$ collecting the remaining $5, 6, 7, ...$ In this way, the sets $\mathscr{E}_a$ and $\mathscr{E}_b$ are those composed by the first four PODs and the remaining infinite PODs, respectively. Then, project Eqns (5.30)-(5.31) over the sets $\mathscr{E}_a$ and $\mathscr{E}_b$ so as to obtain the following set of ODEs:

$$\frac{d\overline{\mathbf{m}}_{z_{2a}}}{dt} = \frac{1}{Pe_{z2}}\langle \Phi_a, \Delta\overline{z}_2 - \nabla\overline{z}_2\rangle_{\mathscr{V}} + B_T B_{cA}\langle \Phi_a, \overline{f}\rangle_{\mathscr{V}} + \beta_T\langle \Phi_a, \overline{u}\rangle_{\mathscr{V}} - \beta_T\langle \Phi_a, \overline{z}_2\rangle_{\mathscr{V}}, \quad (5.32)$$

$$\frac{d\overline{\mathbf{m}}_{z_{2b}}}{dt} = \frac{1}{Pe_{z2}}\langle \Phi_b, \Delta\overline{z}_2 - \nabla\overline{z}_2\rangle_{\mathscr{V}} + B_T B_{cA}\langle \Phi_b, \overline{f}\rangle_{\mathscr{V}} + \beta_T\langle \Phi_b, \overline{u}\rangle_{\mathscr{V}} - \beta_T\langle \Phi_b, \overline{z}_2\rangle_{\mathscr{V}}. \quad (5.33)$$

Note that the control action $\overline{u}$ only applies to the term z_2. Let us now split z_2 into two contributions using the sets $(\mathscr{E}_a, \mathscr{L}_a, \mathcal{N}_a)$ and $(\mathscr{E}_b, \mathscr{L}_b, \mathcal{N}_b)$ so that $z_{2a} = \sum_{i\in\mathcal{N}_a}\phi_i m_{z_2 i}$ and $z_{2b} = \sum_{i\in\mathcal{N}_b}\phi_i m_{z_2 i}$. On this basis, let us choose two Lyapunov functions of the form $\mathcal{B}_a(\overline{z}_2) = 1/2\overline{z}_{2a}^2$ and $\mathcal{B}_b(\overline{z}_2) = 1/2\overline{z}_{2b}^2$. The derivatives of $\mathcal{B}_a$ and $\mathcal{B}_b$ along the trajectories (5.32) and (5.33) lead, respectively, to the following relations (see section 4.4):

$$\dot{\mathcal{B}}_a \leq -\frac{1}{\beta_T}\left(\frac{1}{Pe_{z2}}\lambda_a + \beta_T\right)\frac{\delta_{0a}}{q_{1a}}\mathcal{B}_a + B_T B_{cA}\langle \overline{z}_{2a}, \overline{f}\rangle_{\mathscr{V}} + \beta_T\langle \overline{z}_{2a}, \overline{u}_a\rangle_{\mathscr{V}}$$

$$\dot{\mathcal{B}}_b \leq -\frac{1}{\beta_T}\left(\frac{1}{Pe_{z2}}\lambda_b + \beta_T\right)\frac{\delta_{0b}}{q_{1b}}\mathcal{B}_b + B_T B_{cA}\langle \overline{z}_{2b}, \overline{f}\rangle_{\mathscr{V}} + \beta_T\langle \overline{z}_{2b}, \overline{u}_b\rangle_{\mathscr{V}}$$

where λ_a and λ_b are the minimum eigenvalues of $\mathcal{A}_a = \langle \Phi_a, \Delta\overline{z}_2\rangle_{\mathscr{V}}$ and $\mathcal{A}_b = \langle \Phi_b, \Delta\overline{z}_2\rangle_{\mathscr{V}}$, respectively. If the control law is able to drive $\mathcal{B}_a, \mathcal{B}_b \to 0$, the objective will be reached (see Section 4.4). The first term of the RHS is negative so the control law only must compensate the effects of the reaction term $\overline{f}$. As mentioned before, the exact form of $\overline{f}$ is unknown but we know a bound ζ so that $\zeta > \overline{f}$. According to the previous chapter, the control:

$$\overline{u}_a = \begin{cases} -\frac{1}{\beta_T}\eta_a\frac{\overline{A}_a}{\|\overline{A}_a\|_{\mathscr{V}}} & \text{if} \quad \eta_a\|\overline{A}_a\|_{\mathscr{V}} \geq \theta_a \\ -\frac{1}{\beta_T}(\eta_a)^2\frac{\overline{A}_a}{\theta_a} & \text{if} \quad \eta_a\|\overline{A}_a\|_{\mathscr{V}} < \theta_a \end{cases},$$

$$\overline{u}_b = \begin{cases} -\frac{1}{\beta_T}\eta_b\frac{\overline{A}_b}{\|\overline{A}_b\|_{\mathscr{V}}} & \text{if} \quad \eta_b\|\overline{A}_b\|_{\mathscr{V}} \geq \theta_b \\ -\frac{1}{\beta_T}(\eta_b)^2\frac{\overline{A}_b}{\theta_b} & \text{if} \quad \eta_b\|\overline{A}_b\|_{\mathscr{V}} < \theta_b \end{cases},$$

where $\overline{A}_i = \partial\mathcal{B}_i/\partial z_{2i} = z_{2i}$ and $\eta_i > \|\zeta\|_{\mathscr{V}}$ with $i = a, b$ will stabilise the system in deviation form. Consequently the desired reference will be reached.

A simulation experiment was carried out to illustrate the behaviour of the tubular reactor under this control law acting after $t = 3$. The results of this experiment are

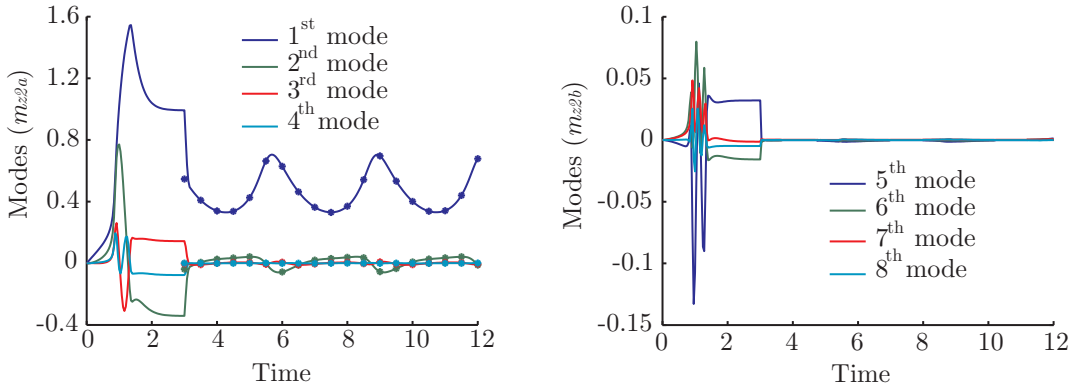

Figure 5.14: Evolution of the modes corresponding to the sets (a) $(\mathscr{E}_a, \mathscr{L}_a, \mathcal{N}_a)$ and (b) $(\mathscr{E}_b, \mathscr{L}_b, \mathcal{N}_b)$, under the control law.

presented in Figures 5.14 and 5.15. On the one hand, Figures 5.14 (a) and (b) show the evolution of the modes corresponding to the sets $(\mathscr{E}_a, \mathscr{L}_a, \mathcal{N}_a)$ and $(\mathscr{E}_b, \mathscr{L}_b, \mathcal{N}_b)$, respectively. As expected the modes $\mathbf{m}_{z_2 b}$ and $\mathbf{m}_{z_2 a}$ start to behave like in the case of $r = 0$, when the control law enters in action at $t = 3$, the modes $\mathbf{m}_{z_2 b}$ are stabilised while the modes $\mathbf{m}_{z_2 a}$ (continuous lines in Figure 5.14 (a)) are forced to follow the reference trajectory given by $\mathbf{m}^*_{z_2 a}$ (marks in Figure 5.14 (a)). On the other hand,

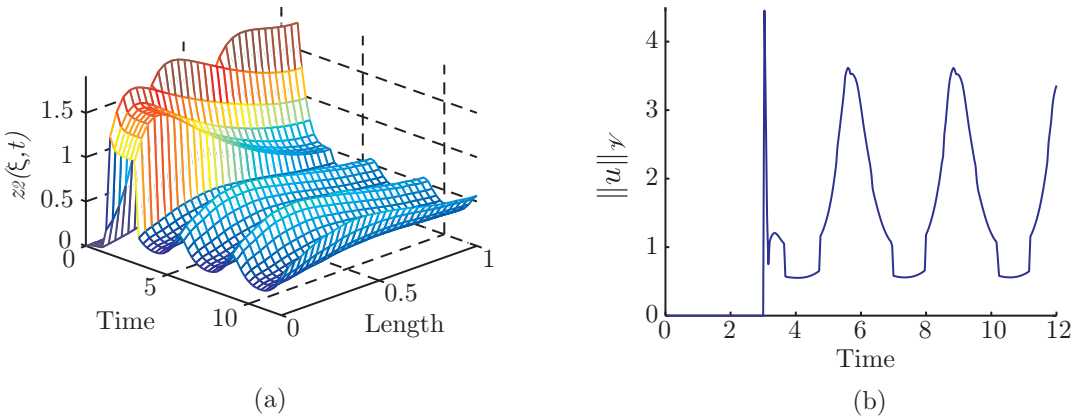

Figure 5.15: (a) Evolution of the field z_2 under the control law. (b) control effort.

the effects of the control law on the field are depicted in Figure 5.15 (a). This figure illustrates that after entering the control at $t = 3$ the field is forced to follow the desired reference. The control effort is depicted in Figure 5.15 (b).

5.5.1 Finite Number of Actuators

In this section, the problem of controlling the tubular reactor using a finite number of actuators is considered. The objective is the same as in the previous section, i.e. to actuate on the tubular reactor with a recycle relation $r = 0$ so as to recover the limit cycle dynamics exhibited when $r = 0.5$.

As shown in the previous section, the projection of the system (5.15)-(5.16) over the four more representative PODs resulted into a ROM able to reproduce the limit cycle dynamics. Furthermore, the evolution of the representative modes (first four modes) in deviation form with respect to the reference trajectory is described by Eqn (5.32). Let us denote by $\mathscr{M}_a$ the set containing the representative modes, i.e. $\mathscr{M}_a = \{\overline{m}_{z2i}\}_{i\in\mathcal{N}_a}$.

As mentioned before, the control device would consist of a number of pipes around the reactor. The temperature of the fluid inside the pipes can be manipulated and is employed to control the temperature inside the reactor. Consider that only seven pipes of diameter $d = L/30$, with L being the reactor length, are available. Alonso et al. (2004b) and Zerrik et al. (2001) showed that for stabilising four modes, at least four zone actuators (pipes) are required. It should be noted that if the control law is able to stabilise the modes of $\mathscr{M}_a$ (that is $\overline{\mathbf{m}}_{z2a} \to \mathbf{0}$), the modes $\mathbf{m}_{z2a}$ will follow the reference given by $\mathbf{m}^*_{z2a}$ since $\overline{\mathbf{m}}_{z2a} = \mathbf{m}_{z2a} - \mathbf{m}^*_{z2a}$. The remaining three pipes will be employed to stabilise the first three modes of the set $\mathscr{M}_b$. It must be stressed that the remaining modes of the set $\mathscr{M}_b$ are assumed to be stable.

The procedure to select the position of the zone actuators which minimises the control effort was presented in Section 4.5. Mainly, it consists of finding the position which maximises the minimum eigenvalue of a given matrix $\mathbf{P}$ constructed from integrals of the PODs over the geometric support of the controller. It must be remarked that the analytical expressions for the PODs are not available. Thus, in order to carry out the integrals, these were approximated by using polynomials of different degrees. In this case, the optimal locations for the four and three actuators employed for stabilising the modes of the set $\mathscr{M}_a$ and $\mathscr{M}_b$, respectively, are:

$$\mathscr{M}_a: \quad \Omega_1 = [0.1, 0.133];\ \Omega_2 = [0.333, 0.367];\ \Omega_3 = [0.567, 0.6];\ \Omega_4 = [0.833, 0.867];$$

$$\mathscr{M}_b: \quad \Omega_5 = [0, 0.033]; \quad \Omega_6 = [0.2, 0.233]; \quad \Omega_7 = [0.967, 1].$$

Figure 5.16 schematically represents such locations. The blank pipes are employed to control the modes of the set $\mathscr{M}_a$ while the objective of the grey pipes is to stabilise the first three modes of the set $\mathscr{M}_b$. The eigenvalues of the matrix $\mathbf{P}$ using these locations are $\underline{\lambda}_a = 0.243$ for the set $\mathscr{M}_a$ and $\underline{\lambda}_b = 0.219$ for the set $\mathscr{M}_b$. Following the steps

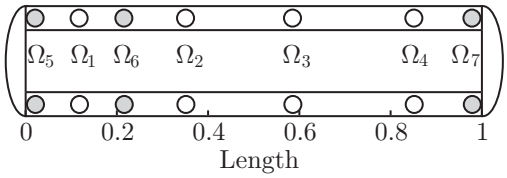

Figure 5.16: Longitudinal section of the tubular reactor showing the optimal position of the zone actuators (pipes). Blank and grey pipes are employed to stabilise the modes belonging to sets $\mathscr{M}_a$ and $\mathscr{M}_b$, respectively.

indicated in Section 4.5, the expression for the control law is $\overline{u} = \overline{u}_a + \overline{u}_b$ with:

$$\overline{u}_a = \begin{cases} -\frac{1}{\beta_T}\eta_a \frac{\overline{A}_a}{\|\overline{A}_a\|_{\mathscr{V}}} & \text{if} \quad \eta_a \|\overline{A}_a\|_{\mathscr{V}} \geq \theta_a \\ -\frac{1}{\beta_T}(\eta_a)^2 \frac{\overline{A}_a}{\theta_a} & \text{if} \quad \eta_a \|\overline{A}_a\|_{\mathscr{V}} < \theta_a \end{cases},$$

$$\overline{u}_b = \begin{cases} -\frac{1}{\beta_T}\eta_b \frac{\overline{A}_b}{\|\overline{A}_b\|_{\mathscr{V}}} & \text{if} \quad \eta_b \|\overline{A}_b\|_{\mathscr{V}} \geq \theta_b \\ -\frac{1}{\beta_T}\eta_b^2 \frac{\overline{A}_b}{\theta_b} & \text{if} \quad \eta_b \|\overline{A}_b\|_{\mathscr{V}} < \theta_b \end{cases},$$

where $\overline{A}_i = \partial \mathcal{B}_i / \partial z_{2i} = z_{2i}$ and $\eta_i > \frac{\|\zeta\|_{\mathscr{V}}}{\underline{\lambda}_i}$ with $i = a, b$. The effects of this control over the modes of the system are depicted in Figure 5.17. Before entering the control law

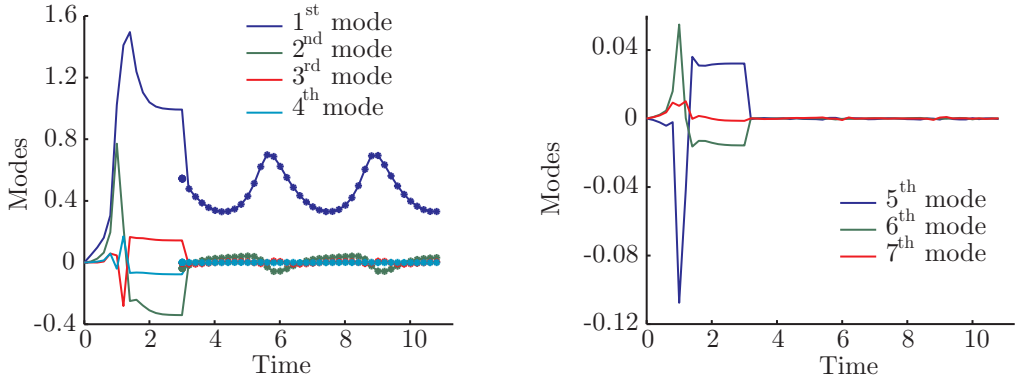

(a) (b)

Figure 5.17: Evolution of the modes corresponding to the sets (a) $(\mathscr{E}_a, \mathscr{L}_a, \mathscr{N}_a)$ and (b) $(\mathscr{E}_b, \mathscr{L}_b, \mathscr{N}_b)$, under the control law.

$(t < 3)$ the evolution of the modes is that corresponding with the tubular reactor with recycle $r = 0$. Once the control law enters in action, and after a short transition period, the first four modes (lines in Figure 5.17 (a)) are forced to follow the reference (marks in Figure 5.17 (a)) while the first three modes of the set $\mathscr{M}_b$ are stabilised (Figure

5.17 (b)). If the field evolution is recovered -Figure 5.18 (a)- one can see that the objective of reproducing the limit cycle is reached. Note that, as expected, in this case

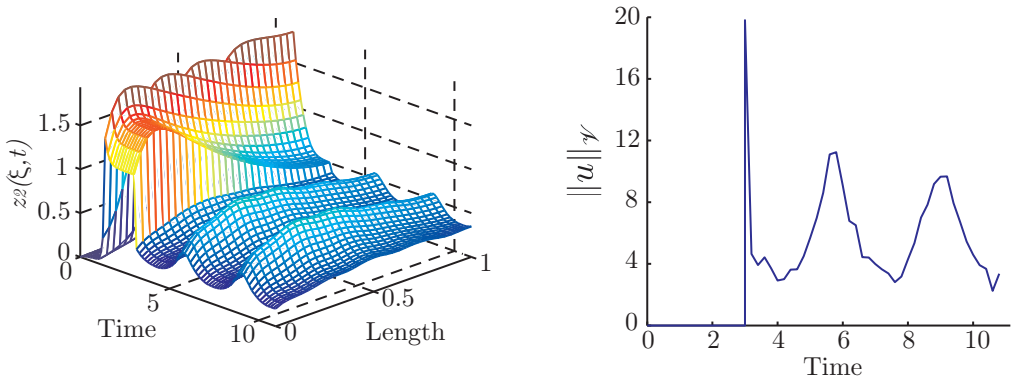

Figure 5.18: (a) Evolution of the field z_2 under the control law using a finite number of actuators. (b) Control effort.

the control effort -Figure 5.18 (b)- is larger than when an infinite number of actuator were available.

Chapter 6

Application 2: The Robust Control of the FitzHugh-Nagumo Model

6.1 Introducción

La evolución espacio-temporal de las señales electroquímicas es el origen de muchos fenómenos biológicos relacionados con la distribución, crecimiento y comunicación de las células (Murray, 2002b; Stelling et al., 2004; Jin et al., 2005). A nivel de tejidos y órganos, la actividad neurológica y los ciclos cardíacos se encuentran entre los ejemplos mejor conocidos de fenómenos biológicos relevantes inducidos por cambios espacio-temporales en las concentraciones de los iones en la membrana. Las señales nerviosas se transmiten en forma de pulsos planos periódicos (frentes) viajando a lo largo de los axones y de los tejidos (Hodgkin and Huxley, 1952b). La actividad normal del corazón está también sostenida por ondas electroquímicas que, producidas por el marcapasos natural del corazón, se extienden a lo largo del tejido cardíaco induciendo la contracción (Fenton and Karma, 1998; Witkowski et al., 1998). Muchas disfunciones cardíacas y neuronales se original mediante inestabilidades dinámicas que producen la ruptura del frente. La arritmia es uno de dichos desórdenes producidos por un frente regular que se rompe para dar lugar a una evolución en forma de espiral (Witkowski et al., 1998). Después de un proceso de ruptura en cadena, la espiral se transforma en un conjunto de espirales desorganizadas que se crean y destruyen continuamente, siendo este patrón característico de la fibrilación (Keener, 2004). La misma clase de mecanismos es responsable interrupciones en las señales nerviosas llevando a desórdenes neurológicos observados por Gorelova and Bures (1983) y Dahlem and Müller (2000).

Con el propósito de idear medios para prevenir dichos desórdenes parece razonable encontrar un enfoque unificado capaz de describir la misma clase de comportamiento observado en estos sistemas biológicos y químicos. Hodgkin and Huxley (1952b) propusieron un modelo matemático para la transmisión de las señales eléctricas en el axón del calamar gigante. Debido a la complejidad de este modelo han surgido otras versiones simplificadas, entre las cuales probablemente la más conocida sea el modelo de FitzHugh-Nagumo (FHN) (FitzHugh, 1961; Nagumo et al., 1962). Pequeñas variaciones de este modelo se han empleado para representar la evolución de sistemas químicos y biológicos. Se recomienda al lector interesado en los detalles acerca del comportamiento del sistema FHN las revisiones de Rinzel (1981) y Murray (2002a,b).

Los mecanismos subyacentes que gobiernan la evolución espacio-temporal de este tipo de señales en diferentes contextos biológicos se describen mediante un paradigma general basado en la interacción entre los fenómenos de difusión y de reacción. Los fundamentos de este paradigma fueron propuestos por Turing (1952) en un artículo que sentó las bases químicas de la morfogénesis. Décadas más tarde, el trabajo experimental en sistemas químicos como las reacciones de Belousov-Zhabotinskii o catalíticas confirmaron la hipótesis siendo capaz de predecir una gran variedad de patrones estacionarios y oscilatorios como se discute en, por ejemplo, Zimmermann et al. (1997), Beaumont et al. (1998), Lebiedz and Brandt-Pollmann (2003) o Lebiedz and Maurer (2004). Este paradigma se ha empleado para entender las rutas que llevan a estos sistemas a la inestabilidad. De esta forma, el análisis dinámico de los sistemas reacción-difusión y en particular el systema FHN, ha sido el objeto de una investigación intensiva, especialmente en lo que se refiere a la detección de condiciones de inestabilidad y análisis de bifurcaciones que lleva a frentes móviles, espirales y formación de otros patrones (Gear et al., 2002; Sweers and Troy, 2003; Bouzat and Wio, 2003).

Además de la derivación de un modelo, también es deseable investigar las formas de interactuar con el sistema mediante controles externos para prevenir la aparición de inestabilidades y por lo tanto preservar la actividad biológica normal. El ámbito del presente capítulo debe inscribirse en este segundo aspecto.

El objetivo de este capítulo es utilizar la teoría presentada en los Capítulos 1-4 para desarrollar lógicas de control capaces de llevar la dinámica del modelo FHN cuando se produce una inestabilidad a la referencia deseada (relacionada con el comportamiento normal del sistema biológico) incluso en la presencia de incertidumbre estructural y/o paramétrica.

6.2 Introduction

The spatiotemporal evolution of chemical or electrochemical signals is at the origin of many biological phenomena related with cell growth and distribution as well as with cell communication -see (Murray, 2002b; Stelling et al., 2004; Jin et al., 2005)-. At the level of tissues and organs, neurological activity or cardiac cycles are among the best known examples of relevant biological phenomena also induced by spatiotemporal changes in the membrane ion concentrations. In this way, nervous signals are transmitted in the form of periodic flat pulses (fronts) travelling along neural axons and tissues (Hodgkin and Huxley, 1952b). Normal heart activity is also sustained by regular electrochemical waves which being produced by the heart's natural peacemaker spread throughout the cardiac tissue and induce contraction (Fenton and Karma, 1998; Witkowski et al., 1998). Many nervous or cardiac dysfunctions are originated by dynamic instabilities that cause front disruption and even breakup. Heart arrhythmia (Witkowski et al., 1998) is one of such disorders produced by a regular front being broken into a wandering spiral. In the last instance and after a chain breaking process, the spiral waves would transform into a disorganised set of multiple spirals continually created and destroyed, being this pattern characteristic of fibrillation (Keener, 2004). The same class of mechanisms is responsible of disruptions in nervous signals leading to neurological disorders as observed by Gorelova and Bures (1983) and Dahlem and Müller (2000).

In the purpose of devising means for preventing such disorders it seems reasonable to find a unifying mechanistic approach able to describe the same class of behaviour observed in such a varied class of chemical and biological systems. Hodgkin and Huxley (1952b) proposed a mathematical description for the neuron firing in the nerve axon of the giant squid. Due to the complexity of such model several simplified versions arose, among which the so-called FitzHugh-Nagumo (FHN) (FitzHugh, 1961; Nagumo et al., 1962) is probably the best known. Slight variations of this model have been employed to represent the evolution of chemical and biological systems. For more details on the behaviour of the FHN system see the revisions by Rinzel (1981) and Murray (2002a,b).

The underlying mechanisms that govern the spatiotemporal evolution of this type of signals in many different biological contexts are now well understood and described by a general paradigm based on the interplay between reaction and diffusion. The essentials of this paradigm were first proposed by Turing (1952) in a seminal article that set up the chemical basis of morphogenesis. Decades later, experimental work in chemical systems such as the Belousov-Zhabotinskii or catalytic driven surface reactions confirmed this

hypothesis by being able to predict a rich variety of stationary as well as oscillatory spatial patterns as discussed in, for instance, Zimmermann et al. (1997), Beaumont et al. (1998), Lebiedz and Brandt-Pollmann (2003) or Lebiedz and Maurer (2004). This paradigm has been also extensively employed to understand the routes that drive these systems to instability. In this way, dynamic analysis of diffusion-reaction systems and in particular the FHN system, has been the subject of intensive research, especially in what refers to the detection of instability conditions and bifurcation analysis leading to moving fronts, spiral waves and pattern formation (Zimmermann et al., 1997; Beaumont et al., 1998; Gear et al., 2002; Sweers and Troy, 2003; Bouzat and Wio, 2003).

In addition, it is also desirable to investigate ways of interacting with the system through external feed-back control systems so as to prevent instabilities and therefore to preserve a normal biological activity. The scope of the present chapter must be inscribed into this second aspect.

The objective of this chapter is to employ the theory presented in Chapters 1-4 so as to develop control logics able to drive the dynamics of the FHN model in the event of instability to a prescribed reference (related to the normal behaviour of the biological system) even in the presence of structural and/or parametric uncertainties.

This chapter is structured as follows: In the first section, the FHN model equations and a brief discussion of its solutions will be presented. After this, the FEM approach will be applied to 2D versions of this model. In Section 6.4, the LSD and POD techniques will be employed to obtain reduced order representations of the original PDE set. Finally, a robust control law able to drive the system to a given reference will be constructed based on the theory presented in Chapter 4. Such reference is given by the ROMs just derived in Section 6.4.

6.3 The model equations

Hodgkin et al. (1949) carried out several experiments in the axon of the giant squid to study the initialisation and propagation of the action potential (Keener and Sneyd, 1998). After two years analysing the experimental data, which were published in Hodgkin and Huxley (1952a), the authors proposed that the membrane of the axon was permeable to certain ions (K^+, Na^+,...) and the permeability depended on the voltage (Hodgkin and Huxley, 1952b). In the same article, they also proposed a model for describing the excitable feature of the axon. This model is briefly described in Appendix A.4. About the middle of the fifties, the biologist Richard FitzHugh searched for a reduced version of the Hodgkin-Huxley model. He observed that the dynamics

of some model variables were much slower than other which rapidly converged to a fix value. He was also able to relate two of these variables arriving to a two variable (V, n) model. Finally, a FitzHugh's additional observation was that the stationary solutions for the equations of V and n, in the physiological range of the variables, had the form of a third order polynomial and a straight line, respectively. These considerations led him to a dimensionless model of the form:

$$\frac{dv}{dt} = g(v) - w + I_a; \quad g(v) = v(a - v)(v - 1), \tag{6.1}$$

$$\frac{dw}{dt} = \varepsilon(\beta v - \gamma w + \delta), \tag{6.2}$$

where v, fast variable, is associated with the membrane potential when representing a biological system. In chemical systems it is usually referred to as *activator*. The slow variable w is associated, in biological systems, with the contribution terms of the ions Na^+, K^+, etc. to the membrane current and it is usually termed as the *inhibitor*. The parameter ε represents the ratio of time scales for the kinetic terms while β, γ and δ are parameters determining the local dynamics (Shvartsman and Kevrekidis, 1998). Nagumo et al. (1962) constructed an electric circuit whose equations were those derived by FitzHugh so the previous model is known as *FitzHugh-Nagumo* (FHN).

In order to understand the solutions of the FHN system, the nullclines[1] of Eqns (6.1) and (6.2) are represented by the red lines in Figure 6.1. Depending on the parameters,

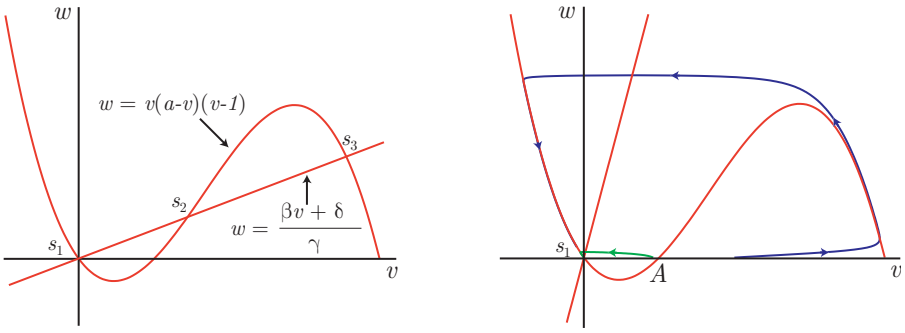

Figure 6.1: Representation in the phase plane of the nullclines of Eqns (6.1) and (6.2) (a) with three steady states and (b) with one steady state and state trajectory under perturbation.

the system can have three (s_1, s_2, s_3 in Figure 6.1 (a)) or one (s_1 in Figure 6.1 (b)) steady states. The parameters in Figure 6.1 (a) are (Murray, 2002a): $a = 0.25$, $I_a = 0$,

[1]The nullclines are the curves resulting from making $\frac{dv}{dt} = \frac{dw}{dt} = 0$.

$\varepsilon = 2 \times 10^{-3}$, $\beta = 0.7$, $\gamma = 1$ and $\delta = 0$ whereas in Figure 6.1 (b), β was changed to $\beta = 0.07$. If the system in the steady state $v = w = 0$ is subjected to a small perturbation $v < A$, then the states will converge rapidly to the steady state (green line). Nevertheless if the perturbation is sufficiently large $v > A$ the states travel across a long way (blue line) before returning to the steady state. This property, known as *excitability*, is the key feature of excitable systems.

So far, the FHN model was presented assuming that the variables are not distributed in space. This assumption works at the level of cells, but at the level of tissues or organs spatial distribution must be considered. Introducing a diffusion term, Eqns (6.1) and (6.2) can be rewritten as follows (Shvartsman and Kevrekidis, 1998):

$$\frac{\partial v}{\partial t} = \kappa \Delta v + g(v) - w + u, \quad g(v) = v(a - v)(v - 1), \tag{6.3}$$

$$\frac{\partial w}{\partial t} = \kappa \rho \Delta w + \varepsilon(\beta v - \gamma w + \delta). \tag{6.4}$$

When describing biological systems, the diffusion coefficient κ is related to the axial current in the membrane of the tissue. The parameter ρ represents the ratio of the diffusivities of v and w. As pointed out in Argentina et al. (2000) in biological systems $\rho \approx 0$, thus the diffusion term in Eqn (6.4) can be neglected. In chemical systems like the Belousov-Zhabotinskii chemical reaction (Winfree, 1984) the ratio of the diffusivities of v and w is of the order of the unity ($\rho \sim 1$). The control input is denoted by u. For the FHN model, no flux boundary conditions are considered:

$$\left| \vec{\mathbf{n}} \cdot \vec{\boldsymbol{\nabla}} v = \vec{\mathbf{n}} \cdot \vec{\boldsymbol{\nabla}} w = 0 \right|_{\mathscr{B}}. \tag{6.5}$$

Using the FEM matrices (Section 2.3), system (6.3)-(6.5) can be approximated as:

$$\frac{d\mathcal{V}}{dt} = -\kappa \mathcal{D}\mathcal{A}^{-1}\mathcal{C}\mathcal{V} + \mathcal{V}(a - \mathcal{V})(\mathcal{V} - 1) - \mathcal{W}, \tag{6.6}$$

$$\frac{d\mathcal{W}}{dt} = -\kappa \rho \mathcal{D}\mathcal{A}^{-1}\mathcal{C}\mathcal{W} + \varepsilon(\beta \mathcal{V} - \gamma \mathcal{W} + \delta), \tag{6.7}$$

where $\mathcal{V}$ and $\mathcal{W}$ are the discrete counterparts of the states v and w, respectively. In the following sections, two cases derived from Eqns (6.3) - (6.5) will be presented.

6.3.1 The FHN Model as a Representation of a Chemical System

In this section a 2D version of the FHN model is considered. The spatial domain is the square surface $\mathscr{V} = \{(\xi_1, \xi_2) / -1 < (\xi_1, \xi_2) < 1\}$ with boundary $\mathscr{B} = \{(\xi_1, \xi_2) / (\xi_1 =$

$\pm 1\ \forall \xi_2 \in [-1,1]), (\xi_2 = \pm 1\ \forall \xi_1 \in [-1,1])\}$. For convenience the example of this section will be usually referred to as *the chemical case*. The model is given by Eqns (6.3) - (6.5). As mentioned before, this system is very sensitive to changes in the parameters and small variations on them give rise to a rich variety of dynamic behaviours. In order to illustrate this point, the original PDE system has been numerically solved using a FEM scheme and two different set of parameters. It should be remarked that since the objective is to represent a chemical reaction system, ρ must be of the order of the unity. The spatial discretisation mesh consists of about 2000 points since larger discretisation schemes do not alter the solution. The initial conditions considered in the chemical case are of the form:

$$v(\boldsymbol{\xi}, 0) = v_0 = \begin{cases} 1 & \text{if} \quad \xi_1 \in [-1, -0.9],\ \forall\, \xi_2 \\ \\ 0 & \text{if} \quad \xi_1 \in (-0.9, 1],\ \forall\, \xi_2 \end{cases} \quad ; \qquad w(\boldsymbol{\xi}, 0) = w_0 = 0,\ \forall\, \xi_1, \xi_2. \tag{6.8}$$

Case 1: The oscillating front evolution

The model parameters were taken from Shvartsman and Kevrekidis (1998) and correspond with: $\kappa = 0.01, \rho = 4, a = -1, \varepsilon = 0.017, \beta = 1, \gamma = 2$ and $\delta = 0.03$. In this case, the solution obtained have the form of a plane front which oscillates between two points in the ξ_1 axis as shown in Figure 6.2 for the state v. It should be remarked that

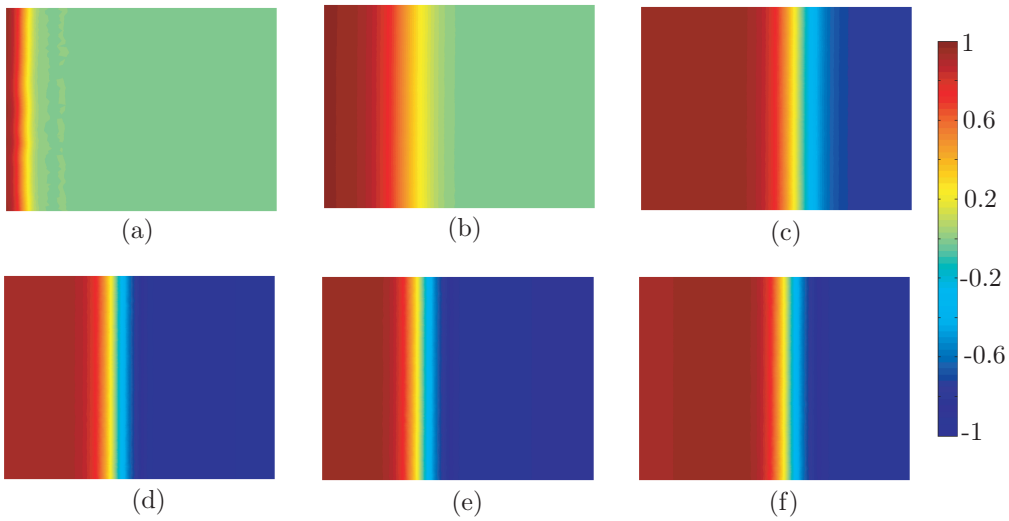

Figure 6.2: Evolution and distribution of the field v for the Case 1. The snapshots from (a) to (f) were taken at different (increasing) sampling times.

the evolution of w is similar to the evolution of v, the difference is that the value of w varies from $w = 0.2$ to $w = -0.2$. When designing the control law, this behaviour, or to be precise a ROM of it, will be employed as the reference trajectory.

Case 2: The "fingerprint" evolution

In this example the model parameters were taken from Vilas et al. (2006) and correspond with: $\rho = 2.5, \kappa = 1 \times 10^{-4}, a = -1, \varepsilon = 0.03, \beta = 1, \gamma = 2$ and $\delta = 0$. With this parameters, the initial front breaks giving rise to the formation of a series of irregular forms (see Figure 6.3). This behaviour will be employed as the system to be controlled in Section 6.5.1.

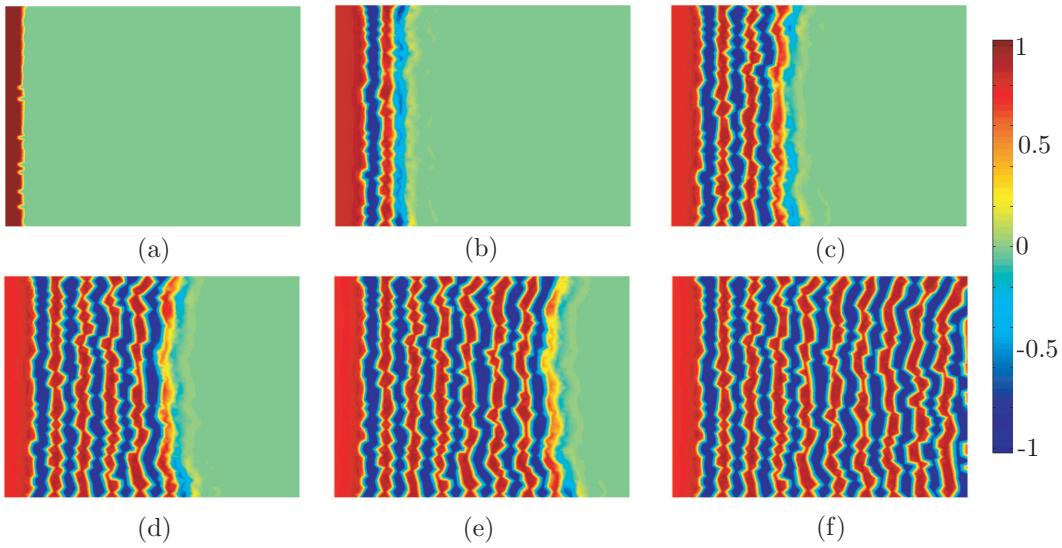

Figure 6.3: Evolution and distribution of the field v for the Case 2. The snapshots from (a) to (f) were taken at different (increasing) sampling times.

6.3.2 The FHN Model as a Representation of a Biological system

Now, the spatial domain covers the square $\mathscr{V} = \{0 \leq (\xi_1, \xi_2) \leq 200\}$ and the boundary corresponds to the sides of such square. This can be formally stated as $\mathscr{B} = \{(\xi_1, \xi_2)/(\xi_1 = 0 \text{ and } \xi_1 = 200\ \forall \xi_2 \in [0, 200]), (\xi_2 = 0 \text{ and } \xi_2 = 200\ \forall \xi_1 \in [0, 200])\}$. In order to distinguish this example from that described in Section 6.3.1 it will be usually referred to as *the biological case*. As pointed out above in biological systems $\rho \approx 0$ thus the diffusive term for w can be neglected. This system is also described by Eqns (6.3) - (6.5). In the context of biological phenomena, such as cardiac or neural activity, the normal behaviour is related to a plane wave which moves along the tissue without changing its shape (travelling plane wave). The FHN system (6.3)-(6.5) reproduces such behaviour by setting the following parameters (Fenton et al., 2002b) $\kappa = 1$, $\rho = 0$,

$a = 0.1$, $\varepsilon = 0.003$, $\beta = 0.5$, $\gamma = 1$ and $\delta = 0$, and with initial conditions:

$$v(0, \boldsymbol{\xi}) = v_0 = \begin{cases} 1 & \text{if} \quad \xi_1 \in [0, 10], \ \forall\, \xi_2 \\ 0 & \text{if} \quad \xi_1 \in (10, 200], \ \forall\, \xi_2 \end{cases}, \quad w(0, \boldsymbol{\xi}) = w_0 = 0 \ \forall\, \xi_1, \xi_2. \tag{6.9}$$

Some snapshots of the v-variable evolution, taken at different times and corresponding to the travelling plane wave behaviour, are plotted in Figure 6.4.

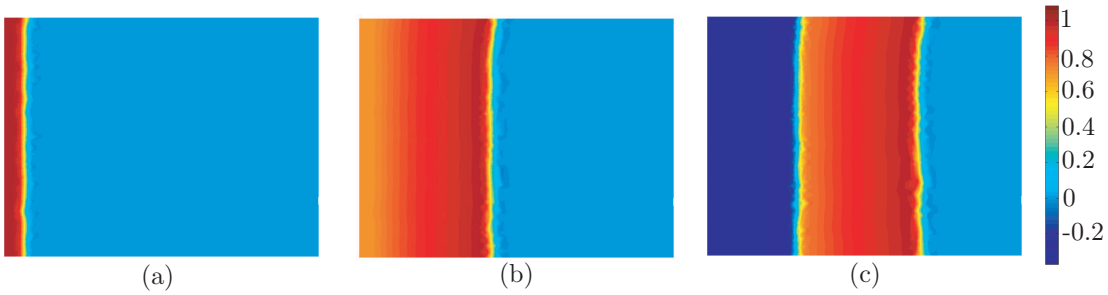

Figure 6.4: Snapshots of FHN system corresponding with the travelling plane wave behaviour.

Under certain circumstances the plane wave can break forcing the front and the back of the wave to meet each other at a given point with undefined phase (Fenton et al., 2002a). Thereafter, the broken wave wanders around this point and gives rise to the formation of a spiral. This class of behaviour is related to neurological disorders (Gorelova and Bures, 1983) or cardiac dysfunctions such as arrhythmia (Witkowski et al., 1998). The FHN model is also able to capture this phenomenon as illustrated in Figure 6.5 (a) and (b). Furthermore, if this spiral is perturbed it may give rise to other

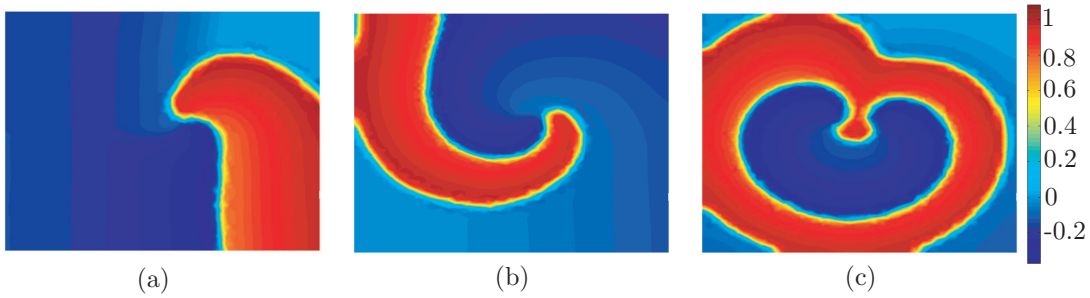

Figure 6.5: Snapshots of the FHN system corresponding with the spiral behaviour and the irregular forms.

irregular forms (see Figure 6.5 (c)) related, in the case of the heart with the fibrillation. The aim of Section 6.5.2 will be *to design a feed-back control scheme (p) which, in the*

event of instability (spiral wave), should be able to drive the system dynamics back to the plane wave behaviour.

Before proceeding with the derivation of ROMs, first let us show that the FHN system is dissipative according to Definition 1.2. To that purpose, let us choose the following convex function and reference:

$$b(v,w) = \frac{1}{2}(\varepsilon\beta v^2 + w^2); \quad [v^*, w^*] = [0,0].$$

The dual $\mathbf{A}$ of the field is computed as the derivative of b with respect to the field (see Section 1.5), so that:

$$\mathbf{A} = \frac{\partial b}{\partial \mathbf{z}} = \begin{bmatrix} \varepsilon\beta v \\ w \end{bmatrix}, \quad \text{where } \mathbf{z} = \begin{bmatrix} v \\ w \end{bmatrix}, \quad \mathbf{A}^* = \begin{bmatrix} 0 \\ 0 \end{bmatrix}.$$

Taking into account that the nonlinear terms are of the form:

$$\mathbf{f} = \begin{bmatrix} v(a-v)(v-1) - w \\ \varepsilon(\beta v - \gamma w + \delta) \end{bmatrix}, \quad \mathbf{f}^* = \begin{bmatrix} 0 \\ \varepsilon\delta \end{bmatrix},$$

substituting this on Eqn (1.41) -see Condition 1.1- and rearranging terms, the following expression for ℓ_μ is obtained:

$$\ell_\mu = \varepsilon\beta v^2(\varepsilon\beta\mu - (a-v)(v-1)) + w^2(\mu + \varepsilon\gamma). \tag{6.10}$$

In the *chemical case* (see Section 6.3.1) $a = -1$ and $\mu, \varepsilon, \gamma > 0$. Thus it is easy to check that the following inequality holds:

$$\ell_\mu \geq \varepsilon v^2(\mu\varepsilon\beta - 1).$$

Note that $\ell_\mu > 0$ for all $\mu > (\varepsilon\beta)^{-1}$. On the other hand, in the *biological case* (see Section 6.3.1) $a = 0.1$ and $\mu, \varepsilon, \gamma > 0$ leading to the following inequality:

$$\ell_\mu \geq \varepsilon v^2(\mu\varepsilon\beta - (0.1-v)(v-1)).$$

Now, $\ell_\mu > 0$ for all $v < 0.1$ or $v > 1$. Furthermore, when $v \in [0.1, 1]$, ℓ_μ is positive if $\mu > \sigma_{min}(\varepsilon\beta)^{-1}$ where $\sigma_{min} = -0.2025$ is the minimum of function $-(0.1-v)(v-1)$.

In Figure 6.6 function ℓ_0 (invariant set) is represented for the first and second examples in the chemical case (Figure 6.6 (a) and (b), respectively) and for the biological case (Figure 6.6 (c)). The thickest line in each plot corresponds with $\ell_0 = 0$. As one can see in the figure, $\ell_0 < 0$ for all points inside this line. Thus, the system is not purely dissipative. On the other hand, note that it is always possible to choose a radius ϱ so that $\ell_0 > 0$ for $\|(v,w)\| > \varrho$, therefore the system is dissipative.

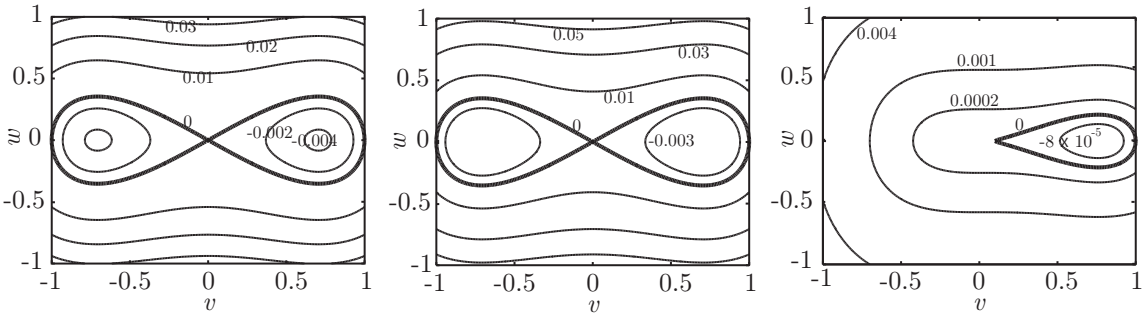

Figure 6.6: Invariant sets (ℓ_0) for the set of parameters corresponding to (a) Case 1 in the *chemical case*, (b) Case 2 in the *chemical case* and (c) the *biological case*.

6.4 Reduced Order Representations

Reduced order models will be employed in this chapter to approximate the reference trajectory to be the one followed by the system to be controlled. As pointed out in the previous section, such reference coincides with the travelling plane wave in both the chemical and biological cases.

6.4.1 ROM in the Chemical Case

Let us begin with the LSD technique. The first step is to obtain the eigenfunctions by solving the eigenvalue equation:

$$\Delta\phi_{\ell m} = -\lambda_{\ell m}\phi_{\ell m}, \tag{6.11}$$

$$\vec{\mathbf{n}}\cdot\vec{\boldsymbol{\nabla}}\phi_{\ell m}|_{\mathscr{B}} = 0. \tag{6.12}$$

For a rectangular domain as that considered in this chapter, the analytical solution of (6.11)-(6.12) has the form:

$$\phi_{\ell m} = \begin{cases} \frac{1}{\sqrt{L_{\xi_1}L_{\xi_2}}}\cos\left(\frac{\ell\pi(\xi_1-\xi_{10})}{L_{\xi_1}}\right)\cos\left(\frac{m\pi(\xi_2-\xi_{20})}{L_{\xi_2}}\right) & \text{if } \ell = m = 0 \\ \frac{\sqrt{2}}{\sqrt{L_{\xi_1}L_{\xi_2}}}\cos\left(\frac{\ell\pi(\xi_1-\xi_{10})}{L_{\xi_1}}\right)\cos\left(\frac{m\pi(\xi_2-\xi_{20})}{L_{\xi_2}}\right) & \text{if } \ell = 0 \text{ or } m = 0, \\ \frac{2}{\sqrt{L_{\xi_1}L_{\xi_2}}}\cos\left(\frac{\ell\pi(\xi_1-\xi_{10})}{L_{\xi_1}}\right)\cos\left(\frac{m\pi(\xi_2-\xi_{20})}{L_{\xi_2}}\right) & \text{otherwise} \end{cases} \tag{6.13}$$

$$\lambda_{\ell m} = \pi^2\left(\frac{\ell^2}{L_{\xi_1}^2} + \frac{m^2}{L_{\xi_2}^2}\right); \quad \ell, m = 0, 1, 2, 3, ... \tag{6.14}$$

where $L_{\xi_1} = L_{\xi_2} = 2$ are the lengths of the rectangle sides and $\xi_{10} = \xi_{20} = -1$ are the coordinates of the left-bottom point of the rectangle. The FEM matrices (see

Section 2.3.2) allows us to approximate the continuous eigenproblem (6.11)-(6.12) by its discrete counterpart, so that:

$$\mathcal{D}\mathcal{A}^{-1}\mathcal{C}\boldsymbol{\phi}_i = -\lambda_i \boldsymbol{\phi}_i \tag{6.15}$$

Three of the most relevant eigenfunctions are plotted in Figure 6.7 (a)-(c). The absolute

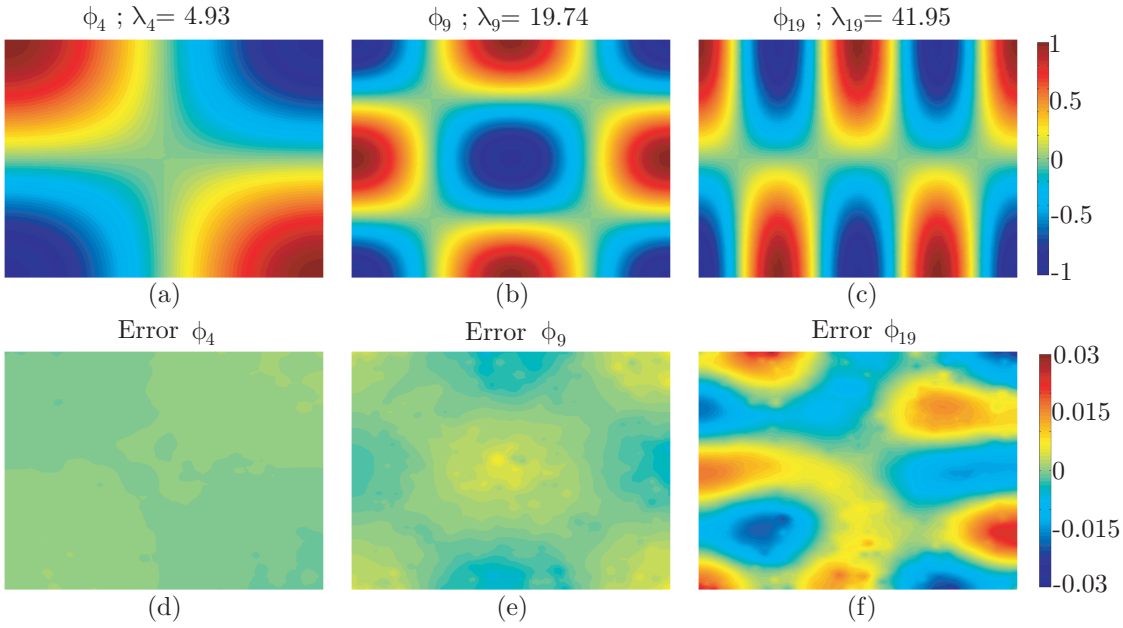

Figure 6.7: (a)-(c) Three eigenfunctions resulted form solving Eqn (6.11). (d)-(f) Absolute error between the eigenfunctions obtained analytically and numerically with the FEM.

errors between the eigenfunctions obtained analytically and with the FEM matrices are depicted in Figures 6.7 (d)-(f). The Figure shows that the FEM is able to approximate the eigenvalue problem with satisfactory accuracy. Note that the eigenvalues resulting from Eqn (6.14) can be ordered so that $\lambda_{\ell m} \to \infty$ as $\ell, m \to \infty$. This fact allows us to arrange the eigenvalues (and therefore their corresponding eigenfunctions) along the set of natural numbers $\mathbb{N}$ so that $\lambda_i \geq \lambda_j$ for $i > j$. It should be remarked that the mode associated with the eigenvalue λ_j will be, in general, more "relevant" than the mode associated with the eigenvalue λ_i. Again, as it is expected, the number of spatial oscillations of the eigenfunction ϕ_i is higher than or equal to that corresponding with the eigenfunction ϕ_j if $i > j$.

Now, let us define the eigenset $(\mathscr{E}, \mathscr{L}, \mathbb{N})$ as that with elements being $\mathscr{E}(\Delta) = \{\phi_i\}_{i\in\mathbb{N}}$ and $\mathscr{L}(\Delta) = \{\lambda_i\}_{i\in\mathbb{N}}$. As in previous chapters, the finite subset of natural numbers $\mathcal{N}_a$ and its complement $\mathcal{N}_b$ allow us to partition the eigenset $(\mathscr{E}, \mathscr{L}, \mathbb{N})$ in two

disjoint sets $(\mathscr{E}_a, \mathscr{L}_a, \mathscr{N}_a)$ and $(\mathscr{E}_b, \mathscr{L}_b, \mathscr{N}_b)$. Projecting Eqns (6.3) and (6.4) over the sets $\mathscr{E}_a$ and $\mathscr{E}_b$, the following set of ODEs is obtained:

$$\frac{d\mathbf{m}_{vi}}{dt} = -\kappa\Lambda_i\mathbf{m}_{vi} + \langle\boldsymbol{\phi}_i, (a-v)(v-1)v\rangle_{\mathscr{V}} - \mathbf{m}_{wi} + \langle\boldsymbol{\phi}_i, p\rangle_{\mathscr{V}}; \quad i = a, b \tag{6.16}$$

$$\frac{d\mathbf{m}_{wi}}{dt} = -\kappa\rho\Lambda_i\mathbf{m}_{wi} - \varepsilon\gamma\mathbf{m}_{wi} + \varepsilon\beta\mathbf{m}_{vi} + \langle\boldsymbol{\phi}_i, \varepsilon\delta\rangle_{\mathscr{V}}; \quad i = a, b \tag{6.17}$$

where Λ_i is a diagonal matrix containing the eigenvalues of $\mathscr{L}_i$ whereas $\boldsymbol{\phi}_i$ is a matrix containing the elements of the set $\mathscr{E}_i$, this is $\boldsymbol{\phi}_i = \left[\phi_{\mathcal{N}_i(1)}, \phi_{\mathcal{N}_i(2)}, ...\right]$. As mentioned in Chapter 3 when the number of elements in the set $(\mathscr{E}_a, \mathscr{L}_a, \mathscr{N}_a)$ is large enough, the modes of the set $(\mathscr{E}_b, \mathscr{L}_b, \mathscr{N}_b)$ converge to zero at exponential rate. Thus, the solution of Eqns (6.3) and (6.4) can be approximated using the solution of (6.16)-(6.17) with $i = a$. The initial conditions for Eqns (6.16) - (6.17) with $i = a$ are obtained by projecting Eqn (6.8) over the set $\mathscr{E}_a$ so that:

$$\mathbf{m}_{va}(0) = \langle\Phi_a, v_0\rangle_{\mathscr{V}}; \quad \mathbf{m}_{wa}(0) = \langle\Phi_a, w_0\rangle_{\mathscr{V}}.$$

By recovering the field from the modes and the eigenfunctions, this is $v = \Phi_a\mathbf{m}_{va}$, $w = \Phi_a\mathbf{m}_{wa}$, one can check the degree of accuracy of the reduced approximation (Figure 6.8). As it can be seen in Figure 6.8(a), projection over the 8 most significant

Figure 6.8: Solutions of the FHN model using the LSD technique with (a) 8 eigenfunctions, (b) 15 eigenfunctions and (c) 20 eigenfunctions

modes is enough to reproduce the qualitative aspects of the front as compared with the finite element solution reproduced in Figure 6.2. Increasing the dimension of the ODE set improves the approximation as depicted in Figures 6.8(b) and (c). In fact, projection over the 20 most dominant eigenfunctions essentially reproduces the "real front". Note that the ROM with 20 eigenfunctions reduces the number of equations of the FEM by two orders of magnitude.

The differences between these ROMs are better appreciated by plotting the modes (see Figure 6.9). As expected the ROM with 20 eigenfunctions (black dotes) approximates much better the FEM modes (blue lines) than the ROM with 8 (green discontinuous line) and 15 (red ×) eigenfunctions. In this particular case, the POD technique

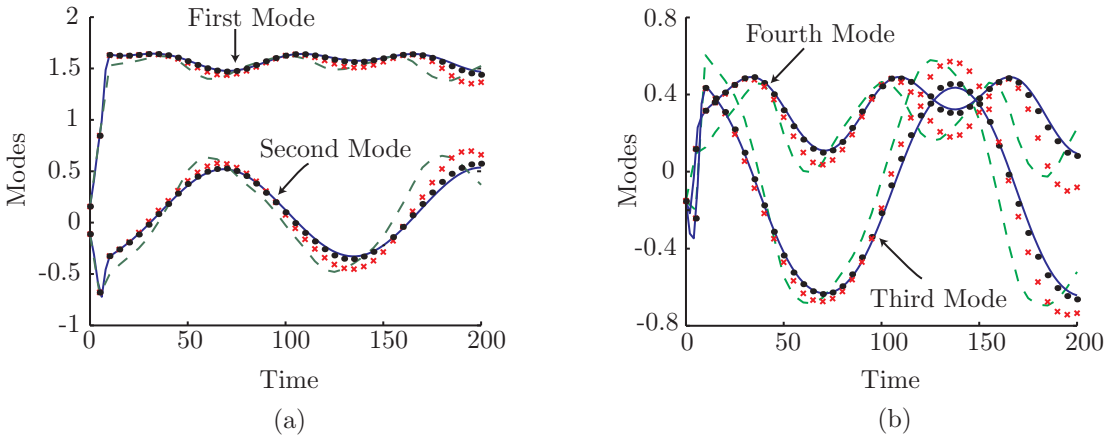

Figure 6.9: First modes of the FHN system (chemical case). Blue lines correspond with the modes obtained using the FEM solution, whereas green dashed lines, red crosses and black dots correspond with ROMs using 8, 15 and 20 eigenfunctions, respectively.

results into a ROM with approximately the same number of equations as the LSD (35 vs. 40). As mentioned in Chapter 3, when this occurs it is preferable to use the LSD since it can be employed for a wider range of conditions. The derivation of the ROM with the POD technique for the chemical case will not be included in this work.

6.4.2 ROM in the Biological Case

Contrary to the previous example, in this case the LSD technique is only able to reduce the number of equations of the FEM in one order of magnitude which translates into solving around 400 ODEs. The POD arises as an alternative to overcome this problem.

The first step to construct the ROM using the POD technique is the derivation of a representative set of data. The snapshots, which will compose the data set, will be obtained by numerically solving system (6.3)-(6.4) using a finite element scheme with initial conditions (6.9) and the set of parameters employed in section 6.3.2. Since the ROM is only required to represent the travelling plane wave behaviour, the snapshots will correspond with this behaviour. For each of the fields v and w, the selected data set is composed of 1000 snapshots collected each 0.4 units of time. This data set is assumed to be representative of the system dynamics. The second step is to compute each POD basis. In this case, since the number of elements of the data set is lower

than the number of discretisation points in the FEM scheme, the method of snapshots is preferable to the direct method (see Section 3.4.2). As a result of this step, two matrices are obtained: $\mathbf{\Phi}_{va} = \left[\boldsymbol{\phi}_{v1}|, \ldots, |\boldsymbol{\phi}_{vk_v}\right]$ and $\mathbf{\Phi}_{wa} = \left[\boldsymbol{\phi}_{w1}|, \ldots, |\boldsymbol{\phi}_{wk_w}\right]$ which have as columns the PODs for the v and w fields, respectively. k_v and k_w indicate two given natural numbers. The sets $\mathscr{E}_{va}$ and $\mathscr{E}_{wa}$ will be composed by the PODs of matrices $\mathbf{\Phi}_{va}$ and $\mathbf{\Phi}_{wa}$, respectively. Some of the PODs for the v field, are represented in Figure 6.10. The picture illustrates that the larger the eigenvalue associated to a POD, the higher the frequency of its spatial oscillations.

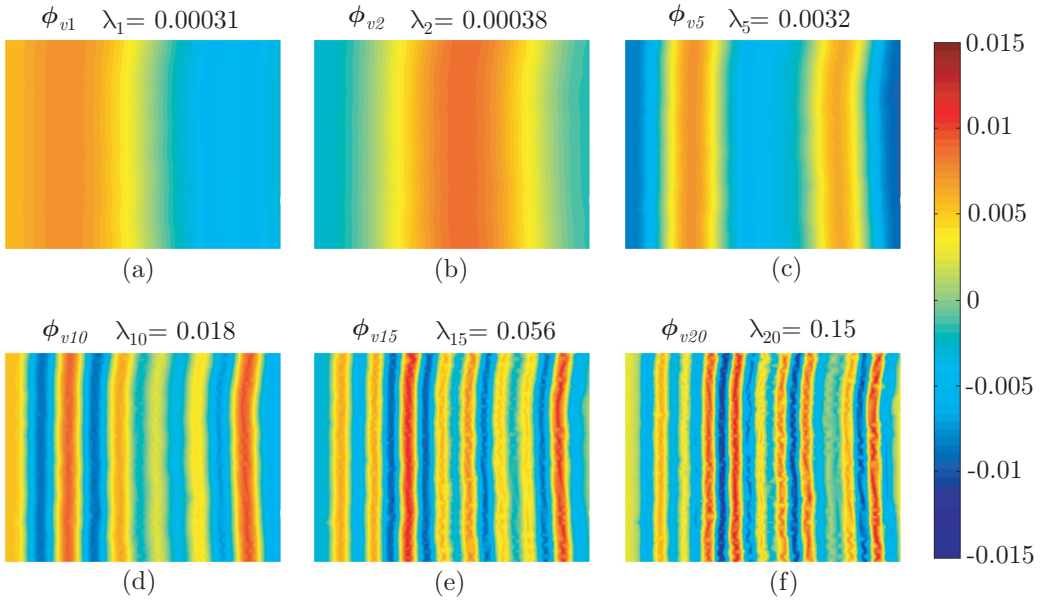

Figure 6.10: Some PODs for the v-field employed for the construction of the ROM.

Finally, the ROM is obtained by projecting Eqns (6.3) and (6.4) over the sets $\mathscr{E}_{va}$ and $\mathscr{E}_{wa}$, respectively. Thus resulting into a system of ODEs of the form:

$$\frac{d\mathbf{m}_{va}}{dt} = \mathcal{A}_a \mathbf{m}_{va} + \langle \Phi_{va}, g \rangle_{\mathscr{V}} - \langle \Phi_{va}, w \rangle_{\mathscr{V}} + \langle \Phi_{va}, u_a \rangle_{\mathscr{V}}, \tag{6.18}$$

$$\frac{d\mathbf{m}_{wa}}{dt} = -\varepsilon\gamma \mathbf{m}_{wa} - \varepsilon\beta \langle \Phi_{wa}, v \rangle_{\mathscr{V}}, \tag{6.19}$$

where $u_a = 0$ and matrix $\mathcal{A}_a$ and vectors $\mathbf{m}_{va}$ and $\mathbf{m}_{va}$ are of the form: $\mathcal{A}_a = \langle \Phi_{va}, \kappa \Delta \Phi_{va} \rangle_{\mathscr{V}}$, $\mathbf{m}_{va} = [m_{v1}, ..., m_{vk_v}]^T$, $\mathbf{m}_{wa} = [m_{w1}, ..., m_{wk_w}]^T$. Similarly, the initial conditions for the resulting ODE system are recovered by projecting (6.9) over the sets $\mathscr{E}_{va}$ and $\mathscr{E}_{wa}$, so that:

$$\mathbf{m}_{v0} = \langle \Phi_{va}, v_0 \rangle_{\mathscr{V}}, \quad \mathbf{m}_{w0} = \langle \Phi_{wa}, w_0 \rangle_{\mathscr{V}}. \tag{6.20}$$

The energy captured by the PODs -see Eqn (3.9)- is represented in Figure 6.11 as a function of the number of PODs. As one can see in it, the lower the number of PODs, the lower the energy captured what may cause poor agreement between the real model and the ROM. In order to illustrate this point, three ROMs constructed with

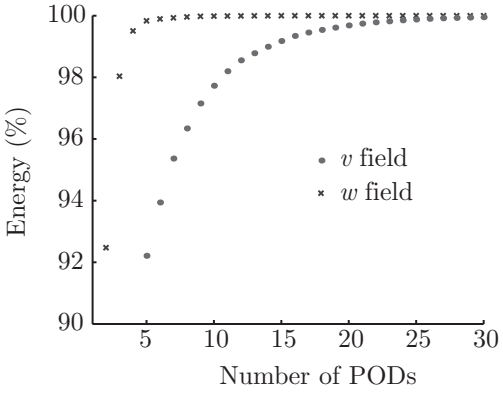

Figure 6.11: Energy captured by the low dimensional set as a function of the number of PODs chosen.

a number of PODs collecting different amounts of energy are considered. Table 6.1 shows a comparison, in terms of captured energy and number of equations, between the different ROMs and the FEM. The Table highlights the fact that ROMs drastically

Method	**Captured Energy (%)**	**N. Eqns (v-field)**	**N. Eqns (w-field)**	**N. Eqns total**
First ROM	99.6	19	5	24
Second ROM	99.8	23	5	28
Third ROM	99.97	33	9	42
FEM	100	2342	2342	4684

Table 6.1: Comparison between the FEM and three ROMs capturing the 99.6%, 99.8% and 99.97% of the energy.

reduce the number of model equations as compared with the FEM. In order to compare the degree of accuracy of the different ROMs, the results (in mode form) obtained with the FEM (lines) are plotted together with the ROM solutions (marks) in Figure 6.12. For clarity reasons, only the four most relevant modes for the v-field were represented. As shown in this picture, the ROMs capturing the 99.6% and 99.8% of the energy (dashed green line and red crosses, respectively) are only able to reproduce the system behaviour at a qualitative level, while the third ROM (circles) results into a much better approximation to the FEM scheme.

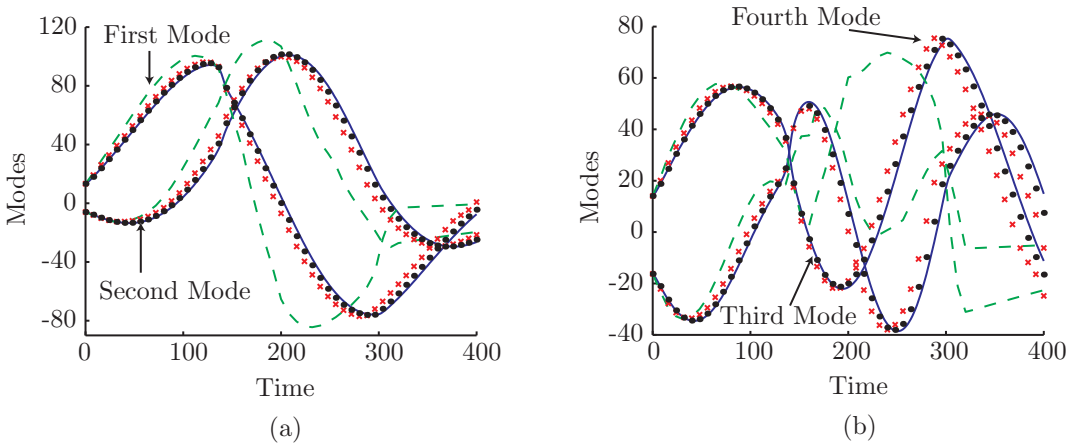

Figure 6.12: Evolution of the modes obtained with the finite element scheme (blue lines) and using ROMs capturing the 99.6% (green dashed lines), 99.8% (red crosses) and 99.97% of the energy. (a) First and second modes, (b) third and fourth modes.

When the time information (modes) is completed with the spatial information (PODs) to recover the field, that is $v = \Phi_{va}\mathbf{m}_{va}$, the same can be concluded as illustrated in Figure 6.13. The fields obtained from the ROMs capturing the 99.6% and

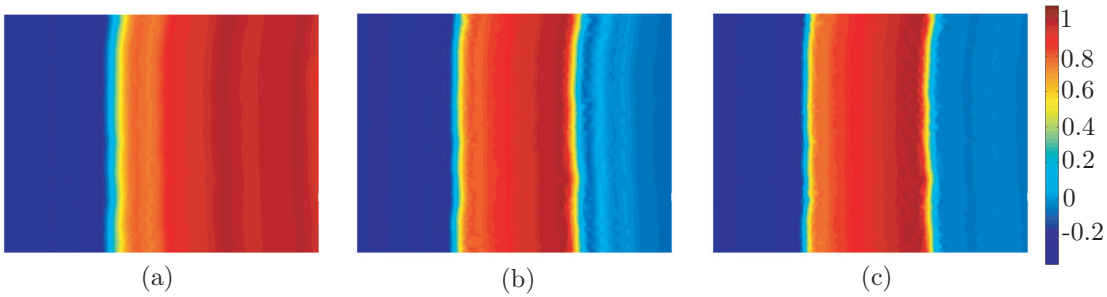

Figure 6.13: v-field snapshots obtained with the ROMs which capture the (a) 99.6%, (b) 99.8% and (c) 99.97% of energy.

99.8% (Figures 6.13 (a) and (b), respectively) are only rough approximations to the real field. However, when using the ROM capturing the 99.97% of the energy, the essential spatio-temporal features of the FEM model are preserved (Figure 6.13 (c)). This third ROM will be employed in Section 6.5.2 as the reference trajectory for the control law.

6.5 Robust Control

In this section, the theory presented in Chapter 4 will be applied to the chemical and biological cases of the FHN model. The objective is to design a control law

able to stabilise a prescribed reference (travelling plane wave) even in the presence of parametric and/or structural uncertainties. It should be remarked that the controllers act only on the activator equation. Controlling this variable seems to be experimentally feasible and for this reason other authors (see Keener (2004); Pumir and Krinsky (1999); Rappel et al. (1999)) have chosen this approach. Other biological or chemical systems might require controlling more than one variable.

6.5.1 Robust Control in the Chemical Case

As mentioned in section 6.3.1 the FHN model is very sensitive to changes in the parameters and two examples were employed so as to illustrate this point. In the first case, the activator v and the inhibitor w evolve in the form of a plane wave which oscillates between two points in the ξ_1 axis (limit cycle). In the second example a number of irregular forms appear. The objective of this section is to design a control law that, acting on the "fingerprint" behaviour, drives the system to the limit cycle. The uncertain terms are: the diffusive parameter κ and the nonlinear term $g(v)$.

As in previous sections, let us partition the eigenset associated to our system into a finite set $(\mathscr{E}_a, \mathscr{L}_a, \mathcal{N}_a)$, where $\mathcal{N}_a$ contains as elements the indexes of the modes we want to drive into the desired limit cycle, and its infinite dimensional complement $(\mathscr{E}_b, \mathscr{L}_b, \mathcal{N}_b)$. The controller is designed so that the modes in $\mathscr{M}_a = \{m_{vi}\}_{i\in\mathcal{N}_a}$ converge to those describing the limit cycle, which is expressed as:

$$\frac{d\mathbf{m}^*_{va}}{dt} = -\kappa^*\Lambda_a\mathbf{m}^*_{va} + \langle\Phi_a, g^*\rangle_{\mathscr{V}} - \mathbf{m}^*_{wa} + \langle\Phi_a, u^*_a\rangle_{\mathscr{V}}, \tag{6.21}$$

while the remaining, which are collected in $\mathscr{M}_b$, are forced to relax so as to reach the following reference:

$$\mathbf{m}^*_{vb} = 0; \quad \mathbf{m}^*_{wb} = 0. \tag{6.22}$$

Projecting Eqn (6.3) over the sets $\mathscr{E}_a$ and $\mathscr{E}_b$ one is led to:

$$\frac{d\mathbf{m}_{va}}{dt} = -\kappa\Lambda_a\mathbf{m}_{va} + \langle\Phi_a, g\rangle_{\mathscr{V}} - \mathbf{m}_{wa} + \langle\Phi_a, u_a\rangle_{\mathscr{V}}, \tag{6.23}$$

$$\frac{d\mathbf{m}_{vb}}{dt} = -\kappa\Lambda_b\mathbf{m}_{vb} + \langle\Phi_b, g\rangle_{\mathscr{V}} - \mathbf{m}_{wb} + \langle\Phi_b, u_b\rangle_{\mathscr{V}}. \tag{6.24}$$

The expression for the evolution of the modes in deviation form is obtained by subtracting Eqns (6.21)-(6.22) from (6.23)-(6.24), respectively. Thus leading to:

$$\frac{d\overline{\mathbf{m}}_{va}}{dt} = -\kappa\Lambda_a\overline{\mathbf{m}}_{va} + \chi\Lambda_a\mathbf{m}^*_{va} + \langle\Phi_a, \overline{g}\rangle_{\mathscr{V}} - \overline{\mathbf{m}}_{wa} + \langle\Phi_a, \overline{u}_a\rangle_{\mathscr{V}}, \tag{6.25}$$

$$\frac{d\overline{\mathbf{m}}_{vb}}{dt} = -\kappa\Lambda_b\overline{\mathbf{m}}_{vb} + \langle\Phi_b, g\rangle_{\mathscr{V}} - \overline{\mathbf{m}}_{wb} + \langle\Phi_b, \overline{u}_b\rangle_{\mathscr{V}}, \tag{6.26}$$

where $\chi = \kappa^* - \kappa$ is unknown since κ and κ^* are unknown. To construct the control law, some information is required on the uncertain terms. In the case of the parametric uncertainty, it is assumed that a function of the form $\chi_b > |\chi|$ is known.

Lemma 6.1 *Let us denote by λ_q the maximum eigenvalue of the set $\mathscr{L}_a$. The modes of the reference trajectory $\mathbf{m}^*_{va}$ and the modes in deviation form $\overline{\mathbf{m}}_{va}$ are related by means of the following inequality:*

$$\chi \overline{\mathbf{m}}^T_{va} \Lambda_a \mathbf{m}^*_{va} \leq \nu \|\overline{v}_a\|_{\mathscr{V}}, \tag{6.27}$$

where $\nu > \lambda_q \chi_b \|v^*_a\|_{\mathscr{V}}$.

The proof of this lemma is included in Appendix B.7. Let us now define the quadratic functions $\mathcal{B}_a = 1/2(\overline{\mathbf{m}}^T_{va}\overline{\mathbf{m}}_{va})$ and $\mathcal{B}_b = 1/2(\overline{\mathbf{m}}^T_{vb}\overline{\mathbf{m}}_{vb})$. Although the exact form of $g(v)$ is unknown, consider that two functions ζ_a and ζ_b so that $\zeta_a \geq \overline{g}$ and $\zeta_b \geq g$ are known. Using these bounds and Eqn (6.27) in lemma 6.1, the time derivatives of $\mathcal{B}_a$ and $\mathcal{B}_b$ along (6.25) and (6.26), lead to:

$$\dot{\mathcal{B}}_a \leq -\kappa\lambda_{1a} 2\mathcal{B}_a + (\nu + \zeta_a)\|\overline{v}_a\|_{\mathscr{V}} - \overline{\mathbf{m}}^T_{va}\overline{\mathbf{m}}_{wa} + \langle \overline{v}_a, \overline{u}_a \rangle_{\mathscr{V}}, \tag{6.28}$$

$$\dot{\mathcal{B}}_b \leq -\kappa\lambda_{1b} 2\mathcal{B}_b + \zeta_b\|\overline{v}_b\|_{\mathscr{V}} - \overline{\mathbf{m}}^T_{vb}\overline{\mathbf{m}}_{wb} + \langle \overline{v}_b, \overline{u}_b \rangle_{\mathscr{V}}, \tag{6.29}$$

where λ_{1a} and λ_{1b} are the minimum eigenvalues of the sets $\mathscr{L}_a$ and $\mathscr{L}_b$, respectively. Control law $\overline{u}_a$ must compensate the terms: ν (related to the parametric uncertainty); ζ_a (related to the structural uncertainty) and $\overline{\mathbf{m}}^T_{va}\overline{\mathbf{m}}_{wa}$. On the other hand, $\overline{u}_b$ must compensate the uncertain term ζ_b and $\overline{\mathbf{m}}^T_{vb}\overline{\mathbf{m}}_{wb}$. As pointed out in Chapter 4 these objectives are attained by selecting the following expressions for the control laws:

$$\overline{u}_a = \begin{cases} \overline{w}_a - \eta_a \frac{\overline{v}_a}{\|\overline{v}_a\|_{\mathscr{V}}} & \text{if} \quad \eta_a\|\overline{v}_a\|_{\mathscr{V}} \geq \theta_a \\ \\ \overline{w}_a - \eta_a^2 \frac{\overline{v}_a}{\theta_a} & \text{if} \quad \eta_a\|\overline{v}_a\|_{\mathscr{V}} < \theta_a \end{cases}, \tag{6.30}$$

$$\overline{u}_b = \begin{cases} \overline{w}_b - \eta_b \frac{\overline{v}_b}{\|\overline{v}_b\|_{\mathscr{V}}} & \text{if} \quad \eta_b\|\overline{v}_b\|_{\mathscr{V}} \geq \theta_b \\ \\ \overline{w}_b - \eta_b^2 \frac{\overline{v}_b}{\theta_b} & \text{if} \quad \eta_b\|\overline{v}_b\|_{\mathscr{V}} < \theta_b \end{cases}, \tag{6.31}$$

where $\eta_a \geq \|(\nu + \zeta_a)\|_{\mathscr{V}}$ and $\eta_b \geq \|\zeta_b\|_{\mathscr{V}}$. In order to illustrate this point, these controls will be applied to the FHN system showing the "fingerprint" behaviour.

As mentioned previously, using too conservative bounds on the uncertain terms can lead to sharp control actions producing chattering. Consider that we know two functions ζ_b and ζ_a of the form:

$$\zeta_b = \begin{cases} 0.1 & \text{if} \quad v \geq 0 \\ 0.75|v| + 0.1 & \text{if} \quad 0 < v \geq 0.6 \\ 0.55 & \text{if} \quad v > 0.6 \end{cases} ; \quad \zeta_a = \zeta_b + |\zeta_c|; \quad \zeta_c = \zeta_b - 0.65, \tag{6.32}$$

which, as shown in Figure 6.14, are bounds for the unknown terms g (dashed line) and $\overline{g}$, respectively. Consider also the control parameters summarised in Table 6.2.

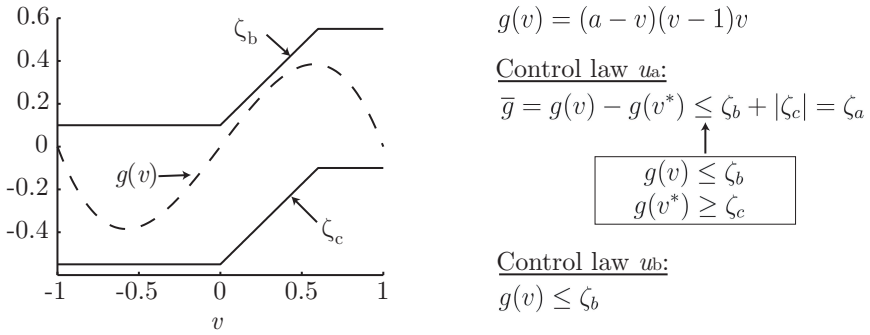

Figure 6.14: Bounds on the nonlinear term $g(v)$.

θ_b	θ_a	χ_b	λ_q	η_b	η_a
1×10^{-4}	1×10^{-4}	0.01	315.11	$\|\zeta_b\|_\mathcal{Y}$	$\|\zeta_a\|_\mathcal{Y}$

Table 6.2: Expressions for the parameters employed in the control law.

The effect of this control law on the FHN system exhibiting a "fingerprint" behaviour (see case 2 in Section 6.3.1) is presented in Figure 6.15. The system, which initially evolves as in the "fingerprint" case (Figure 6.15(a)), is forced to follow the

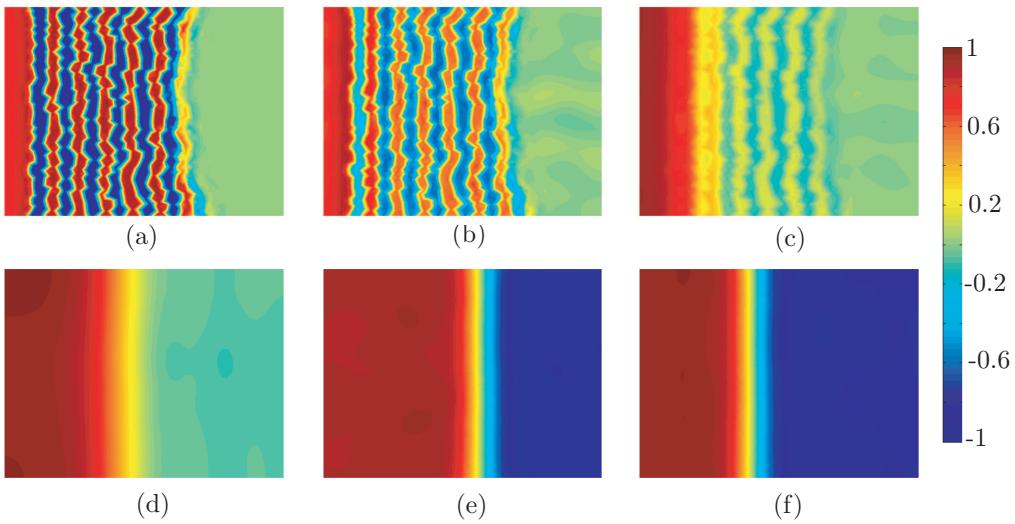

Figure 6.15: Evolution of the FHN system exhibiting the "fingerprint" behaviour under the control logic (6.30)-(6.31), (a) before entering the control, (b)-(d) transition period, (e)-(f) after reaching the reference.

prescribed reference (oscillating front). As shown in Figures 6.15(e)-(f) the objective is reached after a short transition period (Figures 6.15(b)-(d)). The slight differences between the reference (Figure 6.8(c)) and the controlled field (Figure 6.15(e)-(f)) are caused by the presence of uncertainty. Such divergences could be arbitrarily reduced by setting stricter limits on θ_a and θ_b although at the expenses of larger control efforts.

Figure 6.16 depicts the evolution of some modes under this control. For clarity reasons, only a few modes were represented. As shown in Figure 6.16(a), once the

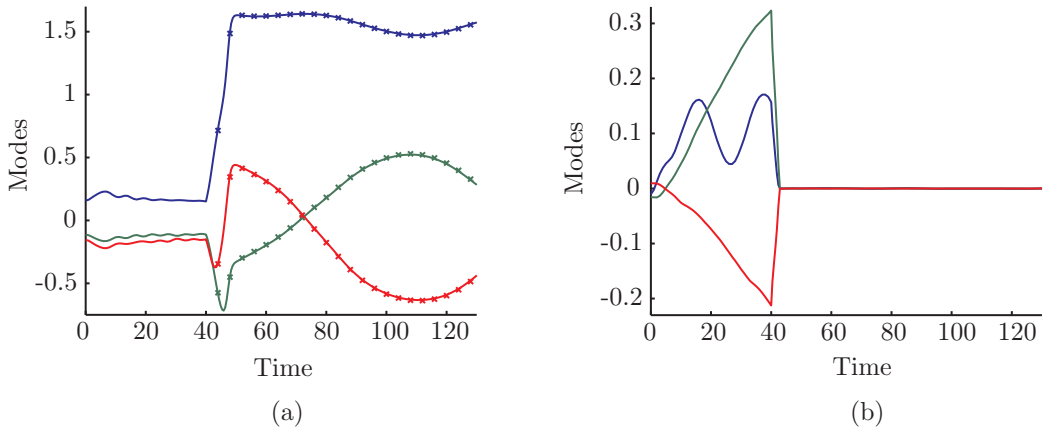

Figure 6.16: Evolution of some modes corresponding to the FHN system. (a) Modes representative of the oscillating front behaviour. The marks represent the reference trajectory. (b) Modes negligible in the oscillating front behaviour.

controller is switched on at $t = 40$, there is a short transition period after which the modes belonging to $\mathscr{M}_a$ (continuous lines) converge to the selected reference (marks). On the other hand, in Figure 6.16(b) one can see that the modes in the set $\mathscr{M}_b$ vanish after $t = 40$.

Finally, the evolution of the control effort for $\overline{u}$, $\overline{u}_a$ and $\overline{u}_b$ in the $\mathcal{L}_2$ norm is represented in Figure 6.17(a). The figure highlights that most of the control effort is employed by $\overline{u}_a$. On the other hand, the value of the control at three different points of the spatial domain is plotted in Figure 6.21(b). The location of these points is $(\xi_1, \xi_2) = (-0.51, 0)$, $(\xi_1, \xi_2) = (0.52, 0.49)$ and $(\xi_1, \xi_2) = (0.50, -0.50)$. It is worth mentioning that other authors (Shvartsman and Kevrekidis, 1998; Shvarstman et al., 2000; Siehr et al., 2007) working in the FHN model, employ control laws producing inputs in the same order of magnitude as those proposed in this work.

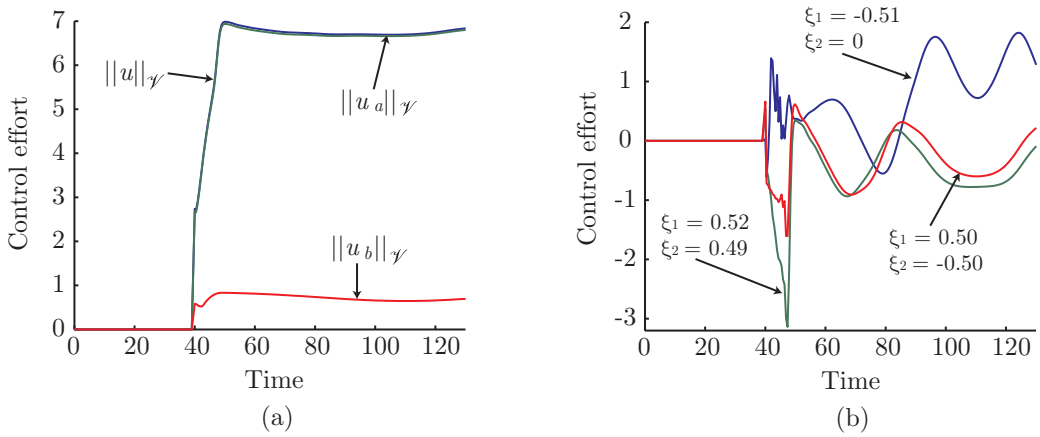

Figure 6.17: Evolution of the control effort. (a) In $\mathcal{L}_2$ norm. (b) In three points distributed in the spatial domain.

6.5.2 Robust Control in the Biological Case

As pointed out in section 6.3.2 when the FHN model represents a biological system, the travelling plane wave solution is usually related to the normal behaviour while a wandering spiral or irregular forms indicate problems such as arrhythmia, fibrillation or neurological disorders. Therefore, the aim of this section is to design a control law which, in the event of instability (spiral), drives the system back to the travelling plane wave. The nonlinear term $g(v)$ is assumed to be unknown.

The same procedure as in the previous section is applied. Thus, the complete set of PODs and the corresponding eigenvalues associated to this system is split into a finite set $(\mathscr{E}_a, \mathscr{L}_a, \mathcal{N}_a)$, where $\mathcal{N}_a$ contains as elements the indexes of the modes we want to drive into the desired behaviour (travelling plane wave), and its infinite dimensional complement $(\mathscr{E}_b, \mathscr{L}_b, \mathcal{N}_b)$. The controller now is designed so that the modes in $\mathscr{M}_a = \{m_{vi}\}_{i\in\mathcal{N}_a}$ converge to those describing the travelling plane wave, which is expressed as:

$$\frac{d\mathbf{m}^*_{va}}{dt} = \mathcal{A}_a\mathbf{m}^*_{va} + \langle\Phi_{va}, g^*\rangle_{\mathcal{V}} - \langle\Phi_{va}, w^*\rangle_{\mathcal{V}} + \langle\Phi_{va}, u^*_a\rangle_{\mathcal{V}}, \tag{6.33}$$

The remaining modes, collected in the set $\mathscr{M}_b$, must be stabilised. Thus the reference is:

$$\mathbf{m}^*_{vb} = 0; \quad \mathbf{m}^*_{wb} = 0. \tag{6.34}$$

For illustrative purposes the initial conditions of the reference, which starts when the control law enters in action, are those indicated in Eqn (6.9). It is worth mentioning that other initial conditions could be employed. Projecting the equations describing

the spiral behaviour over the set $\mathscr{E}_a$, one is led to:

$$\frac{d\mathbf{m}_{va}}{dt} = \mathcal{A}_a\mathbf{m}_{va} + \langle\Phi_{va}, g\rangle_{\mathscr{V}} - \langle\Phi_{va}, w\rangle_{\mathscr{V}} + \langle\Phi_{va}, u_a\rangle_{\mathscr{V}}, \tag{6.35}$$

$$\frac{d\mathbf{m}_{vb}}{dt} = \mathcal{A}_b\mathbf{m}_{vb} + \langle\Phi_{vb}, g\rangle_{\mathscr{V}} - \langle\Phi_{vb}, w\rangle_{\mathscr{V}} + \langle\Phi_{vb}, u_b\rangle_{\mathscr{V}}. \tag{6.36}$$

Note that since the PODs in the set $\mathscr{E}_a$ were obtained only from the snapshots of the travelling plane wave, recovering the field ($v_a = \Phi_{va}\mathbf{m}_{va}$) will not reproduce the spiral. This issue will not affect the control since driving $\mathbf{m}_{va}$ to the reference $\mathbf{m}^*_{va}$ while stabilising $\mathbf{m}_{vb}$, the travelling plane wave will be recovered. The system in deviation form is obtained by subtracting system (6.35)-(6.36) from the reference (6.33)-(6.34):

$$\frac{d\overline{\mathbf{m}}_{va}}{dt} = \mathcal{A}_a\overline{\mathbf{m}}_{va} + \langle\Phi_{va}, \overline{g}\rangle_{\mathscr{V}} - \langle\Phi_{va}, \overline{w}\rangle_{\mathscr{V}} + \langle\Phi_{va}, \overline{u}_a\rangle_{\mathscr{V}}, \tag{6.37}$$

$$\frac{d\overline{\mathbf{m}}_{vb}}{dt} = \mathcal{A}_b\overline{\mathbf{m}}_{vb} + \langle\Phi_{vb}, \overline{g}\rangle_{\mathscr{V}} - \langle\Phi_{vb}, \overline{w}\rangle_{\mathscr{V}} + \langle\Phi_{vb}, \overline{u}_b\rangle_{\mathscr{V}}. \tag{6.38}$$

Control operation will be set up so as to attain the following complementary objectives: $\overline{u}_b$ will stabilise those modes belonging to $\mathscr{M}_b$ (6.36) and $\overline{u}_a$ will force the remaining to follow the reference trajectory given in Eqn (6.33). Now let us choose two Lyapunov functions of the form[2]: $\mathcal{B}_a = \frac{1}{2}\left(\overline{\mathbf{m}}^T_{va}\overline{\mathbf{m}}_{va}\right)$ and $\mathcal{B}_b = \frac{1}{2}\left(\overline{\mathbf{m}}^T_{vb}\overline{\mathbf{m}}_{vb}\right)$. Time derivatives of $\mathcal{B}_a$ and $\mathcal{B}_b$ along the trajectories (6.37)-(6.38) lead to, respectively:

$$\dot{\mathcal{B}}_a = \overline{\mathbf{m}}^T_{va}\mathcal{A}_a\overline{\mathbf{m}}_{va} + \langle\overline{v}_a, \overline{g}\rangle_{\mathscr{V}} - \langle\overline{v}_a, \overline{w}\rangle_{\mathscr{V}} + \langle\overline{v}_a, \overline{u}_a\rangle_{\mathscr{V}} \leq$$

$$\lambda_{ma}\overline{\mathbf{m}}^T_{va}\mathbf{m}_{va} + \langle\overline{v}_a, \overline{g}\rangle_{\mathscr{V}} - \langle\overline{v}_a, \overline{w}_a\rangle_{\mathscr{V}} + \langle\overline{v}_a, \overline{u}_a\rangle_{\mathscr{V}}, \tag{6.39}$$

$$\dot{\mathcal{B}}_b = \overline{\mathbf{m}}^T_{vb}\mathcal{A}_b\overline{\mathbf{m}}_{vb} + \langle\overline{v}_b, g\rangle_{\mathscr{V}} - \langle\overline{v}_b, \overline{w}\rangle_{\mathscr{V}} + \langle\overline{v}_b, \overline{u}_b\rangle_{\mathscr{V}} \leq$$

$$\lambda_{mb}\overline{\mathbf{m}}^T_{vb}\mathbf{m}_{vb} + \langle\overline{v}_b, g\rangle_{\mathscr{V}} - \langle\overline{v}_b, \overline{w}_b\rangle_{\mathscr{V}} + \langle\overline{v}_b, \overline{u}_b\rangle_{\mathscr{V}}, \tag{6.40}$$

The explicit form of the nonlinear function $g(v)$ is assumed to be unknown, but some information on this term is available. Note that $g(v^*)$ and $\overline{g}$ are also unknown. In this case, the information includes two known functions ζ_a and ζ_b so that $\zeta_a \geq \overline{g}$ and $\zeta_b \geq g$. Introducing these functions on inequalities (6.39) and (6.40) and using the Schwarz's inequality, one is led to:

$$\dot{\mathcal{B}}_a \leq 2\lambda_{ma}\mathcal{B}_a + \|\overline{v}_a\|_{\mathscr{V}}\|\zeta_a\|_{\mathscr{V}} - \langle\overline{v}_a, \overline{w}_a\rangle_{\mathscr{V}} + \langle\overline{v}_a, \overline{u}_a\rangle_{\mathscr{V}}.$$

$$\dot{\mathcal{B}}_b \leq 2\lambda_{mb}\mathcal{B}_b + \|\overline{v}_b\|_{\mathscr{V}}\|\zeta_b\|_{\mathscr{V}} - \langle\overline{v}_b, \overline{w}_b\rangle_{\mathscr{V}} + \langle\overline{v}_b, \overline{u}_b\rangle_{\mathscr{V}}.$$

[2]Other convex functions could be employed -see Alonso et al. (2004a); Vilas et al. (2007)-

According to Chapter 4 the control laws:

$$\overline{u}_a = \begin{cases} \overline{w}_a - \omega_a \overline{v}_a - \eta_a \frac{\overline{v}_a}{\|\overline{v}_a\|_\varkappa} & \text{if} \quad \eta_a \|\overline{v}_a\|_\varkappa \geq \theta_a \\ \\ \overline{w}_a - \omega_a \overline{v}_a - \eta_a^2 \frac{\overline{v}_a}{\theta_a} & \text{if} \quad \eta_a \|\overline{v}_a\|_\varkappa < \theta_a \end{cases}, \tag{6.41}$$

$$\overline{u}_b = \begin{cases} \overline{w}_b - \omega_b \overline{v}_b - \eta_b \frac{\overline{v}_b}{\|\overline{v}_b\|_\varkappa} & \text{if} \quad \eta_b \|\overline{v}_b\|_\varkappa \geq \theta_b \\ \\ \overline{w}_b - \omega_b \overline{v}_b - \eta_b^2 \frac{\overline{v}_b}{\theta_b} & \text{if} \quad \eta_b \|\overline{v}_b\|_\varkappa < \theta_b \end{cases}, \tag{6.42}$$

where $\eta_a \geq \|\zeta_a\|_\varkappa$, $\eta_b \geq \|\zeta_b\|_\varkappa$, $\omega_a > 2|\lambda_{ma}|$, $\omega_b > 2|\lambda_{mb}|$ with λ_{ma}, λ_{mb} being the maximum eigenvalues of $\mathcal{A}_a$, $\mathcal{A}_a$, respectively, will attain the objective of this section.

Now, a simulation experiment will be carried out to show that the controller drives the system to the reference. The experiment consists of three parts. (**I**) First, initial conditions (6.9) are used in system (6.3)-(6.9) so as to obtain the travelling plane wave behaviour. (**II**) Then, a perturbation is introduced in order to produce a spiral. Such a perturbation consists of resetting the superior half plane - see Fenton et al. (2002b) for details-. (**III**) Once the spiral is formed, the control law (6.41)-(6.42) is switched on so as to drive the system back to the plane wave behavior.

Consider the control parameters summarised in Table 6.3, where ζ_a and ζ_b are

ω_a	ω_b	θ_a	θ_b	η_a	η_b
2×10^{-6}	0.08	1×10^{-5}	1×10^{-5}	$\|\zeta_a\|_\varkappa$	$\|\zeta_b\|_\varkappa$

Table 6.3: Functions and parameters used in the control law.

stricter bounds on the nonlinear terms as compared with those of the *chemical case*. In this regard, it should be remarked that for the control u_b function $g(v^*) = 0$, thus one has that $\overline{g} = g(v) - g(v^*) = g$. Besides, for the range of values reachable by v it follows that $g(v)$ and $\overline{g}$ are bounded, respectively, by functions ζ_b and ζ_a of the form:

$$\zeta_b = \begin{cases} 0.7|v| & \text{if} \quad v \geq 0 \\ 0.3v & \text{if} \quad 0 < v \geq 0.6 \\ 0.18 & \text{if} \quad 0.6 < v \geq 0.75 \\ 0.18 - 0.514(v - 1.1) & \text{if} \quad 0.75 < v \geq 1.1 \\ 0 & \text{if} \quad v > 1.1 \end{cases} ; \qquad \zeta_a = \zeta_b + 0.7|v^*|. \tag{6.43}$$

Figure 6.18 shows that the nonlinear function $g(v)$ (dashed line) is bounded by ζ_b. Furthermore, note that $\overline{g} = g - g^*$ is bounded by a function of the form $\zeta_a = \zeta_b + 0.7|v^*|$. As mentioned at the beginning of this section, the terms g and g^* are unknown. Consider now that the information we have on g and g^* is ζ_a and ζ_b. With this information we can construct the control law.

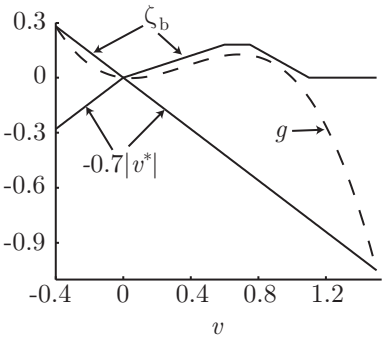

$$g(v) = (a - v)(v - 1)v$$

Control law u_a:

$$\overline{g}(v) = g(v) - g(v^*) \leq \zeta_b + 0.7|v^*| = \zeta_a$$

$$\boxed{\begin{array}{c} g(v) \leq \zeta_b \\ g(v^*) \geq -0.7|v^*| \end{array}}$$

Control law u_b:

$$\overline{g}(v) = g(v) \leq \zeta_b$$

Figure 6.18: Bounds on the nonlinear term $g(v)$.

Figures 6.19(a) and (b) show the evolution of some "relevant" and "non relevant" modes, respectively, under this control law. In this picture one can see that, the

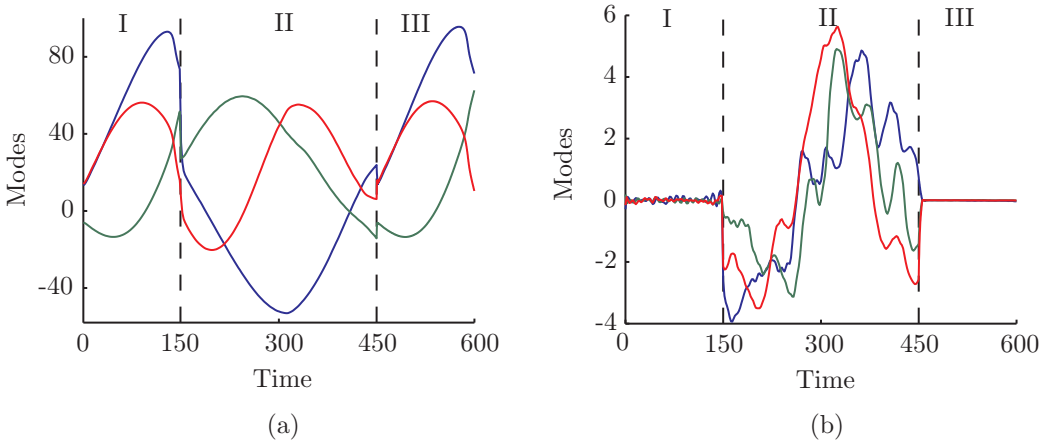

Figure 6.19: Evolution of some modes under the control law (6.41)-(6.42). (a) Three modes which are representative of the plane wave behavior, (b) three modes negligible in the plane wave behavior.

modes start to behave like in the travelling plane wave case. When the perturbation is introduced at $t = 150$ their dynamic behavior completely changes indicating that the spiral is being formed. Note in Figure 6.19(b) **II** that some modes, which in the plane wave case were considered as "non relevant", may become relevant when describing the spiral evolution. This is the reason why they must be stabilised. Finally, when the control law enters in action at $t = 450$ the "relevant" modes are forced to follow the reference trajectory. This can be seen when comparing in Figure 6.19(a), the mode evolution in regions **I** and **III**. At this point ($t = 450$), the "non relevant" modes are stabilised (region **III** in Figure 6.19(b)). The effect of the controller on the v-field is illustrated in Figure 6.20 where six snapshots, taken at different times, are depicted.

Figure 6.20 (a) corresponds with a snapshot of the field before entering the control law

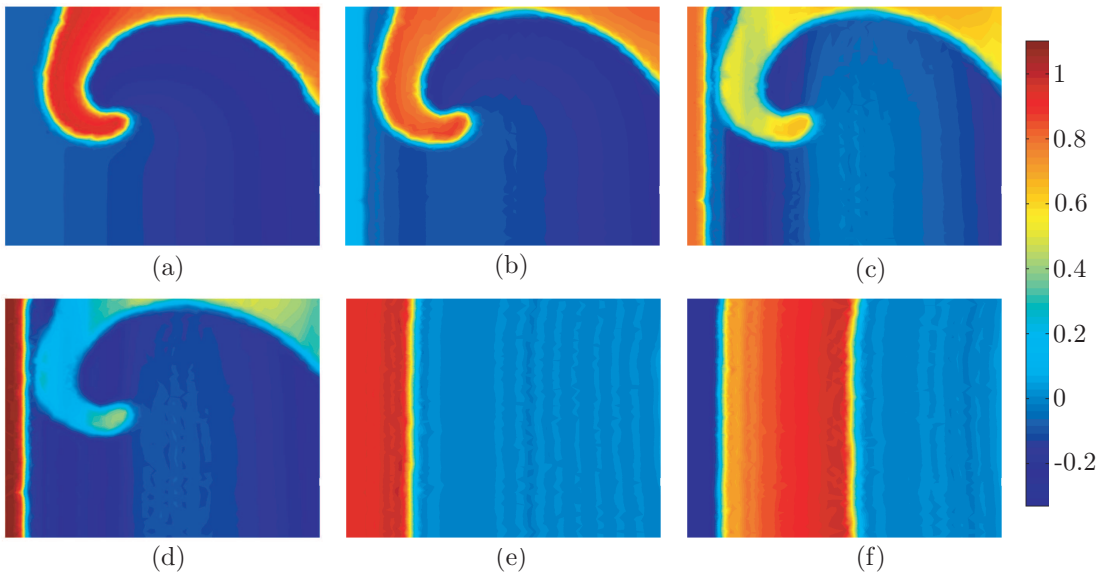

Figure 6.20: Snapshots of the FHN system under the control law (6.41)-(6.42). (a) Before entering the control law, (b)-(e) transition period, (f) system under control.

whereas Figures 6.20 (b)-(d) are snapshots taken in the transition period. Finally, the system under control reaches the reference (see Figures 6.20 (e)-(f)).

The time evolution of the control effort for $\overline{u}_a$ (green line), $\overline{u}_b$ (blue line) and $\overline{u}$ (red line), is represented in Figure 6.21(a) by means of its norm as defined in Eqn (1.27). Figure 6.21(b) shows the value of the of the control law at three different

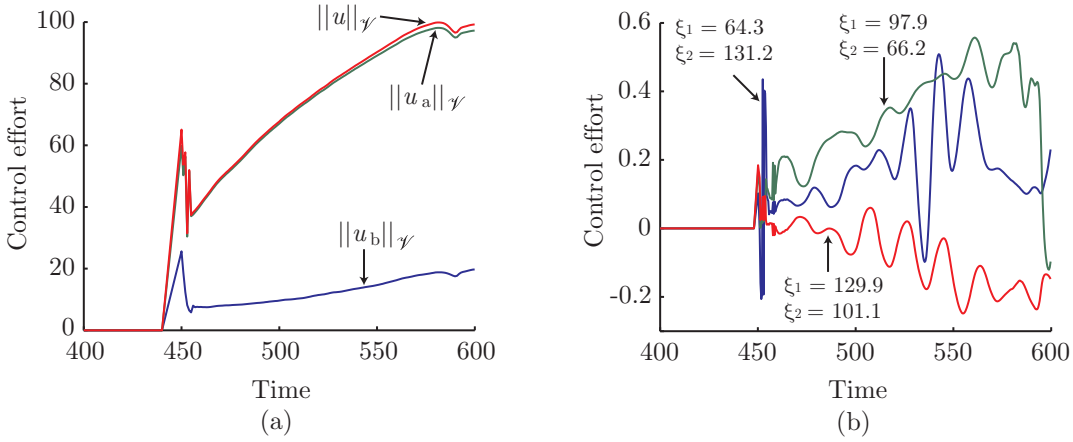

Figure 6.21: Control effort measured (a) using the norm as defined in Eqn (1.27) and (b) using the value of the control law in three points of the spatial domain.

points of the spatial domain. The location of these points is $(\xi_1, \xi_2) = (64.3, 131.2)$, $(\xi_1, \xi_2) = (97.9, 66.2)$ and $(\xi_1, \xi_2) = (129.9, 101.1)$. It is worth mentioning that other

authors (Shvartsman and Kevrekidis, 1998; Shvarstman et al., 2000; Siehr et al., 2007) working in the FHN model, employ control laws producing inputs in the same order of magnitude as those proposed in this work.

Finally, in order to illustrate the importance of $\overline{u}_b$, the experiment has been repeated but this time, without stabilising the modes $\mathbf{m}_{vb}$, i.e. applying only control law $\overline{u}_a$. Figures 6.22 (a) and (b) depict the time evolution of some modes belonging to the sets $\mathscr{M}_a$ and $\mathscr{M}_b$, respectively. As shown in the picture, the modes of the set $\mathbf{m}_{va}$ follow

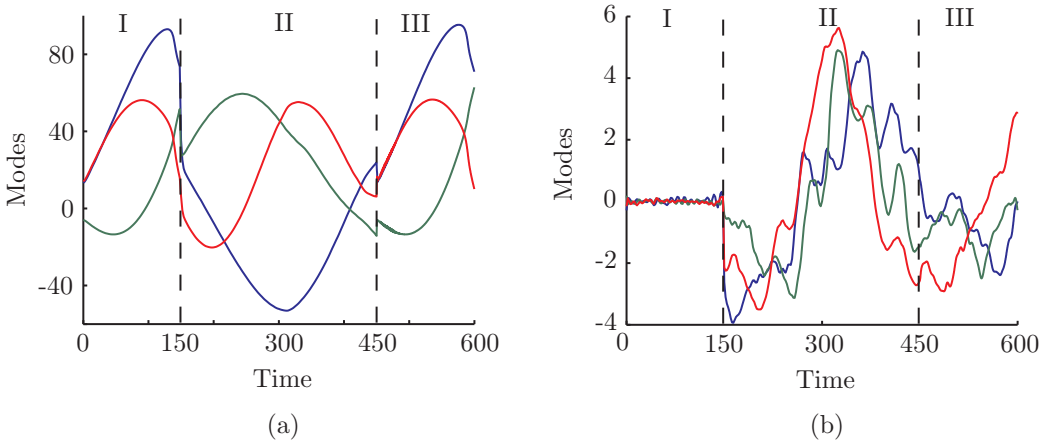

Figure 6.22: Mode evolution of the FHN system when applying only control law $\overline{u}_a$. (a) Three modes belonging to the set $\mathbf{m}_{va}$, (b) three modes belonging to the set $\mathbf{m}_{vb}$.

the reference trajectory $\mathbf{m}^*_{va}$ (see regions **II** and **III** in Figure 6.22(a)) while the modes of the set $\mathbf{m}_{vb}$ may become unstable (compare regions **I** and **III** in Figure 6.22(b)). The effect of the unstable modes of the set $\mathbf{m}_{vb}$ on v is shown in Figure 6.23. This

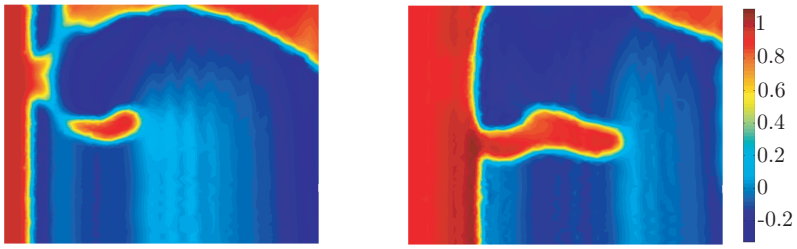

Figure 6.23: Two snapshots of the activator (v-field) showing the effect of the unstable modes $\mathbf{m}_{vb}$.

picture illustrates that such unstable modes prevent the system to reach the reference thus calling for their stabilisation.

Conclusions

The main objective of this work has been the design of a control logic able to drive the dynamics of systems with reaction and/or diffusion and convection (RDC) terms to the desired reference in the presence of structural and/or parametric uncertainty (*robustness*). To that purpose, use has been made of the classical theory of nonlinear robust control on lumped parameter systems, particularly the *Lyapunov Redesign Technique*. This theory has been extended to RDC systems by means of reduced order models (ROMs). In the order reduction techniques, the spatial information of the system (eigenfunctions) is computed off-line and constitutes the basis for the low dimensional subspace. The time information (modes) is obtained by computing a low dimensional system of ODEs (lumped parameter system). Using the Lyapunov redesign technique, the modes of the dynamics to be controlled are driven to those representative of the reference trajectory, this being equivalent to drive the states of the system to the desired reference.

On the first part of the thesis, the theoretical basis associated with the control logic design has been presented. The main results of this part are summarised below:

- The most commonly employed techniques in the derivation of ROMs have been studied. Particularly, special attention has been paid to the most efficient, from the computational cost point of view, approaches: the *Proper Orthogonal Decomposition* (POD) and the *Laplacian Spectral Decomposition* (LSD). The main advantage of the first one is that, in general, it leads to ROMs of lower dimension as compared with the other alternatives. However, since in this method the basis constituting the spatial information are obtained from experimental data, its application is reduced to the zone where the snapshots have been taken. Due to this fact, the second technique will be preferable to the first on those problems in which the difference between the POD and the LSD are not significant.

- Different classical numerical methods for the computation of partial differential equation systems have been compared. Among these, the finite element method

(FEM) has been chosen, firstly due to its flexibility when dealing with problems defined in complex geometries or with different boundary conditions and, secondly because the matrices resulting from the FEM structure allow us to approximate spatial integrals and derivatives using algebraic operations. In this regard, the way in which these approximations are obtained, has been explained in detail. Basically, the contexts of application of these approximations have been:

  - One of the main bottlenecks of ROMs lie in the projections of nonlinear terms. In general, the analytical solution of the spatial integrals involved in the projection is unknown. There exist different alternatives such as the following: the use of quadrature methods and the definition of field transformations such that the form of the nonlinear terms remain polynomial. However, the first alternative is not efficient and the second adds more equations to the original system and cannot be easily systematised since it depends on the form of the nonlinear terms. In this work, the FEM structure has been employed to compute the spatial integrals associated with the projection in a straightforward and systematic procedure.
  - The FEM structure can be also employed to approximate spatial derivatives by means of algebraic operations. In this way, the eigenfunctions of the LSD can be obtained in a systematic manner independently of the domain geometry.

- The application of the Kirchhoff transform has been generalised so as to approach the presence of nonlinear terms in the diffusion coefficients.

- Finally, and using the results summarised above, a robust control logic able to drive the dynamics of a RDC system to the desired reference trajectory has been designed. The following main aspects deserve to be highlighted:

  - The Lyapunov redesign technique has been presented and extended to distributed systems by means of ROM. The basic idea is to drive the representative modes to the reference while stabilising the remaining.
  - This logic has been also applied when only a finite number of actuators are available. In this sense, the minimum number of actuators ensuring the system controlabillity has been shown to coincide with the minimum number of modes representative of the reference trajectory. Furthermore,

the methodology that allows us to compute the spatial distribution of the actuators which ensures the minimum control effort has been developed.

- Problems that arise when too conservative bounds on the uncertain terms are considered have been studied. It has been shown that such bounds can lead to extremely sharp control actions producing the chattering phenomena. Besides, related to the control effort, it has been shown that the selection of an appropriate Lyapunov function collecting the system nonlinearity can help to obtain smoother control actions.
- Thermodynamics has been employed as one of the basis to prove the stability of the control laws and ROM.

The second part of the thesis has been focused on the application of the techniques developed in the theoretical part to systems of interest in fields such as biology and chemical or process engineering.

Future Work:

- The robust control method proposed requires to take measurements of the field at the whole domain. Furthermore, the number of controllers, even after applying the ROM, is still too large specially in 2D or 3D applications. In this regard, the research line proposed is to use robust observers which allow us, on the one hand, to recover the field from a few measurements and, on the other hand, to reduce the dimension of the ROM without affecting its capabilities for reproducing the real behaviour of the system.

- As mentioned previously, the main disadvantage of the POD method is it range of validity. In order to avoid this problem, in the process engineering group (IIM-CSIC) work is being done on developing a systematic procedure for online updating of the PODs.

- In general control actions cannot be arbitrarily large and this issue can affect the system controlabillity. The range of admissible perturbations for which the control actions can ensure the system stability together with the construction of Lyapunov functions collecting the nonlinearity of the system should be studied.

Conclusiones

El objetivo fundamental de este trabajo ha sido el diseño de una lógica de control capaz de conducir la dinámica de sistemas con términos de reacción y/o difusión y convección (sistemas RDC) a la referencia deseada en presencia de incertidumbre estructural y/o paramétrica (*robustez*). Para lograr dicho objetivo se ha hecho uso de la teoría clásica de control robusto no lineal en sistemas de parámetros concentrados, particularmente de la técnica de rediseño de Lyapunov. Esta teoría se ha extendido a sistemas RDC mediante la utilización de los modelos de orden reducido (MOR). En las técnicas de reducción de orden, la información espacial (autofunciones) del sistema se obtiene *off-line* y forma lo que se conoce como base del sistema de dimensión reducida. La información temporal (modos) se obtiene mediante la resolución de un sistema de EDOs de dimensión finita (sistema de parámetros concentrados). Utilizando la técnica de rediseño de Lyapunov, los modos de la dinámica a controlar se hacen converger hacia los modos de la trayectoria de referencia, lo que es equivalente a llevar los estados del sistema a controlar a la referencia deseada.

En la primera parte de la tesis se presenta la base teórica que lleva asociada el diseño de dicha lógica de control. Los principales resultados derivados de esta parte se presentan a continuación:

- Se han estudiado las técnicas más comunmente utilizadas en la derivación de los MOR. En particular se ha prestado especial atención a los dos enfoques más eficientes desde el punto de vista de tiempo de computación: *descomposición ortogonal propia* (DOP) y la *descomposición espectral del Laplaciano* (DEL). La principal ventaja de la primera es que, en general, conduce a MOR de dimensión menor que el resto de alternativas. Sin embargo, dado que en este método las bases que conforman la información espacial se obtienen a partir de datos experimentales, su validez se reduce al rango de perturbaciones en el que se tomaron dichos datos. Debido a esto, en aquellos problemas en los que la diferencia entre DOP y DEL sean poco significativas, el segundo método será preferible al primero.

- Se han comparado los distintos métodos clásicos de resolución de ecuaciones en derivadas parciales. Entre ellos, se ha elegido el método de elementos finitos (MEF) por una parte por su versatilidad a la hora de resolver problemas con distintas geometrías y condiciones frontera y, por otra, porque las matrices resultantes de su estructura nos permiten aproximar derivadas e integrales espaciales mediante operaciones algebraicas. En este sentido se ha explicado detalladamente la forma de llevar a cabo dichas aproximaciones que se han utilizado básicamente en los siguientes contextos:

  - Uno de los principales cuellos de botella de los MOR radica en la proyección de los términos no lineales. En general, no se conoce la solución analítica de las integrales espaciales involucradas en la proyección. Existen alternativas como utilizar métodos de cuadratura o definir transformaciones en el campo, de forma que los términos no lineales sean polinomios. Sin embargo, la primera alternativa es poco eficiente y la segunda añade más ecuaciones al sistema original y no es fácilmente sistematizable ya que depende de la forma del término no lineal. En este trabajo se ha hecho uso de la estructura resultante del MEF para transformar las integrales de la proyección en operaciones algebraicas y, de esta forma, solucionar este inconveniente.
  - La estructura de las matrices MEF también permite aproximar derivadas espaciales por operaciones algebraicas con lo que las autofunciones del método DEL se pueden obtener de forma sistemática independientemente de la geometría del sistema.

- Se ha generalizado la aplicación de la transformada de Kirchhoff para abordar la presencia de términos no lineales en los parámetros difusivos.

- Finalmente, y utilizando como base los resultados presentados anteriormente, se ha desarrollado una lógica de control robusto capaz de llevar la dinámica de un sistema RDC a la trayectoria de referencia deseada. Como principales puntos de dicho desarrollo caben destacar:

  - Se ha presentado la teoría de rediseño de Lyapunov y se ha extendido a sistemas distribuidos mediante la utilización de los MOR. La idea básica es hacer que los modos representativos (que en general son pocos) sigan la trayectoria de referencia mientras se estabiliza el resto.

- Se ha propuesto una lógica de control robusto que funciona cuando se dispone de un número finito de actuadores. En este sentido, se ha visto que el número mínimo de los mismos que aseguran la controlabilidad del sistema coincide con el número de modos necesarios para representar la referencia. Además se ha desarrollado la metodología que permite hallar la distribución espacial de los controladores que produce el menor esfuerzo de control.
- Se ha estudiado la problemática de la selección de cotas demasiado conservadoras en los términos con incerteza y se ha visto que dichas cotas pueden conducir a controles demasiado bruscos provocando el fenómeno de *chattering*. Por otra parte se ha mostrado que, en lo que se refiere a la construcción de la lógica de control, la selección de una función de Lyapunov que recoja la no linealidad del sistema puede ayudar a obtener acciones de control más suaves.
- Se ha hecho uso de la termodinámica como una de las bases para las pruebas de estabilidad tanto de las leyes de control como de los MOR.

La segunda parte de la memoria se ha centrado en la aplicación de las técnicas desarrolladas en la teoría a sistemas de interés en ámbitos tan dispares como la biología o la ingeniería química.

Trabajo Futuro

- El método de control robusto propuesto requiere tomar medidas del campo en todos los puntos del dominio espacial. Además, el número de controladores resultantes, aún después de haber aplicado MOR, sigue siendo demasiado grande en aplicaciones 2D y 3D. En este sentido, la línea de investigación que se propone (y que ya se está empezando a estudiar) es la utilización de observadores robustos que permitan, por una parte, recuperar el campo mediante un número pequeño de medidas y, por otra parte, reducir la dimensión de los MOR sin que se vea afectada su capacidad para reproducir el comportamiento real del sistema.

- Como se ha mencionado anteriormente, la principal desventaja del método DOP es su rango de validez. Para solventar dicho inconveniente, en el grupo de ingeniería de procesos (IIM-CSIC) se está trabajando en una sistemática para la actualización en línea de las autofunciones.

- En general las acciones de control no pueden ser arbitrariamente grandes lo que puede afectar a la controlabilidad del sistema. Se estudiará el rango de perturbaciones admisibles en el sistema para las cuales las acciones de control posibles aseguran su estabilidad además de la selección de funciones de Lyapunov que recojan la no linealidad del sistema.

Appendix A

Further Notions

A.1 Definitions and Theorems

Theorem A.1 (Reynolds Theorem) *Consider an arbitrary function $f : \mathscr{V} \rightarrow \mathbb{R}$. The Lagrangian time derivative of the spatial integral of f can be written as:*

$$\frac{D}{Dt}\int_{\mathscr{V}} f d\xi = \int_{\mathscr{V}} \frac{\partial f}{\partial t} d\xi + \int_{\mathscr{B}} f \overrightarrow{\mathbf{v}} \cdot \overrightarrow{\mathbf{n}} d\xi = \int_{\mathscr{V}} \frac{\partial f}{\partial t} d\xi + \int_{\mathscr{V}} \overrightarrow{\boldsymbol{\nabla}} \cdot (f \overrightarrow{\mathbf{v}}) d\xi$$

where $\mathscr{B}$ is the boundary.

The following Theorem was obtained from (Nocedal and Wright, 1999):

Theorem A.2 (Taylor's Theorem) *Consider that a given function $f : \mathbb{R}^n \rightarrow \mathbb{R}$ is twice differentiable and consider that $\mathbf{z}, \mathbf{z}^* \in \mathbb{R}^n$. Then we have that:*

$$\frac{\partial f(\mathbf{z})}{\partial \mathbf{z}} - \frac{\partial f(\mathbf{z}^*)}{\partial \mathbf{z}} = \int_0^1 \left(\mathbf{M}\mathbf{z} - \mathbf{M}\mathbf{z}^*\right) d\varepsilon,$$

where $\mathbf{M}$ is a matrix with elements:

$$M_{ij} = \frac{\partial f(\mathbf{z}^* + \varepsilon(\mathbf{z} - \mathbf{z}^*))}{\partial z_i \partial z_j}$$

Theorem A.3 (Gauss or Divergence Theorem) *Consider a continuously differentiable vector field $\overrightarrow{\mathbf{v}} \in \mathbb{R}^m$ $(m = 1, 2, 3)$ defined on neighbourhood of the volume $\mathscr{V} \subset \mathbb{R}^m$ with smooth boundary $\mathscr{B}$, then*

$$\int_{\mathscr{B}} \mathbf{u} \cdot \overrightarrow{\mathbf{n}} d\boldsymbol{\xi} = \int_{\mathscr{V}} \overrightarrow{\boldsymbol{\nabla}} \cdot \mathbf{u} d\boldsymbol{\xi}$$

where $\overrightarrow{\mathbf{n}} \in \mathbb{R}^m$ is a unitary vector pointing outwards the boundary.

Definition A.1 (Green's first identity) *This identity is derived from the Gauss theorem:*

$$\int_{\mathscr{V}} \psi \overrightarrow{\boldsymbol{\nabla}} \cdot \left(k \overrightarrow{\boldsymbol{\nabla}} z \right) d\boldsymbol{\xi} = \int_{\mathscr{B}} \psi \overrightarrow{\mathbf{n}} \cdot k \overrightarrow{\boldsymbol{\nabla}} z d\boldsymbol{\xi} - \int_{\mathscr{V}} \overrightarrow{\boldsymbol{\nabla}} \psi \cdot \left(k \overrightarrow{\boldsymbol{\nabla}} z \right) d\boldsymbol{\xi},$$

Definition A.2 (Lyapunov function) *Consider system (1.28) where the space of the states* ($\mathbf{z}$) *is denoted by* $\mathscr{Z}$. *A given function* $\mathcal{B}(\mathbf{z}) : \mathscr{Z} \to \mathbb{R}$ *is said to be a* Lyapunov function *for the system (1.28) if, in a ball* $B(R)$, $\mathcal{B}(\mathbf{z})$ *follows the conditions: it is positive definite for* $\mathbf{z} \neq 0$*; it has continuous partial derivatives; and its time derivative along the state trajectory of system (1.28) is negative semi-definite.*

Definition A.3 *A continuous function* $f : [0, r) \to [0, \infty)$ *is said to belong to class* $\mathcal{K}$ *if it is strictly increasing and* $f(0) = 0$. *Furthermore, if* $r = \infty$ *and* $f(a) \to \infty$ *as* $a \to \infty$, *then* f *is said to belong to class* $\mathcal{K}_\infty$.

Definition A.4 *A continuous function* $f : [0, r) \times [0, \infty) \to [0, \infty)$ *is said to belong to class* $\mathcal{KL}$ *if, for each fixed* b, *the mapping* $f(a, b)$ *belongs to class* $\mathcal{K}$ *with respect to* a *and, for each fixed* b, *the mapping* $f(a, b)$ *is decreasing with respect to* b *and* $f(a, b) \to 0$ *as* $b \to \infty$.

A.2 Alternative development of the state equations

In most of processes the fundamental quantities (FQ) - mass, energy and momentum - cannot be directly measured. The models of these processes should be then based on other measurable variables (temperature, concentration, pressure, etc.), which can be appropriately combined to recovery the FQ (Stephanopoulos, 1984). Such measurable variables are known as the *states* of the process. The balances of the FQ are of the form:

$$\begin{pmatrix}\text{Rate of accumulation of FQ within the system}\end{pmatrix} + \begin{pmatrix}\text{Outlet flow of FQ}\end{pmatrix} = \begin{pmatrix}\text{Inlet flow of FQ}\end{pmatrix} + \begin{pmatrix}\text{Forces acting on the system}\end{pmatrix}. \quad \text{(A.1)}$$

The first term of the left hand side (LHS) relates to the variation of FQ accumulated with the time while the last term of the right hand side (RHS) is related with the forces that actuate over the system (for instance, gravity, reaction terms). The model is completed with the boundary conditions which establish the rate of FQ transfer with the surrounding media. Next, the general explicit form of a model will be derived from the momentum, energy and mass balances. To that purpose, consider a process on a

volume element ($\delta\xi_1\delta\xi_2\delta\xi_3$) where a given fluid moves on an arbitrary direction through the faces of such element. Figure A.1 represents the volume element ($\mathscr{V}$) with z_{ξ_1} being the component ξ_1 of the field $\mathbf{z}^1$ and $\boldsymbol{\sigma}$ is flux density. The states of the model will be

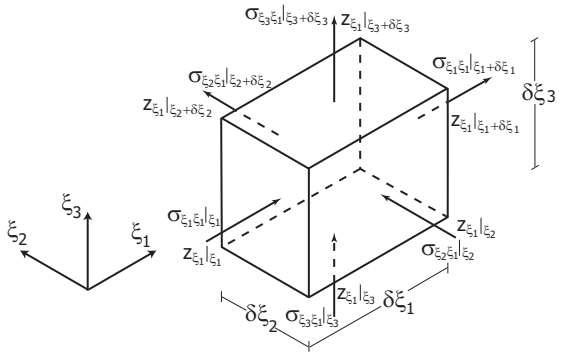

Figure A.1: Volume element $\delta\xi_1\ \delta\xi_2\ \delta\xi_3$. The arrows indicate the direction in which the component z_{ξ_1} is transported.

the fluid velocity vector ($\overrightarrow{\mathbf{v}}$) for the momentum balance, the temperature (T) for the energy balance and the concentration (c) for the mass balance.

A.2.1 Momentum Balance

The rate of accumulation of momentum over $\mathscr{V}$ and on the time interval δt is given by:

$$\delta\xi_1\delta\xi_2\delta\xi_3\frac{\rho v_{\xi_1}|_{t+\delta t} - \rho v_{\xi_1}|_t}{\delta t}.$$

On the other hand, the rate of momentum that enters on the system by means of convection (due to the fluid velocity) and molecular transport (due to velocity gradients) from the face placed on ξ_1 is given by

$$\delta\xi_2\delta\xi_3\left(\alpha\rho v_{\xi_1}\ v_{\xi_1}|_{\xi_1} + \sigma_{\xi_1\xi_1}|_{\xi_1}\right),$$

where the tensor of flux density $\boldsymbol{\sigma}$ when referred to the momentum is usually denoted by $\boldsymbol{\tau}$. Each component $\tau_{\xi_i\xi_j}$ $(i \neq j)$ of $\boldsymbol{\tau}$ is the tangential effort acting over the face ξ_i on the direction ξ_j while $\tau_{\xi_i\xi_i}$ is the normal effort that acts over the face ξ_i. With this new notation, the rate of momentum that enters from the face ξ_1 becomes:

$$\delta\xi_2\delta\xi_3\left(\alpha\rho v_{\xi_1}\ v_{\xi_1}|_{\xi_1} + \tau_{\xi_1\xi_1}|_{\xi_1}\right).$$

[1]Note that if the fundamental quantity is a scalar, the associated field is also a scalar and it will be denoted by z

The rate of momentum that leaves (convection and molecular transport) the system from the face placed on $\xi_1 + \delta\xi_1$ is given by:

$$\delta\xi_2\delta\xi_3 \left(\alpha\rho v_{\xi_1}\, v_{\xi_1}|_{\xi_1+\delta\xi_1} + \tau_{\xi_1\xi_1}|_{\xi_1+\delta\xi_1} \right).$$

The same applies to the remaining faces where the fluid enters and leaves. The pressure forces are computed in the term *forces acting on the system*. In this regard, this term is split into two parts: the pressure forces and the other, like gravity or chemical reactions, represented by $\overrightarrow{\mathbf{f}}(\mathbf{z}) = [f_{\xi_1}, f_{\xi_2}, f_{\xi_3}]^T$. Thus, on the ξ_1 direction, we have $\delta\xi_1\delta\xi_2\delta\xi_3(f_{\xi_1} + (p|_{\xi_1} - p|_{\xi_1+\delta\xi_1})/\delta\xi_1)$. Introducing the transport terms for all the faces, the accumulation term and the other forces into Eqn (A.1), the following expression is obtained after dividing by $\delta\xi_1\delta\xi_2\delta\xi_3$:

$$\frac{\rho v_{\xi_1}|_{t+\delta t} - \rho v_{\xi_1}|_t}{\delta t} + \frac{\rho v_{\xi_1}\, v_{\xi_1}|_{\xi_1+\delta\xi_1} - \rho v_{\xi_1}\, v_{\xi_1}|_{\xi_1}}{\delta\xi_1} + \frac{\rho v_{\xi_2}\, v_{\xi_1}|_{\xi_2+\delta\xi_2} - \rho v_{\xi_2}\, v_{\xi_1}|_{\xi_2}}{\delta\xi_2} +$$

$$\frac{\rho v_{\xi_3}\, v_{\xi_1}|_{\xi_3+\delta\xi_3} - \rho v_{\xi_3}\, v_{\xi_1}|_{\xi_3}}{\delta\xi_3} = \frac{\tau_{\xi_1\xi_1}|_{\xi_1} - \tau_{\xi_1\xi_1}|_{\xi_1+\delta\xi_1}}{\delta\xi_1} + \frac{\tau_{\xi_2\xi_1}|_{\xi_2} - \tau_{\xi_2\xi_1}|_{\xi_2+\delta\xi_2}}{\delta\xi_2}$$

$$+ \frac{\tau_{\xi_3\xi_1}|_{\xi_3} - \tau_{\xi_3\xi_1}|_{\xi_3+\delta\xi_3}}{\delta\xi_3} + f_{\xi_1} - \frac{p|_{\xi_1+\delta\xi_1} - p|_{\xi_1}}{\delta\xi_1},$$

letting $\delta t, \delta\xi_1, \delta\xi_2, \delta\xi_3 \to 0$,

$$\frac{\partial(\rho v_{\xi_1})}{\partial t} + \left(\frac{\partial(\rho v_{\xi_1} v_{\xi_1})}{\partial\xi_1} + \frac{\partial(\rho v_{\xi_2} v_{\xi_1})}{\partial\xi_2} + \frac{\partial(\rho v_{\xi_3} v_{\xi_1})}{\partial\xi_3} \right) =$$

$$- \left(\frac{\partial\tau_{\xi_1\xi_1}}{\partial\xi_1} + \frac{\partial\tau_{\xi_2\xi_1}}{\partial\xi_2} + \frac{\partial\tau_{\xi_3\xi_1}}{\partial\xi_3} \right) + f_{\xi_1} - \frac{\partial p}{\partial\xi_1}. \tag{A.2}$$

Similarly, the expressions for the ξ_2 and ξ_3 momentum components are derived:

$$\frac{\partial(\rho v_{\xi_2})}{\partial t} + \left(\frac{\partial(\rho v_{\xi_1} v_{\xi_2})}{\partial\xi_1} + \frac{\partial(\rho v_{\xi_2} v_{\xi_2})}{\partial\xi_2} + \frac{\partial(\rho v_{\xi_3} z_{\xi_2})}{\partial\xi_3} \right) =$$

$$- \left(\frac{\partial\tau_{\xi_1\xi_2}}{\partial\xi_1} + \frac{\partial\tau_{\xi_2\xi_2}}{\partial\xi_2} + \frac{\partial\tau_{\xi_3\xi_2}}{\partial\xi_3} \right) + f_{\xi_2} - \frac{\partial p}{\partial\xi_2}, \tag{A.3}$$

$$\frac{\partial(\rho v_{\xi_3})}{\partial t} + \left(\frac{\partial(\rho v_{\xi_1} v_{\xi_3})}{\partial\xi_1} + \frac{\partial(\rho v_{\xi_2} v_{\xi_3})}{\partial\xi_2} + \frac{\partial(\rho v_{\xi_3} v_{\xi_3})}{\partial\xi_3} \right) =$$

$$- \left(\frac{\partial\tau_{\xi_1\xi_3}}{\partial\xi_1} + \frac{\partial\tau_{\xi_2\xi_3}}{\partial\xi_2} + \frac{\partial\tau_{\xi_3\xi_3}}{\partial\xi_3} \right) + f_{\xi_3} - \frac{\partial p}{\partial\xi_3}. \tag{A.4}$$

Combining expressions (A.2), (A.3) and (A.4), results

$$\frac{\partial(\rho\overrightarrow{\mathbf{v}})}{\partial t} + \overrightarrow{\boldsymbol{\nabla}}\cdot(\rho\overrightarrow{\mathbf{v}}\,\overrightarrow{\mathbf{v}}) = -\overrightarrow{\boldsymbol{\nabla}}\cdot\boldsymbol{\tau} + \overrightarrow{\mathbf{f}} - \overrightarrow{\boldsymbol{\nabla}}p. \tag{A.5}$$

This equation is the same as that derived in Chapter 1 -see Eqn (1.8)-. For Newtonian fluids, the components of the flux density obey the Newton's law of viscosity[2]:

$$\tau_{\xi_i\xi_j} = -\mu \frac{\partial v_{\xi_j}}{\partial \xi_i}.$$

Next, the same procedure will be employed to construct the energy and mass balances. In Figure A.1 the field $\mathbf{z}$ was a vector and the flux density $\boldsymbol{\sigma}$ a tensor. Since the energy and the mass are scalar quantities, in what follows z will be a scalar quantity while the flux density $\boldsymbol{\sigma}$ will be a vector.

A.2.2 Energy Balance

The *total energy* (e) of a given system is the summation of the *potential energy* (ψ), the *internal energy* (u) and the *kinetic energy* ($\frac{1}{2}v^2$). The potential energy can be included in the term defined as *forces that actuate over the system* of Eqn (A.1) (Bird et al., 2002). In this way, the rate of accumulation of internal and kinetic energy on $V = \delta\xi_1\delta\xi_2\delta\xi_3$ is given by

$$\delta\xi_1\delta\xi_2\delta\xi_3 \frac{\rho u\big|_{t+\delta t} + \frac{1}{2}\rho v^2\big|_{t+\delta t} - \rho u\big|_t - \frac{1}{2}\rho v^2\big|_t}{\delta t}.$$

On the face ξ_1 the convective and conductive inlet flow of internal and kinetic energy is given by:

$$\delta\xi_2\delta\xi_3 \left(v_{\xi_1}\rho u\big|_{\xi_1} + \frac{1}{2}\,\rho v^2\big|_{\xi_1} + q_{\xi_1}\big|_{\xi_1} \right).$$

In the previous expression the notation for the flux density $\boldsymbol{\sigma}$ was replaced by $\overrightarrow{\mathbf{q}}$ which corresponds with the standard notation for the heat flux density. The flow of internal and kinetic energy that leaves the system from the face $\xi_1 + \delta\xi_1$ by means of convection and conduction (due to gradients of energy) is:

$$\delta\xi_2\delta\xi_3 \left(v_{\xi_1}\rho u\big|_{\xi_1+\delta\xi_1} + \frac{1}{2}\,\rho v^2\big|_{\xi_1+\delta\xi_1} + q_{\xi_1}\big|_{\xi_1+\delta\xi_1} \right).$$

As in the momentum balance case, the forces that actuate over the system on the ξ_1 direction are given by $\delta\xi_1\delta\xi_2\delta\xi_3 f_{\xi_1}$. Applying the same procedure to the other faces of $\mathscr{V}$, substituting the result on Eqn (A.1) and dividing by $\delta\xi_1\delta\xi_2\delta\xi_3$, results:

$$\frac{\rho u\big|_{t+\delta t} - \rho u\big|_t}{\delta t} + \frac{\frac{1}{2}\rho v^2\big|_{t+\delta t} - \frac{1}{2}\rho v^2\big|_t}{\delta t} + \frac{v_{\xi_1}\rho u\big|_{\xi_1+\delta\xi_1} - v_{\xi_1}\rho u\big|_{\xi_1}}{\delta\xi_1} + \frac{\frac{1}{2}\,\rho v^2\big|_{\xi_1+\delta\xi_1} - \frac{1}{2}\,\rho v^2\big|_{\xi_1}}{\delta\xi_1} +$$

[2]In complex flux problems, it is necessary to apply other (nonlinear) relations (see Bird et al. (2002))

$$\frac{v_{\xi_2}\rho u|_{\xi_2+\delta\xi_2} - v_{\xi_2}\rho u|_{\xi_2}}{\delta\xi_2} + \frac{\frac{1}{2}\,\rho v^2|_{\xi_2+\delta\xi_2} - \frac{1}{2}\,\rho v^2|_{\xi_2}}{\delta\xi_2} + \frac{v_{\xi_3}\rho u|_{\xi_3+\delta\xi_3} - v_{\xi_3}\rho u|_{\xi_3}}{\delta\xi_3} +$$
$$\frac{\frac{1}{2}\,\rho v^2|_{\xi_3+\delta\xi_3} - \frac{1}{2}\,\rho v^2|_{\xi_3}}{\delta\xi_3} = \frac{q_{\xi_1}|_{\xi_1} - q_{\xi_1}|_{\xi_1+\delta\xi_1}}{\delta\xi_1} + \frac{q_{\xi_2}|_{\xi_2} - q_{\xi_2}|_{\xi_2+\delta\xi_2}}{\delta\xi_2} + \frac{q_{\xi_3}|_{\xi_3} - q_{\xi_3}|_{\xi_3+\delta\xi_3}}{\delta\xi_3} + f$$

Note that contrary to the momentum balance, the nonlinear term (f) is a scalar. Taking the limit when $\delta\xi_1, \delta\xi_2, \delta\xi_3, \delta t \to 0$ it follows that:

$$\frac{\partial\left[\rho\left(u+\frac{1}{2}v^2\right)\right]}{\partial t} + \frac{\partial\left[v_{\xi_1}\rho\left(u+\frac{1}{2}v^2\right)\right]}{\partial\xi_1} + \frac{\partial\left[v_{\xi_2}\rho\left(u+\frac{1}{2}v^2\right)\right]}{\partial\xi_2} + \frac{\partial\left[v_{\xi_3}\rho\left(u+\frac{1}{2}v^2\right)\right]}{\partial\xi_3} =$$
$$-\frac{\partial q_{\xi_1}}{\partial\xi_1} - \frac{\partial q_{\xi_2}}{\partial\xi_2} - \frac{\partial q_{\xi_3}}{\partial\xi_3} + f,$$

or in a more compact form:

$$\frac{\partial\left[\rho\left(u+\frac{1}{2}v^2\right)\right]}{\partial t} + \overrightarrow{\boldsymbol{\nabla}}\cdot\left[\rho\overrightarrow{\mathbf{v}}\left(u+\frac{1}{2}v^2\right)\right] = -\overrightarrow{\boldsymbol{\nabla}}\cdot\overrightarrow{\mathbf{q}} + f. \tag{A.6}$$

The term f can be divided in several contributions (Bird et al., 2002): the work against the volume forces (for instance gravity, $\rho\,(\overrightarrow{\mathbf{v}}\cdot\overrightarrow{\mathbf{g}})$), the work against surface forces (for instance, viscous and pressure forces, $-\overrightarrow{\boldsymbol{\nabla}}\cdot(p\overrightarrow{\mathbf{v}} + \boldsymbol{\tau}\cdot\overrightarrow{\mathbf{v}}) = \boldsymbol{\Pi}\colon(\overrightarrow{\boldsymbol{\nabla}}\overrightarrow{\mathbf{v}})$), the energy transport by radiation $Q_r = A\varepsilon\Theta(T_1^4 - T_2^4)$, the heat produced by a reaction and the heat added to or removed from the system by external mechanisms.

The same procedure can be applied to obtain the variation of internal energy:

$$\frac{\partial\rho u}{\partial t} + \overrightarrow{\boldsymbol{\nabla}}\cdot(\rho u\overrightarrow{\mathbf{v}}) = -\overrightarrow{\boldsymbol{\nabla}}\cdot\overrightarrow{\mathbf{q}} + f. \tag{A.7}$$

Note that since the pressure and viscous forces were included into the nonlinear terms, Eqn (A.7) is equivalent to that derived in Chapter 1 -see Eqn (1.9)-. The internal energy can be expressed as a function that turns out to be much easier to be measured, *the temperature*:

$$du = \left(\frac{\partial u}{\partial V}\right)_T dV + \left(\frac{\partial u}{\partial T}\right)_V dT = \left[-p + T\left(\frac{\partial p}{\partial T}\right)_V\right] dV + c_V dT,$$

where V is the volume and c_V the specific heat at constant volume. Furthermore, on an isotropic medium, the flux density $\overrightarrow{\mathbf{q}}$ can be expressed as a function of the temperature using the Fourier's law:

$$\overrightarrow{\mathbf{q}} = -k\overrightarrow{\boldsymbol{\nabla}}T$$

Introducing the previous expressions on Eqn (A.7) and using again the continuity equation, results:

$$\rho c_V\frac{\partial T}{\partial t} + \rho c_V\overrightarrow{\boldsymbol{\nabla}}\cdot(\overrightarrow{\mathbf{v}}T) = \overrightarrow{\boldsymbol{\nabla}}\cdot\left(k\overrightarrow{\boldsymbol{\nabla}}T\right) - f. \tag{A.8}$$

A.2.3 Mass Balance

The velocity of the component i with respect to steady coordinates will be denoted by $\overrightarrow{\mathbf{v}}_i$ while the mean velocity of mass for a mixture of s components is defined as:

$$\overrightarrow{\mathbf{v}} = \frac{\sum_{j=1}^{s} c_j \overrightarrow{\mathbf{v}}_j}{\sum_{j=1}^{s} c_j} = \frac{\sum_{j=1}^{s} c_j \overrightarrow{\mathbf{v}}_j}{\rho}; \quad \rho_j = \rho c_j,$$

where ρ is the density of the mixture and c_j the mass concentration of the component j. This velocity coincides with the fluid velocity employed in the momentum and energy balances.

The rate of accumulation of mass for the component i on $V = \delta\xi_1\delta\xi_2\delta\xi_3$ is given by

$$\delta\xi_1\delta\xi_2\delta\xi_3 \frac{\rho_i|_{t+\delta t} - \rho_i|_t}{\delta t}.$$

On face ξ_1 (see Figure A.1) the inlet mass flow of a component i of the mixture is

$$\delta\xi_2\delta\xi_3 \; \rho_i v_{i\xi_1}|_{\xi_1} \, ,$$

A new mass flux density vector $\overrightarrow{\mathbf{j}}_i$ can be defined by employing the mean mass velocity $\overrightarrow{\mathbf{v}}$, so that:

$$\overrightarrow{\mathbf{j}}_i = \rho c_i(\overrightarrow{\mathbf{v}}_i - \overrightarrow{\mathbf{v}}) = \rho_i \overrightarrow{\mathbf{w}}_i,$$

so the inlet mass flow of component i from the face ξ_1 can be expressed as

$$\delta\xi_2\delta\xi_3 \left(j_{i\xi_1}|_{\xi_1} + \rho_i \; v_{\xi_1}|_{\xi_1} \right).$$

The outlet mass flow of the component i on the face $\xi_1 + \delta\xi_1$ is

$$\delta\xi_2\delta\xi_3 \left(j_{i\xi_1}|_{\xi_1+\delta\xi_1} + \rho_i \; v_{\xi_1}|_{\xi_1+\delta\xi_1} \right).$$

Computing the inlet and outlet flows on the remaining faces, introducing them in Eqn (A.1) and dividing the result by $\delta\xi_1\delta\xi_2\delta\xi_3$, leads to:

$$\frac{\rho_i|_{t+\delta t} - \rho_i|_t}{\delta t} + \left(\frac{\rho_i v_{\xi_1}|_{\xi_1+\delta\xi_1} - \rho_i \; v_{\xi_1}|_{\xi_1}}{\delta\xi_1} + \frac{\rho_i v_{\xi_2}|_{\xi_2+\delta\xi_2} - \rho_i v_{\xi_2}|_{\xi_2}}{\delta\xi_2} + \frac{\rho_i v_{\xi_3}|_{\xi_3+\delta\xi_3} - \rho_i v_{\xi_3}|_{\xi_3}}{\delta\xi_3} \right) =$$

$$\left(\frac{j_{i\xi_1}|_{\xi_1} - j_{i\xi_1}|_{\xi_1+\delta\xi_1}}{\delta\xi_1} + \frac{j_{i\xi_2}|_{\xi_2} - j_{i\xi_2}|_{\xi_2+\delta\xi_2}}{\delta\xi_2} + \frac{j_{i\xi_3}|_{\xi_3} - j_{i\xi_3}|_{\xi_3+\delta\xi_3}}{\delta\xi_3} \right) + \rho r_i,$$

where r_i is the rate of production/consumption of the component i. Taking the limit when $\delta t, \delta\xi_1, \delta\xi_2, \delta\xi_3 \to 0$, previous equation now reads:

$$\frac{\partial \rho c_i}{\partial t} + \overrightarrow{\boldsymbol{\nabla}} \cdot (\rho c_i \overrightarrow{\mathbf{v}}) = -\overrightarrow{\boldsymbol{\nabla}} \cdot \overrightarrow{\mathbf{j}}_i + \rho r_i. \tag{A.9}$$

Again, this equation is the same as the one derived in Chapter 1 -see Eqn (1.13)-. Fick's law establishes the relationship between the mass flux density vector $\overrightarrow{\mathbf{j}}_i$ and the gradient of concentration to be of the form:

$$\overrightarrow{\mathbf{j}}_i = -D_i \overrightarrow{\boldsymbol{\nabla}} c_i,$$

with D_i being the binary diffusivity for the component i in the mixture. Introducing the Fick's law on Eqn (A.9), it results

$$\frac{\partial c_i}{\partial t} + \overrightarrow{\boldsymbol{\nabla}} \cdot (c_i \overrightarrow{\mathbf{v}}) = \overrightarrow{\boldsymbol{\nabla}} \cdot \left(D_i \overrightarrow{\boldsymbol{\nabla}} c_i \right) + r_i. \tag{A.10}$$

The description of the system must be completed with the FQ transfer between the system and its surroundings which is introduced through the boundary conditions (BC). The general form of the BC correspond with the Robin BC, which for vectorial and scalar fields is:

$$\overrightarrow{\mathbf{n}} \cdot \overrightarrow{\boldsymbol{\nabla}} \mathbf{z} = -\mathbf{H}\mathbf{z} + \mathbf{G}\mathbf{z}^*, \qquad \overrightarrow{\mathbf{n}} \cdot \overrightarrow{\boldsymbol{\nabla}} z = -hz + gz^*. \tag{A.11}$$

where $\mathbf{H}$ is a matrix containing the transfer coefficients and $\mathbf{z}^*$ is the value of $\mathbf{z}$ on the surrounding media. Note that the Neumann BC can be obtained by fixing the transfer coefficients to zero. If the transfer coefficients have large values, BC (A.11) can be considered as an approximation to the Dirichlet BC.

A.3 Initial Value Problem Solvers

The numerical methods for solving PDEs described in Chapters 2 and 3 transform the original PDE into a set of ODEs or initial value problems (IVP) of the form:

$$\frac{d\mathbf{Z}}{dt} = \mathbf{f}(\mathbf{Z}, t); \quad \text{with} \quad \mathbf{Z}(0) = \mathbf{Z}_0. \tag{A.12}$$

In this section a brief description of the numerical solvers for first order IVPs is presented. We restrict to first order since the result of applying any of the methods described in Chapters 2 and 3 to RDC systems is a first order IVP. For a detailed description of initial value problem solvers see, for instance, Silebi and Schiesser (1992); Zill (1997); Ascher and Petzold (1998); Quarteroni et al. (2000) and references therein.

Essentially, the numerical techniques to solve IVPs are based on the discretisation of the time domain and the solution ($\mathbf{Z}$) at a given time (t_i) is approximated, using a Taylor series expansion, by a function of the solution at previous times:

$$\mathbf{Z}_i = \mathbf{g}(\mathbf{Z}_{i-1}, \mathbf{Z}_{i-2}, ...).$$

Although there exist a great deal of different algorithms for solving ODEs, roughly speaking, all of them fall in two categories: *explicit* and *implicit* methods.

A.3.1 Explicit Methods

The simplest technique for solving IVPs is the **Euler explicit** which employs first order Taylor series. The disadvantages of this approach are the slow convergence rate and the small stability region, i.e. the application of this techniques may result into very small step sizes. In order to improve the convergence rate of the Euler method, higher order series expansions can be employed. The techniques that use higher order expansions are known as **Runge-Kutta** methods. Furthermore, the stability of this family of methods can be improved by using variable step size in the expansion (**Adaptive Runge-Kutta**). Finally, it should be remarked that the techniques just mentioned only employ the value of $\mathbf{Z}$ at time t_{i-1}. The precision of the explicit methods can be improved by using information of of $\mathbf{Z}$ at other past times (t_{i-2}, t_{i-3},...). Among these techniques, one of the most employed is the **Adams** method.

In problems with a large time scale separation among states (*stiff problems*), the explicit methods in general are unstable. For this kind of problems the implicit methods, described below, are required.

A.3.2 Implicit Methods

In this case the solution Z at time (t_i) is expressed as:

$$\mathbf{Z}_i = \mathbf{g}(\mathbf{Z}_i, \mathbf{Z}_{i-1}, \mathbf{Z}_{i-2}, ...).$$

Note that now the function $\mathbf{g}$ includes the term $\mathbf{Z}_i$ which implies to solve a nonlinear system. The explicit methods described above have their equivalent implicit version. Apart from the Euler or the Runge-Kutta implicit, one of the most popular implicit methods is the **backward differentiation formula** (BDF) which is nothing else than a generalisation of the Euler implicit. Although there exist techniques for improving the efficiency of the implicit methods, as for instance taking advantage of the Jacobian structure or the sparsity of the resulting matrices, these family of methods are computationally involved as compared with the explicit methods. Therefore, when possible (low stiff problems), a explicit method is preferable.

A.4 The Hodgkin-Huxley Model

Hodgkin et al. (1949) carried out several experiments in the axon of the giant squid to study the initialisation and propagation of the action potential (Keener and Sneyd, 1998). After two years analysing the experimental data, which were published in

Hodgkin and Huxley (1952a), the authors proposed that the membrane of the axon was permeable to certain ions (K^+, Na^+,...) and the permeability depended on the voltage (Hodgkin and Huxley, 1952b). In the same article, they also proposed a model for describing the excitable feature of the axon. In such model, two different contributions to the membrane current (I)[3] were considered. On the one hand, the current generated by individual ions passing through the membrane and, on the other hand, the transmembrane potential, i.e., the contribution of the membrane capacitance. Therefore a basic model for a cellular membrane can be the model of a capacitor and a resistor in parallel:

$$CV_t = -\frac{V - V_{eq}}{R} + I_a, \tag{A.13}$$

where C and R are the membrane capacitance and resistance, respectively, V_{eq} indicates the equilibrium potential between the internal and external membrane surfaces. Finally I_a represents the applied current.

The model proposed by Hodgkin and Huxley has the following form:

$$I_a = I_{Na} + I_K + I_L = g_{Na}m^3h(V - V_{Na}) + g_K n^4(V - V_K) + g_L(V - V_L) \tag{A.14}$$

with I_{Na}, I_K being, respectively, the sodium and potassium currents. I_L represents the trickle current which is related with the other ions, V_{Na}, V_K and V_L are constant equilibrium potential, g_{Na}, g_K and g_L represent constant conductances. Finally, the terms $m, n, h \in [0, 1]$ are variables computed through the following ODEs:

$$m_t = \alpha_m(V)(1 - m) - \beta_m(V)m, \tag{A.15}$$

$$n_t = \alpha_n(V)(1 - n) - \beta_n(V)n, \tag{A.16}$$

$$h_t = \alpha_h(V)(1 - h) - \beta_h(V)h, \tag{A.17}$$

where $\alpha_x(V)$ and $\beta_x(V)$, with $x = m, n, h$, are computed empirically. If a given current $I_a(t)$ is applied and Eqn (A.14) in substituted into Eqn (A.13) the following relation is obtained:

$$CV_t = -g_{Na}m^3h(V - V_{Na}) - g_K n^4(V - V_K) - g_L(V - V_L) + I_a. \tag{A.18}$$

The Hodgkin-Huxley model is the combination of Eqns (A.15)-(A.18). The structure of this model provides the base for almost all systems with excitable membrane behaviour. When $I_a = 0$, the rest state is stable but excitable. Therefore, a sufficiently large perturbation produce a long migration of the system variables before returning to the rest state. Furthermore there is a range of values in which the mechanism describe characteristic limit cycles which have been observed experimentally.

[3]The positive direction of I is the axon output

Appendix B

Proofs of the results

B.1 Proof of Lemma 3.1

The proof begins with the time derivative of $b(\mathbf{z};\mathbf{z}^*)$, which combined with Eqns (1.40) and (1.41) leads to:

$$\dot{b} = \frac{db}{d\overline{\mathbf{z}}}\frac{\partial \overline{\mathbf{z}}}{\partial t} = \overline{\mathbf{A}}^T \Delta\overline{\mathbf{\Gamma}} - \overline{\mathbf{A}}^T \overrightarrow{\overline{\mathbf{\nabla}}} \cdot (\overrightarrow{\overline{\mathbf{v}}}\,\overline{\mathbf{z}}) - \ell_\mu + \mu \overline{\mathbf{A}}^T \overline{\mathbf{A}} + \overline{\mathbf{A}}^T \overline{\mathbf{u}}, \tag{B.1}$$

note that $\overline{\mathbf{A}}$ is defined from the convex function b as $\overline{\mathbf{A}}^T = \frac{\partial b}{\partial \overline{\mathbf{z}}}$. Choosing the output and the input as indicated in Lemma 3.1, integrating expression (B.1) over the spatial domain and denoting $\mathcal{B} = \int_{\mathscr{V}} b(\mathbf{z};\mathbf{z}^*)d\xi$ and $L_\mu = \int_{\mathscr{V}} \ell_\mu(\mathbf{z};\mathbf{z}^*)d\boldsymbol{\xi}$, results:

$$\dot{\mathcal{B}} = \langle \overline{\mathbf{A}}, \Delta\overline{\mathbf{\Gamma}}\rangle_{\mathscr{V}} - \langle \overline{\mathbf{A}}, \overrightarrow{\overline{\mathbf{\nabla}}} \cdot (\overrightarrow{\overline{\mathbf{v}}}\,\overline{\mathbf{z}})\rangle_{\mathscr{V}} - L_\mu + \langle y, \mathbf{u}\rangle_{\mathscr{V}}. \tag{B.2}$$

Applying the Green's formula to the first term of the right hand side (RHS) of equation (B.2):

$$\langle \overline{\mathbf{A}}, \Delta\overline{\mathbf{\Gamma}}\rangle_{\mathscr{V}} = \int_{\mathscr{B}} \overline{\mathbf{A}}^T \mathbf{L}(\mathbf{A}) \left(\overline{\mathbf{n}} \cdot \overrightarrow{\overline{\mathbf{\nabla}}}\overline{\mathbf{A}}\right) d\boldsymbol{\xi} - \langle \overrightarrow{\overline{\mathbf{\nabla}}}\overline{\mathbf{A}}, \mathbf{L}(\mathbf{A})\overrightarrow{\overline{\mathbf{\nabla}}}\overline{\mathbf{A}}\rangle_{\mathscr{V}},$$

due to boundary conditions (1.42) and (1.43) the first term of the RHS is non positive. Since $\mathbf{L}(\mathbf{A})$ is positive definite the second term of the RHS is non negative then $\langle \overline{\mathbf{A}}, \Delta\overline{\mathbf{\Gamma}}\rangle_{\mathscr{V}} \leq 0$. Consider now the second term of the RHS of Eqn (B.2) with the velocity term $\overrightarrow{\overline{\mathbf{v}}}$ constant:

$$-\langle \overline{\mathbf{A}}, \overrightarrow{\overline{\mathbf{\nabla}}} \cdot (\overrightarrow{\overline{\mathbf{v}}}\,\overline{\mathbf{z}})\rangle_{\mathscr{V}} = -\int_{\mathscr{V}} \frac{\partial b}{\partial \overline{\mathbf{z}}} \overrightarrow{\overline{\mathbf{\nabla}}} \cdot (\overrightarrow{\overline{\mathbf{v}}}\,\overline{\mathbf{z}}) d\boldsymbol{\xi} = -\int_{\mathscr{V}} \overrightarrow{\overline{\mathbf{\nabla}}} \cdot (\overrightarrow{\overline{\mathbf{v}}} b) d\boldsymbol{\xi} = -\int_{\mathscr{B}} \overrightarrow{\overline{\mathbf{v}}} \cdot \overrightarrow{\overline{\mathbf{n}}} b d\boldsymbol{\xi}.$$

In the part of the boundary where the fluid enters it follows that $\mathbf{z} = \mathbf{z}^*$ - see Eqn (1.44)- , so according to Eqn (1.30) $b|_{\mathscr{B}_c^-} = 0$. In addition, in $\mathscr{B}_c^+$ it follows that $\overrightarrow{\mathbf{v}} \cdot \overrightarrow{\mathbf{n}} \geq 0$ and since $b(\mathbf{z}, \mathbf{z}^*)$ is non negative, one has that:

$$-\int_{\mathscr{B}} \overrightarrow{\mathbf{v}} \cdot \overrightarrow{\mathbf{n}} b d\boldsymbol{\xi} = -\int_{\mathscr{B}_c^+} \overrightarrow{\mathbf{v}} \cdot \overrightarrow{\mathbf{n}} b d\boldsymbol{\xi} \leq 0.$$

Now, from Condition 1.1, there exists a positive constant μ such that $L_\mu > 0$. Then equation (B.2) can be rewritten as:

$$\dot{\mathcal{B}} \leq \langle y, \mathfrak{u} \rangle_{\mathscr{V}}, \tag{B.3}$$

Note that the time integral of (B.3) over the interval $[t, t+T]$ coincides with the relation (3.16) so the system is passive. Finally, time integration of Eqn (B.3) together with the selection of $\mu = 0$ leads to:

$$\mathcal{B}(\overline{\mathbf{z}}(T)) \leq \mathcal{B}(\overline{\mathbf{z}}(0)) - \int_0^T L_0 dt + \int_0^T \langle \overline{\mathbf{A}}, \overline{\mathbf{u}} \rangle_{\mathscr{V}} dt.$$

and the result follows since ℓ_0 (and thus L_0) are positive in ω'.

B.2 Proof of Lemma 3.2

1. The first statement of the Lemma is proved by using the separation property of the field and its dual and the orthonormality of eigenfunctions:

$$\langle \overline{\mathbf{A}}_b, \frac{\partial \overline{\mathbf{z}}}{\partial t} \rangle_{\mathscr{V}} = \langle \sum_{i \in \mathcal{N}_b} \boldsymbol{\alpha}_i \phi_i, \sum_{i \in \mathbb{N}} \frac{d\mathbf{m}_i}{dt} \phi_i \rangle_{\mathscr{V}} = \sum_{i \in \mathcal{N}_b} \boldsymbol{\alpha}_i^T \frac{d\mathbf{m}_i}{dt} \Rightarrow \langle \overline{\mathbf{A}}_b, \frac{\partial \overline{\mathbf{z}}}{\partial t} \rangle_{\mathscr{V}} = \boldsymbol{\alpha}_b^T \frac{d\mathbf{m}_b}{dt}.$$

2. The proof of the second point is more complicated and begins with the expansions of the field $\overline{\mathbf{A}}$ and of the Kirchhoff transform $\overline{\boldsymbol{\Gamma}}$ as in (3.11) and (3.14), respectively:

$$\langle \overline{\mathbf{A}}_b, \Delta \overline{\boldsymbol{\Gamma}} \rangle_{\mathscr{V}} = \langle \sum_{i \in \mathcal{N}_b} \boldsymbol{\alpha}_i \phi_i, \sum_{i \in \mathbb{N}} \boldsymbol{\gamma}_i \Delta \phi_i \rangle_{\mathscr{V}} = \langle \sum_{i \in \mathcal{N}_b} \boldsymbol{\alpha}_i \phi_i, \sum_{i \in \mathbb{N}} -\boldsymbol{\gamma}_i \lambda_i \phi_i \rangle_{\mathscr{V}} =$$

$$\langle \sum_{i \in \mathcal{N}_b} \boldsymbol{\alpha}_i \phi_i, \sum_{i \in \mathcal{N}_b} -\boldsymbol{\gamma}_i \lambda_i \phi_i \rangle_{\mathscr{V}} = \langle \overline{\mathbf{A}}_b, \Delta \overline{\boldsymbol{\Gamma}}_b \rangle_{\mathscr{V}},$$

now, using the divergence theorem one is led to:

$$\int_{\mathscr{V}} \overrightarrow{\boldsymbol{\nabla}} \cdot (\overline{\mathbf{A}}_b^T \overrightarrow{\boldsymbol{\nabla}} \overline{\boldsymbol{\Gamma}}_b) d\boldsymbol{\xi} = \langle \overrightarrow{\boldsymbol{\nabla}} \overline{\mathbf{A}}_b, \overrightarrow{\boldsymbol{\nabla}} \overline{\boldsymbol{\Gamma}}_b \rangle_{\mathscr{V}} + \langle \overline{\mathbf{A}}_b, \Delta \overline{\boldsymbol{\Gamma}}_b \rangle_{\mathscr{V}} \Rightarrow \int_{\mathscr{B}} \overline{\mathbf{A}}_b^T \left(\overline{\mathbf{n}} \cdot \overrightarrow{\boldsymbol{\nabla}} \overline{\boldsymbol{\Gamma}}_b \right) d\boldsymbol{\xi} =$$

$$\langle \overrightarrow{\boldsymbol{\nabla}} \overline{\mathbf{A}}_b, \overrightarrow{\boldsymbol{\nabla}} \overline{\boldsymbol{\Gamma}}_b \rangle_{\mathscr{V}} + \langle \overline{\mathbf{A}}_b, \Delta \overline{\boldsymbol{\Gamma}}_b \rangle_{\mathscr{V}} = \langle \overline{\mathbf{A}}_b, \mathbf{L}(\mathbf{A}) \overrightarrow{\boldsymbol{\nabla}} \overline{\mathbf{A}}_b \rangle_{\mathscr{V}} + \langle \overline{\mathbf{A}}_b, \Delta \overline{\boldsymbol{\Gamma}}_b \rangle_{\mathscr{V}},$$

rearranging the terms and denoting $\zeta = \min_{\overline{\mathbf{A}}}(\inf_i[\lambda_i(\mathbf{L})]) > 0$, it is obtained:

$$\langle \overline{\mathbf{A}}_b, \Delta\overline{\mathbf{\Gamma}}_b\rangle_{\mathscr{V}} \leq \int_{\mathscr{B}} \overline{\mathbf{A}}_b^T \mathbf{L}(\mathbf{A}) \left(\overline{\mathbf{n}} \cdot \overrightarrow{\boldsymbol{\nabla}} \overline{\mathbf{A}}_b\right) d\boldsymbol{\xi} - \zeta \langle \overrightarrow{\boldsymbol{\nabla}} \overline{\mathbf{A}}_b, \overrightarrow{\boldsymbol{\nabla}} \overline{\mathbf{A}}_b\rangle_{\mathscr{V}}. \tag{B.4}$$

On the other hand, it follows that:

$$\zeta \int_{\mathscr{V}} \overrightarrow{\boldsymbol{\nabla}} (\overline{\mathbf{A}}_b^T \overrightarrow{\boldsymbol{\nabla}} \overline{\mathbf{A}}_b) d\boldsymbol{\xi} = \zeta \langle \overrightarrow{\boldsymbol{\nabla}} \overline{\mathbf{A}}_b, \overrightarrow{\boldsymbol{\nabla}} \overline{\mathbf{A}}_b\rangle_{\mathscr{V}} + \zeta \langle \overline{\mathbf{A}}_b, \Delta\overline{\mathbf{A}}_b\rangle_{\mathscr{V}} \Rightarrow$$

$$\zeta \langle \overrightarrow{\boldsymbol{\nabla}} \overline{\mathbf{A}}_b, \overrightarrow{\boldsymbol{\nabla}} \overline{\mathbf{A}}_b\rangle_{\mathscr{V}} = \zeta \int_{\mathscr{B}} \overline{\mathbf{A}}_b^T \left(\overline{\mathbf{n}} \cdot \overrightarrow{\boldsymbol{\nabla}} \overline{\mathbf{A}}_b\right) d\boldsymbol{\xi} - \zeta \langle \overline{\mathbf{A}}_b, \Delta\overline{\mathbf{A}}_b\rangle_{\mathscr{V}}. \tag{B.5}$$

Substituting equation (B.5) on inequality (B.4):

$$\langle \overline{\mathbf{A}}_b, \Delta\overline{\mathbf{\Gamma}}_b\rangle_{\mathscr{V}} \leq \int_{\mathscr{B}} \overline{\mathbf{A}}_b^T \mathbf{L}(\mathbf{A}) \left(\overline{\mathbf{n}} \cdot \overrightarrow{\boldsymbol{\nabla}} \overline{\mathbf{A}}_b\right) d\boldsymbol{\xi} - \zeta \int_{\mathscr{B}} \overline{\mathbf{A}}_b^T \left(\overline{\mathbf{n}} \cdot \overrightarrow{\boldsymbol{\nabla}} \overline{\mathbf{A}}_b\right) d\boldsymbol{\xi} + \zeta \langle \overline{\mathbf{A}}_b, \Delta\overline{\mathbf{A}}_b\rangle_{\mathscr{V}}.$$

Boundary conditions (1.42)-(1.43) make the term:

$$\int_{\mathscr{B}} \overline{\mathbf{A}}_b^T \mathbf{L}(\mathbf{A}) \left(\overline{\mathbf{n}} \cdot \overrightarrow{\boldsymbol{\nabla}} \overline{\mathbf{A}}_b\right) d\boldsymbol{\xi} - \zeta \int_{\mathscr{B}} \overline{\mathbf{A}}_b^T \left(\overline{\mathbf{n}} \cdot \overrightarrow{\boldsymbol{\nabla}} \overline{\mathbf{A}}_b\right) d\boldsymbol{\xi} \leq 0,$$

then, since the eigenfunctions are orthonormal, one has that:

$$\langle \overline{\mathbf{A}}_b, \Delta\overline{\mathbf{\Gamma}}_b\rangle_{\mathscr{V}} \leq \zeta \langle \overline{\mathbf{A}}_b, \Delta\overline{\mathbf{A}}_b\rangle_{\mathscr{V}} = \zeta \langle \sum_{i\in\mathcal{N}_b} \boldsymbol{\alpha}_i \phi_i, \sum_{i\in\mathcal{N}_b} -\boldsymbol{\alpha}_i \lambda_i \phi_i\rangle_{\mathscr{V}} = -\zeta \boldsymbol{\alpha}_b^T \Lambda_b \boldsymbol{\alpha}_b,$$

where Λ_b is a diagonal matrix containing the eigenvalues of the set $\mathscr{L}_b$. The result follows by choosing λ_ℓ as the minimum eigenvalue of the set $\mathscr{L}_b$.

3. Applying the series expansion to the terms of the third statement of Lemma 3.2, one is led to:

$$-\langle \overline{\mathbf{A}}_b, \overrightarrow{\boldsymbol{\nabla}} \cdot (\overrightarrow{\mathbf{v}}\overline{\mathbf{z}})\rangle_{\mathscr{V}} = -\langle \sum_{i\in\mathcal{N}_b} \boldsymbol{\alpha}_i \phi_i, \overrightarrow{\mathbf{v}} \sum_{i\in\mathbb{N}} \boldsymbol{\tau}_i \phi_i\rangle_{\mathscr{V}} = -\langle \sum_{i\in\mathcal{N}_b} \boldsymbol{\alpha}_i \phi_i, \overrightarrow{\mathbf{v}} \sum_{i\in\mathcal{N}_b} \boldsymbol{\tau}_i \phi_i\rangle_{\mathscr{V}} =$$

$$-\langle \overline{\mathbf{A}}_b, \overrightarrow{\boldsymbol{\nabla}} \cdot (\overrightarrow{\mathbf{v}}\overline{\mathbf{z}}_b)\rangle_{\mathscr{V}}.$$

Now, defining a new convex function b_b of the form of (1.30) for the field $\overline{\mathbf{z}}_b$, the following relations are obtained:

$$\overline{\mathbf{A}}_b^T \overrightarrow{\boldsymbol{\nabla}} \cdot (\overrightarrow{\mathbf{v}}\overline{\mathbf{z}}_b) = \frac{\partial(\overrightarrow{\mathbf{v}} b_b)}{\partial(\overrightarrow{\mathbf{v}}\overline{\mathbf{z}}_b)} \overrightarrow{\boldsymbol{\nabla}} (\overrightarrow{\mathbf{v}}\overline{\mathbf{z}}_b) = \overrightarrow{\boldsymbol{\nabla}} \cdot (\overrightarrow{\mathbf{v}} b_b) \Rightarrow -\langle \overline{\mathbf{A}}_b, \overrightarrow{\boldsymbol{\nabla}} (\overrightarrow{\mathbf{v}}\overline{\mathbf{z}}_b)\rangle_{\mathscr{V}} =$$

$$\int_{\mathscr{V}} \overrightarrow{\boldsymbol{\nabla}} (\overrightarrow{\mathbf{v}} b_b) d\boldsymbol{\xi} = \int_{\mathscr{B}_c^+} \overline{\mathbf{n}} \cdot \overrightarrow{\mathbf{v}} b_b d\boldsymbol{\xi},$$

and the results follows by using the boundary conditions.

4. In the proof of the fourth point use will be made of the integral counterpart of equation (1.41):

$$\langle \overline{\mathbf{A}}, \overline{\mathbf{f}} \rangle_{\mathscr{V}} + L_\mu = \mu \langle \overline{\mathbf{A}}, \overline{\mathbf{A}} \rangle_{\mathscr{V}}. \tag{B.6}$$

On the other hand, making use of the series expansion one has that:

$$\langle \overline{\mathbf{A}}, \overline{\mathbf{f}} \rangle_{\mathscr{V}} = \sum_{i \in \mathbb{N}} \boldsymbol{\alpha}_i^T \boldsymbol{\sigma}_i; \quad \langle \overline{\mathbf{A}}, \overline{\mathbf{A}} \rangle_{\mathscr{V}} = \sum_{i \in \mathbb{N}} \boldsymbol{\alpha}_i^T \boldsymbol{\alpha}_i.$$

Substituting these expressions on Eqn. (B.6), for a given $\mu > 0$, one is led to:

$$\sum_{i \in \mathbb{N}} (\mu \boldsymbol{\alpha}_i^T \boldsymbol{\alpha}_i - \boldsymbol{\alpha}_i^T \boldsymbol{\sigma}_i) = L_\mu \geq 0.$$

In order to this inequality hold for any field satisfying (3.10) it is required that $\mu \boldsymbol{\alpha}_k^T \boldsymbol{\alpha}_k - \boldsymbol{\alpha}_k^T \boldsymbol{\sigma}_k > 0$ for all k. This argument allows us to construct expressions equivalent to (B.6) for each subfield $\overline{\mathbf{A}}_a$ and $\overline{\mathbf{A}}_b$ and for the nonlinear terms $\overline{\mathbf{f}}_a$ and $\overline{\mathbf{f}}_b$. In particular, the following relation holds:

$$\langle \overline{\mathbf{A}}_b, \overline{\mathbf{f}}_b \rangle_{\mathscr{V}} + L_\mu = \mu \langle \overline{\mathbf{A}}_b, \overline{\mathbf{A}}_b \rangle_{\mathscr{V}}.$$

Using Eqn (3.13) and the orthonormality of eigenfunctions it is easy to see that: $\langle \overline{\mathbf{A}}_b, \overline{\mathbf{f}} \rangle_{\mathscr{V}} = \langle \overline{\mathbf{A}}_b, \overline{\mathbf{f}}_b \rangle_{\mathscr{V}}$, so it follows that

$$\langle \overline{\mathbf{A}}_b, \overline{\mathbf{f}} \rangle_{\mathscr{V}} \leq \mu \langle \overline{\mathbf{A}}_b, \overline{\mathbf{A}}_b \rangle_{\mathscr{V}} = \mu \boldsymbol{\alpha}_b^T \boldsymbol{\alpha}_b.$$

B.3 Proof of Proposition 3.1

The projection of system (1.40) over the subfield $\overline{\mathbf{A}}_b$, with $\overline{\mathbf{u}} = 0$, leads to:

$$\langle \overline{\mathbf{A}}_b, \frac{\partial \overline{\mathbf{z}}}{\partial t} \rangle_{\mathscr{V}} = \langle \overline{\mathbf{A}}_b, \Delta \overline{\boldsymbol{\Gamma}} \rangle_{\mathscr{V}} - \langle \overline{\mathbf{A}}_b, \overrightarrow{\boldsymbol{\nabla}} \cdot (\overrightarrow{\boldsymbol{\nabla}} \overline{\mathbf{z}}) \rangle_{\mathscr{V}} + \langle \overline{\mathbf{A}}_b, \overline{\mathbf{f}} \rangle_{\mathscr{V}}. \tag{B.7}$$

Making use of relations (1)-(4) of Lemma 3.2, Eqn. (B.7) can be rewritten as:

$$\boldsymbol{\alpha}_b^T \frac{d\mathbf{m}_b}{dt} \leq (\mu - \zeta \lambda_\ell) \boldsymbol{\alpha}_b^T \boldsymbol{\alpha}_b. \tag{B.8}$$

A new convex function b_b is defined as in Eqn (1.30) for the field $\overline{\mathbf{z}}_b$. The time derivative of b_b yields $\dot{b}_b = \overline{\mathbf{A}}_b^T \frac{\partial \overline{\mathbf{z}}_b}{\partial t}$. Integrating this expression over the spatial domain, results into

$$\int_{\mathscr{V}} \dot{b}_b d\boldsymbol{\xi} = \dot{\mathcal{B}}_b = \langle \overline{\mathbf{A}}_b, \frac{\partial \overline{\mathbf{z}}}{\partial t} \rangle_{\mathscr{V}} = \sum_{i \in \mathcal{N}_b} \boldsymbol{\alpha}_i \frac{d\mathbf{m}_i}{dt} = \boldsymbol{\alpha}_b^T \frac{d\mathbf{m}_b}{dt}. \tag{B.9}$$

On the other hand, that function $\mathcal{B}_b$ is bounded by the field $\overline{\mathbf{z}}_b$ as -see Eqn (1.31)-:

$$q_{0b} \|\overline{\mathbf{z}}_b\|_{\mathscr{V}}^2 \leq \mathcal{B}_b \leq q_{1b} \|\overline{\mathbf{z}}_b\|_{\mathscr{V}}^2 = q_{1b} \mathbf{m}_b^T \mathbf{m}_b,$$

and since $\overline{\mathbf{A}}_b$ relates to $\overline{\mathbf{z}}_b$ through an expression of the form (1.32), we have:

$$\boldsymbol{\alpha}_b^T\boldsymbol{\alpha}_b = \langle\overline{\mathbf{A}}_b, \overline{\mathbf{A}}_b\rangle_{\mathscr{V}} = \langle Q_b\overline{\mathbf{z}}_b, Q_b\overline{\mathbf{z}}_b\rangle_{\mathscr{V}} \geq \delta_0^2\mathbf{m}_b^T\mathbf{m}_b \geq \frac{\delta_{0b}^2}{q_{1b}}\mathcal{B}_b, \tag{B.10}$$

where δ_{0b} is the minimum eigenvalue of Q_b. Substituting (B.9) and (B.10) into (B.8):

$$\dot{\mathcal{B}}_b \leq (\mu - \zeta\lambda_\ell)\frac{\delta_{0b}^2}{q_{1b}}\mathcal{B}_b.$$

Since the eigenvalues have the property that $\lambda_i \to \infty$ as $i \to \infty$, one can always select a number of elements of the set $(\mathscr{E}_a, \mathscr{L}_a, \mathcal{N}_a)$ so that $\lambda_\ell = \max_\lambda \mathscr{L}_a > \mu/\zeta$ and then $(\mu - \zeta\lambda_\ell) < 0$. With this set and by means of the Gronwall-Bellman theorem, it follows that $\mathcal{B}_b$, and thus $\overline{\mathbf{z}}_b$, converge exponentially to zero.

B.4 Proof of Lemma 4.1

1. The steps to be followed in the proof of this statement are similar to those followed in the proof of the second point of Lemma 3.2 for the term $\langle\overline{\mathbf{A}}_b, \Delta\overline{\boldsymbol{\Gamma}}\rangle_{\mathscr{V}}$ so they will not be included in this document.

2. In order to prove the sixth statement use is made of the series expansion:

   $$-\langle\overline{\mathbf{A}}_a, \Delta\boldsymbol{\Gamma}_d\rangle_{\mathscr{V}} = -\langle\sum_{i\in\mathcal{N}_a}\boldsymbol{\alpha}_i\phi_i, \sum_{i\in\mathbb{N}} -\lambda_i\boldsymbol{\gamma}_{di}\phi_i\rangle_{\mathscr{V}} = \sum_{i\in\mathcal{N}_a}\lambda_i\boldsymbol{\alpha}_i^T\boldsymbol{\gamma}_{di} \leq \lambda_q\sum_{i\in\mathcal{N}_a}|\boldsymbol{\alpha}_i|^T|\boldsymbol{\gamma}_{di}|,$$

   where λ_q is the maximum eigenvalue of the set $\mathscr{L}_a$. Finally, using the Hölder inequality one has that:

   $$-\langle\overline{\mathbf{A}}_a, \Delta\boldsymbol{\Gamma}_d\rangle_{\mathscr{V}} \leq \lambda_q\|\boldsymbol{\alpha}_a\|_2\|\boldsymbol{\gamma}_{da}\|_2 = \lambda_q\|\boldsymbol{\gamma}_{da}\|_2\|\overline{\mathbf{A}}_a\|_{\mathscr{V}}.$$

3. This proof is similar to that of point 3 of Lemma 3.2:

   $$-\langle\overline{\mathbf{A}}_a, \overrightarrow{\boldsymbol{\nabla}}\cdot(\overrightarrow{\mathbf{v}}\overline{\mathbf{z}})\rangle_{\mathscr{V}} = -\langle\sum_{i\in\mathcal{N}_a}\boldsymbol{\alpha}_i\phi_i, \overrightarrow{\mathbf{v}}\sum_{i\in\mathbb{N}}\boldsymbol{\tau}_i\phi_i\rangle_{\mathscr{V}} = -\langle\sum_{i\in\mathcal{N}_a}\boldsymbol{\alpha}_i\phi_i, \overrightarrow{\mathbf{v}}\sum_{i\in\mathcal{N}_a}\boldsymbol{\tau}_i\phi_i\rangle_{\mathscr{V}} =$$
   $$-\langle\overline{\mathbf{A}}_a, \overrightarrow{\boldsymbol{\nabla}}\cdot(\overrightarrow{\mathbf{v}}\overline{\mathbf{z}}_a)\rangle_{\mathscr{V}}.$$

   Defining a new convex function b_a of the form of (1.30) for the field $\overline{\mathbf{z}}_a$ one is led to:

   $$-\langle\overline{\mathbf{A}}_a, \overrightarrow{\boldsymbol{\nabla}}\cdot(\overrightarrow{\mathbf{v}}\overline{\mathbf{z}}_a)\rangle_{\mathscr{V}} = \int_{\mathscr{V}}\overrightarrow{\boldsymbol{\nabla}}\cdot(\overrightarrow{\mathbf{v}}b_a)d\boldsymbol{\xi} = \int_{\mathscr{B}_c^+}\overrightarrow{\mathbf{n}}\cdot(\overrightarrow{\mathbf{v}}b_a)d\boldsymbol{\xi}$$

   and the result follows by using the boundary conditions.

4. The last statement is proved by using a known bound on the nonlinear term $\zeta_a \geq \|\overline{\mathbf{f}}_a\|_{\mathscr{V}}$, so by means of the Schwartz inequality

   $$\langle\overline{\mathbf{A}}_a, \overline{\mathbf{f}}\rangle_{\mathscr{V}} \leq \|\overline{\mathbf{A}}_a\|_{\mathscr{V}}\|\overline{\mathbf{f}}\|_{\mathscr{V}} \leq \zeta_a\|\overline{\mathbf{A}}_a\|_{\mathscr{V}}.$$

B.5 Proof of Proposition 4.1

Substituting the control law (4.7) into inequality (4.24), two cases arise:

- If $\eta_a\|\overline{\mathbf{A}}_a\|_{\mathscr{V}} \geq \theta_a$ it is easy to see that:

$$\dot{\mathcal{B}}_a \leq -\zeta\lambda_m\frac{\delta_0^2}{q_1}\mathcal{B}_a,$$

thus by means of Gronwall-Bellman theorem (Khalil, 1996) $\mathcal{B}_a$, and then $\overline{\mathbf{z}}_a$, tend to zero exponentially fast.

- If $\eta_a\|\overline{\mathbf{A}}_a\|_{\mathscr{V}} < \theta_a$ then

$$\dot{\mathcal{B}}_a \leq -\zeta\lambda_m\frac{\delta_{0a}^2}{q_{1a}}\mathcal{B}_a + \eta_a\|\overline{\mathbf{A}}_a\|_{\mathscr{V}} - \frac{\eta_a^2}{\theta_a}\|\overline{\mathbf{A}}_a\|_{\mathscr{V}}^2$$

Let us now define the function Ψ as: $\Psi = \eta_a\|\overline{\mathbf{A}}_a\|_{\mathscr{V}} - \frac{\eta_a^2}{\theta_a}\|\overline{\mathbf{A}}_a\|_{\mathscr{V}}^2$. Since Ψ has a maximum value of $\Psi_m = \frac{\theta_a}{4}$ at $\eta_a\|\overline{\mathbf{A}}_a\|_{\mathscr{V}} = \frac{\theta_a}{2}$, it follows that

$$\dot{\mathcal{B}}_a \leq -\zeta\lambda_m\frac{\delta_{0a}^2}{q_{1a}}\mathcal{B}_a + \Psi_m = -\zeta\lambda_m\frac{\delta_{0a}^2}{q_{1a}}\mathcal{B}_a + \frac{\theta_a}{4} \Rightarrow \lim_{t\to\infty}\mathcal{B}_a(t) \leq \frac{\theta_a q_1}{4\zeta\lambda_m\delta_0^2}.$$

which implies that $\mathcal{B}_a$, and then $\overline{\mathbf{z}}_a$, are ultimately bounded. Note that θ_a can be modified to approximate the limit to zero. □

B.6 Proof of Proposition 4.3

From the application of control law (4.36) to system (4.34), two cases arise:

- If $\eta_a\|\overline{\mathbf{A}}_a\|_{\mathscr{V}} \geq \theta_a$, then the projection of the control law over the intensive variables $\overline{\mathbf{A}}_a$ is given by:

$$\langle\overline{\mathbf{A}}_a, \overline{\mathbf{u}}_a\rangle_{\mathscr{V}} = -\frac{\eta_a}{\|\overline{\mathbf{A}}_a\|_{\mathscr{V}}}\langle\sum_{i\in\mathcal{N}_a}\boldsymbol{\alpha}_i\phi_i, \sum_{k=1}^{m}\mathcal{H}_k\sum_{i\in\mathcal{N}_a}\boldsymbol{\alpha}_i\phi_i\rangle_{\mathscr{V}}.$$

where $\mathcal{H}_k = H(\xi - \xi_k) - H(\xi - (\xi_k + d))$. Following the same procedure as in Section 4.5 and taking into account that $\|\overline{\mathbf{A}}_a\|_{\mathscr{V}} = \|\boldsymbol{\alpha}_a\|_2$ one has that:

$$\langle\overline{\mathbf{A}}_a, \overline{\mathbf{u}}_a\rangle_{\mathscr{V}} = -\frac{\eta_a}{\|\boldsymbol{\alpha}_a\|_2}\boldsymbol{\alpha}_a^T\mathbf{P}\boldsymbol{\alpha}_a \leq -\frac{\eta_a}{\|\boldsymbol{\alpha}_a\|_2}\underline{\lambda}\boldsymbol{\alpha}_a^T\boldsymbol{\alpha}_a = -\eta_a\underline{\lambda}\|\boldsymbol{\alpha}_a\|_2$$

Substituting this expression on inequality (4.34), one is led to:

$$\dot{\mathcal{B}}_a \leq -\zeta\lambda_m\boldsymbol{\alpha}_a^T\boldsymbol{\alpha}_a + (\lambda_q\|\boldsymbol{\gamma}_{da}\|_2 + \zeta_a - \eta_a\underline{\lambda})\|\boldsymbol{\alpha}_a\|_2.$$

Since $\eta_a > \underline{\lambda}^{-1}(\lambda_q\|\boldsymbol{\gamma}_{da}\|_2 + \zeta_a)$ and taking into account that $\mathcal{B}_a \geq \delta_{0a}^2 q_{1a}^{-1}\|\boldsymbol{\alpha}_a\|_2^2$, the previous inequality can be rewritten as:

$$\dot{\mathcal{B}}_a \leq -\zeta\lambda_m \frac{\delta_{0a}^2}{q_{1a}}\mathcal{B}_a.$$

This implies that $\mathcal{B}_a$ (and thus $\overline{\mathbf{z}}_a$) converge exponentially to zero.

- If $\eta_a\|\overline{\mathbf{A}}_a\|_{\mathscr{V}} < \theta_a$. In this case, the projection of the control law over the intensive variables $\overline{\mathbf{A}}_a$ is:

$$\langle \overline{\mathbf{A}}_a, \overline{\mathbf{u}}_{am}\rangle_{\mathscr{V}} = -\frac{\eta_a^2}{\theta_a}\langle \sum_{i\in\mathcal{N}_a}\boldsymbol{\alpha}_i\phi_i, \sum_{k=1}^{m}\mathcal{H}_k\sum_{i\in\mathcal{N}_a}\boldsymbol{\alpha}_i\phi_i\rangle_{\mathscr{V}} =$$

$$-\frac{\eta_a^2}{\theta_a}\boldsymbol{\alpha}_a^T\mathbf{P}\boldsymbol{\alpha}_a \leq -\frac{\eta_a^2}{\theta_a}\underline{\lambda}\boldsymbol{\alpha}_a^T\boldsymbol{\alpha}_a = -\frac{\eta_a^2}{\theta_a}\underline{\lambda}\|\boldsymbol{\alpha}_a\|_2^2.$$

Substituting this expression into inequality (4.34), results:

$$\dot{\mathcal{B}}_a \leq -\zeta\lambda_m\boldsymbol{\alpha}_a^T\boldsymbol{\alpha}_a + (\lambda_q\|\boldsymbol{\gamma}_{da}\|_2 + \zeta_a)\|\boldsymbol{\alpha}_a\|_2 - \frac{\eta_a^2}{\theta_a}\underline{\lambda}\|\boldsymbol{\alpha}_a\|_2^2.$$

Again since $\eta_a > \underline{\lambda}^{-1}(\lambda_q\|\boldsymbol{\gamma}_{da}\|_2 + \zeta_a)$, one has that:

$$\dot{\mathcal{B}}_a \leq -\zeta\lambda_m\boldsymbol{\alpha}_a^T\boldsymbol{\alpha}_a + \eta_a\|\boldsymbol{\alpha}_a\|_2 - \frac{\underline{\lambda}}{\theta_a}\eta_a^2\|\boldsymbol{\alpha}_a\|_2^2.$$

The maximum of function $\Psi = \eta_a\|\boldsymbol{\alpha}_a\|_2 - \frac{\underline{\lambda}}{\theta_a}\eta_a^2\|\boldsymbol{\alpha}_a\|_2^2$ is $\Psi_{\max} = \frac{\theta_a}{4\underline{\lambda}}$ so the previous inequality can be rewritten as:

$$\dot{\mathcal{B}}_a \leq -\zeta\lambda_m\boldsymbol{\alpha}_a^T\boldsymbol{\alpha}_a + \frac{\theta_a}{4\underline{\lambda}} \Longrightarrow \lim_{t\to\infty}\mathcal{B}_a = \frac{\theta_a q_1}{4\zeta\lambda_m\underline{\lambda}\delta_0^2}.$$

This implies that $\mathcal{B}_a$ (and thus $\overline{\mathbf{z}}_a$) are ultimately bounded. Since θ_a is a design parameter of the control law, one can modify it to approach the limit to zero. Finally it should be stressed that the position of the actuators also affects the limit. The best position is that maximising $\underline{\lambda}$.

B.7 Proof of Lemma 6.1

Let us begin the proof by expanding the vector and matrices multiplications, so that:

$$\chi\overline{\mathbf{m}}_{va}^T\Lambda_a\mathbf{m}_{va}^* = \chi\sum_{i\in\mathcal{N}_a}\overline{m}_{vi}\lambda_i m_{vi}^*.$$

Although the term χ is unknown since κ and κ^* are unknown, some information on them is required. With this information one can define a function χ_b so that $\chi_b > |\chi|$. Besides, choosing λ_q as the maximum eigenvalue of $\mathscr{L}_a$, one is led to:

$$\chi \overline{\mathbf{m}}_{va}^T \Lambda_a \mathbf{m}_{va}^* \leq \chi_b \lambda_q \sum_{i \in \mathcal{N}_a} |m_{vi}^* \overline{m}_{vi}|.$$

Using the Hölder inequality, the following relation is obtained:

$$\chi_b \lambda_q \sum_{i \in \mathcal{N}_a} |m_{vi}^* \overline{m}_{vi}| \leq \chi_b \lambda_q \|\mathbf{m}_{va}^*\|_2 \|\overline{\mathbf{m}}_{va}\|_2 =$$

$$\chi_b \lambda_q \left(\sum_{i \in \mathcal{N}_a} |m_{vi}^*|^2 \right)^{\frac{1}{2}} \left(\sum_{i \in \mathcal{N}_a} |\overline{m}_{vi}|^2 \right)^{\frac{1}{2}} = \chi_b \lambda_q \|v_a^*\|_\nu \|\overline{v}_a\|_\nu.$$

Finally, the proof concludes by choosing $\nu = \chi_b \lambda_q \|v_a^*\|_\nu$.

References

Akin, J. E. (2005). *Finite Element Analysis with Error Estimators: An Introduction to the FEM and Adaptive Error Analysis for Engineering Students*. Elsevier, Amsterdam.

Allgöwer, F. and Zheng, A. (1997). *Nonlinear Model Predictive Control*. Birkhäuser Verlag, Basel, Switzerland.

Alonso, A., Banga, J., Moles, C., and Balsa-Canto, E. (2002). Identification and control design numbers in non-linear diffusion-convection reaction processes. In *Proceedings of the 10th Mediterranean Conference on Control and Automation - MED2002, Lisbon, Portugal*.

Alonso, A. A., Banga, J. R., and Sánchez, I. (2000). Passive control design for distributed process systems: Theory and applications. *AIChE Journal*, 46(8):1593–1606.

Alonso, A. A., Fernández, C. V., and Banga, J. R. (2004a). Dissipative systems: from physics to robust nonlinear control. *Int. J. Robust Nonlinear Control*, 14(2):157–179.

Alonso, A. A., Frouzakis, C. E., and Kevrekidis, I. G. (2004b). Optimal sensor placement for state reconstruction of distributed process systems. *AIChE Journal*, 50(7):1438–1452.

Alonso, A. A., Kevrekidis, I. G., Banga, J. R., and Frouzakis, C. E. (2004c). Optimal sensor location and reduced order observer design for distributed process systems. *Computers and Chemical Engineering*, 28(1-2):27–35.

Alonso, A. A. and Ydstie, B. E. (2001). Stabilization of distributed systems using irreversible thermodynamics. *Automatica*, 37(11):1739–1755.

Antoniades, C. and Christofides, P. D. (2000). Computation of optimal actuator locations for nonlinear controllers in transport reaction processes. *Comp. Chem. Eng.*, 24(2-7):577–583.

Antoniades, C. and Christofides, P. D. (2001). Studies on nonlinear dynamics and control of a tubular reactor with recycle. *Nonlinear Analysis*, 47(9):5933–5944.

Argentina, M., Coullet, P., and Krinsky, V. (2000). Head-on collisions of waves in an excitable fitzhugh-nagumo system: a transition from wave annihilation to classical wave behavior. *Journal of Theoretical Biology*, 205:47–52.

Aris, R. (1973). *Análisis de Reactores*. Alhambra, Madrid, Spain.

Aris, R. (1999). *Mathematical Modelling. A Chemical Engineer's Perspective*. Academic Press, San Diego, USA.

Ascher, U. M. and Petzold, L. (1998). *Computer Methods for Ordinary Differential Equations and Diferential-Algebraic Equations*. SIAM, Philadelphia, USA.

Astarita, G. (1989). *Thermodynamics: An Advanced Textbook for Chemical Engineers*. Plenum Press, New York.

Åström, K. and Wittenmark, B. (1995). *Adaptive Control*. Addison-Wesley, Reading, USA, 2nd edition.

Balsa-Canto, E. (2001). *Algoritmos Eficientes para la Optimización Dinámica de Procesos Distribuidos*. PhD thesis, Universidad de Vigo, Vigo.

Balsa-Canto, E., Alonso, A. A., and Banga, J. R. (2002a). A novel, efficient and reliable method for thermal process design and optimization. Part I: Theory. *Journal of Food Engineering*, 52(3):227–234.

Balsa-Canto, E., Alonso, A. A., and Banga, J. R. (2002b). A novel, efficient and reliable method for thermal process design and optimization. Part II: Applications. *Journal of Food Engineering*, 52(3):235–247.

Balsa-Canto, E., Alonso, A. A., and Banga, J. R. (2004). Reduced-order models for nonlinear distributed process systems and their application in dynamic optimization. *Industrial & Engineering Chemistry Research*, 43(13):3353–3363.

Beaumont, J., Davidenko, N., Davidenko, J. M., and Jalife, J. (1998). Spiral waves in two-dimensional models of ventricular muscle: Formation of a stationary core. *Biophysical Journal*, 75:1–14.

Berkooz, G., Holmes, P., and Lumley, L. (1993). The Proper Orthogonal Decomposition in the analysis of turbulent flows. *Ann. Rev. Fluid Mech.*, 25:539–575.

Bird, R. B., Stewart, W. E., and Lightfoot, E. N. (2002). *Transport Phenomena*. John Wiley & Sons, New York, 2^{nd} edition.

Bošković, D., Balogh, A., and Krstić, M. (2003). Backstepping in infinite dimension for a class of parabolic distributed parameter systems. *Mathematics of Control, Signals and Systems*, 16:44–75.

Bouzat, S. and Wio, H. S. (2003). Influence of boundary conditions on the dynamics of oscillatory media. *Physica A*, 317:472–486.

Brezis, H. (1984). *Análisis Funcional. Teoría y Aplicaciones*. Alianza, Madrid, Spain.

Brigham, E. O. (1974). *The Fast Fourier Transform*. Prentice-Hall, Englewood Cliffs, NJ.

Callen, H. (1985). *Thermodynamics and an Introduction to Thermostatistics*. 2nd. Edition. John Wiley & Sons.

Camacho, E. F. and Bordons, C. (1999). *Model Predictive Control*. Springer Verlag, London, UK.

Christofides, P. D. (2001). *Nonlinear and Robust Control of PDE Systems: Methods and Applications to Transport-Reaction Processes*. Birkhäuser, Boston.

Christofides, P. D. and Daoutidis, P. (1996). Nonlinear control of diffusion-convection-reaction processes. *Comp. Chem. Eng.*, 20:s1071–s1076.

Conde, J. C., González, P., Lusquiños, F., Chiussi, S., Serra, J., and León, B. (2005). Analytical and numerical calculations of the temperature distribution in si and ge targets irradiated by excimer lasers. *Applied Surface Science*, 248(1-4):455–460.

Constantinides, A. and Mostoufi, N. (1999). *Numerical Methods for Chemical Engineers with MATLAB Applications*. Prentice Hall PTR.

Cooley, J. W. and Tukey, J. W. (1965). An algorithm for machine calculation of complex fourier series. *Mathematics of Computation*, 19(90):297–&.

Corless, M. (1993). Control of uncertain nonlinear-systems. *Journal of Dynamic Systems, Measurements and Control - Transactions of the ASME*, 115(2B):362–372.

Courant, R. and Hilbert, D. (1989). *Methods of Mathematical Physics*. John Wiley & Sons, New York, USA, 1st edition.

Curtain, R. F. and Pritchard, A. J. (1977). *Functional Analysis in Modern Applied Mathematics*. Academic Press, London, UK.

Dahlem, M. A. and Müller, S. C. (2000). Image processing techniques applied to excitation waves in the chicken retina. *Methods*, 21:317–323.

Demirel, Y. (2002). *Nonequilibrium Thermodynamics*. Elsevier: Amsterdam.

Dochain, D., Babary, J., and Tali-Maamar, N. (1992). Modelling and adaptive control of nonlinear distributed parameter bioreactors via orthogonal collocation. *Automatica*, 28(5):873–883.

Eidelman, Y., Milman, V., and Tsolomitis, A. (2004). *Functional Analysis. An Introduction*. American Mathematical Society, USA.

Everson, R. and Sirovich, L. (1995). Karhunen-loeve procedure for gappy data. *Journal of the Optical Society of America*, 12(8):1657–1664.

Fenton, F. H., Cherry, E. M., Hastings, H. M., and Evans, S. J. (2002a). Multiple mechanisms of spiral wave breakup in a model of cardiac electrical activity. *Chaos*, 12:852–892.

Fenton, F. H., Cherry, E. M., Hastings, H. M., and Evans, S. J. (2002b). Real-time computer simulations of excitable media: Java as a scientific language and as a wrapper for c and fortran programs. *Biosystems*, 64:73–96.

Fenton, F. H. and Karma, A. (1998). Vortex dynamics in three-dimensional continuous myocardium with fiber rotation: Filament instability and fibrillation. *Chaos*, 8:20–47.

FitzHugh, R. (1961). Impulses and physiological states in theoretical models of nerve membrane. *Biophys. J.*, 1:445–466.

Fletcher, C. A. J. (1984). *Computational Galërkin Methods*. Springer-Verlag, New York.

Fogler, H. S. (1992). *Elements of Chemical Reaction Engineering*. Prentice Hall, NJ, USA, 2nd edition.

Garcia, C. E. and Morari, M. (1982). Internal model control-1. a unifying review and some new results. *Industrial & Engineering Chemistry Process Design and Development*, 21(2):308–323.

García, M. R., Vilas, C., Banga, J. R., and Alonso, A. A. (2007). Optimal field reconstruction of distributed process systems from partial measurements. *Industrial & Engineering Chemistry Research*, 46(2):530–539.

Gear, C. W., Kevrekidis, I. G., and Theodoropoulos, C. (2002). "coarse" integration/bifurcation analysis via microscopic simulators: micro-galerkin methods. *Computers & Chemical Engineering*, 26:941–963.

Gorban, A. N., Karlin, I. V., Zmievskii, V. B., and Dymova, S. V. (2000). Reduced description in the reaction kinetics. *Physica A*, 275(3-4):361–379.

Gorelova, N. A. and Bures, J. (1983). Spiral waves of spreading depression in the isolated chicken retina. *Journal of Neurobiology*, 14(5):353–363.

Gottlieb, D. and Orszag, S. A. (1977). *Numerical Analysis of Spectral Methods: Theory and Applications*. Society for Industrial and Applied Mathematics, Philadelphia, Pennsylvania.

Gundepudi, P. and Friedly, J. (1998). Velocity control of hyperbolic partial differential equation systems with single characteristic variable. *Chem. Eng. Sci.*, 53(24):4055–4072.

Henson, M. A. and Seborg, D. E. (1997). Feedback linearizing control. In Henson, M. A. and Seborg, D. E., editors, *Nonlinear Process Control*. Prentice Hall PTR, NJ, USA.

Hirschfelder, J. O., Curtiss, C. F., and Bird, R. B. (1954). *Molecular Theory of Gases and Liquids*. John Wiley & Sons, New York.

Hodgkin, A. L. and Huxley, A. F. (1952a). Measurement of current-voltage relations in the membrane of the giant axon of loligo. *Journal of Physiology*, 116(4):424–448.

Hodgkin, A. L. and Huxley, A. F. (1952b). A quantitative description of membrane current and its application to conduction and excitation in nerve. *J. Physiol.*, 117:500–544.

Hodgkin, A. L., Huxley, A. F., and Katz, B. (1949). Ionic currents underlying activity in the giant axon of the squid. *Archives des Sciences Physiologiques*, 3(2):129–150.

Holmes, P., Lumley, J. L., and Berkooz, G. (1996). *Turbulence, Coherent Structures, Dynamical Systems and Symmetry*. Cambridge University Press.

Holmes, P. J., Lumley, J. L., Berkooz, G., Mattingly, J. C., and Wittenberg, R. W. (1997). Low-dimensional models of coherent structures in turbulence. *Physics Reports*, 287(4):338–384.

Hoo, K. and Zheng, D. (2001). Low-order control-relevant models for a class of distributed parameter systems. *Chemical Engineering Science*, 56(23):6683–6710.

Jin, Y., Xu, J., Zhang, W., Luo, J., and Xu, Q. (2005). Simulation of biological waves in single-species bacillus system governed by birth and death-diffusion dynamical equation. *Mathematics and Computers in Simulation*, 68:317–327.

Jou, D., Casas-Vazquez, J., and Lebon, G. (1993). *Extended Irreversible Thermodynamics*. Springer-Verlag, Berlin.

Keener, J. (2004). The topology of defibrillation. *Journal of Theoretical Biology*, 203:459–473.

Keener, J. and Sneyd, J. (1998). *Mathematical Physiology*. Springer, New York.

Khalil, H. K. (1996). *Nonlinear Systems*. Prentice Hall, Upper Saddle River, New Jersey, 2nd edition.

Lapidus, L. and Pinder, G. (1999). *Numerical Solution of Partial Differential Equations in Science and Engineering*. John Wiley & Sons, Inc.

Lebiedz, D. and Brandt-Pollmann, U. (2003). Manipulation of self-aggregation patterns and waves in a reaction-diffusion system by optimal boundary control strategies. *Physical Review Letters*, 91(20):208301.

Lebiedz, D. and Maurer, H. (2004). External optimal control of self-organisation dynamics in a chemotaxis reaction diffusion system. *IEE Systems Biology*, 2:222–229.

Lemouel, A., Neirac, F., and Maisi, N. (1994). Heat-transfer equation - modeling by rational hankel approximation methods. *Revue Generale de Thermique*, 33(389):336–343.

Levenspiel, O. (1962). *Chemical Reactor Engineering, An Introduction to the Design of Chemical Reactors*. John Wiley, NY.

Levenspiel, O. (2004). *Ingeniería de las Reacciones Químicas*. John Wiley & Sons, Mexico, 3rd edition.

Ljung, L. (1999). *System Identification. Theory for the User.* Prentice Hall, New Jersey, USA, 2nd edition.

Lorenz, E. N. (1960). Energy and numerical weather prediction. *Tellus*, 12(4):364–373.

Morari, M. and Zafiriou, E. (1989). *Robust process control.* Prentice-Hall, New Jersey.

Murray, J. D. (2002a). *Mathematical Biology I: An Introduction.* Springer-Verlag, Berlin, 3rd edition.

Murray, J. D. (2002b). *Mathematical Biology II: Spatial Models and Biomedical Applications.* Springer-Verlag, Berlin, 3rd edition.

Nagumo, J., Arimoto, S., and Yoshizawa, Y. (1962). Active pulse transmission line simulating nerve axon. *Proc. Inst. Radio. Eng.*, 50:2061–2070.

Nicolis, G. and Nicolis, C. (1999). Thermodynamic dissipation versus dynamical complexity. *Journal of Chemical Physics*, 110(18):8889–8898.

Nocedal, J. and Wright, S. (1999). *Numerical Optimization.* Springer, New York, USA.

Norgaard, M., Ravn, O., Poulsen, N. K., and Hansen, L. K. (2000). *Neural Networks for Modelling and Control of Dynamic Systems.* Springer.

Ogunnaike, B. A. and Ray, W. H. (1994). *Process dynamics, modelling, and control.* Oxford University Press, Inc.

Onsager, L. (1931a). Reciprocal relations in irreversible processes. I. *Physical Review*, 37(4):405–426.

Onsager, L. (1931b). Reciprocal relations in irreversible processes. II. *Physical Review*, 38(12):2265–2279.

Orszag, S. A. (1980). Spectral methods for problems in complex geometries. *Journal of Computational Physics*, 37(1):70–92.

Orszag, S. A. and Kruskal, M. D. (1968). Formulation of theroy of turbulence. *Physics of Fluids*, 11(1):43–&.

Park, H. M., Kim, T., and Cho, D. (1998). Estimation of parameters in flow reactors using the Karhunen-Loève decomposition. *Comput. & Chem. Eng.*, 23:109–123.

Polyanin, A. D. (2002). *Handbook of Linear Partial Differential Equations for Engineers and Scientists*. Chapman & Hall/CRC, Boca Raton.

Prigogine, I. (1967). *Introduction to Thermodynamics of Irreversible Processes*. John Wiley & Sons, New York, 3^{rd} edition.

Pumir, A. and Krinsky, V. (1999). Unpinnig of a rotating wave in cardiac muscle by an electric field. *J. Theor. Biol.*, 199:311–319.

Quarteroni, A., Sacco, R., and Saleri, F. (2000). *Numerical Mathematics*. Springer-Verlag, New York, U.S.A.

Rappel, W. J., Fenton, F. H., and Karma, A. (1999). Spatiotemporal control of wave instabilities in cardiac tissue. *Physical review Letters*, 83(2):456–459.

Reddy, B. (1998). *Introductory Functional Analysis: With Applications to Boundary Value Problems and Finite Elements*. Springer-Verlag, New York.

Reddy, J. N. (1993). *An Introduction to the Finite Element Method*. McGraw-Hill, 2nd edition.

Rico-Martínez, R., Krischer, K., and Kevrekidis, Y. (1995). *Neural Networks in Chemistry and Chemical Engineering*, chapter Nonlinear systema identification using neural networks: dynamics and instabilities. A. Bulsari.

Rinzel, J. (1981). *Models in Neurobiology*. Plenum Press.

Rudin, W. (1973). *Functional Analysis*. McGraw Hill, USA.

Saro, O., Nonino, C., and Comini, G. (1995). *An enthalpy-based algorithm for the analysis of phase change in nonhomogeneous media*, pages 127–134. Computational Mechanics Publications, Southampton.

Sasane, A. (2002). Hankel norm approximation for infinite-dimensional systems - introduction. *Lecture Notes in Control and Information Sciences*, 277:1.

Scheerlinck, N., Verboven, P., Fikiin, K., De Baerdemaeker, J., and Nicolai, B. (2001). Finite element computation of unsteady phase change heat transfer during freezing or thawing of food using a combined enthalpy and kirchhoff transform method. *Transactions of the ASAE*, 44(2):429–438.

Seborg, D. E. and Henson, M. A. (1997). *Nonlinear Process Control*, chapter Introduction. Prentice Hall PTR, NJ, USA, henson, m. a. and seborg, d. e. edition.

Sepulchre, R., Jankovic, M., and Kokotovic, P. (1997). *Contructive Nonlinear Control*. Springer-Verlag, London.

Shi, D., El-Farra, N. H., Li, M. H., Mhaskar, P., and Christofides, P. D. (2006). Predictive control of particle size distribution in particulate processes. *Chemical Engineering Science*, 61(1):268–281.

Shvarstman, S. Y., Theodoropoulos, C., Rico-Martínez, R., Kevrekidis, I. G., Titi, E. S., and Mountziaris, T. J. (2000). Order reduction for nonlinear dynamic models of distributed reacting systems. *J. of Proc. Cont.*, 10:177–184.

Shvartsman, S. Y. and Kevrekidis, I. G. (1998). Nonlinear model reduction for control of distributed systems: A computer–assisted study. *AIChE Journal*, 44(7):1579–1595.

Siehr, J., Mommer, S., Slaby, O., and Lebiedz, D. (2007). Targeting characteristic wave properties in reaction-diffusion systems by optimization of external forcing. *Physical Review E*, 76(5):056211.

Silberman, I. (1954). Planetary waves in the atmosphere. *Journal of Meteorology*, 11(1):27–34.

Silebi, C. A. and Schiesser, W. E. (1992). *Dynamic Modeling of Transport Process Systems*. Academic Press, London.

Sirovich, L. (1987). Turbulence and the dynamics of coherent structures. Part I: Coherent structures. *Quaterly of Appl. Math.*, 45(3):561–571.

Slotine, J. and Li, W. (1991). *Applied Nonlinear Control*. Prentice Hall, Englewood Cliffs, New Jersey.

Smith, J. M., Van Ness, H. C., and Abbott, M. M. (1996). *Introduction to Chemical Engineering Thermodynamics*. McGraw-Hill, New York, 5th edition.

Smoller, J. (1994). *Shock Waves and Reaction-Diffusion Equations*. Springer-Verlag, New york, 2nd edition.

Stelling, J., Sauer, U., Szallasi, Z., Doyle III, F. J., and Doyle, J. (2004). Robustness of cellular functions. *Cell*, 118(6):675–685.

Stephanopoulos, G. (1984). *Chemical Process Control: An Introduction to Theory and Practice*. Prentice Hall, New Jersey, USA.

Sweers, G. and Troy, W. C. (2003). On the bifurcation curve for an elliptic system of fitzhugh-nagumo type. *Physica D-Nonlinear phenomena*, 177:1–22.

Syafiie, S., Tadeo, F., and Martinez, E. (2007). Model-free learning control of neutralization processes using reinforcement learning. *Engineering Applications of Artificial Intelligence*, 20(6):767–782.

Tombs, M. and Postlethwaite, I. (1987). Truncated balanced realization of stable, non-minimal state-space systems. *Int. J. Control*, 46:1319–1330.

Truesdell, C. (1984). *Rational Thermodynamics*. Springer-Verlag, New York, 2^{nd} edition.

Turing, A. M. (1952). The chemical basis of morphogenesis. *Phil. Trans. R. Soc. London B*, 237:37–72.

van den Bosch, P. P. J. and van der Klauw, A. C. (1994). *Modeling, Identification and Simulation of Dynamical Systems*. CRC Press, Florida.

Varga, A. (1991). Efficient minimal realization procedure based on balancing. In A. El Moudui, P. Borne, S. G. T., editor, *Proc. Of IMACS/IFAC Symp. MCTS*, pages 42–46 (vol.2), Lille, France.

Vilas, C., García, M. R., Banga, J. R., and Alonso, A. A. (2006). Stabilization of inhomogeneous patterns in a diffusion-reaction system under structural and parametric uncertainties. *Journal of Theoretical Biology*, 241(2):295–306.

Vilas, C., García, M. R., Banga, J. R., and Alonso, A. A. (2007). Robust feed-back control of distributed chemical reaction systems. *Chemical Engineering Science*, 62(11):2941–2957.

White, D. A. and Sofge, D. A. (1992). *Handbook of Intelligent Control - Neural, Fuzzy, and Adaptive Approaches.* Van Nostrand Reinhold, New York, USA.

Winfree, A. T. (1984). The prehistory of the belousov-zhabotinsky oscillator. *Journal of Chemical Education*, 61(8):661–663.

Witkowski, F. X., Leon, L. J., Penkoske, P. A., Giles, W. R., Spano, M. L., Ditto, W. L., and Winfree, A. T. (1998). Spatiotemporal evolution of ventricular fibrillation. *Nature*, 392:78–82.

Ydstie, B. E. and Alonso, A. A. (1997). Process systems and passivity via the clausius-plank inequality. *Syst. & Cont. Letters*, 30(5):253–264.

Zerrik, E., Boutoulout, A., and Bourray, H. (2001). Boundary strategic actuators. *Sensors and Actuators A - Physical*, 94(3):197–203.

Zienkiewicz, O. C., Taylor, R. L., and Zhu, J. Z. (2005). *The Finite Element Method: Its Basis & Fundamentals*. Elsevier, Amsterdam, 6^{th} edition.

Zill, D. G. (1997). *Ecuaciones diferenciales con aplicaciones de modelado*. International Thomson, Mexico, 6th edition.

Zimmermann, M. G., Firle, S. O., Natiello, M. A., Hildebrand, M., Eiswirth, M., Bär, M., Bangia, A. K., and Kevrekidis, I. G. (1997). Pulse bifurcation and transition to spatiotemporal chaos in an excitable reaction-diffusion model. *Physica D*, 110:92–104.

Contributions

Articles published in SCI Journals

Antonio A. Alonso, **Carlos V. Fernández** and Julio R. Banga (2004). Dissipative Systems: from physics to robust nonlinear control. *International Journal of Robust and Nonlinear Control*, 14(2): 157-179.

Carlos Vilas, Míriam R. García, Julio R. Banga and Antonio A. Alonso (2006). Stabilization of inhomogeneous patterns in a diffusion-reaction system under structural and parametric uncertainties. *Journal of Theoretical Biology*, 241(2): 295-306.

Míriam R. García, **Carlos Vilas**, Julio R. Banga and Antonio A. Alonso (2007). Optimal Field Reconstruction of Distributed Process Systems from Partial Measurements. *Industrial & Engineering Chemistry Research*, 46(2): 530-539.

Carlos Vilas, Míriam R. García, Julio R. Banga and Antonio A. Alonso (2007). Robust feed-back control of distributed chemical reaction systems. *Chemical Engineering Science*, 62(11): 2941-2957.

Maya N. Ignatova, Velislava N. Lyuvenova, Míriam R. García, **Carlos Vilas** and Antonio A. Alonso (2008). Indirect adaptive linearizing control of a class of bioprocesses - Estimator tuning procedure. *Journal of Process Control*, 18: 27-35.

Carlos Vilas, Míriam R. García, Julio R. Banga and Antonio A. Alonso (2008). Desarrollo de una librería de componentes en EcosimPro para la operación de plantas de procesamiento térmico de alimentos. *Revista Iberoamericana de Automática e Informática Industrial (RIAI)*, 5(1): 51-65.

Carlos Vilas, Míriam R. García, Julio R. Banga and Antonio A. Alonso (2008). Feed-Back Robust Control of Spiral Waves in Distributed Biological Systems. *Available online at www.sciencedirect.com.* D.O.I. 10.1016/j.physd.2008.02.019.

Míriam R. García, **Carlos Vilas**, Julio R. Banga and Antonio A. Alonso (2008). Exponential Observers for Distributed Tubular (Bio)Reactors. *Accepted for publication*

in AIChE Journal.

Book Chapters

Carlos Vilas, Míriam R. García, María R. Fernández, Eva Balsa-Canto, Julio R. Banga and Antonio A. Alonso (2004). On Systematic Model Reduction Techniques for Dynamic Optimization and Robust Control of Distributed Process Systems. In *European Symposium on Computer Aided Process Engineering - 15.* 841-846. Elsevier.

Míriam R. García, **Carlos Vilas**, Julio R. Banga and Antonio A. Alonso (2005). An Efficient Real-Time Dynamic Optimization Architecture for the Control of Non-Isothermal Tubular Reactors. In *European Symposium on Computer Aided Process Engineering - 15*, L. Puigjaner Editor. 1339-1344. Elsevier.

Carlos Vilas, Míriam R. García, Julio R. Banga and Antonio A. Alonso (2006). Robust Stabilization of Inhomogeneous Patterns in a Reaction-Diffusion Biological System. In *Understanding and Exploiting Systems Biology in Biomedicine and Bioprocesses*, Cánovas, M. and Iborra, J. L. and Manjón, A. Editors. 93-100. Fundación CajaMurcia.

Contributions to Conferences

Antonio A. Alonso, **Carlos Vilas**, Míriam R. García, Marcos Villafín, Julio R. Banga (2003). *Embedding Software and Hardware for Real-Time Integral Control in Food Processing Plants.* International Workshop Information Technologies and Computing Techniques for the Agro-Food Sector, AfoT 2003. Barcelona (Spain), November, 27-28.

Carlos Vilas, Míriam R. García, Marcos Villafín, Julio R. Banga, Antonio A. Alonso (2004). *An Efficient Dynamic Simulation Environment for the Operation of Food Processing Plants.* International Congress on Engineering and Food (ICEF9). Montpellier (France), March, 7-11.

Míriam R. García, **Carlos Vilas**, Julio R. Banga, Antonio A. Alonso (2004). *Observer Design and Parameter Estimation Tools for Food Processing Plants.* International Congress on Engineering and Food (ICEF9). Montpellier (France), March, 7-11.

Antonio A. Alonso, **Carlos Vilas**, Julio R. Banga (2004). *On the Robust Control of Biological Waves.* International Conference on Systems Biology (ICSB5). Heidelberg (Germany), October, 9-13.

Carlos Vilas, Míriam R. García, María R. Fernández, Eva Balsa-Canto, Julio R. Banga, Antonio A. Alonso (2004). *On systematic model reduction techniques for dynamic optimization and robust control of distributed process systems.* European Symposium on Computer Aided Process Engineering (ESCAPE 14). Lisbon (Portugal), May, 16-19.

Míriam R. García, Eva Balsa-Canto, **Carlos Vilas**, Julio R. Banga, Antonio A. Alonso (2005). *An Efficient Real-Time Dynamic Optimization Architecture for the Control of Non-Isothermal Tubular Reactors.* European Symposium on Computer Aided Process Engineering (ESCAPE 15). Barcelona (Spain), June, 29 - July, 1.

Maya N. Ignatova, Velislava N. Lyubenova, **Carlos V. Fernández**, Míriam R. García, Antonio A. Alonso AA (2005). *Model for control of gluconic acid fermentation by Aspergillus Niger and its application for observers design.* Agricultural and Food Sciences, Processes and Technologies. Sibiu (Rumania), December, 12-13.

Carlos Vilas, Míriam R. García, Julio R. Banga, Antonio A. Alonso (2005). *Control Robusto de Sistemas Reacción-Difusión.* XXVI Jornadas de Automática. Alicante (Spain), September, 7-10.

Míriam R. García, Eva Balsa-Canto, **Carlos Vilas**, Julio R. Banga, Antonio A. Alonso (2005). *Optimización en tiempo real para el control de reactores tubulares no isotermos.* XXVI Jornadas de Automática. Alicante (Spain), September, 7-10.

Carlos Vilas, Míriam R. García, Julio R. Banga, Antonio A. Alonso (2005). *Robust Control of Inhomogeneous Patterns in Reaction-Diffusion Systems Using Reduced Order Models.* AIChE 2005 Annual Meeting. Cincinnati (USA), October, 30 - November, 4.

Míriam R. García, **Carlos Vilas**, Julio R. Banga, Velislava N. Lyubenova, N. Ignatova, Antonio A. Alonso (2005). *State Reconstruction in Spatially Distributed BioProcess Systems using Reduced Order Models: Application to the Gluconic Acid Production.* CDC-ECC'05. Seville (Spain), December, 12-15.

Carlos Vilas, Míriam R. García, Julio R. Banga, Antonio A. Alonso (2006). *Control of Travelling Waves in Reaction-Diffusion Biological Systems.* 5^{th} MathMod. Vienna (Austria), February, 8-10.

Carlos Vilas, Míriam R. García, Julio R. Banga, Antonio A. Alonso (2006). *Robust Stabilization of of Inhomogeneous Patterns in a Reaction-Diffusion Biological System.*

1^{st} International Symposium on Systems Biology (SysBiol). Murcia (Spain), June, 1-2.

Carlos Vilas, Míriam R. García, Marcos Villafín, Julio R. Banga, Antonio A. Alonso (2006). *Entorno Eficiente de Simulación Dinámica para la Operación de Plantas de Procesamiento de Alimentos.* XXVII Jornadas de Automática. Almería (Spain), September, 6-9.

Maya N. Ignatova, Velislava N. Lyubenova, **Carlos Vilas**, Míriam R. García (2006). *Adaptive Linearizing Control of Gluconic Acid Fermentation by Aspergillus Niger.* 2^{nd} International BioInfo'2006 Workshop on Computational Inteligence in Bioinformatics. Sophia (Bulgaria), October, 5.

Míriam R. García, **Carlos Vilas**, Julio R. Banga, Antonio A. Alonso (2006). *Optimal Field Reconstruction of Distributed Process Systems from Partial Measurements.* 2006 AIChE Annual Meeting. San Francisco (USA), November, 12-17.

Míriam R. García, **Carlos Vilas**, Lino O. Santos, Antonio A. Alonso (2006). *A Robust and Stabilizing Multi-Model Predictive Control Approach to Command the Operation of Distributed Process Systems.* 2006 AIChE Annual Meeting. San Francisco (USA), November, 12-17.

Juan Manuel Escao, Carlos Bordóns, Míriam R. García, **Carlos Vilas**, Antonio A. Alonso (2007). *Control Predictivo basado en Modelo Neuroborroso de un Autoclave Industrial.* XXVIII Jornadas de Automática. Huelva (Spain), September, 5-7.

Carlos Vilas, Míriam R. García, Julio R. Banga, Antonio A. Alonso (2008). *A Library of Software Components for the Operation of Thermal Food Processing Plants.* Model-It. Madrid (Spain), June, 9-11.

Míriam R. García, **Carlos Vilas**, Antonio A. Alonso, Eva Balsa-Canto (2008). *Real Time Optimization of the thermal processing of bioproducts in batch units.* Model-It. Madrid (Spain), June, 9-11.

S. Syafiie, **Carlos Vilas**, Míriam R. García, Fernando Tadeo, Antonio A. Alonso and Ernesto Martinez (2008). *Intelligent Control Based on Reinforcement Learning for Batch Thermal Sterilization of Canned Foods.* IFAC'08. Seul (Korea), July, 6-11.

Publicaciones del Departamento de Matemática Aplicada II de la Univerdidad de Vigo
Sección 1. Tesis Doctorales.

1.- Estudio matemático y numérico del modelo de Reynolds-Koiter y de los modelos tribológicos en lectura magnética. J. Jesús Cendán Verdes. 2005.

2.- Polinomios ortogonales en varias variables discretas. Jaime Alberto Rodal Vila. 2008.